THE EFFECT OF VIBRATIONAL LOADING ON GEAR SCUFFING

Anthony George Douglas Smith
D.I.C., B.Sc., A.C.G.I.

A thesis submitted for the degree of
DOCTOR OF PHILOSOPHY
of the University of London

October 1977

Lubrication Laboratory
Department of Mechanical Engineering,
Imperial College,
London, S.W.7.

A B S T R A C T

This thesis is concerned with investigating the effect of applying vibration to a pair of gear teeth by simulating the system on a disc machine.

The main results from the imposed vibrations were:

(a) The scuffing load was reduced, and the extent of this reduction was dependent upon the frequency of the applied load changes.

(b) The disc surface temperature, coefficient of friction and asperity contact were all increased.

(c) The pitting life was appreciably reduced at 15 Hz.

The mechanisms causing these changes were investigated using a range of experimental techniques, including:

(i) Measurement of the disc surface temperature with an infra-red microscope.

(ii) Electrical resistance and voltage discharge techniques for measuring the average film thickness.

(iii) Measuring the pitting life at several frequencies.

(iv) Using discs with different surface roughnesses.

A Fourier analysis of the pressure waveforms resulting from vibration showed that for a latter series of tests, the waveform was virtually constant with applied frequency.

After the examination of four other hypotheses, a probable explanation for the changes occurring with a vibrating load was deduced, based upon work by Lee and Cheng. This indicated that with each change in load an entrapment was formed temporarily in the discs' surface. This led to a considerably lower minimum film thickness, accompanied by a higher peak pressure and flash temperature rise. Substantial support

was provided for this explanation by an examination of the data from the disc machine investigations.

Work by Hunt and Kauzlarich was used to provide the tentative hypothesis that the dependence of the scuffing load on frequency occurred because a squeeze film bearing was created between the discs. At high frequencies this was supporting a portion of the load, and thus reducing the effect of the vibrations.

Further work is suggested to substantiate these deductions, including combining, by computer, the traditional equations for rolling with sliding line contact and the findings by Cheng and Lee.

A C K N O W L E D G E M E N T S

The author gratefully acknowledges the following for their assistance in this study:-

Professor A. Cameron for his many excellent ideas, supervision and advice.

Dr. P.B. Macpherson for his encouragement, recommendations and interest in each stage of the work.

Mr. R. Dobson and Mr. A. Wymark for their helpful technical advice and suggestions.

All members of the Lubrication Laboratory for a congenial academic environment, and many productive discussions.

Mr. P.T. Jeffs for his assistance with infra-red measurement of surface temperatures.

The Science Research Council for providing a grant.

Mrs. R. Baldwin for the excellent typing.

Finally, Miss Mary-Alice Brown for her encouragement and help with proof-reading.

LIST OF CONTENTS

		Page
Abstract		i
Acknowledgements		iii
List of Figures		xii
Nomenclature		xvi
CHAPTER 1	INTRODUCTION AND OUTLINE OF APPROACH	1
1.1	Introduction	1
1.2	Outline of Chapters Two to Seventeen	2
CHAPTER 2	THE HYDROSTATIC BEARING DISC MACHINE AND STANDARD TEST PROCEDURE	6
2.1	Introduction and Background	6
2.2	Description of the Test Machine	7
	2.2.1 Instrumentation	12
2.3	Discussion of the Operation of the Disc Machine	12
2.4	Explanation of the Standard Test Procedure	14
	2.4.1 Simulation of Gears	14
	2.4.2 Description of Setting-up and Running a Standard Test	14
2.5	Variations on the Standard Test	16
	2.5.1 Fatigue Test	16
	2.5.2 Type A Test	17
CHAPTER 3	THE INFLUENCE OF RETAINED AUSTENITE ON GEAR TEETH SCUFFING	18
3.1	Introduction	18
3.2	Retained Austenite, Advantage or Disadvantage?	18
	3.2.1 Literature Review	19
3.3	Scuffing Tests on the Disc-Machine	20
3.4	Results and Torque Traces	21
3.5	Discussion	21

		Page
3.6	Conclusions, Effect of Sub-Zero Treatment on EN 39B	24
3.7	Pitting of EN 31, EN 39B (Treated and Untreated)	25
	3.7.1 Tests and Results from Disc-Machine	25
3.8	Discussion of Pitting Tests	25
	3.8.1 Conclusions and Disappointment in Sub-Zero Treatment	26
3.9	Performance of Used Oil	26
CHAPTER 4	INFLUENCE OF SURFACE COATINGS ON GEAR SCUFFING	28
4.1	Introduction and Reasons for Surface Coatings	28
4.2	Surface Coatings for Testing	29
	4.2.1 Description of Surface Coatings	30
4.3	Testing on the Disc-Machine	30
4.4	Results and Torque Traces	31
4.5	Discussion and Reasons for Apparent Disadvantageous Treatments	32
4.6	Conclusions and Recommendations	33
CHAPTER 5	THE INFLUENCE OF LUBRICANT ADDITIVES ON PISTON-RING SCUFFING	34
5.1	Synopsis	34
5.2	Introduction and History	35
5.3	Modification of a Petter AV1 Lab Engine to Enable Scuffing to be Observed	36
	5.3.1 Identification of Scuffing	36
5.4	Test Procedure	41
5.5	Description of the Test Engine and its Modifications	42
5.6	Test Lubricants	42
	5.6.1 The Fuel	42
5.7	Pre-Test Procedure	43

		Page
	5.7.1 Running-in a New Piston-Ring	43
	5.7.2 Running-in Between Tests	43
	5.7.3 Oil Changes	43
5.8	Scuffing Test Procedure	45
5.9	Petter Engine Scuffing Test Results	46
5.10	Discussion of Results	47
	5.10.1 Base Oil plus Detergent	47
	5.10.2 Base Oil plus Extreme Pressure Additive	47
	5.10.3 Base Oil plus Detergent plus Extreme Pressure Additive	48
5.11	Tests with only One Oil Control Ring	48
5.12	Conclusions	49
5.13	Summary of Conclusions	51
CHAPTER 6	EXAMINATION OF PREVIOUS WORK ON DYNAMIC LOADS IN GEARS	52
6.1	Introduction	52
6.2	Buckingham, E.	52
6.3	Post Buckingham Work on internally excited Dynamic Loads	58
6.4	Bishop and Johnson and the Use of Complex Notation	59
6.5	Application of Electrical Measurements	64
6.6	Resonances in Gears	64
6.7	Merritt's Simulation of Gears on a Disc-Machine	66
6.8	The Effect of Damping in Gearboxes	68
6.9	A Method of Eliminating known Rig Vibrations from Test Results	69
6.10	Temperatures in the Contact	72
6.11	Kohler, Pratt and Thompson's work on Noise	74
6.12	Surface Roughness related to Scuffing Resistance	77
6.13	Modal Analysis of the System Response	78
6.14	Conclusions	78

		Page
CHAPTER 7	DYNAMIC LOADING TESTS, EXPERIMENTAL DETAILS	81
7.1	Introduction	81
7.2	Description of the Servovalve	83
7.3	Use of the Servovalve on the Disc Machine	83
7.4	Calibration and Use	88
7.5	Alteration of the Standard Test Procedure When using the Servovalve	90
7.6	Variations on the Type B Test	92
7.7	Type C Test	92
7.8	Types D and E Tests	93
7.9	Types F, I and J Tests	93
7.10	Type H Tests	93
7.11	Type K Tests	93
7.12	Type L Tests	93
7.13	Type M Tests	94
7.14	Table of Test Conditions	94
7.15	Other Experimental Details	96
7.16	Test Results at Frequencies Below 10 Hz.	97
7.17	Electrical Measurement of Asperity Contact	97
7.18	Oil Film Thickness by Voltage Discharge and Resistance Techniques	99
7.19	Test 224, Effect of Vibrations on Coefficient of Friction	102
7.20	Test 221, Effect of Vibration on the Disc Surface Temperature	102
CHAPTER 8	THE RESULTS FROM TESTS WITH A FLUCTUATING LOAD	105
8.1	Explanation of Figures in Tables of Results	105
8.2	Disc Machine Test Results	106
8.3	Type B Tests	107
8.4	Type D Tests	109
8.5	Type E Tests	111
8.6	Type F Tests	113
8.7	Type H Tests	115
8.8	Type I Tests	117
8.9	Type J Tests	119
8.10	Type K Tests	121
8.11	Type C Tests	123
8.12	Type L Tests	124
8.13	Type M Tests	126

		Page
8.14	Summary	128
8.15	Electrical Investigation of Asperity Contact	128
8.16	Resistance Measurement of Film Thickness	128
8.17	Results of Film Thickness Measurements by Voltage Discharge	132
8.18	Results from Test 224, Coefficient of Friction and Disc Surface Temperature for different Applied Load Frequencies	133
8.19	Preliminary Analysis of the Results	133
8.20	Effect of Vibrations on the Scuffing Load	133
8.21	Effect of Vibrations on the Coefficient of Friction	136
8.22	Effect of Vibrations on the Disc Surface Temperature	139
	8.22.1 Effect of Oil Viscosity on the Coefficient of Friction	139
8.23	Effect of Vibrations on Film Thickness	143
	8.23.1 Film Thickness and λ Ratio	144
8.24	Effect of Vibrations on the Pitting Life	145
	8.24.1 Calculation of Stress required to cause Pitting	146
8.25	Effect of Using Discs with a Rougher Surface	147
8.26	Effect of Using a Vibration Level of $\pm$ 12%	147
8.27	Effect of Changes in the Mean Disc Speed	147
8.28	Effect of Changes in the Slide/Roll Ratio	149
8.29	Summary of Results	149
CHAPTER 9	GENERAL DISCUSSION	152
9.1	Introduction	152
9.2	Mechanism of Scuffing	152
9.3	Main Hypothesis to explain the Effect of a Vibrating Load on the Scuffing Load	152
CHAPTER 10	SURVEY OF PREVIOUS WORK ON THE EQUATIONS FOR SQUEEZE FILMS	154
10.1	Introduction	154
10.2	Reynolds' Assumptions	154
10.3	Evolution of the Analysis	154
10.4	Squeeze Films between Plates	156
10.5	Evolution of Squeeze Film Equations	157
10.6	Reynolds Squeeze Film Equation	157
10.7	Rectangular Plates	158

		Page
10.8	Non-Newtonian Fluids	163
10.9	The Influence of Rough Surfaces and Asperities	168
10.10	Iterative Solutions for the Inertia Forces	172
10.11	One Surface Subjected to Normal Sinusoidal Excitation	173
10.12	Christensen's Work	176
10.13	Experimental Measurements During Transient Loading	180
10.14	Hydraulic Squeeze Film Bearing	182
10.15	Cavitation	183
10.16	Elastic Impact of Cylinders	184
10.17	Total Temperature at Scuffing	185
10.18	Pressure and Deformation Between Normally Approaching Lubricated Cylinders	187
10.19	Scuffing of Circumferentially Ground Discs	188
10.20	Conclusions	189
CHAPTER 11	HYPOTHESIS THAT LOW SCUFFING LOADS WERE ATTRIBUTABLE TO RESONANCE	191
11.1	Introduction	191
11.2	Investigation of the Disc Machine using a Mobility Meter	191
	11.2.1 Test 1	191
	11.2.2 Test 2	191
	11.2.3 Test 3	193
11.3	Discussion of Mobility Meter Results	193
11.4	Examination of the Torque For Disc Resonances	196
11.5	Results from Displaying the Torque on the Oscilloscope	196
11.6	Checking the Flexible Pipes for Hydraulic Resonances	197
11.7	Results from Installing the Pressure Transducer adjacent to the Disc Housing	197
11.8	Discussion	199
11.9	Comparison of the Disc and Applied Load Frequencies	199
11.10	Conclusions	201
CHAPTER 12	HYPOTHESIS THAT CAVITATION WAS CAUSING THE REDUCED SCUFFING LOADS	
12.1	Introduction	202
12.2	Cavitation	202

		Page
12.3	Conclusions	203
CHAPTER 13	HYPOTHESIS THAT SCUFFING OCCURRED AT CONSTANT TOTAL TEMPERATURE	204
13.1	Critical Temperature Hypothesis	204
13.2	Total Temperatures in the Disc Machine	204
13.3	Conclusions	206
CHAPTER 14	HYPOTHESIS THAT SURFACE FATIGUE WAS INDUCING SCUFFING	208
14.1	Introduction	208
14.2	Application of Miner's Law	208
14.3	Conclusions	210
CHAPTER 15	HYPOTHESIS THAT SCUFFING WAS INITIATED BY THE FORMATION OF A TEMPORARY ENTRAPMENT	211
15.1	Introduction	211
15.2	The Pressure and Deformation Profile between Two Cylinders in Normal Approach	211
15.3	Oil Film In a Closing Gap	212
15.4	Elastohydrodynamic Squeeze Film between two Cylinders in Normal Approach	218
15.5	Elastohydrodynamics of Normal Approach	220
15.6	The Pressure and Deformation Profiles between Two Normally Approaching Lubricated Cylinders	221
15.7	Results Produced Using a Composite-Exponential Lubricant	226
15.8	Discussion	229
15.9	Pressure Profile for the Contact	230
15.10	Film Profile for the Contact	230
15.11	Flash Temperature Rise	232
15.12	Conclusions from Lee and Cheng's Work	233
15.13	Coefficient of Friction and Asperity Contact	233
15.14	Disc Surface Temperature	234
15.15	Disc Surface Stress	235
15.16	Mechanism of Scuffing	235
15.17	Conclusions	236
CHAPTER 16	HYPOTHESIS TO ACCOUNT FOR VARIATION OF THE SCUFFING LOAD WITH FREQUENCY	238
16.1	Introduction	238
16.2	Hydraulic Squeeze Bearing	238
16.3	Pressure Distribution in a Plane Fluid Film Subjected to Normal Sinusoidal Excitation	240

		Page
16.4	Discussion	240
16.5	Lubrication of Rough Surfaces	242
16.6	Scuffing Load at Low Frequencies	243
16.7	Experimental Investigations	244
16.8	Conclusions	245
CHAPTER 17	SUMMARY, CONCLUSIONS AND RECOMMENDATIONS FOR FUTURE WORK	246
17.1	Summary	246
17.2	Conclusions	247
17.3	Recommendation for Future Work	249
Appendix 1	Description of the Test Engine for the Investigation of Piston Ring Scuffing	251
1.1	The Petter AV1 Laboratory Engine	251
1.2	Cylinder Liner Modifications	251
1.3	Piston Modifications	252
1.4	Liner Heater	252
1.5	Optical and Recording System	254
1.6	Oil and Water Systems	254
1.7	Engine Instruments	254
Appendix 2	Surface Roughness and Hardness Details of EN 31 Discs	257
Appendix 3	Surface Roughness and Hardness Details of EN 39B Discs	258
Appendix 4	Composition and Qualities of EN 31	259
Appendix 5	Composition and Qualities of EN 39B	260
Appendix 6	Deep Freezing Treatment Procedure for EN 39B Discs	261
Appendix 8	Transition Temperature Measurement for Eng. R.D.2487	263
Appendix 9	Calculation of the Accuracy of the Total Temperatures	265
Appendix 10	Calculation of Central Pressure, Using Lee and Cheng's Results (72), For a Load of 1000 lbf.	266
Appendix 11	Statistical Analysis of Scuffing Loads	267
Appendix 12	Fourier Analysis of the Pressure Waveforms	270
12.2	Fourier Analysis of Pressure Waveforms for Type M Tests	273
12.3	Computer Program for Fourier Analysis of Pressure Waveforms	298
References		303

LIST OF FIGURES

Figure No.	Title	Page No.
2.2a	General View of the Disc Machine	8
2.2b	The Test Discs	8
2.2c	Diagram Showing the Hydrostatic Pockets	10
2.2d	Exploded View of the Disc Driving Arrangement	10
2.2e	The Back Half of the Disc Housing	11
2.2f	Two Discs Mounted On their Spigots	11
5.3	Liner Heater Arrangement	37
5.3.1a	Early Stage of Ring Scuffing	39
5.3.1b	Severe Scuff	39
5.3.1c	Arrangement of Strobe Light and Microscope	40
5.3.1d	Ring Surface viewed directly through the Microscope	40
5.7.1a	Run-in Piston Ring	44
5.7.1b	The Ring after 1 hour's running	44
6.4a	Arrangement used by Bishop and Johnson	60
6.4b	Relative Motion of Gear Masses	63
6.9a	One Cycle of Variation of Gearbox Input Power	71
6.9b	Determination of the Working Curve for the Gear with Zero Vibratory Power	73
6.11	Transmission Error for a Reduction Gear Pair, Ratio 3:1	76
7.2	Diagram of Servovalve and Connections	82
7.3a	Electrical and Hydraulic Circuits associated with the Servovalve	84
7.3b	View of the Rig and Electrical Equiptment	86
7.3c	The Servovalve and Pressure Transducer	86
7.3d	Ancillary Electrical Equiptment	92
7.13	Servovalve Installed on the Disc Housing	95
7.17	Circuit Diagram for Electrical Measurement of Asperity Contact	98
7.18a	Circuit Diagram for Measurement of Electrical Resistance of the Oil Film	100
7.18b	Circuit Diagram for Voltage Discharge Measurement of the Oil Film Thickness	101
7.20	Disc Machine plus Infra-Red Microscope	104
8.3	Results from Type B Tests	108
8.4	Results from Type D Tests	110
8.5	Results from Type E Tests	112
8.6	Results from Type F Tests	114

Figure No.	Title	Page
8.7	Results from Type H Tests	116
8.8	Results from Type I Tests	118
8.9	Results from Type J Tests	120
8.10	Results from Type K Tests	122
8.13	Results from Type M Tests	127
8.15a	Electrical Investigation of Asperity Contact	129
8.15b	Electrical Investigation of Asperity Contact	129
8.15c	Electrical Investigation of Asperity Contact	130
8.15d	Electrical Investigation of Asperity Contact	130
8.15e	Electrical Investigation of Asperity Contact	131
8.15f	Electrical Investigation of Asperity Contact	131
8.18	Disc Surface Temperature and Coefficient of Friction from Test 224	134
8.19	Tabulation of Information from Tests	135
8.20a	Extent of the Reduction in the Scuffing Load at different Oil Film Thicknesses	137
8.21a	Coefficients of Friction for the Eight types of test	138
8.21b	Coefficient of Friction plotted against the load at Scuffing	140
8.22	Mean Disc Surface Temperature for the two Discs plotted against the Scuffing Load	141
8.22.1	Surface Temperature, Friction, Oil Film Thickness and Viscosity for Test 224	142
8.27	Scuffing Load / Sliding Speed	148
8.28	Scuffing Load / Slide to Roll ratio	150
10.6a	Flat Plate approaching a Flat Parallel Surface	159
10.6b	Effect of W or μ on the Sinkage Rate	159
10.7	f(B/L) for Rectangular Plates	161
10.8a	Squeeze Film Pressures For Impact Loading	161
10.8b	Co-ordinates for Inclined Sinkage	167
10.8c	The effect of β on the Sinkage Rate	169
10.9a	Effect of Surface Roughness on the Sinkage Rate	171
10.9b	Effect of Surface Roughness on the Sinkage Rate	171
10.11	Variation of $p_{max}/\mu\omega$ with a/h	175
10.12a	Configuration used by Herrebrugh	179
10.12b	Dimensionless Film Profile	179
11.2.1	Vibration Response of Left Hand Disc	192
11.2.2	Vibration Response of Right Hand Disc to Casing Excitation	194
11.2.3	Vibration Response of Right Hand Disc to Excitation of Left Hand Disc	195

Figure No.	Title	Page No.
11.6	Pressure Transducer Installed next to the Disc Housing	198
13.2	Total Temperature / Load at Scuffing	205
15.3a	Non-Dimensional Load as a Function of Central Film Thickness, h_o	215
15.3b	Film and Pressure Profiles for h_o= 99	217
15.4	Minimum Film Thickness as a Function of Film Thickness Parameter	219
15.6a	Pressure and Deformation Profiles for a "Straight Exponential" Lubricant	222
15.6b	Viscosity as a Function of Pressure for a "Composite Exponential" Lubricant	225
15.7a	Pressure and Deformation Profiles for a "Composite Exponential" Lubricant	227
15.7b	Variation of Load with Center Film Thickness, H_o	228
15.9	Pressure and Deformation Profiles for a "Composite Exponential" Lubricant, p_o=75,000 lbf./in^2 , G =3180	231
16.2	Squeeze Film Forces during a Pressure Cycle calculated from Kauzlarich's results	239
16.3	Squeeze Film Pressures during a Pressure Cycle calculated from Hunt's results	241
1.3	Modified Piston and it's New Ring Pack	253
1.5	General View of the Diesel Engine Rig	253
1.7	Control Panel, T.V. and Video Recorder	256
8	Slow Speed Friction measurement for Disc Machine Oil and EN 31	264
12.1	Mean Failure Loads for each Type of Test / Applied Load Frequency	272
12a	10 Hz. Waveform	274
12b	Fourier Components of 10 Hz. Waveform	275
12c	12½ Hz. Waveform	276
12d	Fourier Components of 12½ Hz. Waveform	277
12e	15 Hz. Waveform	278
12f	Fourier Components of 15 Hz. Waveform	279
12g	20 Hz. Waveform	280
12h	Fourier Components of 20 Hz. Waveform	281
12i	30 Hz. Waveform	282
12j	Fourier Components of 30 Hz. Waveform	283
12k	60 Hz. Waveform	284
12l	Fourier Components of 60 Hz. Waveform	285
12.2a	10 Hz. Waveform	286
12.2b	Fourier Components of 10 Hz. Waveform	287

Figure No.	Title	Page No.
12.2c	12½ Hz. Waveform	288
12.2d	Fourier Components of 12½ Hz. Waveform	289
12.2e	15 Hz. Waveform	290
12.2f	Fourier Components of 15 Hz. Waveform	291
12.2g	20 Hz. Waveform	292
12.2h	Fourier Components of 20 Hz. Waveform	293
12.2i	30 Hz. Waveform	294
12.2j	Fourier Components of 30 Hz. Waveform	295
12.2k	60 Hz. Waveform	296
12.2l	Fourier Components of 60 Hz. Waveform	297

NOMENCLATURE

a	half the amplitude of vibration of a surface (used in the equation $h = h_o + a \sin \omega t$).
A	area of the plate in squeeze film equations.
b	half the Hertzian contact width.
d	total tooth deflection under load.
e	measured error of a pair of gear teeth in contact.
E	modulus of elasticity.
g	gravitational acceleration.
h	film thickness.
h_o	minimum oil film thickness.
H	height of the tooth.
L	length of the contact.
m_1	effective mass acting at pitch line of pinion.
m_2	effective mass acting at pitch line of gear.
n	number of cycles.
N	number of cycles to failure.
p_{max}	Hertzian contact stress.
r_1	radius of tooth or one surface of the contact.
r_2	radius of tooth or other surface of the contact.
R	radius.
R'	reduced radius of contact.
t	temperature ^oC.
t_f	flash temperature rise in the contact.
v	sliding speed.
W	load on the contact.
W_d	dynamic load on gear tooth.

k	thermal diffusivity.
K	thermal conductivity.
α	pressure-viscosity coefficient.
η	viscosity, Poises.
η_o	viscosity of fluid at inlet to the contact.
λ	ratio of theoretical oil film thickness/combined r.m.s. surface roughness.
μ	coefficient of friction.
ρ	specific gravity.
σ	Poisson's ratio.
τ	shear stress.
ω	excitation frequency, Hz.

A waveform which varied between (100 - x)% and (100 + x)% of its mean value was defined as having an amplitude of $\pm$ x%.

British units were used throughout this thesis, unless otherwise specified.

CHAPTER ONE

INTRODUCTION AND OUTLINE OF APPROACH

1.1 INTRODUCTION

To provide the necessary knowledge on all aspects of gear performance a substantial quantity of research has been undertaken. However, the life to failure, from tooth surface damage in a highly stressed gear pair was considerably more variable than could be accounted for by manufacturing tolerances. An analysis of failures in helicopter transmissions revealed that the discrepancies were possibly related to the effect of vibrations occurring in the gears.

Dynamic tooth loads have been investigated theoretically, and papers presented discussing the level of vibrational load in a gear pair. None of the authors though, had examined the effect of applying a controlled vibration to a gear pair.

The intention of this thesis was to apply a fluctuating load, of controlled frequency and amplitude to a pair of simulated gear teeth. This work, the results and analysis are described in Chapters Six to Sixteen. Before commencing the investigation it was considered that in addition to the examination of the previous theoretical studies of the subject, introductory work was essential. The aim of this was to provide a more thorough understanding of the following:-

(a) The conditions occurring in a modern highly stressed gear pair.

(b) The effect of repeated contact and dynamic loads,

and the influence of surface coatings and surface metallurgy on the scuffing resistance of simulated gear teeth.

(c) The criteria affecting scuffing under the conditions of unsteady load, as experienced in an alternative scuffing environment.

All the chapters are now discussed and the evolution of the thesis explained.

1.2 OUTLINE OF CHAPTERS TWO TO SEVENTEEN

A disc-machine is a test apparatus designed to kinematically simulate gear teeth under any desired operating condition. It was intended to use a highly sophisticated version for the majority of the practical work. Chapter Two describes the disc-machine and standard test procedure.

The following chapter relates to the first of the introductory work. Gear teeth in operation suffer a complete stress cycle with each pass through the contact, as a practical introduction into the metallurgical aspects of scuffing under repeated stressing, the influence of the percentage of retained austenite in the surface of the discs was investigated.

Gears made from EN31, EN29B or similar gear steels are prone to premature scuffing during running-in. A new gear pair can sieze and scuff at loads of less than half that at which they will operate continuously when run-in. To protect the gears during this stage of their life a surface coating is sometimes applied. The effect of eight different surface treatments was examined in Chapter Four and helped to provide a practical knowledge about the contribution of

surface chemistry to gear teeth lubrication.

A completely separate occurrence of scuffing under conditions of dynamic load and repeated contact was investigated next, to provide a wider practical knowledge of scuffing causes and situations. The case in particular was that of scuffing between a piston ring and cylinder in a diesel engine. Chapter Five describes work done to enable the progress of ring scuffing in action to be observed and reproduced in a naturally aspirated laboratory diesel engine. The subsequent testing of four basic lubricating oils enabled the ability of the oil additives in preventing scuffing to be examined under realistic operating conditions.

Chapter Six presents a literature survey of previous work on both internally and externally generated vibrations in gear teeth, the theoretical analysis of dynamic loads, and practical findings by other workers.

To enable the disc-machine to be used to simulate gears subjected to an unsteady load it was necessary to modify it. This is described in Chapter Seven. The changes entailed in the standard test procedure are discussed, and ten different types of test, to be used with an oscillating load described.

In the following chapter the results from these tests are tabulated. This is accompanied by a brief analysis of this data. It was essential to have an exact knowledge of the conditions in the contact. This was to ensure that the actual situation existing between the discs was identical with that intended by the author. It was also necessary in order to provide evidence which would lead to the causes of

the results obtained. To these ends extensive investigations were carried out on the disc machine. These included Fourier analyses of the applied pressure waveforms, electrical determination of asperity contact and film thickness, and infra-red measurement of the disc surface temperature.

For an understanding of the theory of squeeze films and impact loaded oil films a second literature survey was conducted in Chapter Ten.

In Chapters Eleven to Sixteen a range of possible failure mechanisms were examined in the light of the disc machine data. It was seen that the test results were possibly caused by the combined interactive effects of more than one mechanism. By calculation it was possible, to a certain extent, to quantify the contribution of each mechanism and thus examine the accuracy of their predicted effects, in relation to the actual figures obtained.

Chapter Seventeen includes a brief summary of the work, detailed conclusions from Chapters Fifteen and Sixteen and gives recommendations for further work.

CHAPTER TWO

THE HYDROSTATIC BEARING DISC MACHINE AND STANDARD TEST PROCEDURE

2.1 INTRODUCTION AND BACKGROUND

In order to investigate scuffing and pitting in gears two basic types of machine were available. A gear machine such as the I.A.E. or FZG (21) gear test apparatus or a disc machine. The degree of repeatability and reproducibility of the I.A.E. machine were investigated under the aegis of the Institute of Petroleum, and the results produced as reference 22. These results, coupled with experience by Macpherson (3) indicated that a gear machine would not be very suitable for the work, as the load carrying capacity of some of the lubricants to be studied was above a realistic limit, imposed by tooth deflections for the machine. This was because the conditions to be investigated were very highly stressed gear teeth operating with an oil containing extreme pressure additives.

Macpherson (3) thus decided to build a disc machine. The concept of using discs, which are kinematically equivalent to gears has a long history.

The main advantage lies with the ability to select an appropriate slide/roll ratio, speed, oil temperature and contact stress to simulate any given point on a gear tooth under chosen operating conditions. Further, the cost and problems associated with producing a small quantity of precision gears are eliminated.

One such arrangement of discs was used in a machine designed by Kelley and Benedict of Caterpillar Tractor (23). However this relied upon a mechanical loading of the one disc against the other, which meant that it was not possible to ensure even loading across the track width. By 1971 the hydrostatic bearing machine hereafter referred to as a disc-machine, had been developed (24). This used self aligning hydrostatic bearings, thus maintaining full contact across the tracks of the discs, and resulting in a high capacity laboratory-type machine. The first machine to this design was used in the Mobil Oil Company Laboratories, and it was this type of machine which was selected as being suitable for the work envisaged.

2.2 DESCRIPTION OF THE TEST MACHINE

A full description of the test machine can be found in reference 3. For convenience, a brief description is included here.

A general view of the machine is shown in Figure 2.2a. Figure 2.2b shows a photograph of the two rings, referred to as discs, which are the test members. These are 3.26" outside diameter, 1.0" axial width and have a wall thickness of 0.375". As can be seen the one disc is lightly chamfered at 4^{o} to provide a o.25" wide track. The intention being to provide physical support to the track and reduce the influence of edge effects. An examination of the discs used shows that scuffing can occur anywhere across the track.

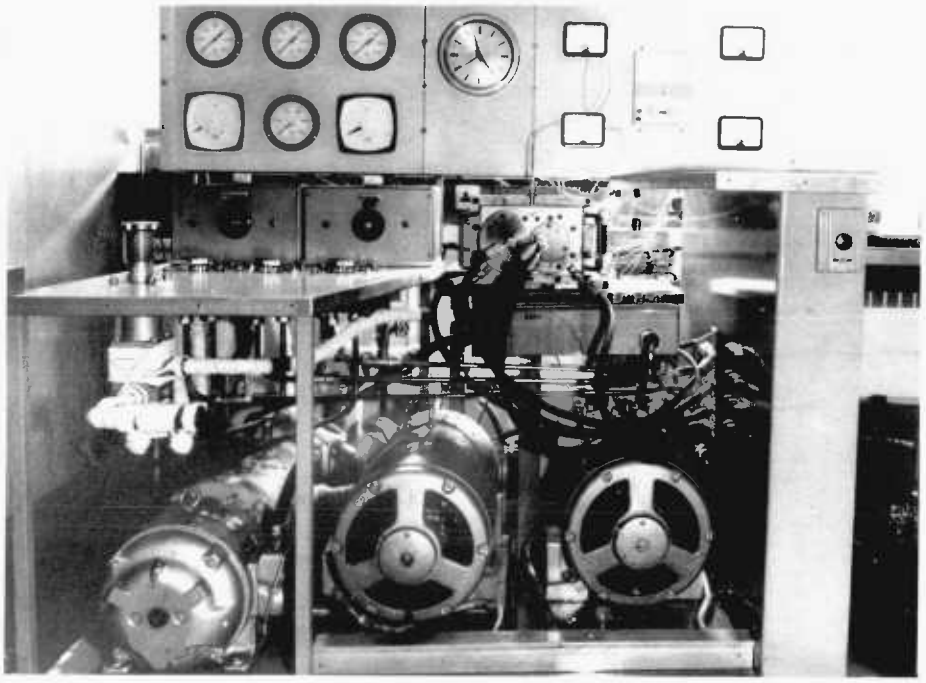


Figure 2.2a. General View of the Disc Machine.



Figure 2.2b. The Test Discs.

The discs are arranged as shown in Figure 2.2c each forming the outer rotating member of a hydrostatic bearing. They are loaded against each other by the 3 high pressure oil pockets, which form a stable self-aligning arrangement, thus ensuring even loading across the track. The discs are driven through shear pins from drive rings, which are in turn rotated by driving blades centrally clamped onto the input shafts. This arrangement forms an Oldham coupling which allows for any misalignment. An exploded view of the hydrostatic bearing and disc driving arrangement is shown in Figure 2.2d. A view of the disc assemblies and inside of the hinged door is shown in Figures 2.2e and 2.2f. Strain gauges are glued to the driving blades, and their leads taken out down the input shafts to slip ring assemblies, and thus form a pair of strain gauge bridges, the leads from which are connected to the pen recorder, providing a permanent record of the torque traces for the right and left hand discs.

The discs are driven and braked by a pair of "Dynadrive" units, which are squirrel cage motors matched to electromagnetic coupling units. Control of the "Dynadrive" units to enable constant speeds to be maintained, independent of torque, was achieved by electronic feedback control circuits. This has been highly satisfactory in practice and during prolonged pitting tests only very infrequent adjustments to the speed settings have proved necessary. Timing belts were used to drive the shafts for the discs.

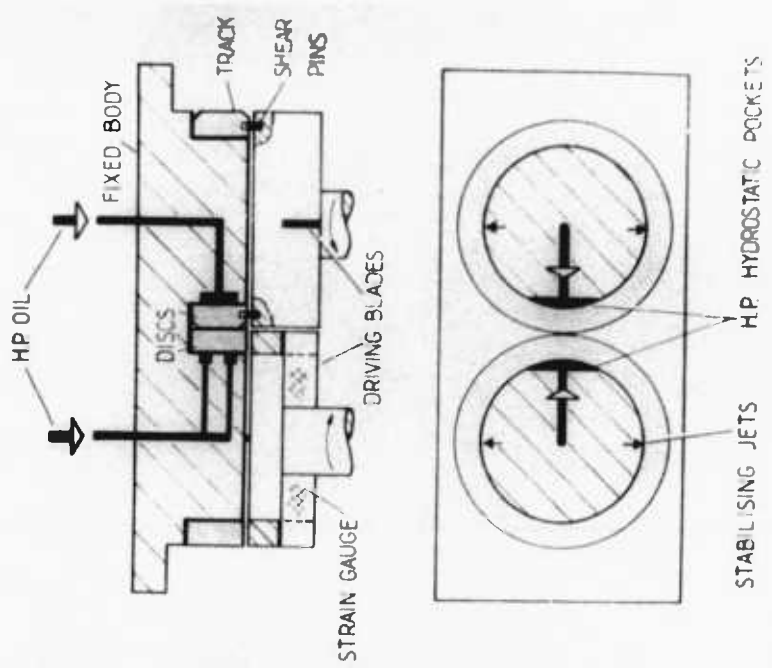


Figure 2.2c. Diagram showing the Hydrostatic Pockets.

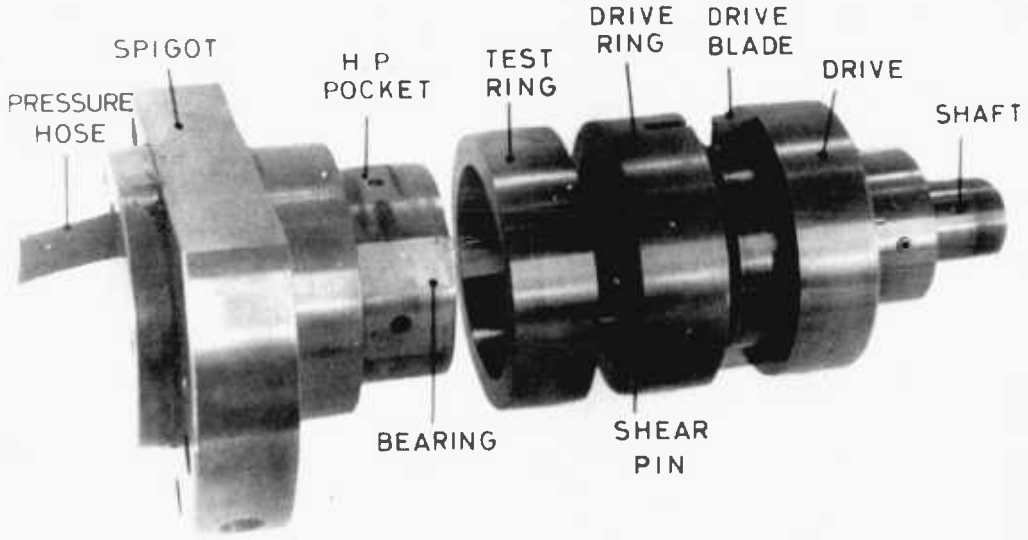


Figure 2.2d. Exploded View of the Disc Driving Arrangement.

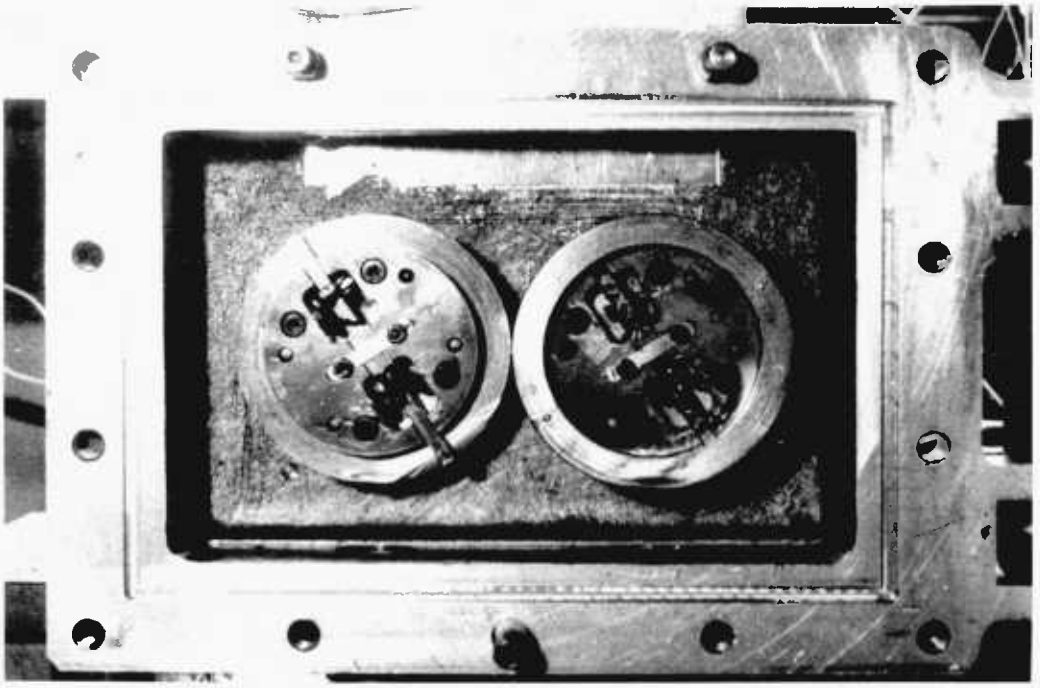


Figure 2.2e. The Back half of the Disc Housing.

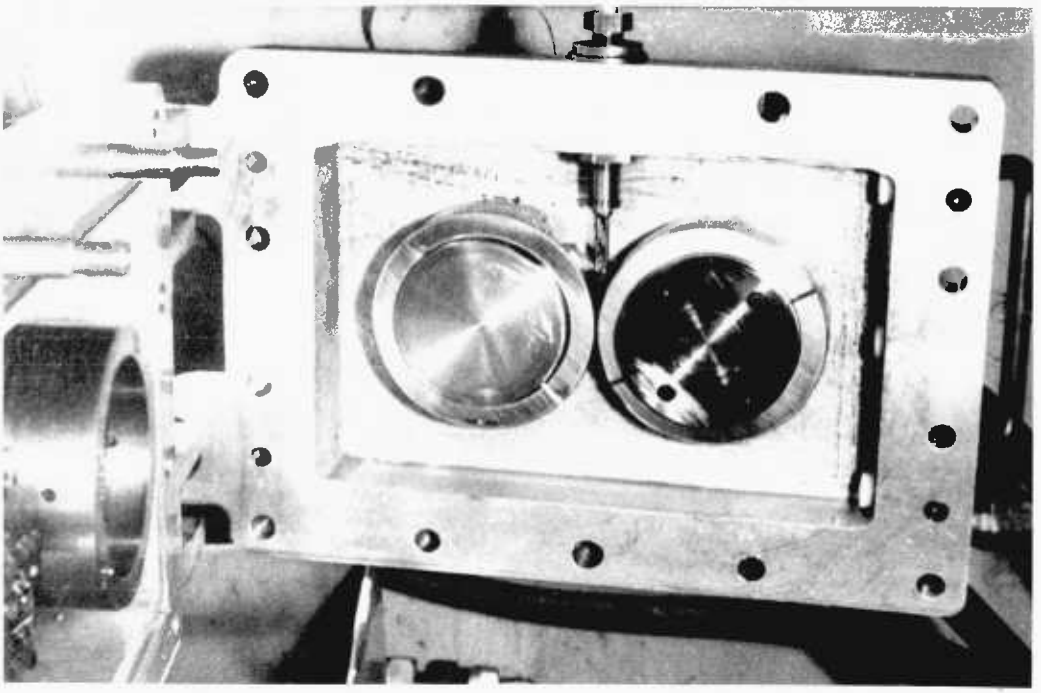


Figure 2.2f. Two Discs Mounted on their Spigots.

The remainder of the apparatus consisted of electronic monitoring equipment, plus a high pressure oil pump, filter and control valves, adjustable orifices, two water cooled oil coolers, a 3 KW oil heater, header tank and associated pipework, an electrical distribution board, low voltage supply, voltmeters and ammeters.

The surface temperature of the discs was measured by means of two trailing thermocouples, see Figure 2.2f.

2.2.1 Instrumentation

This comprised the following:-

A two channel pen recorder providing a continuous trace of the torque from the left and right hand disc.

A multi-channel electronic thermometer, so that the temperature of the oil at positions of interest around the circuit and the disc surface temperature could be monitored.

Two tachometers for the disc speeds.

Three pressure gauges to give the supply pressure to the oil pockets.

A millivoltmeter to zero the strain gauge bridges and check the readings of the pen recorder.

2.3 DISCUSSION OF THE OPERATION OF THE DISC MACHINE

Macpherson (3) after building the test machine, calibrated the load on the discs and found that it agreed well with the calculated figure in that each lbf/in^2 supplied to the high pressure pockets produced 1 lbf. load

between the discs with an overall accuracy of $\pm$ 2%.

The strain gauge bridges were calibrated by using a load arm and dead weights. This has been repeated recently and the figures found to be unchanged.

Initially it was found that at oil temperatures over 60 to 70°C the amount of oil escaping from the hydrostatic bearings prevented operation at high pressures with the ordinary high pressure oil pump. However the introduction of a loose plunger, accommodating the pressure pocket, into the spigot for the left-hand disc eliminated this problem. The plunger was arranged to follow the movement of the bore of the left-hand disc, by providing a 0.5% bias, towards the discs across the plunger. Hence the clearance was controlled and the oil pump was now capable of maintaining a pressure of 2,500 lbf/in^2. even when the oil temperature was 80°C.

The discs are relatively cheap, being produced from the forgings intended as inner races for ball bearings. However owing to inflation a new disc machine is being developed by Macpherson which will use much smaller cylinders.

The speed of the shafts is checked occasionally using a hand-held stroboscope, though this is generally unnecessary owing to the satisfactory characteristics of the "Dynadrive" system, with its electronic feedback system.

The use of trailing thermocouples to obtain the disc surface temperature leads to the results being somewhat dependant upon the particular operator. A high load

on the thermocouple leading to temperature rises through frictional heating. Vice-versa, insufficient pressure merely results in the temperature of the oil near the surface being measured. To overcome this problem, a few millivolts were applied between the thermocouple and the disc. When a current flowed the thermocouple was rubbing on the disc surface, and so it could be screwed back slightly to obtain a true reading.

2.4 EXPLANATION OF THE STANDARD TEST PROCEDURE

2.4.1 Simulation of Gears

An investigation programme, including infra-red work, was being carried out on a helicopter tail rotor gearbox in another part of the Lubrication Laboratory. Accordingly the conditions chosen were those occurring in this gear pair, at the point on the teeth which is most prone to scuffing. This is known as the standard test condition, which entailed having the discs rotating at 1100 r.p.m. and 500 r.p.m., with an oil inlet temperature of 50^{o}C.

Most of the tests were conducted following this standard test procedure and a full description is given here. However, later tests were conducted with altered conditions and these will be discussed briefly after the standard test description.

2.4.2 Description of Setting-up and Running a Standard Test

Two discs, one plain and one chamfered, were cleaned. They are normally covered with a protective layer

which is removed using toluene, which also acts as a good general purpose solvent, and then dried using paper tissue.

The rings were mounted on their spigots (see Figures 2.2e and 2.2f) and the hinged door closed, thus connecting with their drive rings. Using the milli-voltmeter, the strain gauge bridges for the left and right-hand torque measurement were zeroed. The pen recorder traces of the output from the strain gauge bridges were also zeroed. The lateral scale for the chart was 1 mV/in., and the paper was run at 6 cm/hr. As the test was to be run at 50°C oil inlet temperature, the oil pump (with the pressure relief valve set at 0 lbf/in^2.) and heater were switched on. The oil used was to Specification ENG. R.D. 2487, which is a synthetic, 7½ centi-stoke (at 210°F), ester based oil containing an anti-oxidant, which also serves as a mild extreme-pressure additive.

The "Dynadrive" motors were started and the discs counter-rotated at 500 r.p.m. under low load until the oil temperature reached 50°C. Standard test speeds were 1100 r.p.m. and 500 r.p.m. so the left and right hand discs were then adjusted to these speeds.

Over a period of 5 minutes load was gradually applied between the discs by rotating the control on the oil pressure relief valve, to bring the pressure up to 400 lbf/in^2., which constituted the first load stage. The oil heater was switched off and the pair of water cooled oil coolers used from this point onwards to main-

tain an inlet oil temperature of 50 $\pm$ 1°C.

The rig was run under these conditions for 5 minutes. Readings were then taken of the right and left hand torque figures, and the two-disc surface temperatures. Over the next minute the load between the discs was raised to 500 lbf. and held there for four minites. Readings were taken and the process repeated at 600 lbf., and so on, raising the load by 100 lbf. every 5 minutes.

This was continued until the torque trace suddenly started to rise in a "run-away" condition, indicating that the discs were scuffing. The stop button was pressed which switched off the drive and brake units, plus the oil pump. This prevented further damage to the discs, as owing to the low inertia of the system they stopped within a couple of revolutions. If the test was not terminated, scuffing would continue, with a consequent rise in torque until the shear pins failed.

The discs were then removed for examination, the surfaces initially being viewed under a low power (x 90) stereo microscope. Before the next test the discs were labelled, coated in protective lanolin and stored for future reference.

2.5 VARIATIONS ON THE STANDARD TEST

In Chapters Three and Four two other types of test were used, and differed from the standard test as follows.

2.5.1 Fatigue Test

This was conducted as the standard test but the

load was held steady after it reached 800 lbf. and the torque trace was watched for signs of pitting. Occasionally the output from the trailing thermocouple was applied to the chart recorder, any increase or instability indicating that conditions in the contact had deteriorated. The discs could easily be removed at intervals for examination under the stereo microscope. This was necessary as occasionally the formation of pits would not be reflected in a change in the torque trace.

2.5.2 Type A test

Type A test was exactly the same as the standard test but the oil inlet temperature was controlled to 80 $\pm$ 2°C. To achieve this extra lagging had to be applied to the oil pump, pipes and header tank.

CHAPTER THREE

THE INFLUENCE OF RETAINED AUSTENITE ON GEAR TEETH SCUFFING

3.1 INTRODUCTION

It is believed that the percentage of retained austenite in gear-tooth steel has an effect on the scuffing resistance of the gears, in that the lower the level of retained austenite, the greater the scuffing resistance. However, owing to the limited and conflicting nature of the literature available on this matter it was decided to conduct a series of tests to help to clarify the point.

3.2 RETAINED AUSTENITE, ADVANTAGE OR DISADVANTAGE?

It is common practice in America and Great Britain to apply a sub-zero temperature treatment to gears intended for highly-stressed usage, thus reducing the amount of retained austenite in the surface. However, the French are opposed to this on the grounds that the process lowers the fatigue endurance stress level of the parent metal in reverse bending, and would accordingly affect rolling fatigue in a similar manner. Possibly this would result from the fact that the transformation to martensite while undergoing fatigue stressing could set up large localised stresses as a result of austenite/martensite reaction, and these would initiate cracks.

3.2.1 Literature Review

A literature survey reveals that not much information is available on this matter, and that it is conflicting in its conclusions.

There is complete agreement on the fact that it is essential to minimise the amount of retained austenite in precision bearing applications for reasons of volumetric stability. Transformations of austenite will arise during the course of bearing operation and these would bring about changes in metal volume and introduce out of balance forces. On all other factors the influence of austenite is a matter of controversy.

Popov and Brykov (25) found that an increase of 1% in the retained austenite in a 15% Cr, 0.6% Ni, 3.16% C steel decreased the resistance to wear by 1.2%. Balter and Turovakii (26) advocated an unspecified amount of austenite to be retained to maximise resistance to pitting. Nieman and Lechnev (27) showed that resistance to scuffing is inversely related to the percentage of retained austenite. However, as they tested a variety of different steels to obtain their range of austenite content, and the composition of their steels varied widely in nickel content (from 0 to 20%), their results appear to be of little value.

The main worthwhile work known to the author, which has been carried out in connection with scuffing was reported by Grew (28). He showed that the temperature of desorption of chemicals on to the metal surface is lowered slightly as the amount of retained austenite is

increased and concludes from this that the resistance to scuffing varies inversely with austenite content. The austenite is non-reactive, hence the extreme-pressure additive cannot react. This conclusion is nevertheless open to question. It can logically be argued that in a gearing application the lower the temperature at which desorption arises the better for then more protection can be derived hydrodynamically as the viscosity is higher. Recently Matveevsky et al (29) showed that the percentage of retained austenite appeared to have but a small influence on the scuffing resistance. They concluded that the composition of the steel had far greater effect.

Consequently a series of 23 tests were planned to determine the ranking order for combinations of steels in an endeavour to ascertain the influence of retained austenite on scuffing.

3.3 SCUFFING TESTS ON THE DISC-MACHINE

The test discs were either EN 31 untreated, EN 39B which had undergone a sub-zero treatment to reduce the austenite content, or EN 39B untreated. (See Appendices (2) and (3) for details of the Surface Hardness and Roughness, Appendices (4) and (5) give details of the composition, qualities and uses for steels). These were run in pairs covering all the combinations possible.

The oil used was to specification ENG. R.D. 2487, at an inlet temperature of 50^{o}C, and the disc speeds were 1,100 r.p.m. and 500 r.p.m. respectively.

3.4 RESULTS AND TORQUE TRACES

Disc Material. For convenience the following code was introduced.

		% retained austenite
A	Untreated EN 31	20%
B	Sub-zero treated EN 39B	15%
C	Untreated EN 39B	35%

Table 3.4

Results from Tests Investigating Retained Austenite

Material Disc 1	Material Disc 2	No. of Tests	Mean Failure Load (lbs.)	Range of Results	Comparison with EN 31/EN 31
A	A	2	1300	1300-1300	100%
B	B	4	875	700-1000	67%
C	C	4	1200	1000-1400	92%
A	B	2	1050	1000-1100	81%
B	A	4	1075	900-1300	83%
A	C	2	650	600-700	50%
C	A	3	800	700-900	62%
B	C	2	750	600-900	58%
C	B	2	750	700-800	58%

Oil:- to specification ENG. R.D. 2487.

Inlet temperature 50°C.

Disc speeds:- N_1 = 1100 r.p.m. N_2 = 500 r.p.m.

3.5 DISCUSSION

The only difference between the deep-frozen EN 39B and the untreated EN 39B was that the former had a lower percentage of retained austenite and this was demonstrated in that it had a Vickers Hardness Number which was 50 higher (i.e. 850 as opposed to 800). The only relevant

difference bwtween EN 31 and EN 39B was thought to be the nickel content which was nil for the former and approximately 4% for the latter. Nickel is relatively non-reactive.

Specimens from the metals were ground, etched and examined under a microscope to measure the austenite content. It was estimated as being A - 20%, B - 15%, and C - 35%. The above mentioned case hardness difference of 50 V.H.N. between B and C tended to substantiate this. However it was seen from the above results that there was actually an appreciable difference between the performance of the various steels.

When running similar pairs together the ranking order was expected to be A, B, C. Surprisingly B came out considerably worse than C. A total of 4 tests for each of these pairs was run, and though the scatter was greater than had previously been experienced with EN 31 the extra tests confirmed the above result. The higher speed disc runs hotter than the low speed disc, and the time out of contact is shorter, but still 0.05 sec. More chemical reaction would be expected to occur on the faster moving surface. Thus, by interchanging the disc materials, improved performance would possibly, but by no means certainly be obtained when the higher speed disc was made of the more reactive material. By running both forms of EN 39B with EN 31 it was hoped to establish a clue which would lead to an explanation as to why the B-B combination was so very much inferior to C-C.

At first sight it might appear reasonable to suppose that the index (comparison with EN 31/EN 31) ob-

tained by running dissimilar discs together would bear a relationship to the indices for running each against its own partner. For example the index for A-A is 100%, and that for B-B is 67%, hence an A-B or B-A combination would on this basis, have an index of $\frac{1}{2}(100 + 67) = 83\%$. This did in fact happen.

However with an A-C combination an index of 50% was obtained as opposed to the calculated value of 96%. Similarly with the B-C or C-B combination the result was worse than expected. No firm reason for this discrepancy has been established. In both the A and B, and A and C combinations it can be seen that they came out slightly better when the EN 31 was allocated as the low speed disc. With B and C discs it appeared immaterial which disc was the low-speed one.

It is interesting to observe that the C-C pair performed better than the B-B pair, but when only one of the above was used in conjunction with an EN 31 disc the order of performance was reversed.

When running EN 31 discs together the torque traces reveal a feature which was pointed out by Macpherson (3). An increase in applied load results in an instantaneous increase in transmitted torque. During the 5 minute running stage at constant load, the torque falls more than can be explained by the combined effects of an improvement in surface finish brought by running-in, from about 10μ ins. before the tests to 4μ ins. C.L.A., and a reduction in surface temperature. It is possible that some form of chemical film being formed on the surface

is responsible for the reduction in torque. After a test had been run there was frequently a very thin brownish layer on and just adjacent to the track which could be wiped off. Furthermore if this was done half way through a test the torque readings would be slightly higher for a while when restarting the test. An attempt was made to have this film analysed, but it was not possible to collect sufficient quantity. At the stage in which scuffing arises a much smaller drop in torque was always recorded. It was thought that a study of the torque traces might provide an indication of the relative reactivity of the surfaces.

It was noted that with the C-C combination the reduction in torque in all stages was very little. This also applied to the B-B combination, except for one stage in the middle where the torque reduction was similar to that experienced with an A-A combination. The only conclusion to be drawn from these observations was that EN 31 was more reactive than EN 39B. This was expected on account of there being no nickel in EN 31.

A considerable amount of effort was expended in an attempt to derive some form of pattern from the above results and the torque traces. This was unsuccessful.

3.6 CONCLUSIONS, EFFECT OF SUB-ZERO TREATMENT ON EN 39B

It can be concluded that when a pair of gears are both produced from EN 39B it is beneficial not to treat them at sub-zero temperatures. But, if the second gear is say EN 31, then a slight advantage appears to be gained from the reduction of austenite by a sub-zero treatment. The spread

of the results suggest that a fuller examination is required.

3.7 PITTING OF EN 31, EN 39B (Treated and Untreated)

To provide a possible further insight into the effect of reducing the austenite content of EN 39B it was decided to run a series of 5 tests at a constant load of 800 lbs. to obtain an idea of the hours to pitting for the steels. (Sometimes known as the "Fatigue Scuffing" life, when run at such a high load relative to the instantaneous scuffing load).

3.7.1 Tests and Results from Disc-Machine

The five tests were run as shown in the results below.

Table 3.7.1

"Fatigue Scuffing" Test Results

Disc 1	Disc 2	Hours to Failure
A	A	13
B	B	25
C	C	48
B	A	26
C	A	51

Oil to ENG. R.D. 2487. Inlet Temp 50°C.

N1 = 1100 r.p.m. N2 = 500 r.p.m.

A - EN 31 Untreated.

B - EN 39B Sub-zero treated.

C - EN 39B Untreated.

3.8 DISCUSSION OF PITTING TESTS

With EN 31 a clear indication of the onset of pitting was indicated on the torque trace. As shown by

Macpherson (3) this could be regarded as fairly reliable. However, no such obvious indication arose with the EN 39B steels, or combination of them with EN 31. Thus it was necessary to inspect the discs under a stereo microscope at regular intervals for pits. The tests were terminated when the surface damage was considered to be comparable with that for EN 31. The results in Table 3.7.1 should be regarded as indicating no more than a trend as only a single test was made for each steel combination.

3.8.1 Conclusions and Disappointment in Sub-Zero Treatment

However, despite the above, it is possible to deduce the following:-

(a) EN 39B in both forms is more resistant to pitting under traction and sliding than EN 31.

(b) The untreated EN 39B was superior to the sub-zero treated EN 39B with regards to pitting both when running on its own, and when in combination with EN 31.

More work is required in this field and a new disc-machine, specifically designed for pitting, has just been completed in the Lubrication Laboratory at Imperial College.

3.9 PERFORMANCE OF USED OIL

In general all tests on the disc-machine are carried out with virtually unused oil. It was thought that possibly the effectiveness of the oil, and especially the action of the additives, might decrease in use. So

a representative series of 4 tests were run with oil to specification ENG. R.D. 2487 which had been removed from a Westland Wessex main gearbox after 600 hours flying time with the Royal Navy. At 50°C and 80°C two tests were run at the standard slide roll ratio (disc speeds 1100 r.p.m. and 500 r.p.m.). The failure loads and torque traces were found to be identical with those for a new oil, and thus it appears that there is no deterioration of the oil with use.

CHAPTER FOUR

INFLUENCE OF SURFACE COATINGS ON GEAR SCUFFING

4.1 INTRODUCTION AND REASONS FOR SURFACE COATINGS

The disc-machine described in Chapter 2 was used to examine the effect of eight different surface treatments on the scuffing resistance of gears operating under highly stressed conditions. In all cases the coatings were applied to discs of EN 31 steel. (See Appendix (2) for surface roughness and hardness details. Also Appendix (4) for composition). EN 31 was chosen as it is a widely-used gear steel. It has been common practice to apply a surface treatment to gear teeth operating under highly stressed conditions such as found in the aviation industry.

These treatments were intended as an aid to running-in. However most of them were developed before the introduction and widespread use of synthetic oils using an extreme pressure additive. Accordingly it was thought possible that some of the treatments were uncompatible with ester-based oils.

It has been demonstrated by Whyte (30) when working on damage arising in automobile rear axles in 1966 that there was a temperature range over which the gears were unable to carry a high load without wearing. This was considered to occur because at low temperatures the oil viscosity was sufficient to provide a satisfactory

film between the gear teeth and also the oiliness additive was not desorbed. At high temperatures the action of the extreme pressure agent prevented the gears from scuffing.

Macpherson (3) in investigating this phenomenon referred to it as the "surface temperature distress gap". He carried out tests on the disc-machine using a Mobil oil. This was a standard 7½ centi-stoke di-ester oil to specification ENG. R.D. 2487 with an added phosphor extreme-pressure additive. He showed that the scuffing capacity was average at 50°C, and quite high at an inlet temperature of 80°C. It fell as the temperature was increased beyond 50°C and was very poor at an inlet temperature of 70°C, though the film thickness at 70°C was reasonably large. Further experience at Westland Helicopters in testing helicopter spiral-bevel gear pairs in a "back-to-back" rig demonstrated this point. It was thought that the use of a suitable surface coating might help to overcome this "surface temperature distress gap", especially during running-in.

4.2 SURFACE COATINGS FOR TESTING

Coatings were selected on three bases:-

(1) because they were already in common usage, such as black oxide, molybdenum di-sulphide and Parco Lubrite.

(2) They had performed well in other applications, such as zinc and lead phosphate, or

(3) because they were a new treatment, for example Sulf. B.T.

4.2.1 Description of Surface Coatings

The surface coatings tested were:-

Black Oxide.

M_oS_2 commercially bonded to the surface.

M_oS_2 sputtered on the surface.

Parco-Lubrite commercially applied to the surface.

Zinc Phosphate.

Lead Phosphate.

Parco-Lubrite applied to the surface by GKN using a new very rapid process.

Sulf. B.T., an experimental coating produced by I.C.I., and similar to Parco-Lubrite, but using a sulphur base.

4.3 TESTING ON THE DISC-MACHINE

A series of 18 tests were run on the disc machine to evaluate the coatings when operating with an ester-based oil, containing a mild extreme-pressure additive, to specification ENG. R.D. 2487, at an inlet temperature of 50°C, and with disc speeds of 1100 and 500 r.p.m.

As the repeatability of the disc machine had been checked by Macpherson (3) and found to be acceptable, it was decided to limit the tests to two of each surface coating.

4.4 RESULTS AND TORQUE TRACES

Table 4.4

Results of Tests on Discs with Treated Surfaces

Surface Treatment	Failure Load lbs. Test 1	Failure Load lbs. Test 2	Average Failure Load lbs.	Comparison with untreated EN 31
Plain	1300	1300	1300	100%
Black Oxide	900	900	900	69%
M_oS_2 bonded	1100	1200	1150	88%
M_oS_2 sputtered	1100	1500	1300	100%
Parco-Lubrite	1600	1700	1650	127%
Zinc Phosphate	600	900	750	58%
Lead Phosphate	1100	1500	1300	100%
Parco-Lubrite, GKN	1900	2100	2000	154%
Sulf. B.T., I.C.I.	2000	2100	2050	158%

Disc Material: EN 31. Disc speeds: N_1 = 1100 r.p.m. N_2 = 500 r.p.m.

Slide/Roll Ratio: 0.375. Oil Inlet Temperature 50°C.

Oil: Castrol to specification ENG. R.D. 2487.

4.5 DISCUSSION AND REASONS FOR APPARENT DISADVANTAGEOUS TREATMENTS

It can thus be seen that Black Oxide and Molybdenum Disulphide which are standard industrial treatments, along with Zinc Phosphate all fared worse than the bare EN 31. However when performing the tests it was observed that all the coated discs were much less prone to premature scuffing at loads of 400 to 500 lbf., which occasionally occurs with standard discs, and that the torque trace was also smoother. This is important for it meant that less care had to be exercised during the early stages of a test.

At this stage it is necessary to speculate on the reason why most of the coatings resulted in no improvement over bare metal, and the three already mentioned gave worse results. The presence of the coatings was probably interfering with the normal mechanisms of lubrication in that they were preventing the surfactant molecules from attaching themselves to the metal surfaces. These organic polar compounds would have adsorbed on the surface and provided better lubrication than the applied coatings, in the cases where the load carrying capacity was less than 100%. Where the load capacity was substantially unaltered it was assumed that the coating had been worn off. Visual inspection did not help here for all coatings, including those with the highest index, appeared to have been removed when inspected at the end of a test.

In the case of the two Parco-Lubrite and the Sulf. B.T. coatings it was assumed that the phosphorus and sulphur protecting molecules had penetrated into the

surface to provide long-term protection. The Parco-Lubrite applied by GKN's new process produced better results than that applied by the normal method. The new process is considerably quicker and produces a different grain structure. It was included to ensure that its lubricating qualities were equal to those obtained with the old method.

It was expected that the Sulf. B.T. would rank well because the coating is rather similar to the well proven Sulfinuz one, but has an advantage that the process is carried out at a much lower temperature. Unfortunately this exceeds the limiting one of S. 82 steels, and this probably eliminates it for current gearing work such as found in helicopters.

4.6 CONCLUSIONS AND RECOMMENDATIONS

It would appear that the use of Black Oxide and Molybdenum Di-sulphide for gear teeth treatments should be discontinued in favour of Parco-Lubrite, the use of which will enable the "surface temperature distress gap" to be overcome, provided it does not then interfere with the reactions of the extreme-pressure additive. However it is clear that much more should be done to investigate surface coatings when used in combination with modern synthetic oils. Further research would include detailed chemical analysis of the surface films.

CHAPTER FIVE

THE INFLUENCE OF LUBRICANT ADDITIVES ON PISTON-RING SCUFFING

5.1 SYNOPSIS

A field in which a great deal of work has been carried out with regard to scuffing, under conditions of an oscillating load and continuously varying sliding speed, is that of diesel engine piston-ring scuffing. However the exact influence of the additives in preventing a scuff has not been evaluated under running conditions.

It was decided to design a realistic test routine and thus evaluate the influence of diesel engine anti-scuffing lubricants in an actual diesel engine. The basic problem in investigating scuffing in an operating engine is that it needs to be stripped after every test to examine the state of the piston ring and liner. This is time consuming and unsatisfactory as the point at which a ring began to scuff during test is undeterminable merely from post-test examination. Furthermore scuffing failures unless severe can heal themselves, and thus for useful results an examination of the piston-ring whilst in operation is essential.

This chapter discusses work done at Imperial College by M.W. Bailey, T.J. Crooks and the author to enable the progress of ring scuffing in action to be observed and reproduced in a naturally aspirated Petter AV1 laboratory diesel engine.

Four lubricants were then evaluated in terms of

their ability to prevent scuffing under conditions of increasing operating severity.

5.2 INTRODUCTION AND HISTORY

Piston ring scuffing has been a recurring problem since the 1930's. Its increasing occurrence during the 1960's caused many manufacturers to make alterations to their surface finishing methods, piston ring design and materials, and in some cases modifying the engine block design. In 1969 Neal (31) surveyed the situation and found that scuffing was encountered mainly during running-in and was due to the interaction of many variables. However experience by users and manufacturers has resulted in some agreement over the combinations of surface finish, materials, coatings, etc. Consequently it was thought justifiable, as interest was focussed on the influence of additives, to limit tests to one set-up, i.e. a chromium-plated piston ring with a honed cast-iron bore of standard surface finish.

Though engine oils contain additives to improve the following:- anti-corrosion, detergency, disperency, anti-wear, anti-oxidation, Viscosity Index improvers, and extreme pressure additives, the ones with the greatest influence on scuffing are the extreme-pressure and detergent additives.

Testing of lubricants in simulated piston-ring/liner rigs is useful in providing background work, and for screening purposes. The final testing of oils for scuffing resistance must still be done in an engine.

5.3 MODIFICATION OF A PETTER AV1 LAB ENGINE TO ENABLE SCUFFING TO BE OBSERVED

In 1969 it was shown, in a paper to the S.A.E. (32) that scuffing could be initiated in the Petter AV1 engine by heating part of the liner to temperatures over 300°C. This had been suspected as previous experience had shown that when engines with "siamesed" bores scuffed, the scuffed area was generally on the hotter portion of the bore.

It was thus decided to use heating of the cylinder bore to produce scuffing. One critical problem that had to be overcome was that of obtaining conditions severe enough to promote ring scuffing while avoiding large scale seizure of the whole of the piston. A system was evolved whereby a narrow vertical strip of liner was heated using a low voltage, high current electric element clamped to the outside of the liner, inside, but shielded from the water jacket. This enabled bore temperatures of over 400°C to be achieved. These temperatures were measured with a thermocouple placed just below the liner surface, in the region of the heating element. Figure (5.3) shows the arrangement.

5.3.1 Identification of Scuffing

Returning to the problem of identifying when the piston-ring scuffs, radioactive rings have been used to enable their wear to be monitored by counting the radioactive debris in the oil. A sudden increase in this indicating that the wear rate had increased. However this need not necessarily be due to scuffing, and there

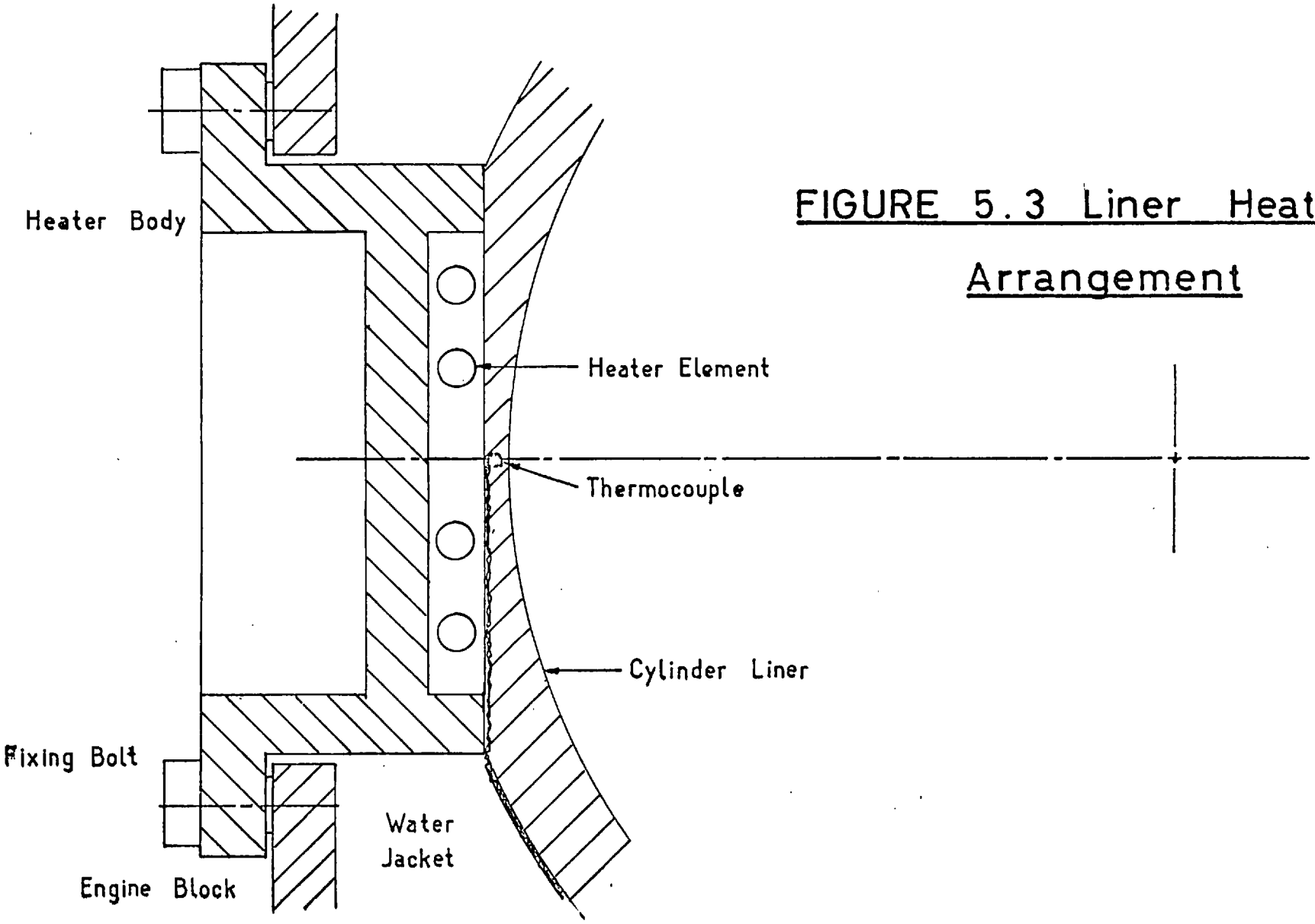


FIGURE 5.3 Liner Heater Arrangement

is an inevitable delay of about 4 minutes between the wear taking place and its detection by the monitoring equipment.

In 1963 Bäumler (33) reported a method of observing a ring whilst in a running engine. He found that by drilling a small hole through the liner and illuminating the reciprocating piston with a stroboscope, the state of the ring surface could be seen. Scuffing can thus be detected, as the surface finish of the ring deteriorates rapidly when scuffing, and this deterioration can be seen to spread across the ring surface (see Figures 5.31a and 5.31b).

A closed-circuit television camera, in conjunction with a microscope and video-tape recorder were used to monitor the ring surface and permit a record of the test runs to be produced (see Figure 5.31c). The use of closed circuit television led to a slight loss of definition compared with cinematography, but in fact definition was found to be acceptable. Figure 5.31d is a view through the microscope of the ring surface shown on the television screen in Figure 5.31a. Illumination was provided by a stroboscope triggered from a photo-electric pick-up working off the end of the camshaft. This enabled the piston-ring to be viewed at the end of the induction stroke as opposed to the firing stroke, when blow-by gases tended to obscure the picture. The problem of oil mist and spray obscuring the picture was overcome by the use of air jets in front of the lens of the microscope. The observation hole was naturally positioned on the same side of the liner as the heater.

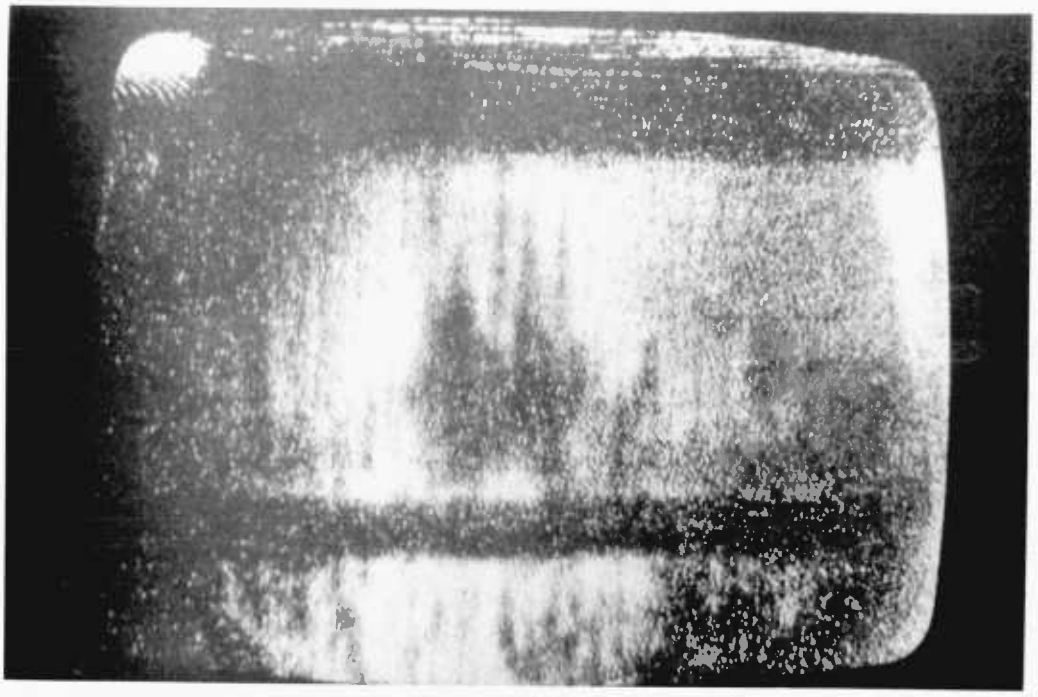


Figure 5.3.1a. Early Stage of Ring Scuffing.

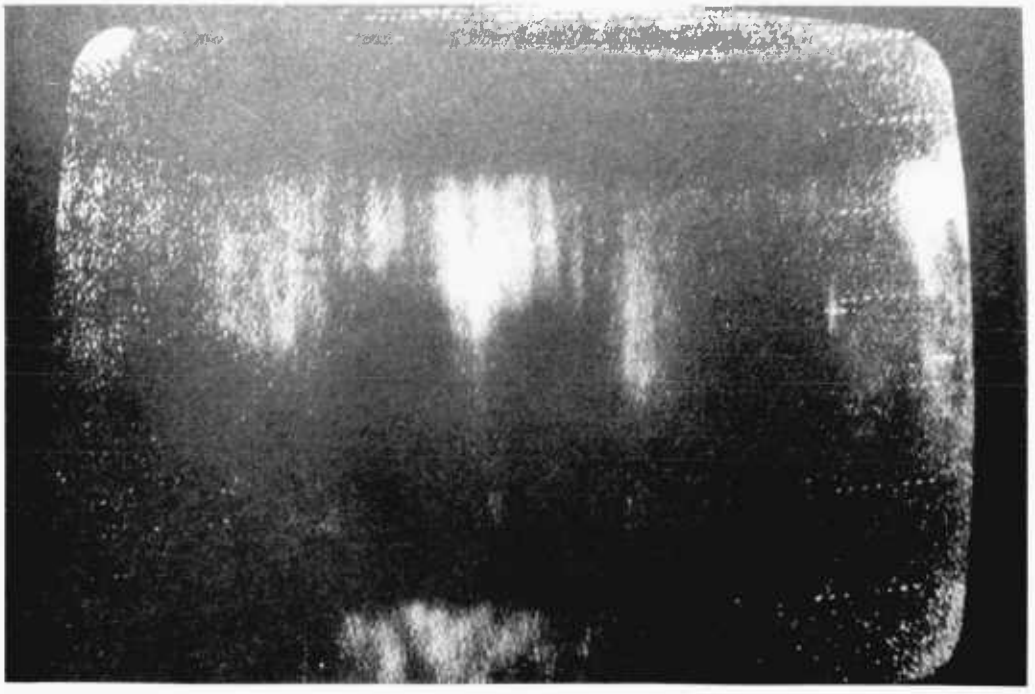


Figure 5.3.1b. Severe Scuff.

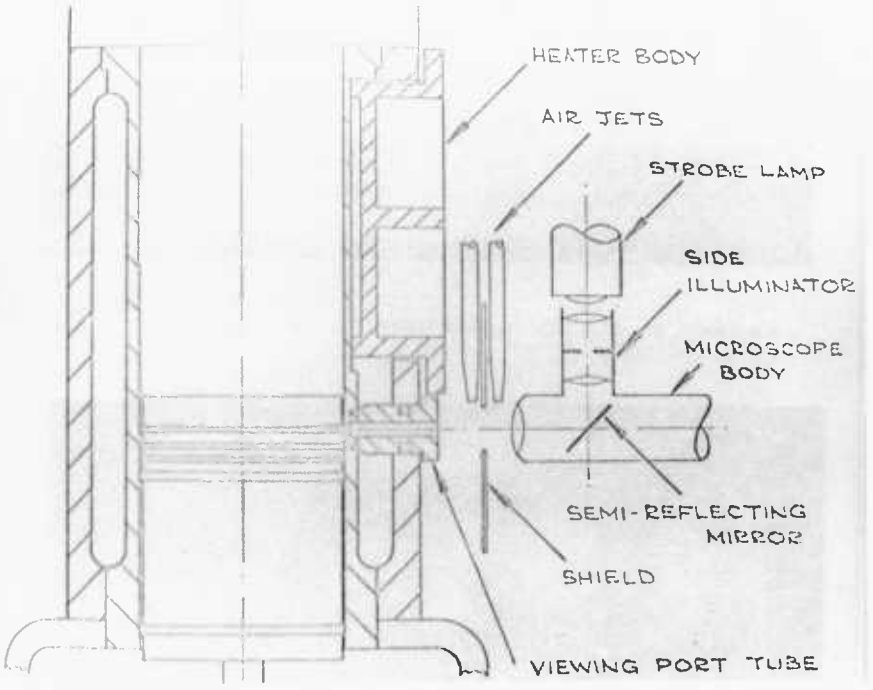


Figure 5.3.1c. Arrangement of Strobe Light and Microscope.

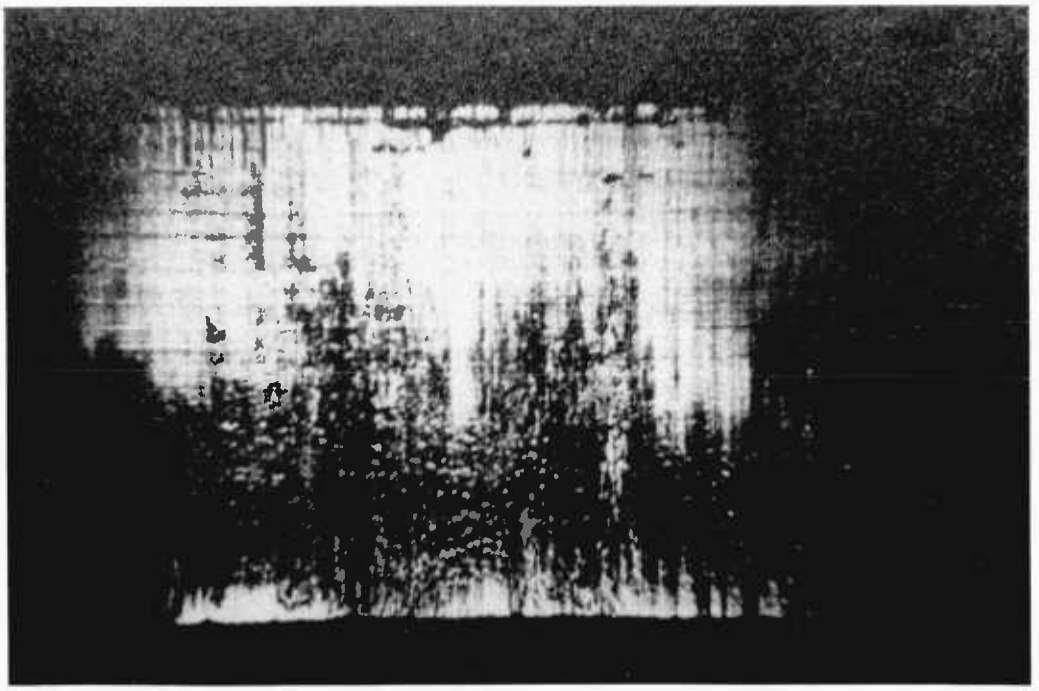


Figure 5.3.1d. Ring Surface Viewed directly through the Microscope.

With experience the recognition of a scuff became fairly certain. This was helped by the slow rotation of the ring in its groove, when points on its surface would move with it, whereas oil marks were sometimes fixed in position as they were caused by scores on the liner or the influence of the viewing hole. Furthermore it became possible to distinguish the rapid development of dark markings caused by a true scuff from the background of patches of dark laquer film produced by the oil and blow-by gases (see Figures 5.31a and 5.31b).

Another problem concerned with ring rotation was that scuffing would not necessarily be initiated in front of the viewing hole. Thus it could be that the ring-scuff was out of sight, and so not necessarily be detected. However as each temperature stage lasted for 5 minutes, and the ring was continually moving slightly the chance of this was considered remote. As a consequence of the ring movement, the piston-ring gap appeared occasionally.

5.4 TEST PROCEDURE

Tests on the lubricants chosen were conducted by running the engine at constant speed and raising the load and then the temperature of the heated portion of liner in stages up to 400^{o}C. A constant watch was kept on the conditions of the top piston-ring. The stage at which the surface began to deteriorate was taken as the scuffing point for that lubricant.

5.5 DESCRIPTION OF THE TEST ENGINE AND ITS MODIFICATIONS

This can be found in Appendix 1.

5.6 TEST LUBRICANTS

Four lubricants were blended for investigation, to be used in the modified Petter engine.

1. The Base Oil

This was a standard SAE 30 grade Gulf "Paramid". Sulphur content was 0.6%, blended with 2% Lubrizol 1202. Lubrizol 1202 was a light detergent additive, added to prevent excessive ring laquering.

2. Base Oil plus Detergent Additive

This comprised lubricant 1 above, blended with 5% (vol.) Lubrizol OS 27409. This was a calcium detergent additive, TBN = 80, 4.8% (wt.) calcium, 3.0% (wt.) sulphur. The sulphur was classed as being inactive.

3. Base Oil plus Extreme Pressure Additive

Lubricant 3 comprised lubricant 1 plus 2% (vol.) Lubrizol OS 18877. This was a highly active sulphur extreme pressure additive, 46% (wt.) sulphur.

4. Base Oil plus Detergent plus Extreme Pressure Additive

This consisted of the base oil, 1, with 5% Lubrizol OS 27409 and 2% OS 18877 by volume.

5.6.1 The Fuel

The fuel used was a commercially supplied diesel oil. This contained a small percentage of sulphur to assist in preventing scuffing. Bailey (34) had checked to ensure

that its influence was not sufficient to effect the performances of the test oils.

5.7 PRE-TEST PROCEDURE

5.7.1 Running-in a New Piston-Ring

Whenever a new piston ring was used in the engine it had to be run-in until it presented a smooth shiny surface, see Figure 5.71a. This required up to 50 hours running, and Figure 5.71b shows a ring after 1 hour's running. As the ring is slightly taper faced the lower edge becomes polished first. The running-in was carried out using the base oil. During all running-in the oil and water coolers were left switched on resulting in an oil temperature of 40^{o}C and a water temperature (at outlet from the block) of 45^{o}C.

5.7.2 Running-in Between Tests

On completion of a test the engine was run at 5 Bar bmep. and 1500 r.p.m. for between 8 and 12 hours to heal the scuff marks. If after 15 hours the ring surface was still unhealed then a new ring or piston assembly was installed.

5.7.3 Oil Changes

The oil was always changed before and after a test. In addition if the next test required a different oil then it was also changed mid-way through the running-in period. Hence there had always been a minimum of 3 oil changes with a particular oil before any test.

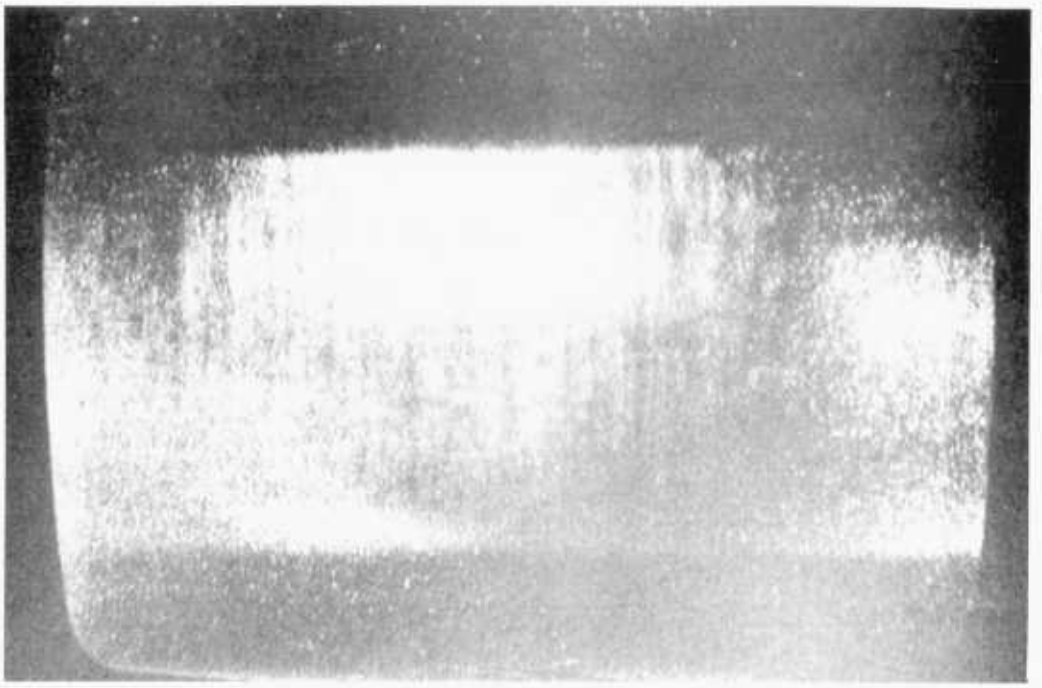


Figure 5.7.1a. Run-in Piston Ring.

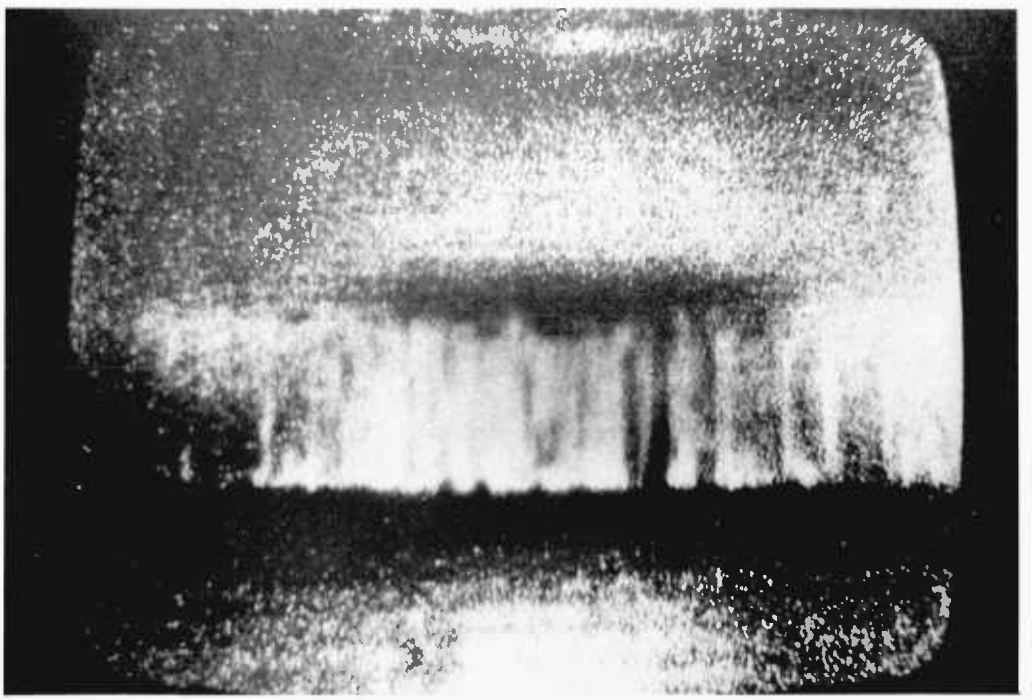


Figure 5.7.1b. The Ring after 1 hour's running.

5.8 SCUFFING TEST PROCEDURE

The engine was warmed up by running at 1250 r.p.m. and 3 Bar bmep. until the oil and water temperatures reached 95°C. The load was reduced to 1 Bar bmep. and the engine speed set at that for the test. The test was started. With the liner heater off the load was increased at 5 minute intervals to the desired load. Thereafter, the liner temperature was raised in steps of 25°C every 5 minutes until scuffing was observed, or a liner temperature of 400°C was reached, at which point the test was terminated. A coding system was adopted to enable any particular stage in a test to be referred to. A demonstration example is shown in Table 5.8.

Table 5.8

Test Stages for Scheduled 6 Bar Test

Test Stage	Load Bar bmep.	Liner Temperature °C
1	1	
2	2	
3	3	Liner
4	4	Unheated
5	5	
6	6	
6/175	6	175
6/200	6	200
6/225	6	225
6/250	6	250
6/275	6	275
6/300	6	300
6/325	6	325
6/350	6	350
6/375	6	375
6/400	6	400

5.9 PETTER ENGINE SCUFFING TEST RESULTS

The results for the series of tests for the four oils are shown in Tables 5.91 to 5.94.

Table 5.91

Test Results - Oil 1, Base Oil

Speed (r.p.m.)	Scheduled Test Load (Bar bmep.)	Scuffing Point (Load/Temp °C)
1500	6	6/200
1500	6	6/175
1500	6	6/225
1500	6	6/175
2000	6	5/150
2000	6	4/150
1500	4½	4½/300
1500	4½	No Scuff
1500	4½	4½/275
2000	4½	4½/160
2000	4½	4½/200

Table 5.92

Test Results - Oil 2, Base Oil plus Detergent

Speed (r.p.m.)	Scheduled Test Load (Bar bmep)	Scuffing Point (Load/Temp °C)
1500	6	No scuff
1500	6	No scuff
2000	6	6/175
2000	6	6/350
2000	6	6/250
2000	6	6/175

Table 5.93

Test Results - Oil 3, Base Oil plus Extreme Pressure Additive

Speed (r.p.m.)	Scheduled Test Load (Bar bmep)	Scuffing Point (Load/Temp °C)
1500	6	6/225
1500	6	6/225
2000	6	6/200
2000	6	6/175

Table 5.94

Test Results - Oil 4, Base Oil plus Detergent plus E. P. Additive

Speed (r.p.m.)	Scheduled Test Load (Bar bmep)	Scuffing Point (Load/Temp ^{o}C)
1500	6	6/200
1500	6	6/275
1500	6	6/225
2000	6	6/200
2000	6	6/200

5.10 DISCUSSION OF RESULTS

5.10.1 Base oil plus Detergent

It can be seen that the addition of the detergent additive resulted in much higher scuffing points relative to those produced by the base oil on its own. At 1500 r.p.m. the Base Oil failed at stage 6/200. However with detergent added, failure was not observed up to 6/400.

At 2000 r.p.m. the base oil plus detergent results show considerable scatter, for which no satisfactory explanation has been found. Close inspection of the video-tape records for the tests which failed at 6/350 and 6/250 showed no signs of failure at 6/175. Possibly stage 6/175 was a critical one (approximately the stage at which the base oil alone was prone to failure) which, if passed through would permit much higher temperatures to be reached before scuffing occurred.

5.10.2 Base oil plus Extreme Pressure Additive

The presence of the extreme pressure additive in the base oil yielded an almost negligible improvement over

the base oil alone.

5.10.3 Base Oil plus Detergent plus Extreme Pressure Additive

When added to the base oil plus detergent the extreme pressure additive had a very marked effect. The high scuffing points obtained with the base oil plus detergent were no longer present. In fact, the scuffing points were now similar to those of the base oil alone.

This is extremely significant since although the highly active extreme pressure additive had little or no effect on raising the scuffing resistance of the base oil, it was very effective in negating the good scuff resistant qualities of the detergent additive.

5.11 TESTS WITH ONLY ONE OIL CONTROL RING

To study the effect of increasing the lubricant supply rate to the top piston ring the second and third oil control rings were removed (see Appendix 1). Immediately more oil could be seen around the top ring.

To examine the influence of this extra oil, two further tests were carried out and the results shown in Table 5.11, see over.

Table 5.11

Effect of Oil Control Rings on Scuffing Point

No. of oil control rings	Speed (r.p.m.)	Test Load (Bar, bmep)	Scuffing Point (Load/Temp ^{o}C)
3	1500	6	6/200
3	1500	6	6/175
3	1500	6	6/225
3	1500	6	6/175
1	1500	6	6/250
1	1500	6	6/275

As can be seen, removing two of the three oil scraper rings raised the scuffing point significantly. This was not unexpected and reinforces the view that in some cases engine scuffing problems can be accounted for by inadequate lubricant supply.

5.12 CONCLUSIONS

The above tests on the Petter engine showed that from the scuffing point of view the detergent additive was the most effective. The extreme pressure additive, which was chosen because of its high degree of reactivity, as previously determined in a pin-on-disc machine and in rotating four-ball type machines by Bailey (34) was not effective in increasing the scuffing resistance of the base oil.

With any of the lubricants an increase in engine speed resulted in a lowering of the scuffing point. Also, expectedly, a reduction in the load, that is the bmep., raised the scuffing point.

Returning to the ineffective performance of the extreme pressure additive. The reason postulated for this

behaviour was based on the theory that there was insufficient time during the critical parts of the stroke for effective chemical reaction to occur. Around the dead-centre positions the friction is highest and hydrodynamic oil film thinest. The sections of the liner in these two regions are passed over twice in a very short time interval, once as the ring approaches the dead-centre position and again as it recedes. It was calculated that at 1000 r.p.m. the liner 0.5mm. below the lower surface of the ring at T.D.C. was scraped twice in 2 milliseconds. This is the order of the length of time needed for chemical reaction to take place, as shown by Bailey (35). Hence, if a chemical film was destroyed on the first pass (towards top dead centre), there was insufficient time for an effective chemical film to be built before the second pass. A rig is at present being developed by T. Mills of the Lubrication Laboratory to investigate this matter further.

Unfortunately not only is the extreme pressure additive ineffective as an anti-scuffing agent in the diesel engine, but Table 5.94 showed that it actually destructively interfered with the performance of the detergent additive, when both were present.

The final series of tests showed that an increase in oil supply to the top ring raised the scuffing point. This indicates that the oil film thickness plays a part in the scuffing mechanism, and that the mode of lubrication is probably physical adsorption rather than chemical.

5.13 SUMMARY OF CONCLUSIONS

These are as follows:-

(a) A repeatable engine scuffing test has been established.

(b) The detergent additive was shown to have good effective anti-scuffing properties.

(c) The extreme pressure additive was seen to have little effect as an anti-scuffing additive and also destructively interfered with the detergent.

(d) With all lubricants an increase in speed and/or load reduced the scuffing point.

(e) Increasing the supply of oil to the ring raised the scuffing point significantly.

CHAPTER SIX

EXAMINATION OF PREVIOUS WORK ON DYNAMIC LOADS IN GEARS

6.1 INTRODUCTION

In order to understand the conditions experienced between a pair of gear teeth running under load, a review of the previous work on the subject was undertaken, special attention being paid to the quantity and quality of the dynamic loads upon the teeth. Work on the subject is split into two sections. Considered initially are papers on dynamic loads arising from defects in the tooth profile. Secondly attention is given to the work done on the consequences of external sources of vibration.

6.2 BUCKINGHAM, E.

The consideration and analysis of dynamic loads upon gear teeth was investigated theoretically by E. Buckingham (1) in 1949, and his book "Analytical Mechanics of Gears" with his basic equations has remained the standard text to the present day.

Starting from first principles Buckingham considered the effect on the gear teeth as a high spot entered the contact area. Previous work on the Lewis machine (66) had shown that it was the magnitude rather than the nature of the error that was important. Thus as a basis for his work Buckingham considered a cylinder rolling up a step.

The following nomenclature was used.

σ = Poisson's Ratio

W = Load on the contact, lbf.

L = Length of the contact along the tooth, ins.

E = Modulus of Elasticity, lbf/in^2.

r_1 = Radius of curvature of one contact surface, ins.

r_2 = Radius of curvature of second contact surface, ins.

He showed that the amount of compressive deformation of the gear teeth d_1 could be found from

$$d_1 = 2W\ (1-\sigma^2)(2/3 + \log\ (1.548\ EL\ (r_1+r_2)/W))/\pi EL \quad (1)$$

When,

H_1 = the distance from the point of application of the load to the tip of the tooth, ins.

h_1 = the thickness of the tooth at the point of application of the load, ins.

h_2 = the thickness of the tooth at its base, ins.

The deflections, d_2 from the combined effects of bending and shearing was equal to

$$d_2 = \frac{12\ W\ H^3}{E\ L\ h_2^{\ 3}}\left(\left[\frac{3}{2} - \frac{H_1}{2H}\right]\left[\frac{H_1}{H} - 1\right] + \log \frac{H}{H_1}\right) + \frac{4W}{L}\ \frac{(H-H_1)\ (1+\sigma)}{(h_1-h_2)\ E} \quad (2)$$

Hence the total deflection of the teeth, d is equal to equation (1) plus equation (2). However from measurements it has been shown that the following approximate equation is sufficiently accurate

$$d = (W/L)\ (E_1\ z_1 + E_2\ z_2)/\ E_1\ z_1\ E_2\ z_2 \quad (3)$$

Where,

E_1 and E_2 = Modulus of elasticity for the two materials, lbf/in^2.

z_1 and z_2 = Elasticity form factor for the two gear teeth respectively, and can be found from equation (3A).

y = Lewis tooth-form factor.

H = Height of the tooth, ins.

$$z = y / (0.242 + 7.25y) \quad (3A)$$

Buckingham then defined the limiting acceleration load, f_L as that which was required to deform the teeth by the amount of the effective error. Hence,

$$f_L = W ((e/d) + 1) \quad (4)$$

Where,

e is the measured error of a pair of gear teeth, ins.

d is the total deformation of mating teeth under load, ins.

The effective masses of the gear and pinion are calculated as usual from inertia considerations, the effective mass of the pair at their pitch line is equal to

$$m = m_1 m_2 / (m_1 + m_2) \quad (5)$$

He showed that this could cause the teeth to separate as follows.

As the error enters the contact area it causes the driver to be slowed down and the follower to be accelerated. With elastic bodies the accelerating force, in addition to changing the velocities of the gears will cause increased deformation of them. This deformation will also tend to separate the bodies, but is opposed by the load between the teeth. Equating the work done by the two forces leads to:-

$$W(k + d_m) = f_a (e - d_m + d) + \tfrac{1}{2} (f_a + W) dm \quad (6)$$

Where,

k is the separation of the surfaces, ins.

f_a is the acceleration force.

d_m deformation set up by the total load, ins.

This rearranges to

$$k = (f_a/W)\ e - (d/2)((f_a/W)^2 + 1) \qquad (7)$$

If k is negative the two surfaces do not separate and k is the magnitude of the minimum amount of deformation. With k positive the surfaces separate, reach a point of maximum separation when both surfaces are travelling at the same speed and then come together again with an impact under the closing force of the applied load. Of interest is the intensity of the maximum load Wd during this impact.

$$Wd = W\ (1 + (1 + 2\ k/d)^{\frac{1}{2}}) \qquad (8)$$

Buckingham relates the above equation to particular types of gears other than external spur gears. For spiral-bevel gears the effective mass m_c on the pitch line of the gear is determined from

$$m_d = (B^2 + 4AC)^{\frac{1}{2}} - B)/2A \qquad (9)$$

Where,

m_a = full effective mass of connected bodies on pinion shaft at R_1, = Ia/R_1^2.

m_b = effective mass of m_a at pitch line of pinion.

m_c = full effective mass of connected bodies on gear shaft at R_2, = I_c/R_2^2.

m_d = effective mass of m_c at pitch line of gears.

Z_2 = elasticity factor of connecting member on gear shaft.

Z_1 = elasticity factor of connecting member on pinion shaft.

$$A_2 = G\ m_c\ V^2 \cos \psi$$

$$B_2 = (m_1 + m_2)\ A_2 + e\ m_1\ Z_2$$

$$C_2 = e\ m_c\ m_1\ Z_2$$

For $14\frac{1}{2}^{o}$ gears

$$G = 0.00086 \ (\cos \gamma_1/R_1) + (\cos \gamma_2/R_2)$$

For 20^{o} gears

$$G = 0.00120 \ (\cos \gamma_1/R_1) + (\cos \gamma_2/R_2)$$

γ_1 = pitch cone angle of bevel pinion.

V = pitch-line velocity of gears, ft./min.

γ_2 = pitch-cone angle of bevel gear.

R_1 = mean pitch radius of bevel pinion, ins.

R_2 = mean pitch radius of bevel gear, ins.

m_1 = effective mass acting at pitch line of bevel pinion.

m_2 = effective mass acting at pitch line of bevel gear.

ψ = helix angle at pitch line.

Similarly the effective mass of m_a on the tooth profile of the pinion is determined from

$$m_b = ((B_1^2 + 4 A_1 C_1)^{\frac{1}{2}} - B_1) / 2A_1 \qquad (10)$$

Where, $A_1 = G \ m_a \ V^2 \cos^2$

$B_1 = (m_1 + m_2) \ A_1 + e \ m_2 \ Z_1$

$C_1 = e \ m_a \ m_2 \ Z_1$

The acceleration force is then calculated from

$$f_a = f_1 \ f_2 \ / \ (f_1 + f_2) \qquad (11)$$

f_1 = force required to accelerate the masses as rigid bodies, lbf.

f_2 = force required to deform the teeth the amount of the effective error, lbf.

and thus the dynamic load can be calculated from a form of equation (8)

$$Wd = W + (f_a \ (2 \ f_2 - f_a)^{\frac{1}{2}}) \qquad (12)$$

He pointed out with respect to fatigue lives, the gears are not subjected to a number of dynamic loads proportional to the number of errors, but to twice this, as there is also an acceleration load on the gears before the separation, as well as the dynamic load experienced at impact. However with regard to surface stressing the two do not occur at exactly the same place on the gear tooth surface, as the gears have moved during the separation and recombination of the two surfaces.

This work is related to modern high speed gears in which the extent of the effective error is reduced. This occurs because the time interval between successive contacts is too short to permit the full double-load cycle to act, either because of fine pitches or high pitch-line velocities. Buckingham modified his equations to encompass this effect by modifying e to e' as follows.

$$t = 30/n \ N_1 \qquad (13)$$

$$e' = 6 \ W \ t^2 \ / \ m \qquad (14)$$

$$n_c = (30/N_1) (\phi W e m)^{\frac{1}{2}}$$

Where, n = r.p.m. of spiral bevel pinion.

N_1 = number of teeth on the pinion.

When e' is greater than e then the latter will be used in the dynamic load equations. When e' is smaller than e, then e' will be used. The maximum value of the dynamic load will occur when the pinion is running at speed n_c. Thus if the gears are to operate most of the time at speeds above n_c, then stresses greater than the endurance limits

for the steels may be used. However if the gear pair is to operate at varying speeds encompassing n_c then the dynamic stresses must lie within the endurance limit for the material for a useful gear life. In his book Buckingham provides examples of gear pairs and calculates the dynamic loads for them.

6.3 POST BUCKINGHAM WORK ON INTERNALLY EXCITED DYNAMIC LOADS

In 1953 Tuplin (2) theoretically investigated the effect of gear tooth errors by considering an analogy of a thin wedge inserted between a surface and a follower, spring, mass system. He was interested in determining the allowable nominal loads at high speeds assuming that it was solely the dynamic load which governed this condition. Starting with the stiffness of the gear teeth and blank, and assuming that one of the masses is infinitely large, he considered the wedge of thickness e, to be inserted in time t_1. Assuming that the teeth of the two gears did not separate he showed that in such a simplified system the maximum load F_1 on the surface could be calculated from

$$F_1 = k\ e\ /\ 1 + 2\ n\ \pi^2\ (t_1/T)^2 \qquad (16)$$

This is analogous to the maximum acceleration load before tooth separation calculated by Buckingham.

In the above equation n is a form factor for the shape of the wedge, being ½ if it is a straight wedge, greater than a half for a convex wedge, and smaller for a concave one. k is the stiffness of the teeth and gear, mass m. $T = 2\pi\ (m/k)^{\frac{1}{2}}$.

The remainder of the paper considers the com-

pliance of the gear wheel rim and associated stiffnesses, but does not warrant further discussion due to the somewhat over-simplified approach used.

6.4 BISHOP AND JOHNSON AND THE USE OF COMPLEX NOTATION

Bishop and Johnson (4) discussed "displacement excitation". This they defined as excitation arising from gear cutting errors, which caused periodic variations in the velocity ratio of mating components. Complex notation was used for convenience.

With the arrangement shown in Figure 6.4a, the gear having a nominal ratio of n:1

$$x_1 = X_1 e^{iwt} = \beta_{11} F_1 e^{iwt} \tag{17}$$

$$x_2 = X_2 e^{iwt} = \gamma_{22} F_2 e^{iwt} \tag{18}$$

Assuming that there is a gearing error at the interface between the two gears, which gives a compatability condition such that $x_2 = nx_1 + E\, e^{iwt}$

$E \ll nx_1$ and therefore $X_2 = n\, X_1 + E$

w will usually be a multiple of one of the shaft speeds.

However for a closed system $F_1 \times 1 = -F_2 \times n$

When the last two equations are substituted into the first pair they become

$$x_1 = \frac{-n\ \beta_{11}\ E\ e^{iwt}}{\gamma_{22} + n^2\ \beta_{11}} \quad \text{and} \quad x_2 = \frac{\gamma_{22}\ E\ e^{iwt}}{\gamma_{22} + n^2\ \beta_{11}} \tag{19}$$

These equations now represent the responses at the junctions of the systems B and C, in terms of their receptances. It was shown that for resonance

$$\gamma_{22} + n^2\ \beta_{11} = 0 \tag{20}$$

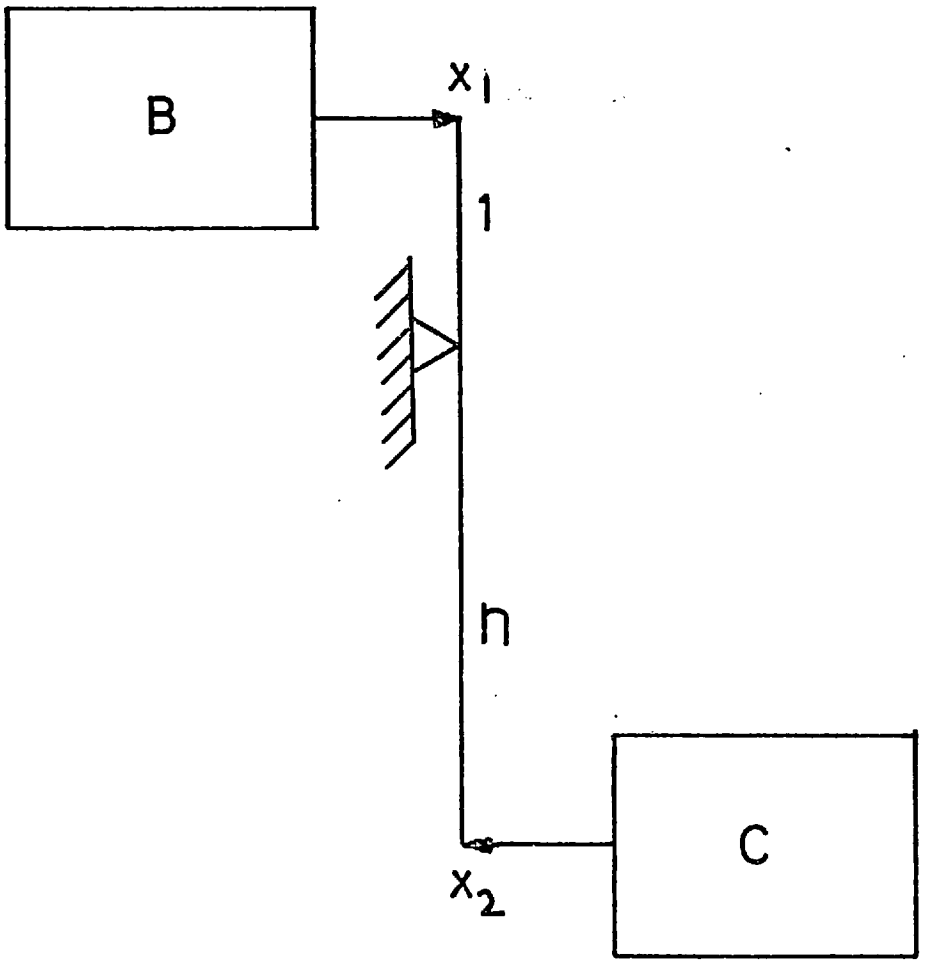


FIGURE 6.4.a

But this equation is also the frequency equation of the gearing system with an error. Bishop and Johnson stated, as demonstrated above that frequently the application of harmonic forces to a system is most simply considered in terms of their receptances and the use of complex notation. A prime source of harmonic loading is the eccentric mounting of one, or both of the gear pair.

Buckingham's work was extended by Reswick (5) in 1955 to cover the cases of heavily loaded gears. He used the same analogy of a wedge being inserted between two teeth, but this time the wedge is considered to represent a high tooth, and the effect of this is examined as the load is transferred to it. The profile of the wedge is taken as a parabola and the height is equal to the tooth effective error e. It was shown that the tooth entering the contact very quickly takes part of the load, especially if it is a "high" one. To determine the maximum tooth deflection vibration the motion of the gears is examined. This work differs from that of Buckingham in that the wedge is profiled to yield a constant acceleration on the gear tooth and the load is assumed to be supported by two teeth. The following assumptions were made:-

(a) The tooth deflection, $\delta t \gg$ the manufactured error, e_m.

(b) The inertias of the gears is finite, and represented by an effective mass at the pitch point $m = I/R^2$.

(c) Inertias of other items are ignored if connected by a shaft.

(d) Spring constant for tooth deflection is constant and equal to k based on the loading at the tooth end.

(e) Viscous damping is negligible.

(f) Pitch line velocities at instant of engagement are equal.

By the solution of the equations produced Reswick showed that the motion of the teeth was as shown in Figure 6.4b.

Thus the maximum resulting force Td will be given by $Td = k\ (e/2 + x_{ar}')$ (21)

where e is the effective error and

$$x_{ar}' = (A^2 + B^2)^{\frac{1}{2}} \quad (22)$$

is the equation for the final motion where

$$A = e\ B_a\ (B_a \sin (1/B_a) - 1)$$

$$B = e\ B_a^{\ 2}\ (\cos (1/B_a) - 1)$$

$$B_a = (V/w_{na})\ (c/e)^{\frac{1}{2}} \qquad w_{na} = (2\ k/m)^{\frac{1}{2}}$$

$$C = 0.129\ (1/R_1 + 1/R_2) \text{ for } 14\tfrac{1}{2}^{\circ} \text{ gears.}$$

$$C = 0.183\ (1/R_1 + 1/R_2) \text{ for } 20^{\circ} \text{ gears.}$$

It can be seen that despite the differing initial conditions for Reswick's work, the final result is very similar to that of Buckingham. Reswick showed that this solution was valid for e_m increasing from zero to a value equal approximately to δt. The dynamic load on the teeth varies from zero to ek/2 and the peak loads on the teeth reach a maximum of ek at high pitch line velocities ($e = e_m + \delta t$). The second part of his work covered the

Relative Motion of Gear Masses

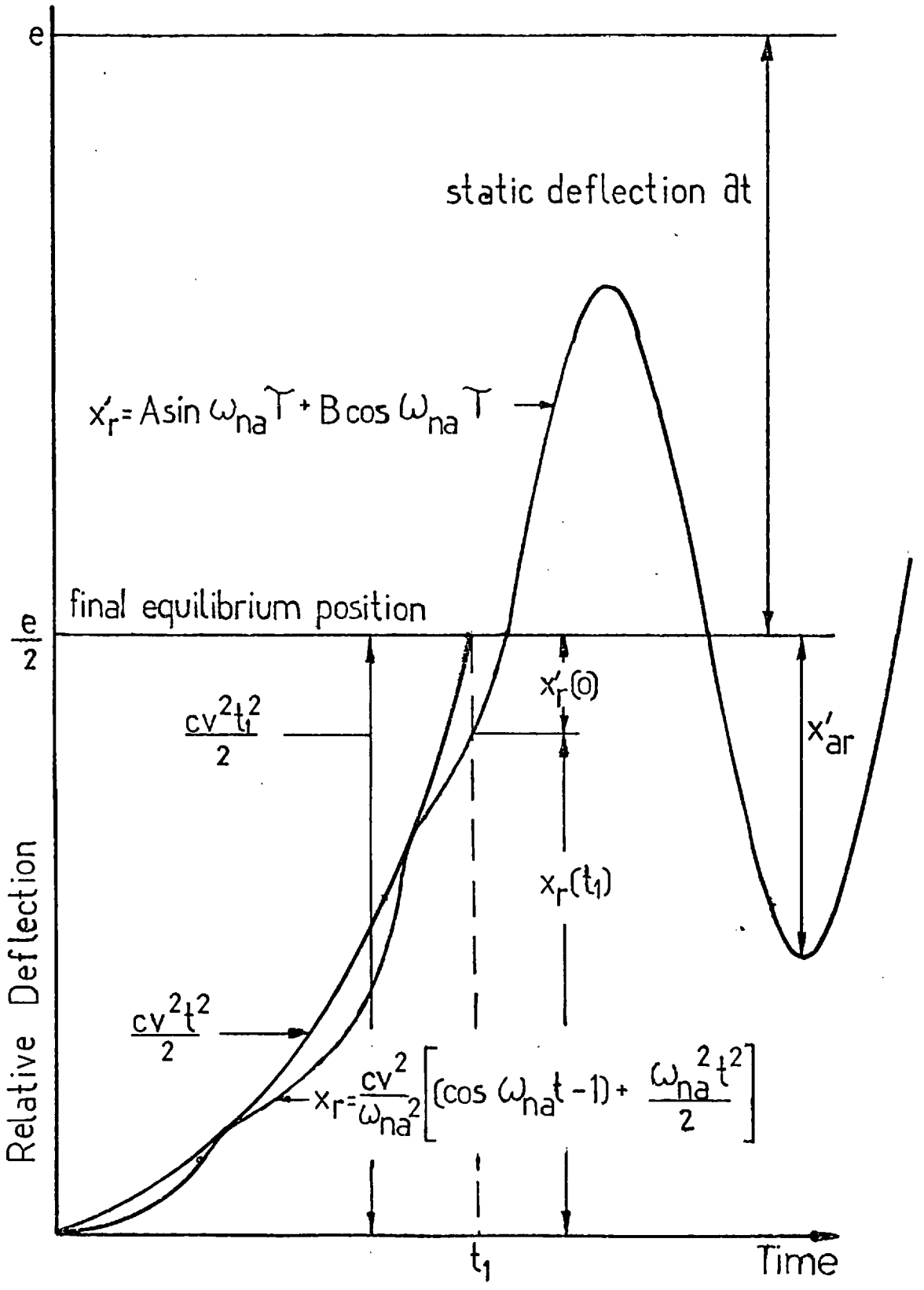


FIGURE 6.4.b

case of lightly loaded teeth, which is not relevant to this investigation.

6.5 APPLICATION OF ELECTRICAL MEASUREMENTS

In 1957 Crook (6) showed that there was considerable metal-to-metal contact initially between a pair of discs in a disc machine. After 10 hours, corresponding to 10^6 revolutions the average electrical resistance of the contact increased to 5×10^4 ohms. This was equivalent to an oil film thickness of about 1×10^{-5} inch. He paralleled his electrical measurements with Talysurf recordings, and showed that the peaks on the surface of the work were progressively removed as running continued. By increasing the load it was found that with mild steel discs a hydrodynamic film was still in existance up to the point at which considerable plastic deformation of the surfaces was possible.

6.6 RESONANCES IN GEARS

In 1958 the Institution of Mechanical Engineers held an International Conference on Gearing, at which Johnson (7) highlighted the need to avoid resonance in a gear system. Care must be exercised in ensuring that the meshing frequency of the gears was not similar to the natural frequency on their shafts, nor to any natural frequency of the support structure, otherwise a positive feedback setup would arise. Any improvement in tooth-to-tooth damping that could be obtained would reduce the dynamic load on the teeth and the tendency to resonate. Further in the case of resonance the ratio of

tooth amplitude to error causing the amplitude would be greatly reduced by improved damping.

Bishop (8) in 1962 reported a case of failure through resonance in a set of four centrifugal compressors. They were mounted axially in line and the common shaft was driven through a step-up gear pair. A brittle fatigue failure occurred in the output shaft adjacent to this gear pair. A Holzer analysis of an idealised representation of the system showed that the fifth harmonic torsional frequency of the system lay in the operating speed range. A node for the fifth principal mode was found to occur at the point of failure of the shaft.

After replacing the shaft with an identical spare, just to bring the machine back into operation, it was found that the Holzer prediction of resonant frequencies was confirmed, and that the amplitude experienced was sufficient to cause fatigue failure of the shaft. From this case study Bishop drew the following conclusions.

(a) With centrifugal machines the torque transmitted through the system increases steeply with speed. This tends to "lock-up" couplings and thus higher modes of vibration do not experience as much damping as anticipated. Doubt had been experienced as to the possibility of experiencing significant distortions in such a high mode as the fifth. However the measurements on the second shaft showed that the torsional vibrations had not been eliminated.

(b) With the low damping the magnification of the system (Q factor) at resonance in the fifth mode was

approximately 40 for any error in gear meshing. As it is almost impossible to remove completely the errors detuning was necessary.

(c) It can be seen that when detuning, all modes up to the fifth must be checked.

Of the other papers presented at the Conference, the one with the most relevance was that by Cleare (9) discussing gear tooth failures in highly stressed transmission gears. Presented with his paper were an interesting series of photographs depicting a wide range of severe gear failures. These point to the need for attention to detail in the rigidity of the casing and the grinding and inspection of the tooth roots.

6.7 MERRITT'S SIMULATION OF GEARS ON A DISC-MACHINE

In a nominated lecture to the Institution of Mechanical Engineers in 1962 Merritt (10) discussed simulation work on a disc machine, from theoretical and experimental aspects. His work on chain connected discs, with opposite velocities through the contact showed that even with these very severe conditions of lubrication a hydrodynamic film was produced, and he obtained coefficients of friction for glycerol, mineral and castor oil.

The life of a disc will be greater than that experienced by gear teeth as errors in tooth alignment and profile error will cause higher localised contact pressures. A brief summary of the conditions affecting scuffing was given, which was as follows:-

(a) The results of scuffing tests on gears are only

repeatable within a fairly wide tolerance band. This may be due to the rate of flow of oil, an inadequate supply of which can induce or accelerate the scuffing.

(b) Teeth which are hand dressed after scuffing will then sometimes work perfectly well, which may be explained by insufficient original tip profile relief.

(c) Scuffing, especially during running in can be inhibited by suitable surface coatings, such as copper plating or a Parco-Lubrite treatment.

(d) Extreme-pressure additives are highly beneficial in preventing scuffing, and are essential in many modern gearboxes.

(e) Scuffing can be seen to progress from the tip of a tooth towards the root, which is probably caused by the high sliding speed at the root.

(f) The scuffing resistance for some pairs of materials is much lower than either of the failure loads for the materials on their own.

(g) Initial assumptions were that lower coefficients of friction for the contact meant a larger film thickness, and secondly that scuffing occurred due to a breakdown of the oil film. However it was found that glycerol had a scuffing resistance of only one tenth of that of the reference mineral oil, despite having a much lower coefficient of friction.

(h) An inadequate supply of oil to the contact can easily result in the onset of scuffing under conditions where scuffing is avoidable.

6.8 THE EFFECT OF DAMPING IN GEARBOXES

An interesting paper covering the dynamic behaviour of spur gears was presented to the Institution of Mechanical Engineers in 1963 by Gregory, Harris and Munro concerning the role of damping in gearboxes. In a previous paper Harris (11) had shown theoretically that due to positive feedback large vibrations could occur in a pair of spur gears. This would happen at certain speeds if the damping was less than about 0.07 of critical. The authors set out to investigate the dynamic behaviour of a typical pair of precision spur gears and thus determine whether Harris' predictions had any relevance to real effects.

Using an exceptionally well designed back-to-back gear test rig they were able to measure transmission error continuously by an optical method. (A back-to-back gear test rig is one in which two or more identical gear test pairs are connected together such that the output from one pair is fed back into the input for the other pair. By this means and suitable pre-torqueing of the gear shafts only the losses from friction in the gears need to be supplied. This enables a 400 horse power gear pair to be tested under operating conditions using a 100 horse power motor, and eliminates the need for a brake, capable of dissipating 350 horse power). Knowing the stiffness and inertia of the system they were thus able to calculate the tooth contact loads, as they were principally interested in the peak tooth loads. Over 400 records were made at speeds up to twice that of resonance and at loads

of ¼, ¾, 1 and 1¼ times the design load. They specified the design load as that which gave a constant transmission error at low speed. This was 1700 lbf/in. face width, as opposed to the theoretical design load of 2000 lbf/in., the difference being due to the teeth being more flexible than Weber's (12) figures suggest, probably because of the greater depth of tooth.

It was found that the maximum dynamic load on any one tooth never exceeded about 2¼ times the design load. However this figure could be approached even when the applied load was well below the design load, due to tooth separation. Consequently excessive profile modification should be avoided. Great care was taken to produce a rig with a very low level of damping. However the actual figure of 0.02 of critical, though small was fortunately still a useful amount of damping, and thus real gears benefited from more damping than could be deduced from calculations. This extra damping would serve to reduce the dynamic content of the tooth load.

The authors concluded that tooth separation and serious dynamic loads occur, as predicted by Harris (11), even with precision gears, running at their design load, without external excitation.

6.9 A METHOD OF ELIMINATING KNOWN RIG VIBRATIONS FROM TEST RESULTS

In 1960 Westland Aircraft Ltd. produced a stress report entitled "A method for deriving the Power/N curve for a gear from test results which include unwanted but known rig vibration". As this paper (13) demonstrated

a useful method of obtaining a more realistic fatigue curve from a set of results the work in it is discussed fairly fully now. The authors, A.D. Hall and D. Hill stated that for a gearbox on fatigue test it was obvious that ideally it should be run under conditions of constant power. However, in practice unwanted power fluctuations were present in a test rig, superimposed upon the mean power level. The value of these fluctuations could be obtained by measurement. Applying the cumulative damage hypothesis (Miner's Law) to a typical cycle of vibratory power the damping effect of these fluctuations could be taken into account.

The following notation was used:-

P_M was the mean power level.

P_V was the vibratory power level.

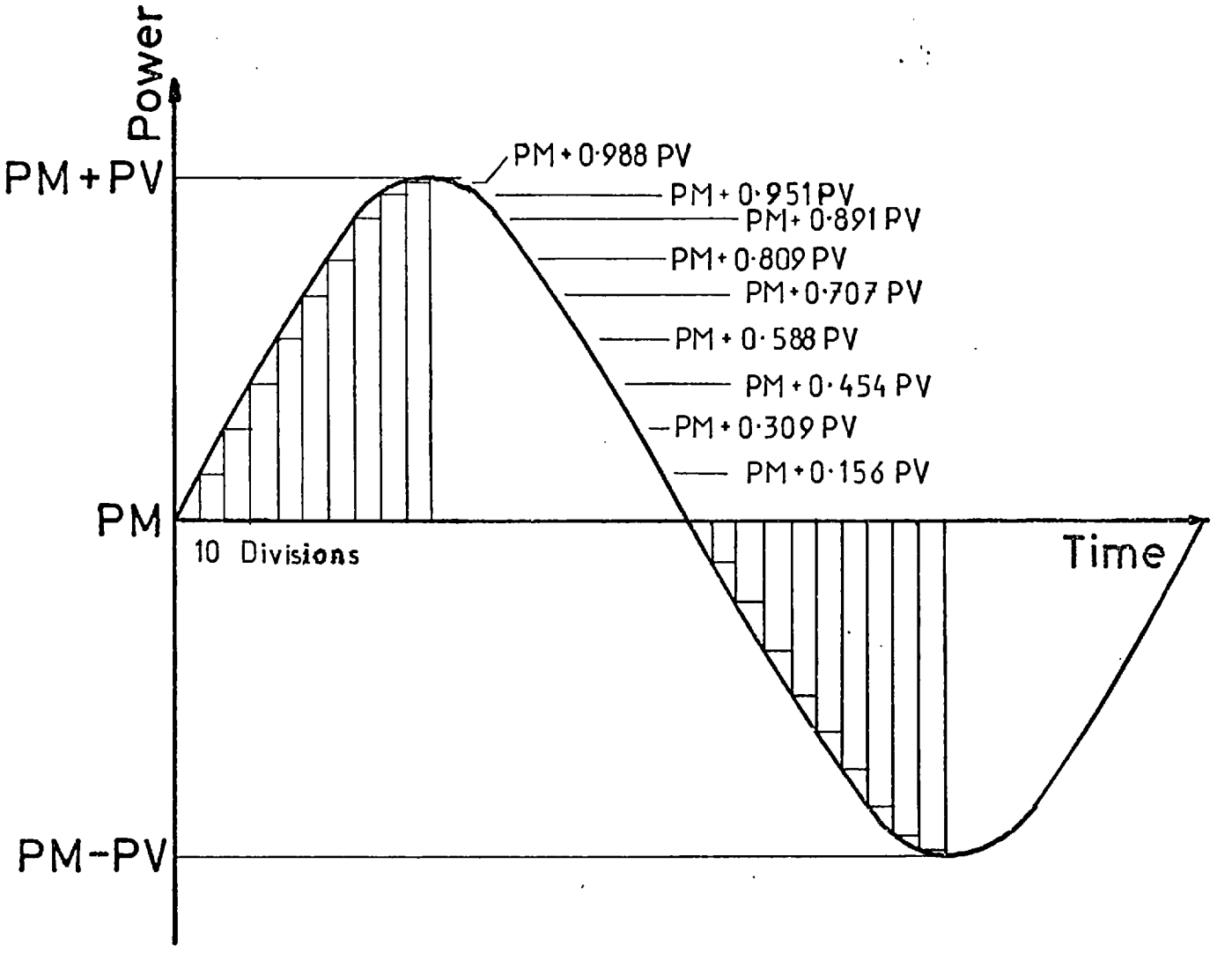
N_T total number of cycles to failure.

P equivalent steady power level producing failure at N_T cycles.

It was assumed that the shape of the Power/N curve was known, which for gear steels is well documented. The procedure was as follows. Figure 6.9a shows one cycle of the power level to which a gear is subjected.

It can be seen that the applied power is split into 20 levels, each of equal duration. The levels are selected on the concave side of the curve to enable a pessimistic result to be obtained. (Higher powers have far more effect upon the fatigue life than lower powers). Shown on Figure 6.9a are the fractions of vibratory power K, corresponding to each of the 20 power levels. The total number of cycles, n, of applied tooth loading

FIGURE 6.9.a One Cycle of Variation of Gearbox Input Power



at a given power level of $P_m + K P_V = N_T/20$. Power/N cycles are then drawn to establish the particular one which will satisfy the condition that $\Sigma n/N = 1$, which for this case means that $(N_T/20)\ \Sigma 1/N = 1$.

The procedure for an actual example is as follows. From the data obtained during a test run, P_M, P_V and N_T can be obtained. A curve is then plotted for the Power/N which from previous work, paper S.D. 721 Westlands Aircraft Ltd., had shown could be represented as follows.

Number of cycles	10^5	10^6	10^7	2×10^7
Power level (relative figures)	1.17	1.045	1.005	1.0

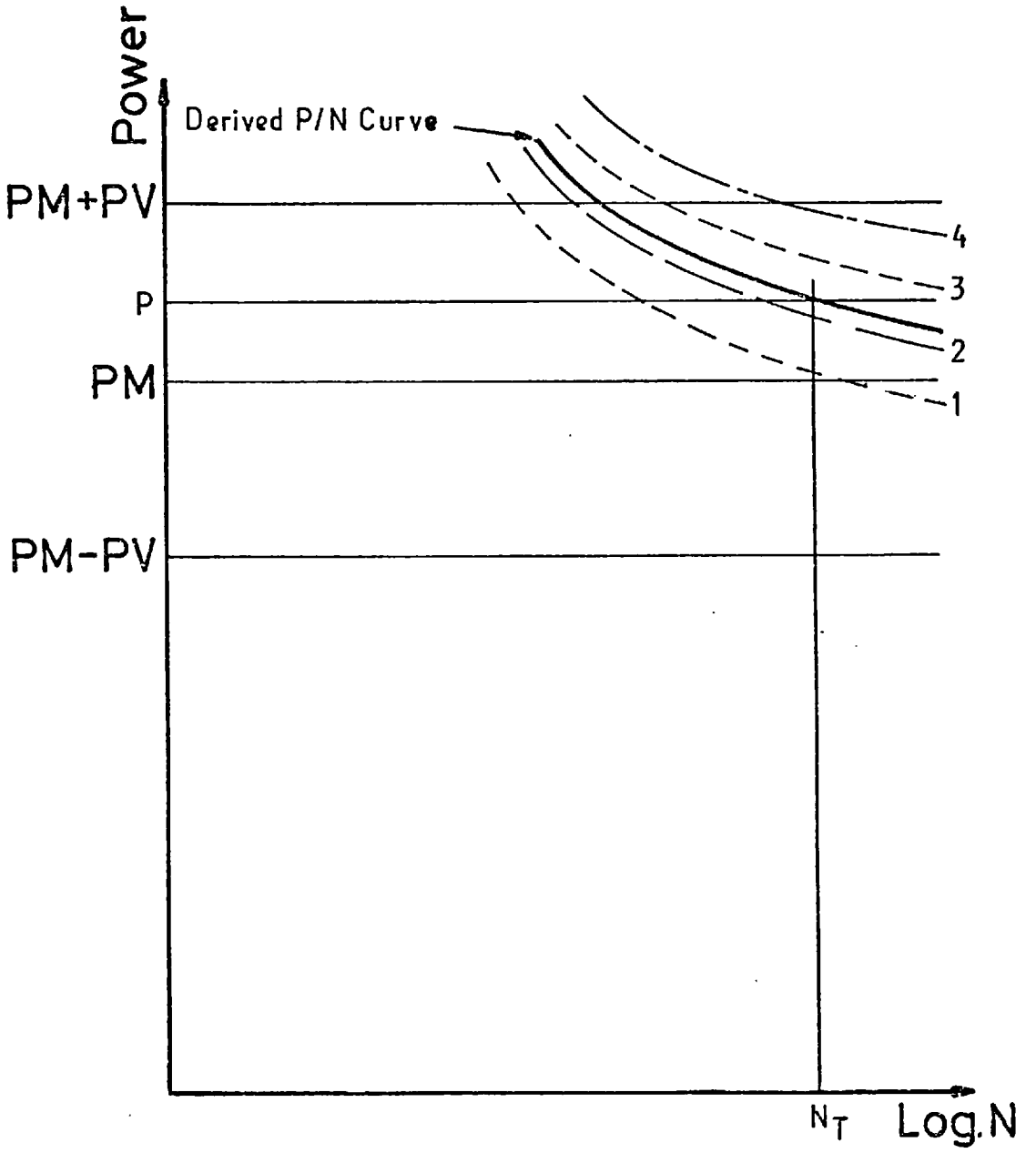
It is not necessary to know the actual power level as the shape of the curve is the same for different levels.

For each of the 20 levels a figure for $P_M + K P_V$ is obtained and thus a value for $(N_T/20)\ \Sigma 1/N$. This is plotted against a power for N_T cycles. The value of P at the intersection of this curve and the line $(N_T/20)\Sigma 1/N = 1$ is found. A P/N curve may then be drawn through this value of P and N_T to obtain the working curve for the gear with zero vibratory power, see Figure 6.9b.

6.10 TEMPERATURES IN THE CONTACT

Manton, O'Donoghue and Cameron (14) carried out a very thorough investigation into the temperature profiles in the fluid and in both surfaces in a rolling with sliding elastohydrodynamic contact, and in particular for a pair of gear teeth. They found, using numerical methods, large thermal gradients through the film, several orders of mag-

FIGURE 6.9.b Determination of the Working Curve for the Gear with Zero Vibratory Power



nitude greater than those along the film, and that whilst the oil in the centre of the film would rise to 380°F, in the particular case they were studying the surface temperature of the metals had merely reached about 100°F, with an inlet temperature of 80°F. From their results they were slightly uncertain as to the ratio of the nett temperature rise in the two metal surfaces, and referred to earlier experimental work by Merrit (15). It had been found using a disc machine operating under elastohydrodynamic conditions that the faster disc carried away more heat. Due to shear in the oil, as the temperature of the faster metal surface increases the peak oil temperature moves nearer that side of the oil film and increases the heat flow into it. Though it appears that the situation becomes unstable, the blank temperature rises to a steady value where the heat from the contact is conducted away to other surfaces of the disc. The authors discussed the effect of the heat of compression of the oil in the contact and showed that it was very much a second order term, and its greatest effect was to move the peak of the temperature distribution towards the faster moving surface.

6.11 KOHLER, PRATT AND THOMPSON'S WORK ON NOISE

In 1970 Kohler, Pratt and Thompson (16) gave a general account of gear dynamic tooth loads and noise. From a study of previous work they concluded that the best description of the excitation function in a gear pair is the gear transmission error under load. The transmission

error being defined as the departure of the driven gear from its theoretical position as the input gear is rotated under load at constant speed. Earlier work such as that by Buckingham (1) has examined the effect of a single tooth error, but it is essential to realise that the dynamics and noise of gearing is a continuous, repeating process. The authors considered that the system to be modelled should at least include the rotating parts together with the stiffness of the supporting members. Typical transmission error is shown in Figure 6.11 for a reduction gear pair with 15 and 45 teeth, centre distance 8.0 ins., face width 3 ins.

This trace is the nett result of a large number of different errors in the gears, shafts, bearings, housings etc. It was found that almost all harmonics of the basic tooth contact period were present. The vibrational and acoustic responses and correlation between excitation and response were covered. They were able to conclude that examination of the transmission error trace explained the occurrence, at times, of vibratory components at frequencies corresponding to neither shaft nor tooth contact frequencies.

To reduce dynamic loads in high quality gearing it is necessary to avoid resonances between significant transmission error components and system natural frequencies. To this end helical gears are preferable to spur gears because of their inherently smaller transmission error. For the control of noise they recommended that more attention should be paid to the gear case.

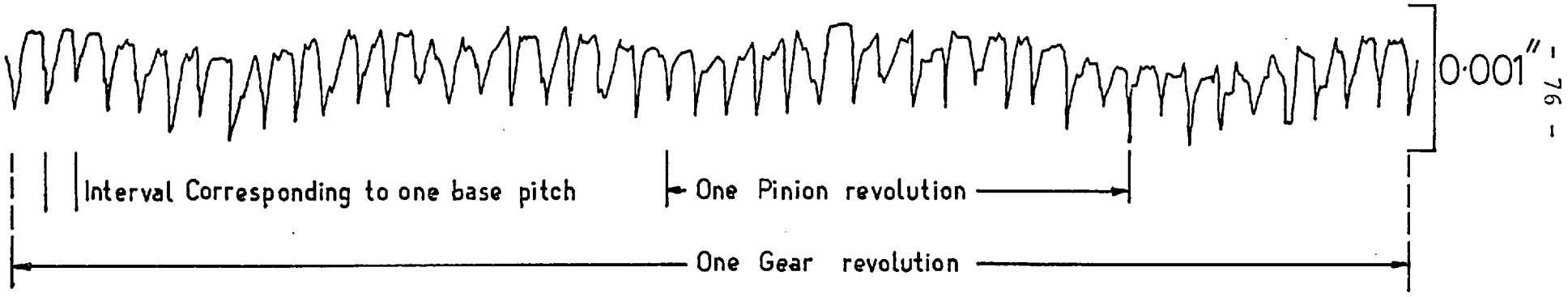


FIGURE 6.11 Transmission Error for a Reduction Gear Pair

Ratio 3:1

Continuing in the same sort of work Welbourn (17) set out to evaluate the magnitude of the adjacent pitch errors of gears in terms of Fourier series, and hence assess the relative importance of different sources of error from the point of view of obtaining quiet gears.

He used the approach that all gears must and do have errors, and covered the effects of base circle eccentricity, pitch error, dropped tooth, tooth bending under load and involute error. His assumption that the total error on the pitch circle is often randomly distributed was checked on two different types of gears using an air gauging method, which yielded an accuracy of $\pm$ ¼µm. When predicting noise levels he found that the above data gave more importance to eccentricity ratio than it in fact warranted, but that industry in general did not give it enough attention. He concluded that attention should also be drawn to the occurrence of "rogue" gears, with a high noise level, owing to statistical chance.

6.12 SURFACE ROUGHNESS RELATED TO SCUFFING RESISTANCE

In 1971 Dowson and Whomes (18) with a relatively simple analysis using the Martin theory for rough cylinders were able to show that when surfaces such as rollers were cylindrically ground there is an improvement in the lubricating conditions over those for smooth rollers. Load capacity, horizontal force and surface traction all increase with increasing roughness, but since the load capacity increases most rapidly, the coefficient of fric-

tion falls. This obviously only occurs up to a certain point, after which conditions deteriorate. The analysis was able to support previously obtained results on rough rollers (19). However, the present author found that under the more severe conditions occurring in the disc-machine, the scuffing failure load was quite strongly influenced by surface roughness. But, with the opposite results, as will be shown later.

6.13 MODAL ANALYSIS OF THE SYSTEM RESPONSE

Mahalingham and Bishop (20) returning to the problem of the dynamic loads on gear teeth, were able to obtain the response of the system to dynamic loads, using a modal analysis. It was shown that this could also be applied to a cam-follower system. Finally they used a numerical example and for it were able to calculate the natural frequencies, and principal modes. Investigating the case of resonance in the highest mode of free vibration they were able to calculate the dynamic torque on the gear shafts.

6.14 CONCLUSIONS

From the above papers it is apparent that gears are always subjected to internal or external dynamic load. Gregory, Harris and Munro showed that at any level of loading, the gears could experience peak loads of up to 2¼ times design value. The same authors also showed that in general much more damping is provided in a gear-box than could be estimated by calculation and this had

probably helped to prevent failures in gearboxes before they were designed with dynamic loads in mind.

Bishop had shown that resonance between gears and drive shafts could, however, increase the effect of gear tooth errors considerably. In a set of gear driven centrifugal compressors the Q factor at resonance was approximately 40 for any gear error. The problems of resonance had been previously highlighted by Johnson at the 1958 International Conference on Gearing.

By the later 1960's the approach to theoretically analysing gear tooth errors changed. In early work by Buckingham and Reswick the situation of a single high or low tooth entering the contact was investigated. Alternatively the effect of a high spot on a tooth face was analysed. In later work the gear pair were considered to be subject to a continuously varying transmission error and that a perfect tooth did not exist. This was analysed as a Fourier series by workers such as Welbourn. Mahalingham and Bishop used a Modal analysis to obtain the response of the system to dynamic loads.

It was obvious that the application of a dynamic load to the discs whilst they were running would produce more realistic operating conditions. However at this stage it was uncertain as to the effects which would result from this. But it did appear that at one or more frequencies there was likely to be a change in load carrying capacity. Part of the reason for the uncertainty in knowing what results to expect lay in the lack of previous research in the field. Though work had

been undertaken analysing the dynamic loads on gears and similar lubrication conditions, no-one had applied a damaging dynamic load at a known frequency. It was hoped to be able to run the disc machine under an unsteady load, both the amplitude and frequency of which were controlled.

CHAPTER SEVEN

DYNAMIC LOADING TESTS, EXPERIMENTAL DETAILS

7.1 INTRODUCTION

This chapter looks at the experimental procedures used in carrying out dynamic loading disc machine tests. The results are presented in the next chapter. Parts 7.2 to 7.5 describe the modifications made to the disc machine to enable it to operate under dynamic loading. Sections 7.6 to 7.14 discuss the various test procedures used in testing. Finally parts 7.15 to 7.20 look at ancillary measurement techniques.

The modifications by Macpherson (3), whereby he installed a floating plunger in the left-hand spigot of the disc machine, resulted in the discs running under steady loading conditions. This is the condition in which the machine has been operated subsequently. Furthermore, in other work (41) and (42) on test gears and other mechanically loaded disc machines, trouble has been taken to ensure that fluctuations between the gear teeth or discs do not occur. In practice the load on gear teeth fluctuates appreciably, as discussed in the literature survey in Chapter Six, consequently it was thought that these conditions were unrealistic and probably yielding optimistic results.

In the disc machine load between the discs is directly proportional to the pressure in the high pressure oil system. Accordingly, if the pressure could be made to fluctuate then this would simulate a vibrating load upon the gear teeth. The easiest method of obtaining a fluctuating pressure is to use a solenoid controlled bleed-off valve, called a servovalve.

Diagram of Servovalve and Connections

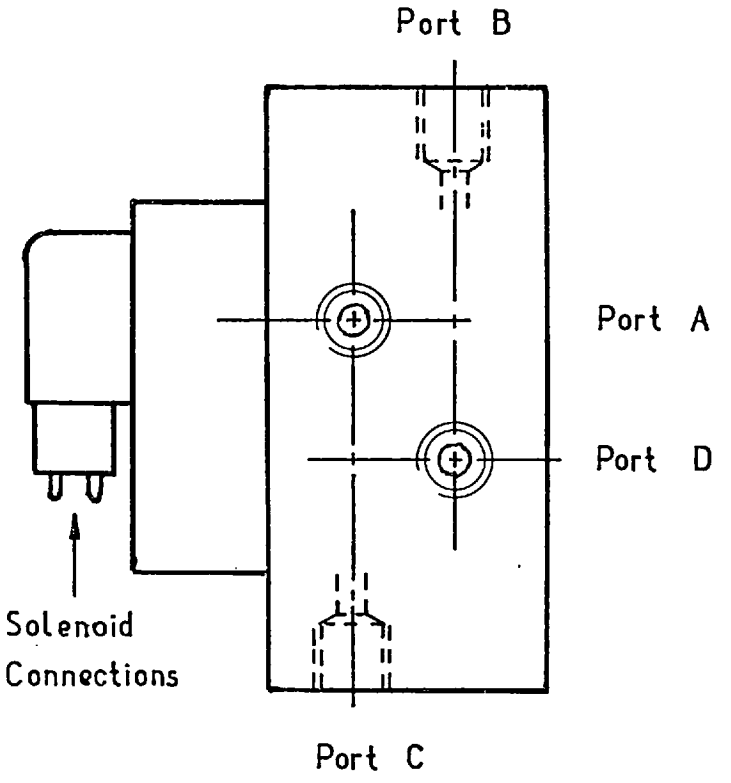


FIGURE 7.2

7.2 DESCRIPTION OF THE SERVOVALVE

The servovalve was Dual Input Servovalve (produced by Moog Servocontrols Inc.) having two high pressure inlets, though only one was used, and two outlets. When no voltage was supplied to the solenoid connections on the servovalve, the oil supplied to port A emerged unaffected through port B. However when 15 Volts were supplied to the connections they caused the solenoid to operate a two-stage valve which resulted in a proportion of the oil emerging from port C. This continued until the 15 Volts were disconnected. The proportion of the oil which could be by-passed could be varied between 0 and 25%, by means of a balance screw on the two stage valve. Thus the pressure of the outlet was equal to that of the input when no electrical signal was supplied to the valve and could be controlled between 75 and 100% of the input when 15 Volts were applied. This occurred at any of the pressures at which the valve was used. Further the valve would hydraulically follow an electrical signal at frequencies from 0 to 60 Hertz, though at the high frequencies only 10% of the oil could be by-passed if instability was to be avoided. Although it would have been preferable to have studied frequencies higher than 60 Hertz including up to those of blade vibrations, the present servovalve was not able to operate at these higher frequencies.

7.3 USE OF THE SERVOVALVE ON THE DISC MACHINE

Figure 7.3a shows a schematic diagram of the lay-out of the electrical and hydraulic circuits connected with

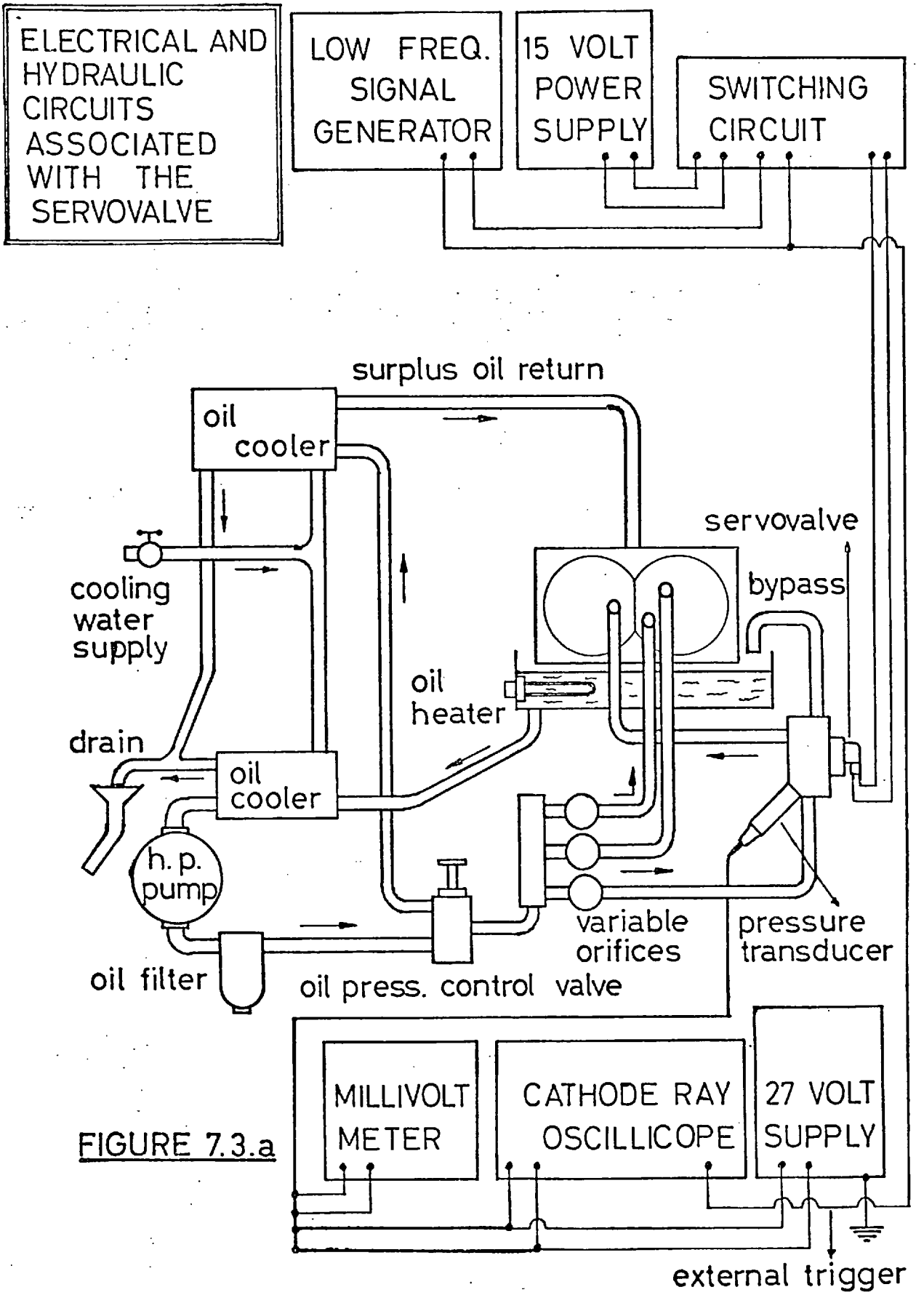

ELECTRICAL AND HYDRAULIC CIRCUITS ASSOCIATED WITH THE SERVOVALVE
LOW FREQ. SIGNAL GENERATOR
15 VOLT POWER SUPPLY
SWITCHING CIRCUIT
surplus oil return
oil cooler
servovalve
bypass
cooling water supply
oil heater
drain
oil cooler
h. p. pump
variable orifices
pressure transducer
oil filter
oil press. control valve
MILLIVOLT METER
CATHODE RAY OSCILLICOPE
27 VOLT SUPPLY
external trigger

FIGURE 7.3.a

the servovalve.

Figure 7.3b shows a general view of the rig and electrical equipment to operate the servovalve. The oil flow circuit is as follows:- The header tank has a capacity of just over 1 gallon, contains a 3 KW heater, and is located beneath the housing for the discs. Oil flows from it through a large water cooled oil cooler and thus to the high pressure pump which had a rated outlet pressure of 2,5000 psi. at a flow rate of 2½ gallons/ minute. A Fairey high pressure oil filter with a nominal maximum particle size of 5 microns was used to clean the oil, and the outlet pressure to the discs was controlled by a large, calibrated, mechanical pressure-relief valve. The bypass from this valve was fed through a small water-cooled oil cooler and used to splash lubricate the two discs. The temperature after the cooler was measured by two thermocouples. Adjustment of the flow rates to the three oil pockets, to produce a self-stabilising load system was provided by the adjustable orifices.

From here it flowed directly to the two right hand pockets via flexible hoses. For the left-hand pocket the oil flowed via the servovalve and a flexible hose. The operation of the servovalve was as outlined above, but just downstream from it a Pye-Ether Strain Gauge Bridge Pressure Transducer was used to obtain the instantaneous value of the oil pressure. Figure 7.3c shows the installed pressure transducer and servovalve.

The power supply for the pressure transducer was three 9 volt batteries mounted in a screened case. The

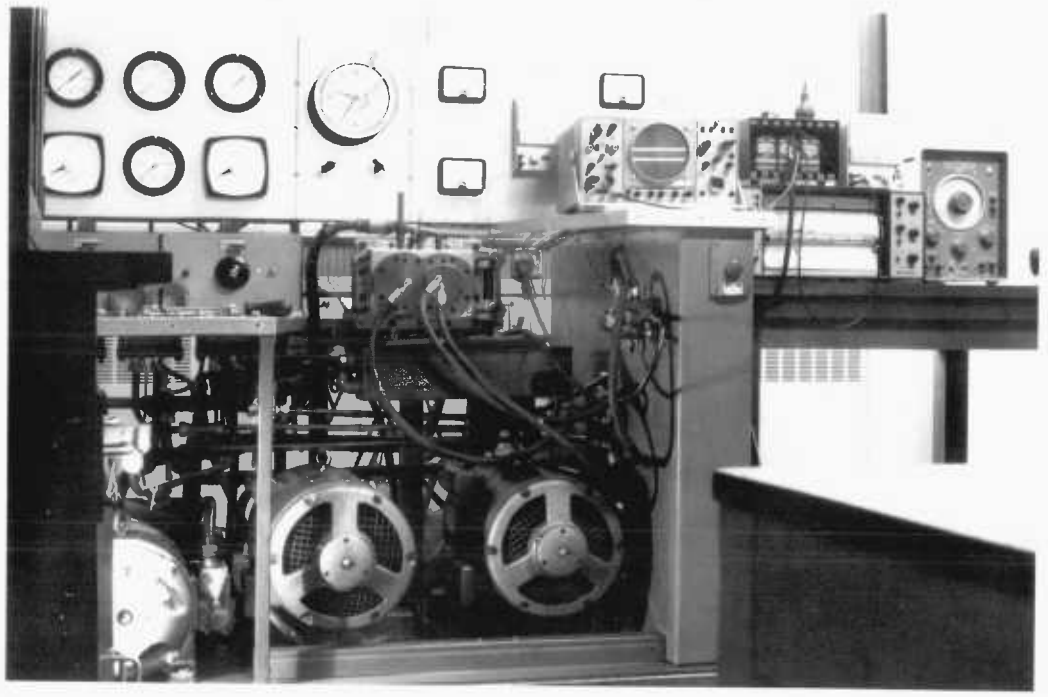


Figure 7.3b. View of the Rig and Electrical Equipment.

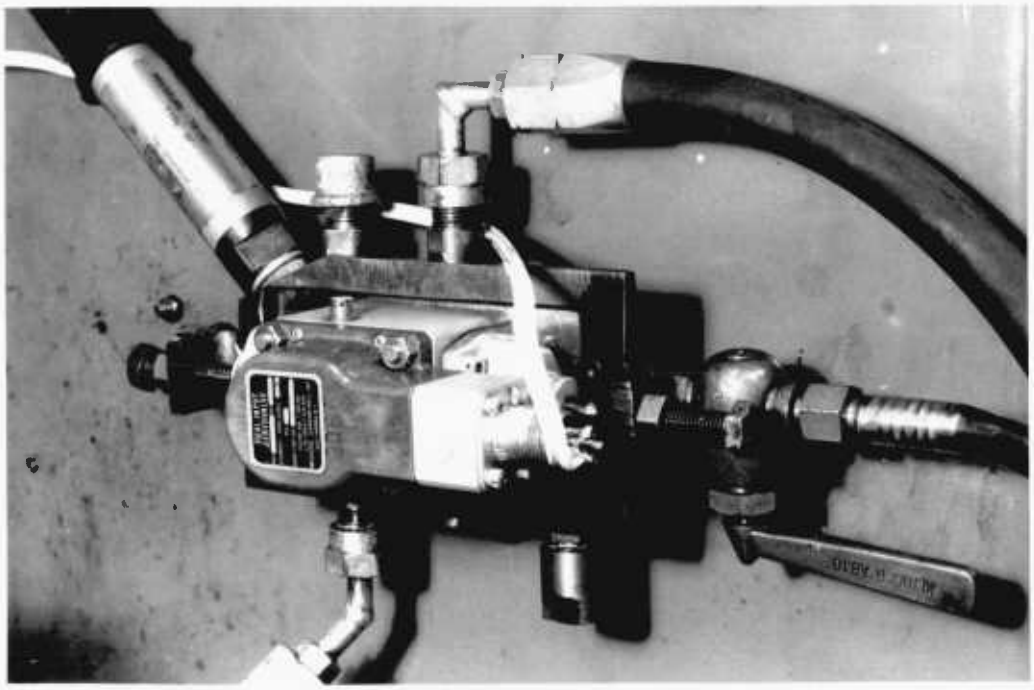


Figure 7.3c. The Servo-Valve and Pressure-Transducer.

output from the transducer found to be 0.66 mV per 100 lbf./in^2., was sufficient to produce a satisfactory trace on a cathode ray oscilloscope. The output from the pressure transducer was also fed to a Comark millivoltmeter so that the mean output pressure could be measured at any time. A strain-gauge bridge pressure transducer was used as opposed to a piezo-electric type, as the former produced an output which was independent of rate of change of pressure and was thus easily calibrated. The response time was more than adequate as the resonant frequency was over 10 kHz.

To provide the electrical signal to switch the servovalve a Marconi Low Frequency signal generator was used, which covered the anticipated frequency spectrum and could produce sine, saw tooth or square waves. As the output was only 8 volts an amplifier was required to boost this signal to the 15 volts required by the servovalve. At this stage a 15 volt (output) signal generator was borrowed, and after a few experiments it was realised that for the initial testing the only signal required was square waveform. This arose because the natural damping in the hydraulic circuit to the left-hand disc resulted in the pressure waveform being milder than the electrical signal. Thus even with a square wave electrical signal the hydraulic waveform was more rounded (see Appendix 12 and Figures 12a, 12c, 12e, 12g, 12i and 12k taken from the pressure transducer). It was decided that the pressure changes when sine wave electrical signals were used were too mild for an initial examination programme. Saw tooth or ramp waveforms

were eliminated as being rather more difficult to control and analyse. Though a reasonable response to the drop in the waveform was obtained, the linear increase in electrical signal was not matched hydraulically.

As only square waves were needed for the servovalve this meant that the 8 volt signal generator would be perfectly adequate if used with a 15 volt power supply and a switching circuit.

A switching circuit was designed and built. The servovalve could now be used with the disc machine. Figure 7.3d shows a view of the auxillary electrical equipment connected with the servovalve.

7.4 CALIBRATION AND USE

The pressure transducer was calibrated from 0 to 2,500 lbf/in^2. and was found to be linear with no detectable hysteresis. Since installation it has functioned correctly without drift.

The servovalve was originally bench tested by Westland Helicopters and has performed as expected. Experience is necessary in using it as it becomes unstable at frequencies greater than 40 Hertz if attempts are made to by-pass more than 10% of the oil flow. It ceases to oscillate and remains in the by-pass mode. Several tests were ruined by this failure in the early stages of the work. In order to determine the percentage of oil by-passed the oscilloscope was used to monitor the reading produced by the pressure transducer. With the oscillo-

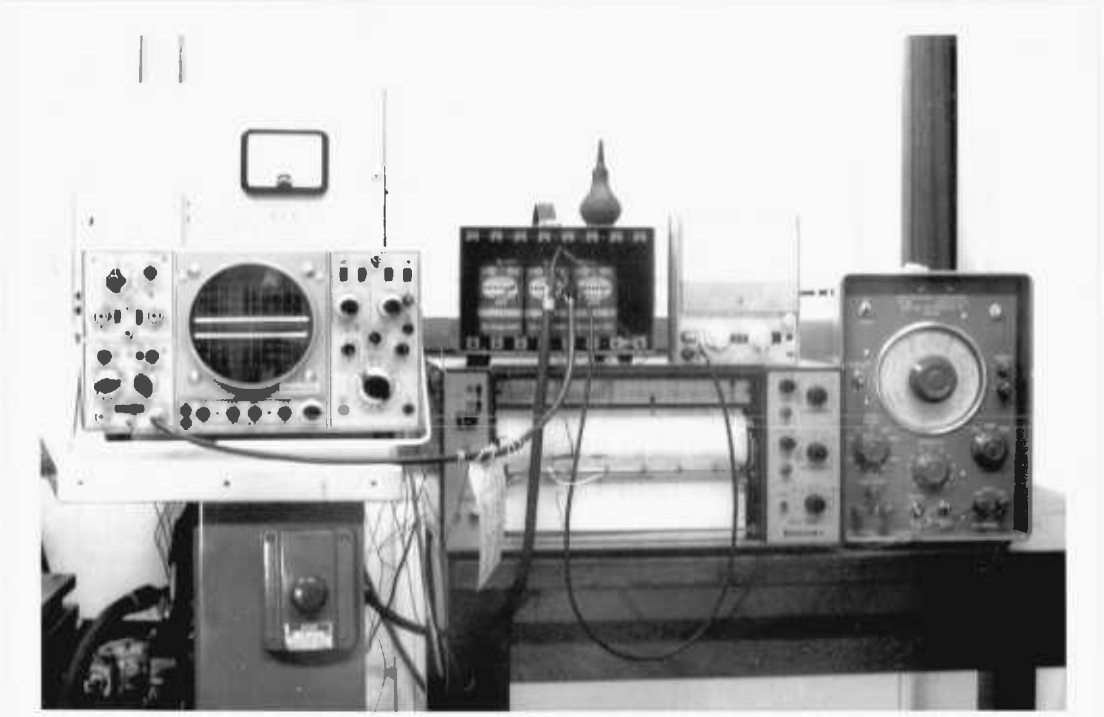


Figure 7.3d Ancillary Electrical Equipment

scope set on AC input the display showed the pressure fluctuations (see Figure 7.3 for a typical waveform), and thus having calibrated the transducer one could adjust the by-pass with the balance screw on the servovalve.

When raising the pressure from one stage to the next during a test the valve would continue to function, but would by-pass a slightly lower percentage, thus requiring adjustment with each load stage. However it was found to be very consistent with time and could be left unaltered on the occasions when it was in use during a pitting test.

The frequencies of the signal generator were checked with the oscilloscope and found to be accurate within the accuracy of the measurement. The vertical scale of the oscilloscope was checked by comparison with the readings on the millivoltmeter. To facilitate ease of viewing, the oscilloscope was triggered by a connection to the signal generator, thus producing a stationary display showing the oil pressure waveform.

This meant that the hydrostatic disc machine could now be run whilst the discs were experiencing a fluctuating load, both the amplitude and frequency of which could be controlled.

7.5 ALTERATION OF THE STANDARD TEST PROCEDURE WHEN USING THE SERVOVALVE

When the servovalve was incorporated into the test procedure the alterations to the standard test were as follows.

At the 400 lb. load stage the signal generator,

15V power supply, switching circuit, oscilloscope, millivoltmeter and 27 volt supply were switched on. However, as the balance control on the servovalve had been previously adjusted to the end of its travel, no oil was by-passed. The millivoltmeter showed the mean oil pressure in the pipe supplying the left-hand disc. The trace on the oscilloscope showed the fluctuations in the oil pressure caused by the oil pump, though these were less than $\pm$ 1% of the mean level.

The signal generator was set to the frequency applicable for the test, and the position of the balance control adjusted until the desired percentage of the oil was by-passed (usually 10%, but occasionally 25%). The amplitude and shape of the resulting pressure waveform was visible on th oscilloscope. The test was now run as in a standard test except that after raising the pressure between load stages the balance control was adjusted to maintain the by-pass ratio. This type of test with disc speeds of 1100 and 500 r.p.m. and an oil inlet temperature of 50^{o}C was designated as a Type B test. (The standard test, and Type A test were described in Chapter 2).

7.6 VARIATIONS ON THE TYPE B TEST

As will be shown in Chapter 8 and discussed in Chapter 9, one of the most interesting results arising from the use of the servovalve is that the scuffing load, using Type B test procedure is dependent upon the frequency of load fluctuations. To investigate this effect further a number of other test procedures were employed, which established the vibrating system as in Type B tests, but varied successively.

(a) Applied load frequency for pitting and scuffing under a dynamic load.

(b) Mean disc speed.

(c) Slide/roll ratio.

(d) Amplitude of applied load vibration.

(e) Disc surface roughness.

These test procedures were designated Types C to M, and were as follows.

7.7 TYPE C TEST

To examine whether the vibrations affected the pitting life of the discs three tests were run at a load of 760 lbf., with $\pm$5% load fluctuations at 15 Hz. Very careful running-in was ncecssary, with the discs at a steady load, to prevent immediate scuffing.

Pitting was detected by noting:-

(a) an increase in friction, or

(b) a change in the disc surface temperature.

At intervals the discs were removed for examination under a microscope, as occasionally the formation of pits could pass undetected.

7.8 TYPES D AND E TESTS

These were conducted under conditions identical to Type B, except that the mean disc speeds were altered by 25% to 1000 and 600 r.p.m. respectively.

7.9 TYPES F, I AND J TESTS

Types F, I and J tests were all conducted at disc speeds chosen to make the slide/roll ratio 0.259. This was the minimum value at which scuffing could be achieved by the disc machine using a mean disc speed of 800 r.p.m. The tests had mean disc speeds of 675, 800 and 1000 r.p.m. respectively.

7.10 TYPE H TESTS

Type H Tests examined the effect of surface roughness on the failure loads under a steady or fluctuating load. For this series, the surface roughness was between 16 and 20 μ ins. C.L.A., as opposed to the normal value of between 8 and 12 μ ins. C.L.A.

7.11 TYPE K TESTS

At the termination of Type J tests a large range of mean disc speed had been covered at slide/roll ratios of 0.375 and 0.259. To provide further data the intermediate slide/roll ratio of 0.318 was also tested. The most pronounced variations in scuffing load had been obtained when the oil film thickness was low, so a mean disc speed of 600 r.p.m. was used.

7.12 TYPE L TESTS

A series of five Type B tests were conducted with

amplitude fluctuations of $\pm$ 12½%, and designated as Type L. Time did not permit a full range of tests to be conducted at two levels of vibration. For the remainder of the tests a vibrational level of $\pm$ 5% was used, as the analyses in Chapter Six indicated that this was reasonable.

7.13 TYPE M TESTS

The aim of this series was to run tests in which the applied pressure waveform was independent of frequency. When this was a variable the results at different frequencies could not necessarily be directly related. This will be discussed again in Appendix Twelve, when a Fourier analysis of the waveforms is computed. It was thought that these vibrations were produced by the servovalve. In practice the flexible pipe from the servovalve to the disc-machine was flexing with each pressure change. This was the reason the valve could not function above 60 Hz. It also caused the "rounding" of the waveform at higher frequencies.

Subsequent to consultations with Dowty Hydraulics, the servovalve was repositioned on the disc housing itself (see Figure 7.13). It was now feeding into a small "rigid" volume and a considerable improvement in the frequency response was obtained. A very consistent waveform was obtained between 5 and 100 Hz.

7.14 TABLE OF TEST CONDITIONS

See over.

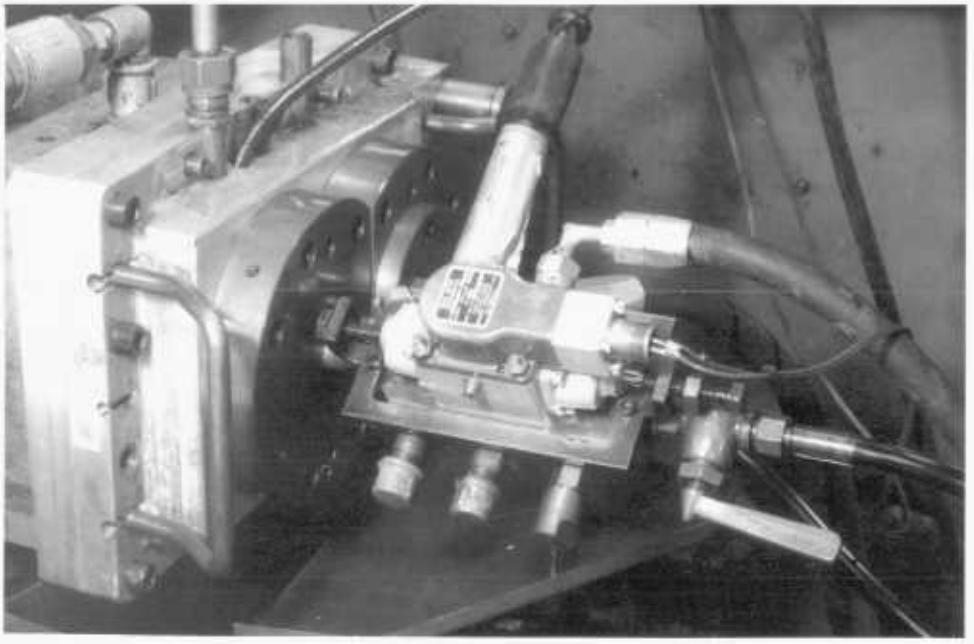


Figure. 7.13 Servovalve Mounted Directly on the Disc Machine

Table 7.14 Test Conditions

Type of Test	S/R Ratio	Mean Disc Speed r.p.m.	Surface Roughness μ ins. C.L.A.	Vibration Amplitude ± %	Comments
Standard Test	0.375	800	8-12	0	Reference
B	0.375	800	8-12	5	
C	0.375	800	8-12	5	Fatigue
D	0.375	1000	8-12	5	
E	0.375	600	8-12	5	
F	0.259	675	8-12	5	
H	0.259	1080	16-20	5	Surface Roughness
I	0.259	800	8-12	5	
J	0.259	1000	8-12	5	
K	0.318	600	8-12	5	
L	0.375	800	8-12	12½	Vibration Amplitude
M	0.375	800	8-12	5	Improved Waveform

7.15 OTHER EXPERIMENTAL DETAILS

The trailing thermocouples were located in "Araldite", but this tended to break up with use. Consequently there are no surface temperature figures for some of the tests.

The absence of torque figures from some of the tables of results was caused by drift in the zero of the pen recorder producing invalid readings.

Though readings were taken of the torque and disc surface temperature at five minute intervals during each test,

only the figures obtained immediately prior to scuffing are given in Chapter Eight.

7.16 TEST RESULTS AT FREQUENCIES BELOW 10 Hz.

The object of this section was to explain why only a limited number of tests were conducted at frequencies below 10 Hz.

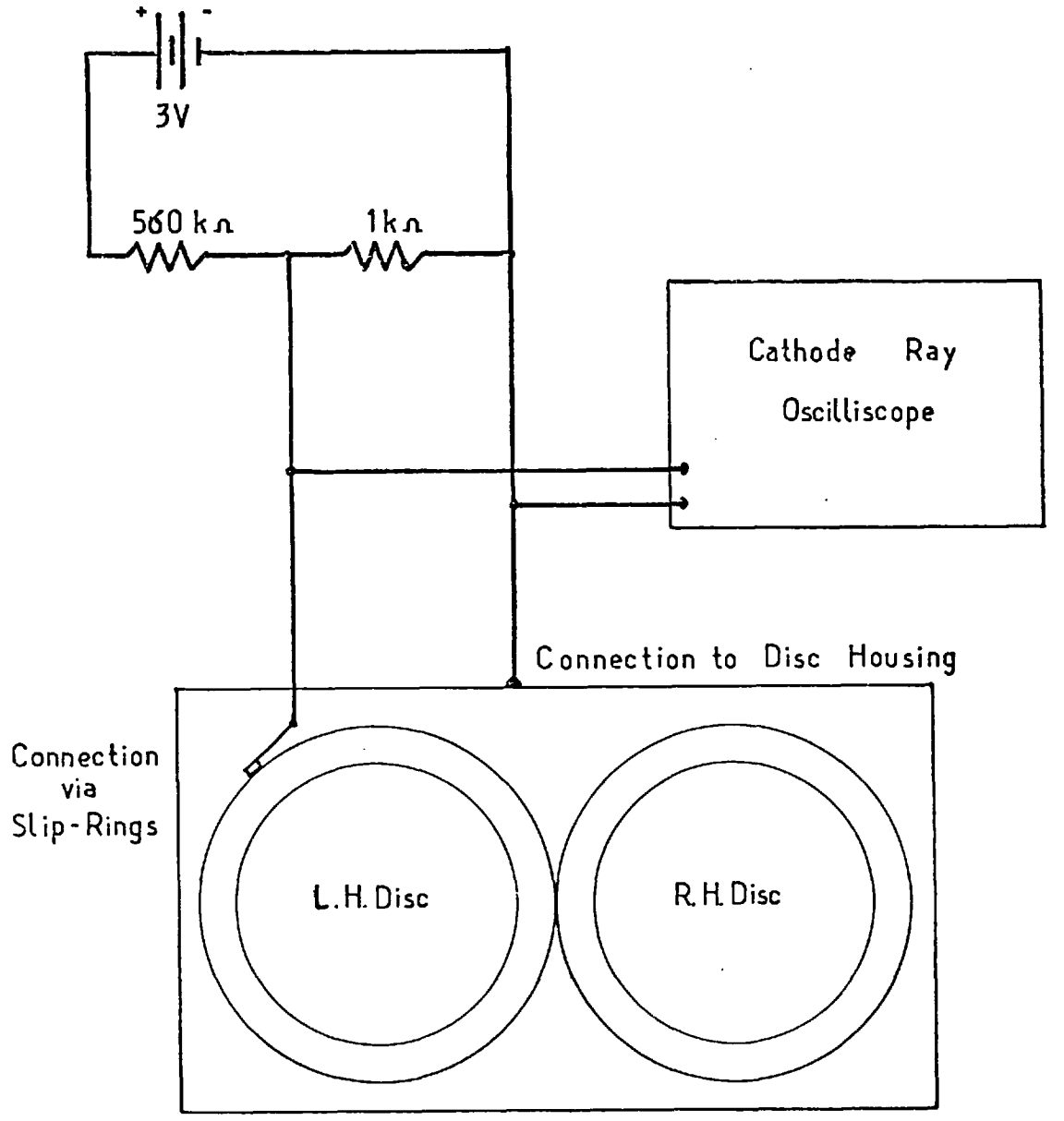
From the nine tests which had been run at 7½ and 5 Hz.it appeared that unless there was a reduction in the failure load at 10 Hz. it was unlikely that at 7½ Hz. the failure load would be less than that when there were no load fluctuations. When the applied load frequency was 5 Hz. a fall-off in load capacity had not been experienced. Accordingly it was decided that no further tests would be conducted at frequencies below 10 Hz. unless the failure load at this frequency was less than that obtained with a steady load.

7.17 ELECTRICAL MEASUREMENT OF ASPERITY CONTACT

An electrical investigation of asperity contact (87)was used as an additional tool to investigate the extent of metallic contact occurring during disc-machine tests. This was conducted as follows.

The ends and bore of a chamfered left-hand disc were ground so that it could be insulated from its surroundings by a layer of "Tufnol". An electrical contact was made with the disc and an insulated lead taken back to the slip rings. A second connection was made with the housing for the discs, which is in electrical contact with the right hand disc. 5mV was applied across the contact, the current being limited to 5 μ A, to prevent arcing. The circuit is shown in Figure 7.17.

FIGURE 7.17 Circuit for Electrical Investigation of Asperity Contact



The occurrence of asperity contacts was observed with an oscilloscope, as was the waveform from the pressure transducer. The discs were run at 1100 and 500 r.p.m. The load was held at 760 lbf., fluctuated at $\pm$ 5% and 15 Hz. with an inlet oil temperature of 50°C.

The results are given in Chapter Eight.

7.18 OIL FILM THICKNESS BY VOLTAGE DISCHARGE AND RESISTANCE TECHNIQUES

These two techniques were used to determine whether the average oil film thickness changed when a fluctuating load was used.

The two electrical circuits for this subsidiary work are shown in Figures 7.18a and 7.18b, and the corresponding results in Chapter Eight. The tests were run with pure rolling and an oil temperature of 50°C.

Resistance methods of measuring film thickness require pairs of resistors to be selected until the average voltage, displayed on the oscilloscope, across the contact is 7½ mV. At this point the contact resistance is the same as the resistance A in the voltage divider. Unfortunately the oil film resistance fluctuated so much that a steady value could not be obtained. Values were thus estimated to the nearest value of resistance A.

As the resistivity of the oil was unknown, an absolute value for the thickness of the oil film could not be calculated.

For the voltage discharge measurements, the variable resistor in Figure 7.18b was adjusted until the voltage across the fixed resistor, B, corresponded with a current of 2 amps.

FIGURE 7.18a Circuit Diagram for Measurement of Electrical Resistance of the Oil Film

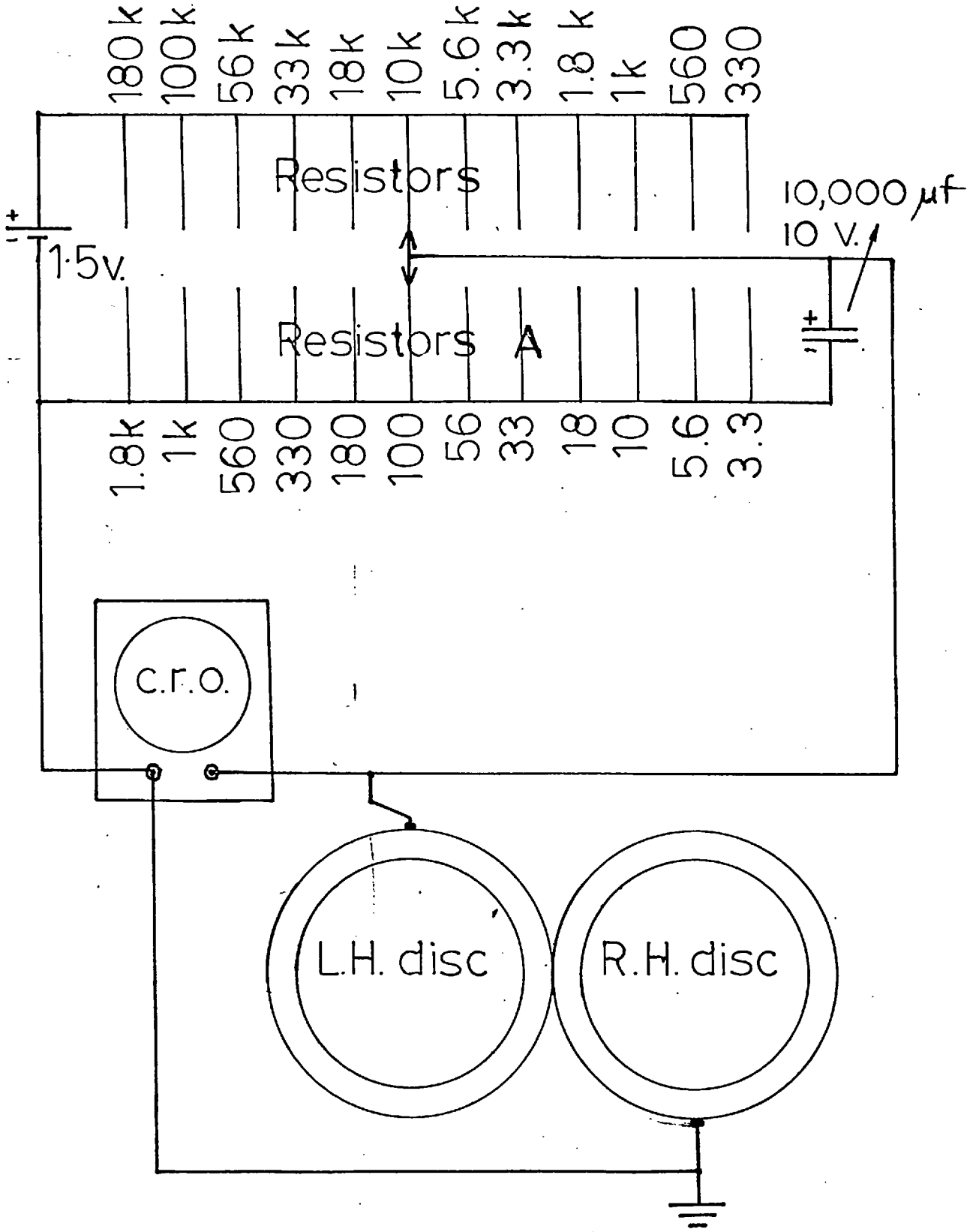
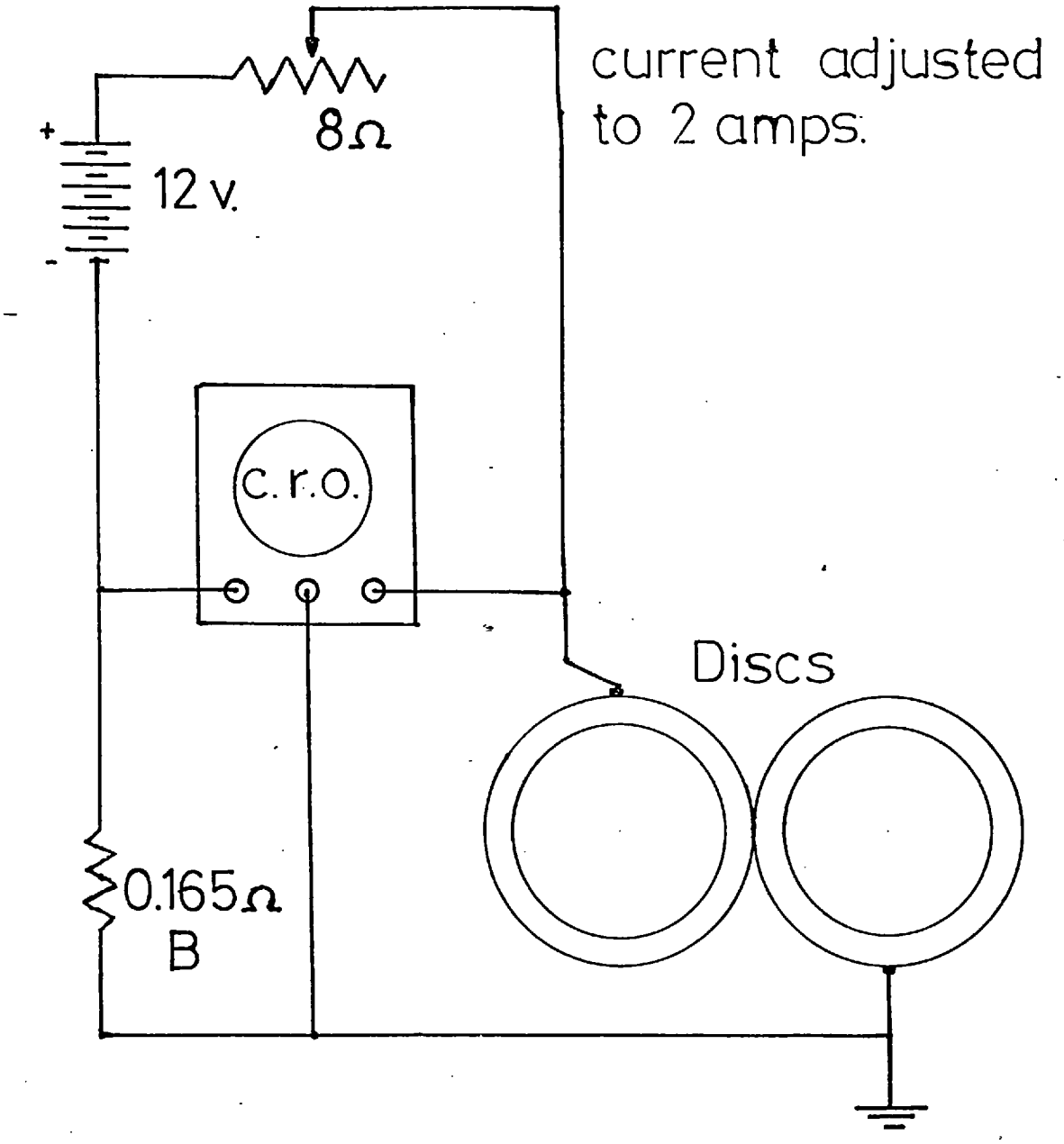


FIGURE 7.18 b Circuit Diagram for Voltage Discharge Measurement of the Oil Film Thickness



The voltage across the contact could then be seen on the oscilloscope. This fluctuated between approximately zero, as asperity interactions occurred, and a higher level, corresponding to a full film. The results are given in Chapter Eight.

7.19 TEST 224, EFFECT OF VIBRATIONS ON COEFFICIENT OF FRICTION

This test was conducted to examine the effect of the frequency of applied load upon the coefficient of friction for the contact.

The disc machine was operated as in a Type B test, at a mean load of 760 lbf. Whilst maintaining an amplitude ratio of $\pm$ 5%, the applied load frequency was swept up and down through the range from 2½ to 60 Hz. Readings were taken of the torque and are given in Chapter Eight.

7.20 TEST 224, EFFECT OF VIBRATION ON THE DISC SURFACE TEMPERATURE

This subsidiary work was undertaken to provide more accurate disc surface temperatures. As explained in section 2.3 the accuracy of the trailing thermocouples was approximately $\pm$ 5°C. To improve this the disc-machine was modified for infra-red disc surface temperature measurement.

The infra-red microscope used was very suitable as it had the following qualities:-

(1) Response time was 1 mS.

(2) Accuracy was $\pm$ 1°C.

(3) The spot-size of the area where the temperature was measured was 0.40 ins. diameter.

(4) Its optical system enabled it to be positioned and

focused exactly on the disc track.

Before it could be used it was necessary to do the following:-

(a) Machine the disc housing.

(b) Construct a cantilever structure to support the infra-red microscope.

(c) Evolve a method of wiping the excess oil from the disc surface, to leave a consistent thin film only.

(d) Calibrate the output from the infra-red microscope under running conditions, throughout the expected temperature range.

Figure 7.20 shows the disc machine plus infra-red microscope.

To investigate the effect of the frequency of applied load fluctuation Test 224 was conducted, as described in 7.19. The surface temperature measurements recorded during it are shown in Chapter Eight.

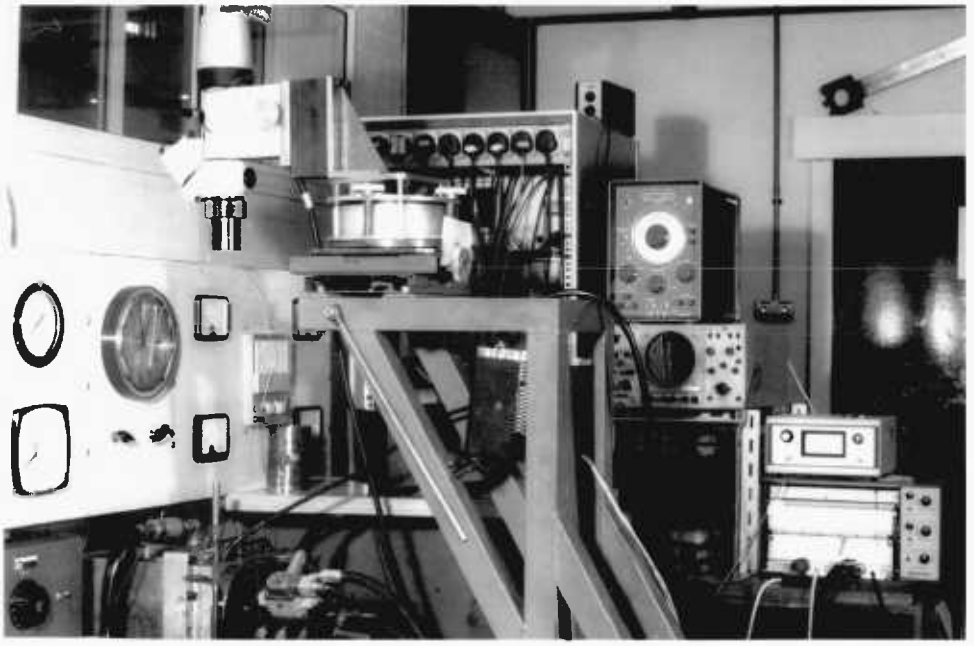


Figure 7. 20 Disc-Machine plus Infra-Red Microscope

CHAPTER EIGHT

THE RESULTS FROM TESTS WITH A FLUCTUATING LOAD

8.1 EXPLANATION OF FIGURES IN TABLES OF RESULTS

This chapter presents the results of the bulk of the test work carried out using the modified disc machine.

For convenience each of the columns of data was given a symbol and these are explained here.

ω The frequency of the applied load fluctuations in Hz.

L_s The load at which scuffing occurred. With a fluctuating load this is the mean value. In lbf.

T/L The torque in mV. and the load at which i was measured, which was usually that preceeding the scuffing load. Sometimes however the discs would fail just after a reading, as the load was being increased.

T1 The surface temperature of the high speed disc, as measured by the trailing thermocouple about ½ inch ahead of the contact. In ^{o}C.

μ The coefficient of friction for the contact just before failure, measured by the strain gauges on the torque arm of the slow speed disc. It is obtained knowing the geometry of the rig, the calibration of the torque trace (i.e. 1 mV. = 1.68 ft. lbf.) and the applied load.

T2 As T1, but for the slow speed disc. In ^{o}C.

h_o The minimum oil film thickness calculated from

$$h_o = (0.88)\ \alpha^{0.6}\ E^{0.03}\ \eta^{0.7}\ U^{0.7}\ R^{0.43}\ (L/W)^{0.13} \quad (24)$$

which was produced by Dowson and Higginson (38). C.G.S. units are used in this equation, and an inlet temperature of 50°C used. It should be noted that $U = U_1 + U_2$, and that the formula is for the case when both materials have the same value of E. In micro-inches.

p The Hertzian maximum contact stress obtained from reference (39)

$$p = (1.055 \times E \times W/(\pi \times L \times R))^{\frac{1}{2}} \quad (25)$$

In lbf./in.^{2}

TF The flash temperature rise in the contact calculated from (75)

$$TF = 2q\ (Bk/\pi)^{1/2}\ (1/(U_1^{1/2} + U_2^{1/2}))/K$$

Where B is the Hertzian contact width from

$$B = (32 \times W \times R/\pi \times L \times E)^{\frac{1}{2}} \quad \text{in cms.}$$

Both of the above equations use C.G.S. units and the flash temperature rise is in °C.

TT The total temperature in the contact. The sum of the calculated flash temperature rise plus the mean of the two disc surface temperatures. In °C.

8.2 DISC MACHINE TEST RESULTS

For the tests the oil used was to specification ENG. R.D. 2487. All the tests except Type L were run with a load oscillation amplitude of $\pm$ 5% about the mean.

8.3 TYPE B TESTS

Disc Speeds 1100 and 500 r.p.m.

Slide/Roll ratio 0.375.

Mean disc speed 800 r.p.m.

Test No.	ω Hz	Ls lbf.	T/L mV/lbf.	T1 °C	T2 °C	TF °C	TT °C	μ	h_o ins x 10^{-6}	p lbf x 10^3
23	0	1200							47.5	168
27	0	1200	4.4/1100	104	89	84	181	.049	47.5	168
1	0	1300	5.0/1200			93		.051	47.0	175
2	0	1300	4.6/1200			86		.047	47.0	175
22	0	1300							47.0	175
24	0	1300	4.8/1200	98	88	89	182	.049	47.0	175
28	0	1300	4.6/1200	102	89	86	181	.047	47.0	175
29	0	1300							47.0	175
26	0	1400							46.5	181
74	7½	1330	5.7/1235			106		.057	46.8	177
75	12½	1140		96	85				47.7	163
76	12½	1140	5.0/1045	91	81	98	184	.059	47.7	163
215	15	760							50.4	133
65	15	855	4.2/855			81		.061	49.6	142
66	15	855	4.3/855			83		.062	49.6	142
214	15	855							49.6	142
77	15	950		96	87				48.9	149
78	20	950	4.0/855			84		.058	48.9	149
79	20	1045							48.3	156
70	30	855	3.7/760			80		.060	49.6	142
69	30	950	4.4/855			91		.063	48.9	149
54	30	1140	4.0/1045			78		.047	47.7	163
218	40	1045							48.3	156
217	40	1140							47.7	163
67	60	1140	4.8/1140			86		.052	47.7	163
68	60	1140	4.7/1045			91		.055	47.7	163

Mean values of μ, steady running 0.049
fluctuating load 0.057

Mean value of h_o, micro-inches 480

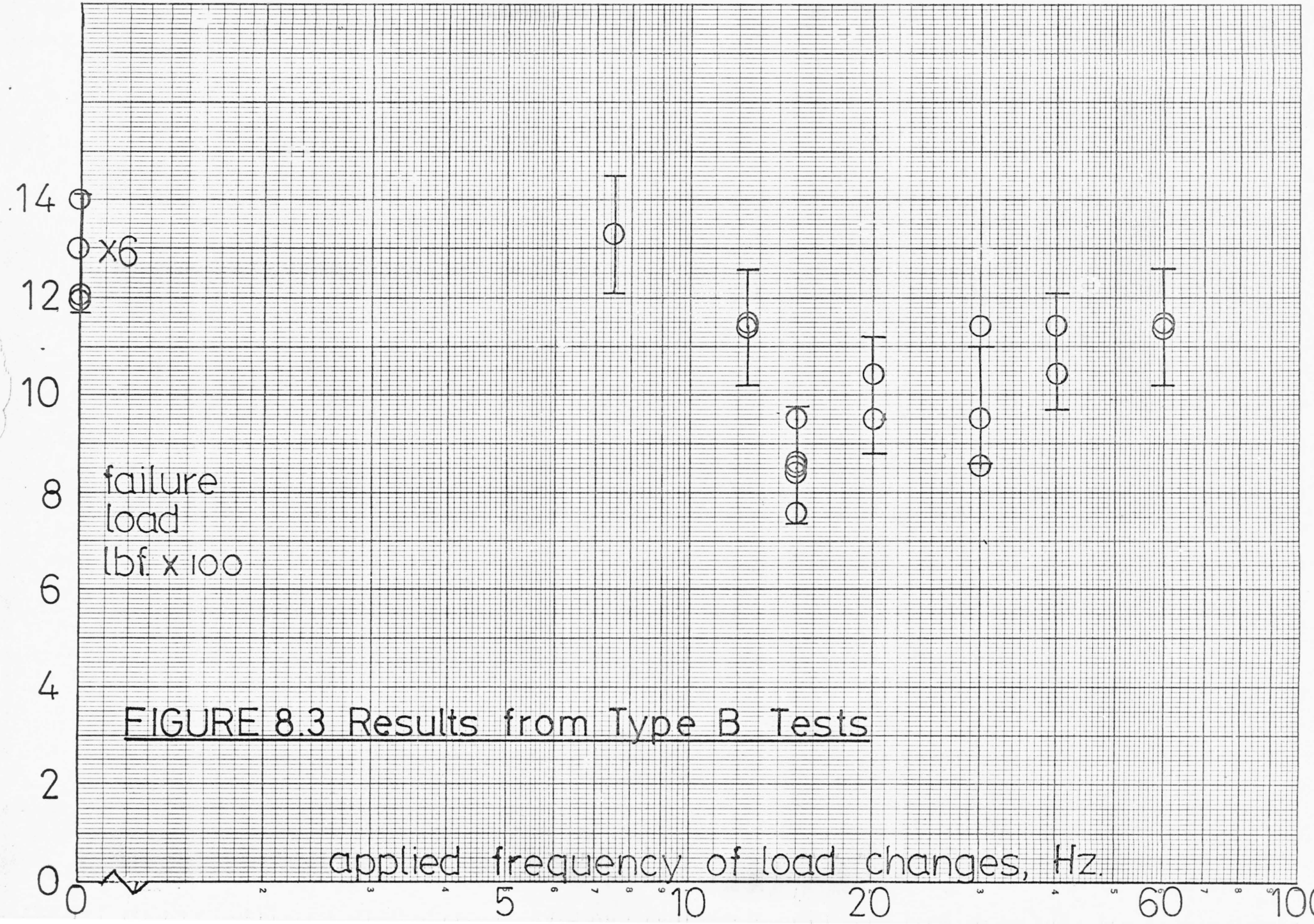


FIGURE 8.3 Results from Type B Tests

8.4 TYPE D TESTS

Disc speeds 1375 and 625 r.p.m.

Slide/Roll ratio 0.375

Mean Disc Speed 1000 r.p.m.

Test No.	ω Hz	Ls lbf.	T/L mV/lbf.	T1 °C	T2 °C	TF °C	TT °C	μ	h_o ins x 10^{-6}	p lbf x 10^3
90	0	1000		109	88				56.8	153
91	0	1200	4.5/1100	118	87	98	200	.051	55.5	168
201	0	1200							55.5	168
140	5	1045	4.7/950	116	103	106	215	.061	56.5	156
141	5	1235	5.7/1235			106		.057	55.3	170
120	7½	665	3.1/570	98	88	83	176	.067	60.0	125
121	7½	760		105	95				58.9	133
119	7½	1045	4.4/950	115	109	99	206	.057	56.5	156
99	10	760	3.2/665	97	81	81	170	.059	58.9	133
100	10	760	3.5/665	91	79	89	174	.065	58.9	133
85	15	665		98	86				60.0	125
101	15	665		89	75				60.0	125
84	15	950	4.4/855	115	95	101	206	.063	57.2	149
86	20	855		108	86				58.0	142
87	20	855	3.9/760	110	88	94	193	.063	58.0	142
88	30	855		107	81				58.0	142
89	30	950	3.9/855	106	83	90	183	.056	57.2	149
98	60	1140	4.8/1045	101	90	105	200	.057	55.9	163
97	60	1330	6.0/1235	109	96	122	224	.059	54.8	177

Mean values of μ, steady running 0.051
fluctuating load 0.060

Mean value of h_o, micro-inches 57.5

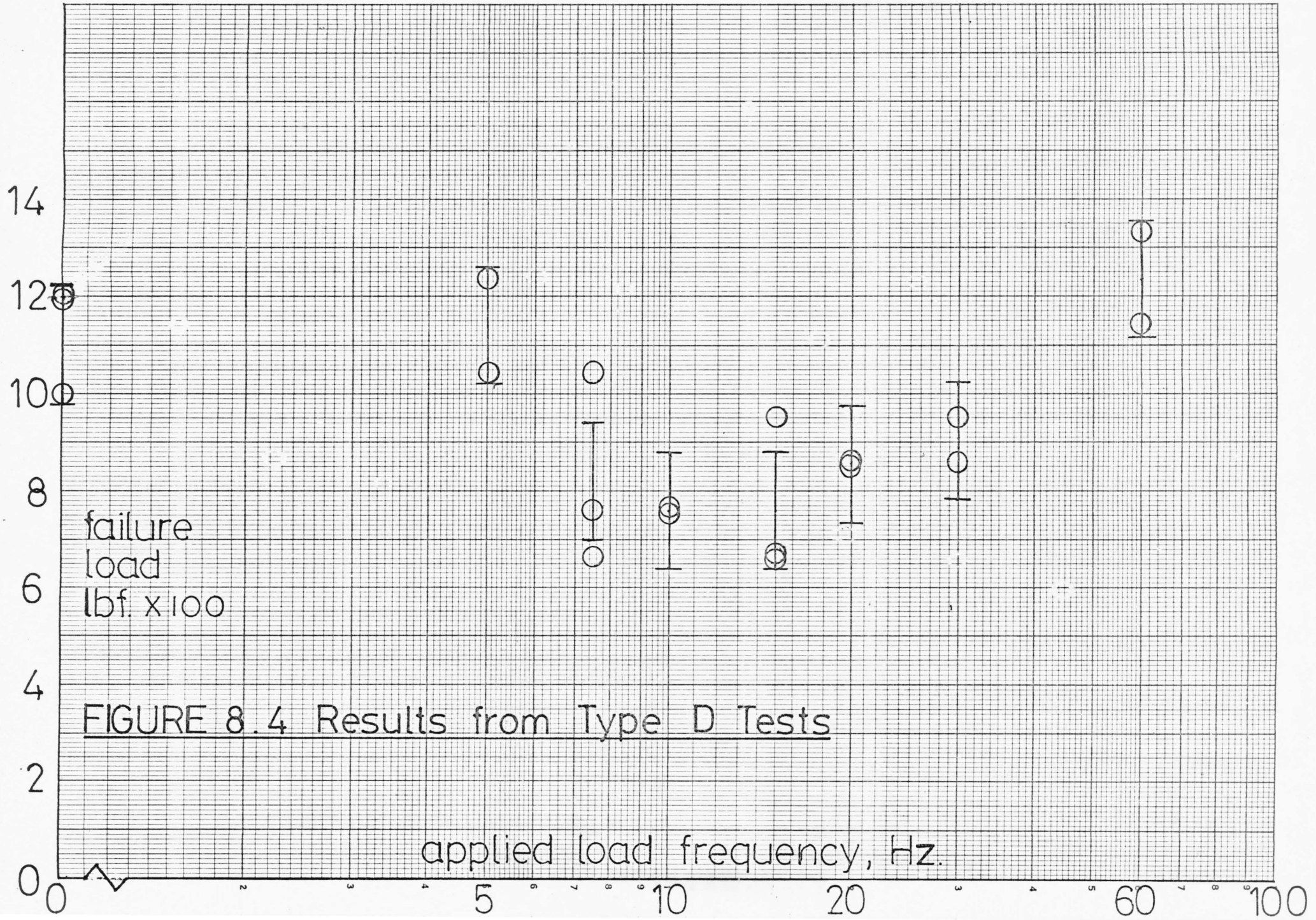


FIGURE 8.4 Results from Type D Tests

8.5 TYPE E TESTS

Disc Speeds 825 and 375 r.p.m.

Slide/Roll ratio 0.375.

Mean Disc Speed 600 r.p.m.

Test No.	ω Hz	Ls lbf	T/L mV/lbf.	T1 °C	T2 °C	TF °C	TT °C	μ	h_o insx10^{-6}	p lbfx10^3
105	0	1200	6.2/1100		81	105	192	.070	38.8	168
104	0	1400	7.3/1300	94	82	115	203	.069	38.0	181
204	7½	1330							38.3	177
117	10	1045	5.8/950	104	95	101	200	.075	39.5	156
113	10	1140		101	88				39.1	163
114	10	1235	6.1/1140	101	93	100	197	.066	38.7	170
118	10	1235	7.1/1235	105	97	108	209	.071	38.7	170
106	15	760			74				41.2	133
107	15	760	4.3/665			83		.079	41.2	133
108	20	1045	4.3/950			75		.056	39.5	156
109	20	1235	7.1/1140	104	87	117	212	.077	38.7	170
126	20	1425	6.9/1330	106	94	108	208	.069	38.0	183
124	30	1235	6.6/1235	108	96	100	202	.066	38.7	170
111	30	1235	5.9/1140	104	92	97	196	.064	38.7	170
110	30	1425	7.7/1425	108	96	113	215	.067	38.0	183
115	60	1235	6.4/1140	104	93	105	207	.069	38.7	170
125	60	1235	6.7/1140	98	89	109	202	.072	38.7	170

Mean value of μ, steady load 0.069
fluctuating load 0.069

Mean value of h_o, micro-inches 39.0

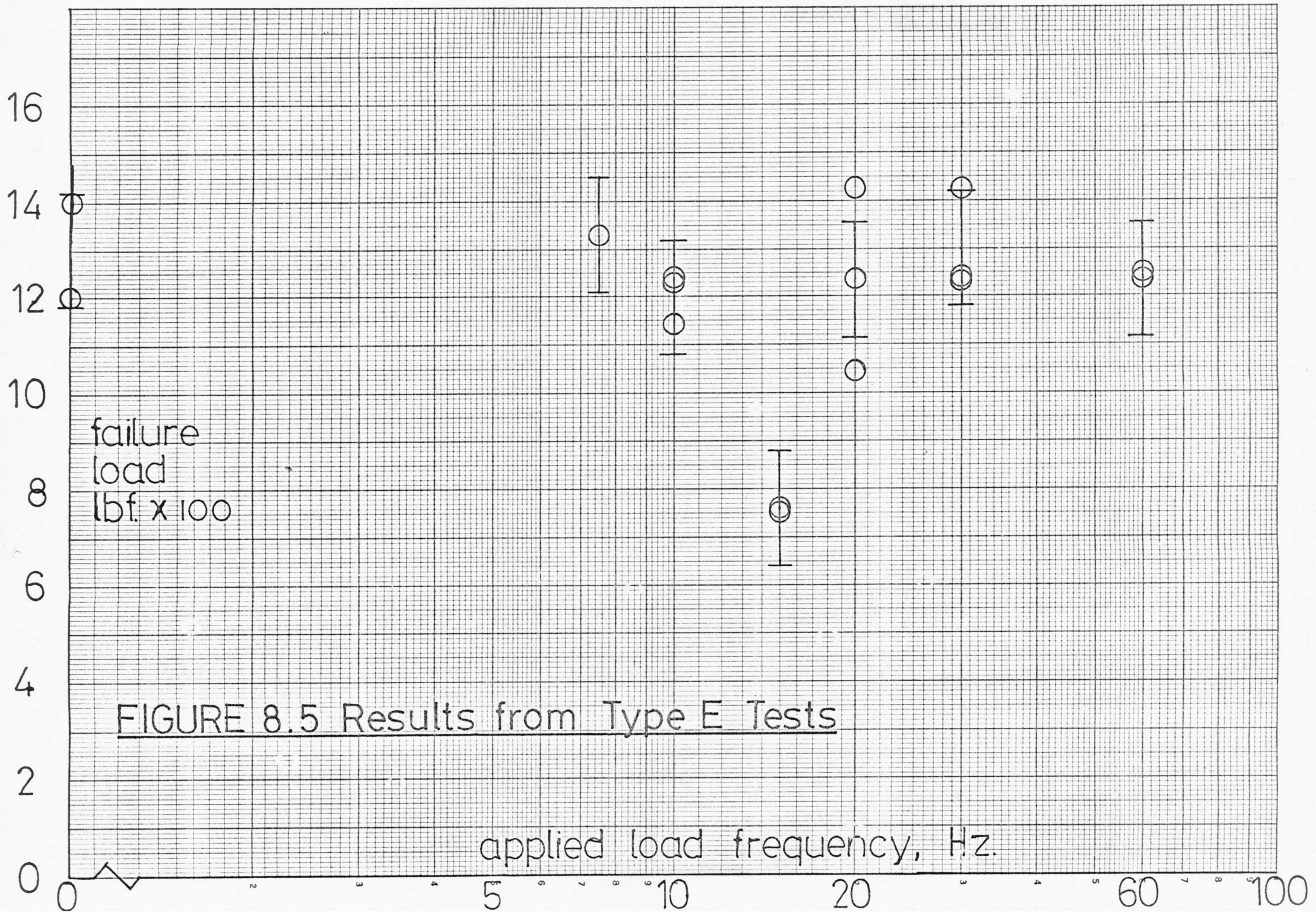


FIGURE 8.5 Results from Type E Tests

8.6 TYPE F TESTS

Disc Speeds 850 and 500 r.p.m.

Slide/Roll ratio 0.259.

Mean Disc Speed 675 r.p.m.

Test No.	ω Hz	Ls lbf.	T/L mV/lbf.	T1 °C	T2 °C	TF °C	TT °C	μ	h_o insx10^{-6}	p lbfx10^3
130	0	1800	9.4/1800	108	99	94	197	.064	40.0	206
129	0	1900	9.2/1800	107	95	96	197	.063	39.7	211
137	10	1710	9.4/1615	107	98	101	203	.072	40.2	200
132	15	1615		104	97				40.5	195
131	15	1710	9.4/1615	101	92	101	197	.072	40.2	200
133	20	1235		97	93				42.0	170
205	20	1425							41.2	183
134	20	1520	8.4/1425	103	91	94	189	.073	40.9	189
139	20	1615	9.1/1520	101	94	100	197	.074	40.5	195
219	25	1520							40.9	189
138	25	1805	10.0/1805	107	97	100	202	.068	40.0	207
135	30	1710	9.3/1615	102	92	100	197	.071	40.2	200
136	30	1710	9.3/1615	107	97	103	205	.073	40.2	200
128	60	1805							40.0	206

Mean values of μ, steady running 0.063
fluctuating load 0.072

Mean value of h_o, micro-inches 40.5

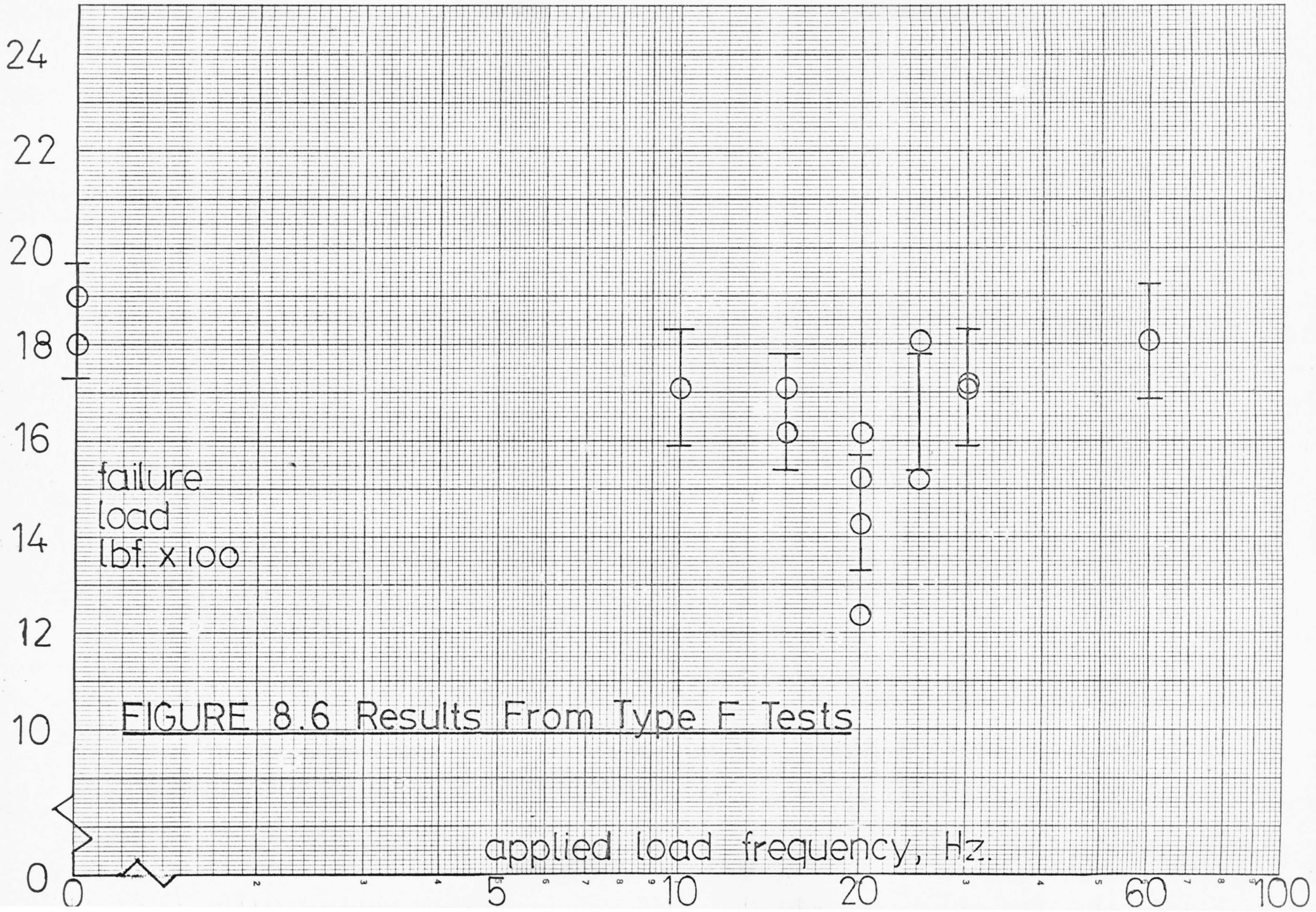


FIGURE 8.6 Results From Type F Tests

8.7 TYPE H TESTS

Disc Speeds 1360 and 800 r.p.m.

Slide/Roll ratio 0.259.

Mean Disc Speed 1080 r.p.m.

Test No.	ω Hz	Ls lbf.	T/L mV/lbf.	T1 °C	T2 °C	TF °C	TT °C	μ	h_o insx10^{-6}	p lbfx10^3
145	0	1900	9.2/1800			121		.063	55.2	211
202	0	1900	8.4/1800			112		.058	55.2	211
203	0	2000							54.8	216
206	10	1900	9.3/1800			123		.064	55.2	211
150	10	2090	9.5/2090			116		.056	54.5	221
148	15	1710	8.0/1615			109		.061	55.7	200
149	15	1900	9.6/1805			127		.066	55.2	211
146	20	1615	7.6/1520	121	106	106	219	.062	56.3	195
147	20	1805	8.8/1710	112	100	118	224	.064	55.5	207
151	30	1900	9.0/1805			120		.062	55.2	211
207	30	1995							54.8	216
152	60	2185	9.6/2185			116		.054	54.2	226
209	60	2185							54.2	226

Mean values of μ, steady running 0.060
fluctuating load 0.061

Mean value of h_o, micro-inches 55.1

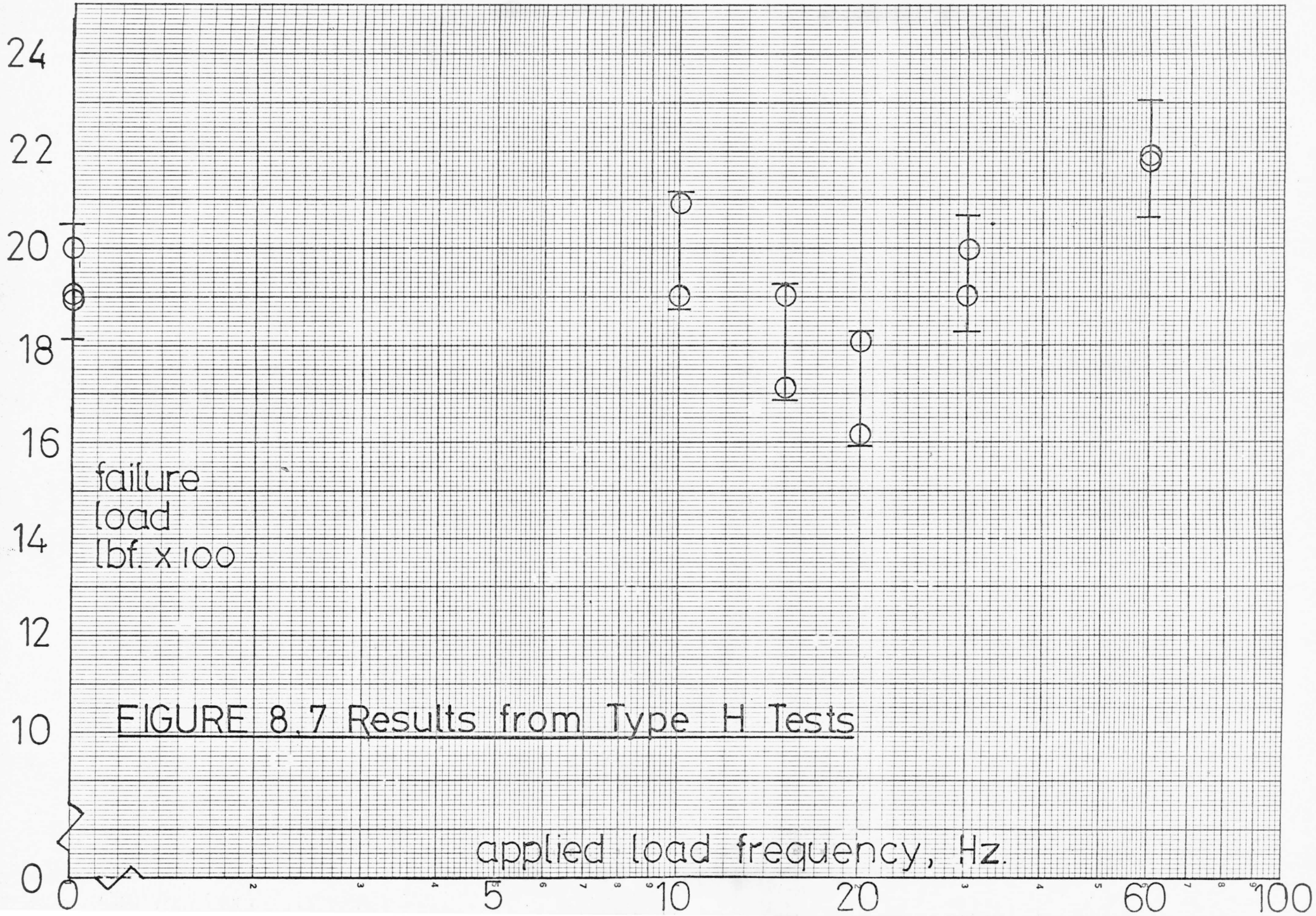


FIGURE 8.7 Results from Type H Tests

8.8 TYPE I TESTS

Disc Speeds 1007 and 593 r.p.m.

Slide/Roll ratio 0.259.

Mean Disc Speed 800 r.p.m.

Test No.	ω Hz	Ls lbf.	T/L mV/lbf	T1 °C	T2 °C	TF °C	TT °C	μ	h_o insx10^{-6}	p lbfx10^3
162	0	2300	8.3/2100			94		.049	43.6	232
161	0	2400	8.8/2300			93		.047	43.4	237
170	7½	1900	9.2/1805			104		.063	44.7	211
169	7½	2090	8.9/1995			100		.056	44.2	221
165	10	1710	8.9/1710			98		.064	45.3	200
168	10	1805	8.9/1805			97		.061	45.0	207
164	15	1805	9.3/1710			107		.067	45.0	207
180	15	1805	9.1/1805	104	93	99	197	.062	45.0	207
167	20	1900	8.6/1900			94		.057	44.7	211
166	20	1995	8.7/1900			98		.057	44.4	216
163	30	2280	8.8/2185			95		.050	43.7	231
172	60	2185	8.5/2090			92		.050	43.9	226
210	60	2375							43.4	236

Mean values of μ, steady load 0.048
fluctuating load 0.059

Mean value of h_o, micro-inches 44.3

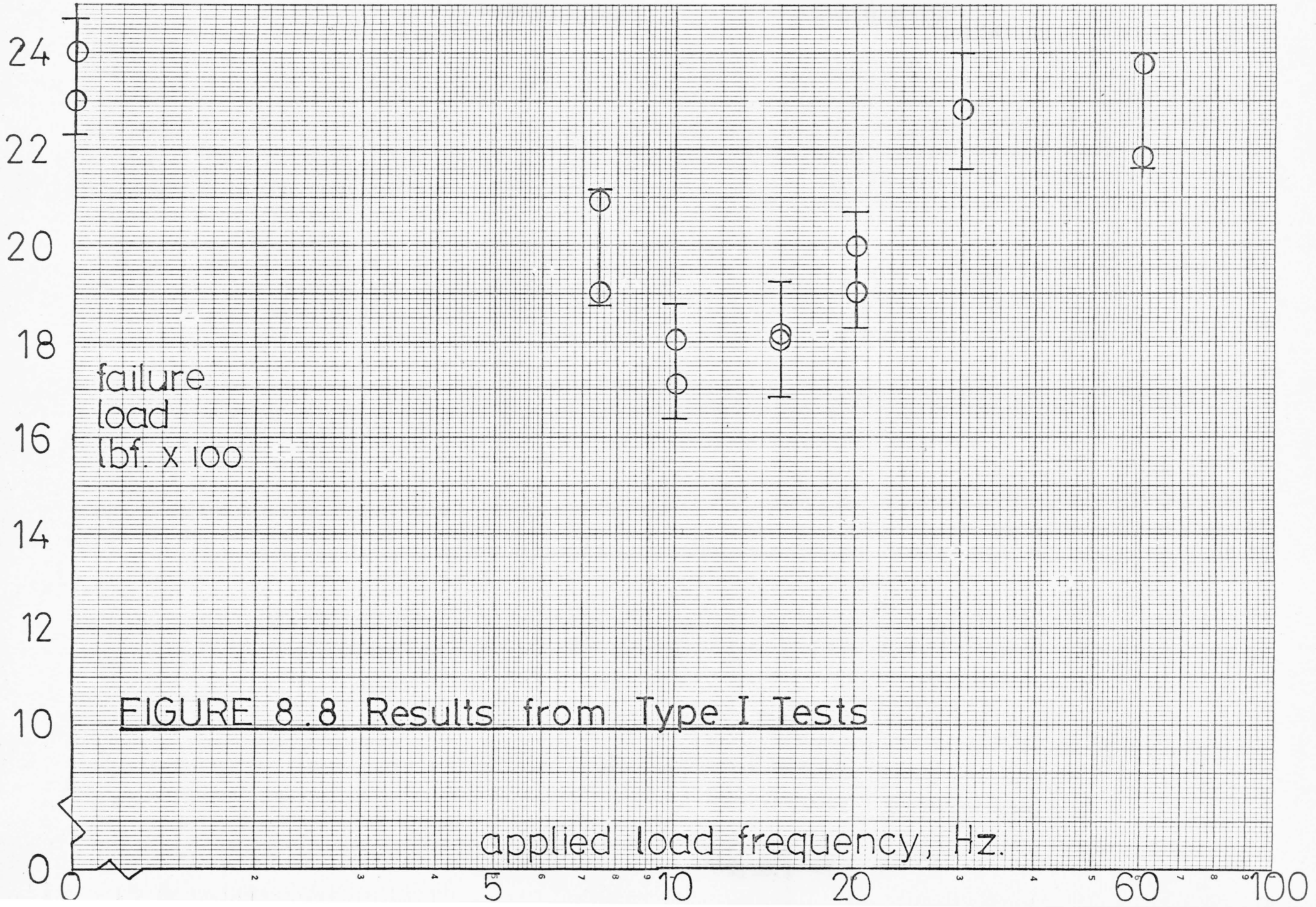


FIGURE 8.8 Results from Type I Tests

8.9 TYPE J TESTS

Disc Speeds 1260 and 741 r.p.m.

Slide/Roll ratio 0.259.

Mean Disc Speed 1000 r.p.m.

Test No.	ω Hz	Ls lbf.	T/L mV/lbf	T1 °C	T2 °C	TF °C	TT °C	μ	h_o insx10^{-6}	p lbfx10^3
173	0	2100	7.5/2000			92		.046	51.6	222
174	0	2100	8.4/2100			98		.049	51.6	222
176	10	2185	7.1/1995			91		.044	51.3	226
211	15	2185							51.3	226
212	15	2185							51.3	226
177	15	2375	8.9/2280	108	97	105	207	.048	50.8	236
175	20	2090	7.5/1995			92		.046	51.6	221
178	30	1995	8.4/1900	109	100	106	210	.055	51.9	216
179	60	1995	9.1/1900	112	103	112	219	.059	51.9	216
213	60	2090							51.6	221

Mean values of μ, steady load 0.047
fluctuating load 0.050

Mean values of h_o, micro-inches 51.5

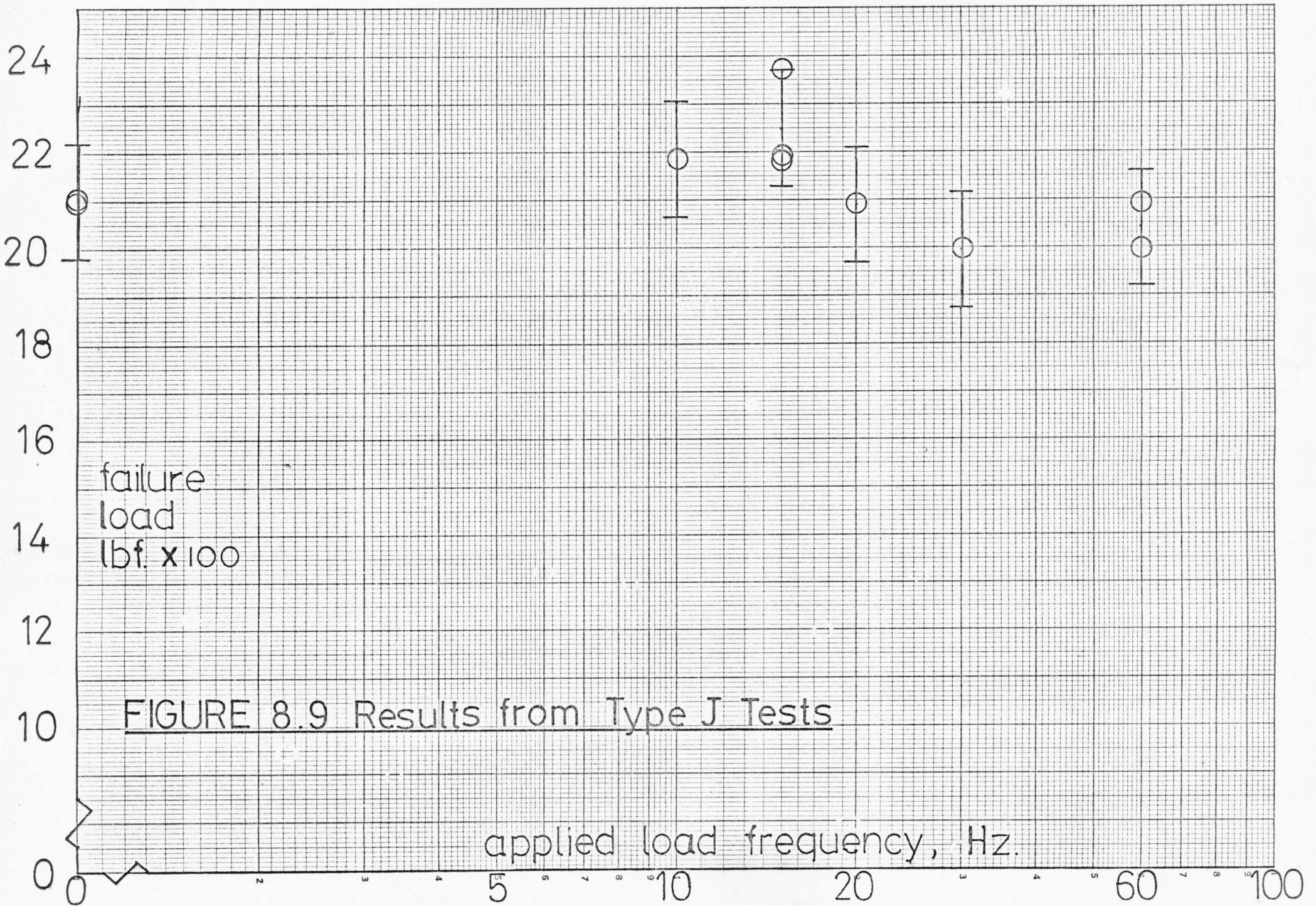


FIGURE 8.9 Results from Type J Tests

8.10 TYPE K TESTS

Disc Speeds 790 and 410 r.p.m.

Slide/Roll ratio 0.317

Mean Disc Speed 600 r.p.m.

Test No.	ω Hz	Ls lbf.	T/L mV/lbf	T1 °C	T2 °C	TF °C	TT °C	μ	h_o insx10^{-6}	p lbfx10^3
182	0	2100	8.4/2000			101		.053	36.1	222
183	0	2200	9.0/2100			106		.054	35.9	227
187	10	2185	9.2/2090	87		106	188	.054	35.9	226
184	15	2185	9.2/2090			106		.054	35.9	226
189	20	1520	7.7/1425	81		100	176	.067	37.6	189
185	20	1615	7.4/1520	90	80	94	179	.060	37.3	195
190	25	1805	8.2/1710	80		100	175	.059	36.8	207
191	25	1900	8.4/1805	84		102	181	.058	36.6	211
186	30	2090	8.7/2090	88		97	180	.051	36.1	221
188	60	1995	8.8/1900	89		104	188	.057	36.3	216

Mean values of μ, steady loads 0.053
fluctuating loads 0.057

Mean value of h_o, micro-inches 36.5

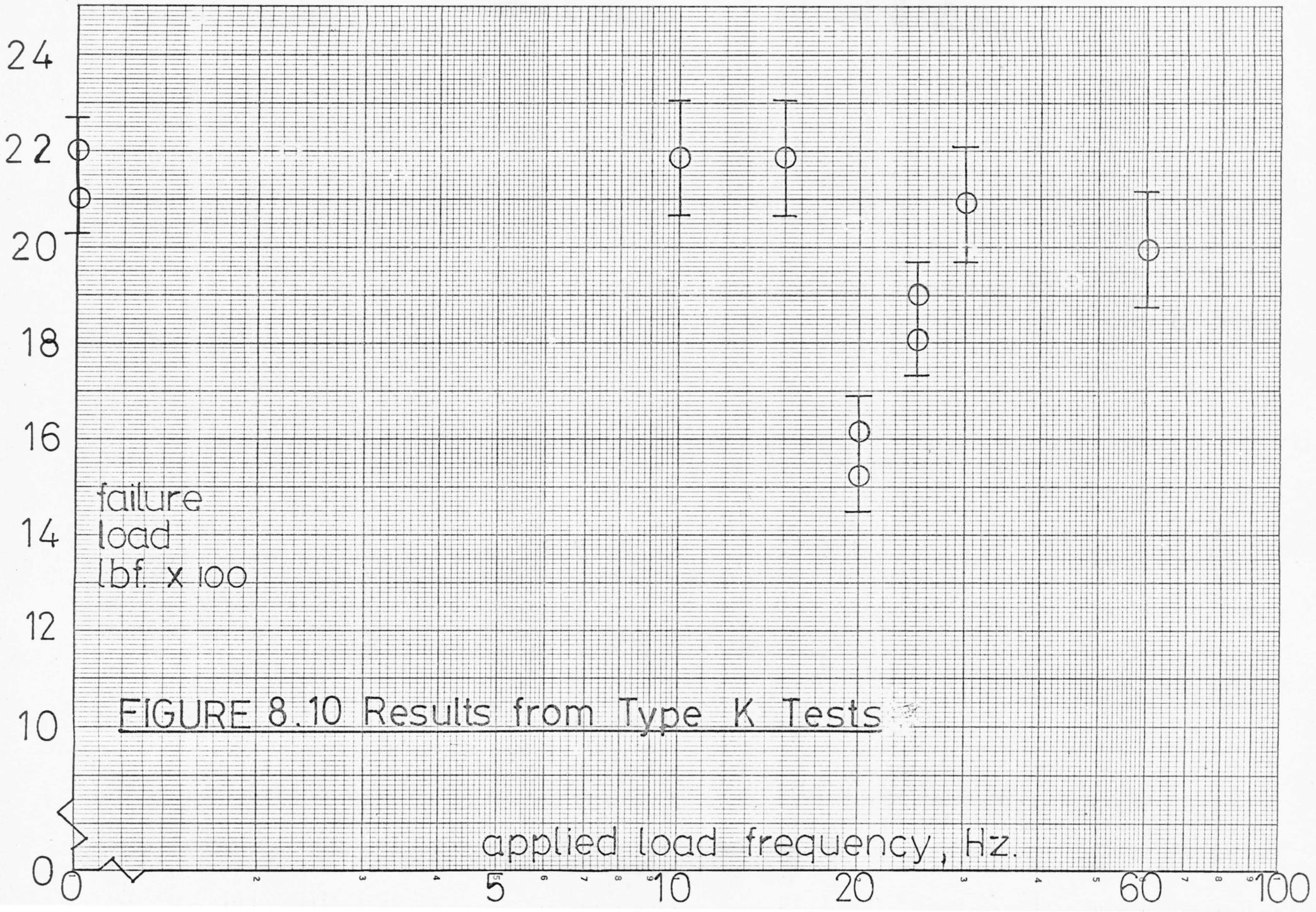


FIGURE 8.10 Results from Type K Tests

8.11 TYPE C TESTS

Disc speeds 1100 and 500 r.p.m.

Slide/roll ratio 0.375.

Mean disc speed 800 r.p.m.

Hertzian contact stress 132,000 p.s.i.

Mean oil pressure level 760 p.s.i.

Oil pressure fluctuated between 720 and 800 p.s.i. at 15 Hertz.

Mean oil film thickness 50.1 micro-inches.

Test 80

Time Hrs.	Time Mins.	T mV	T1 °C	T2 °C	μ
0	0	4.7	97	77	0.076
0	20	4.1	93	76	0.068
1	00	3.8	90	74	0.062
3	00	3.7	89	73	0.060
6	20	3.6	89	69	0.058

Test stopped as inspection revealed a few small pits on the surface and an oblique line of scuffing across the track width.

Test 81

Time Hrs.	Time Mins.	T mV	T1 °C	T2 °C	μ
0	0	3.3	94	82	0.054
1	0	3.2			0.052
3	20	3.2			0.052

Test stopped for inspection. The track had a few small pits.

Test 82

Time Hrs.	Time Mins.	T1 °C	T2 °C
0	0	96	77
1	10		

Stopped for inspection. Again the track was pitted.

Test 83

Load reduced to 665 lbf. to increase the time to scuffing.

Time		T	T1	T2	μ
Hrs.	Mins.	mV	°C	°C	
0	0	3.4	91	70	0.063
0	30				

Stopped for examination. The track was pitted.

Test 216

Load fluctuation frequency changed to 60 Hz. Mean load 760 lbf.

Time		T	T1	T2	μ
Hrs.	Mins.	mV	°C	°C	
0	0	3.6			0.058
1	30	3.2			0.052
5	00	3.0			0.049
9	00	3.0			0.049
11	00	3.2			0.052

Inspection of the tracks revealed slight pitting, so the test was terminated.

8.12 Type L tests

Type B tests, but with a load fluctuation level of ± 12½%.

Test No.	ω Hertz	L_s lbf.	T/L mV/lbf	T1 ^oC	T2 ^oC	μ	h_o insx10^{-6}	p lbfx10^3	TF ^oC
58	15	1225	6.3/1145			0.068	47.1	169	43
60	15	1225	6.8/1145			0.073	47.1	169	46
55	30	1050	4.5/960			0.060	48.0	157	31
73	30	1050	5.3/960			0.068	48.0	157	36
71	30	1225	6.5/1145			0.070	47.1	169	44

8.13 TYPE M TESTS

Disc Speeds 1100 and 500 r.p.m.

Slide/Roll ratio 0.375.

Mean Disc Speed 800 r.p.m.

Test No.	ω Hz	Ls lbf.	T/L mV/lbf.	T1 °C	T2 °C	TF °C	TT °C	μ	h_o insx10^{-6}	p lbfx10^3
23	0	1200							47.5	168
27	0	1200	4.4/1100	104	89	84	181	.049	47.5	168
1	0	1300	5.0/1200			93		.051	47.0	175
2	0	1300	4.6/1200			86		.047	47.0	175
22	0	1300							47.0	175
24	0	1300	4.8/1200	93	88	89	182	.049	47.0	175
28	0	1300	4.6/1200	102	89	86	181	.047	47.0	175
29	0	1300							47.0	175
26	0	1400							46.5	181
233	10	1235							47.3	170
234	10	1330							46.8	177
223	12½	950							48.9	149
221	12½	1140							47.8	163
235	15	760							50.4	133
220	15	855							49.6	142
226	20	760							50.4	133
225	20	1045							48.3	156
228	30	950							48.9	149
227	30	1045							48.3	156
232	40	1045							48.3	156
231	40	1235							47.3	170
229	60	1045							48.3	156
230	60	1235							47.3	170

Mean value of h_o, micro-inches 47.9

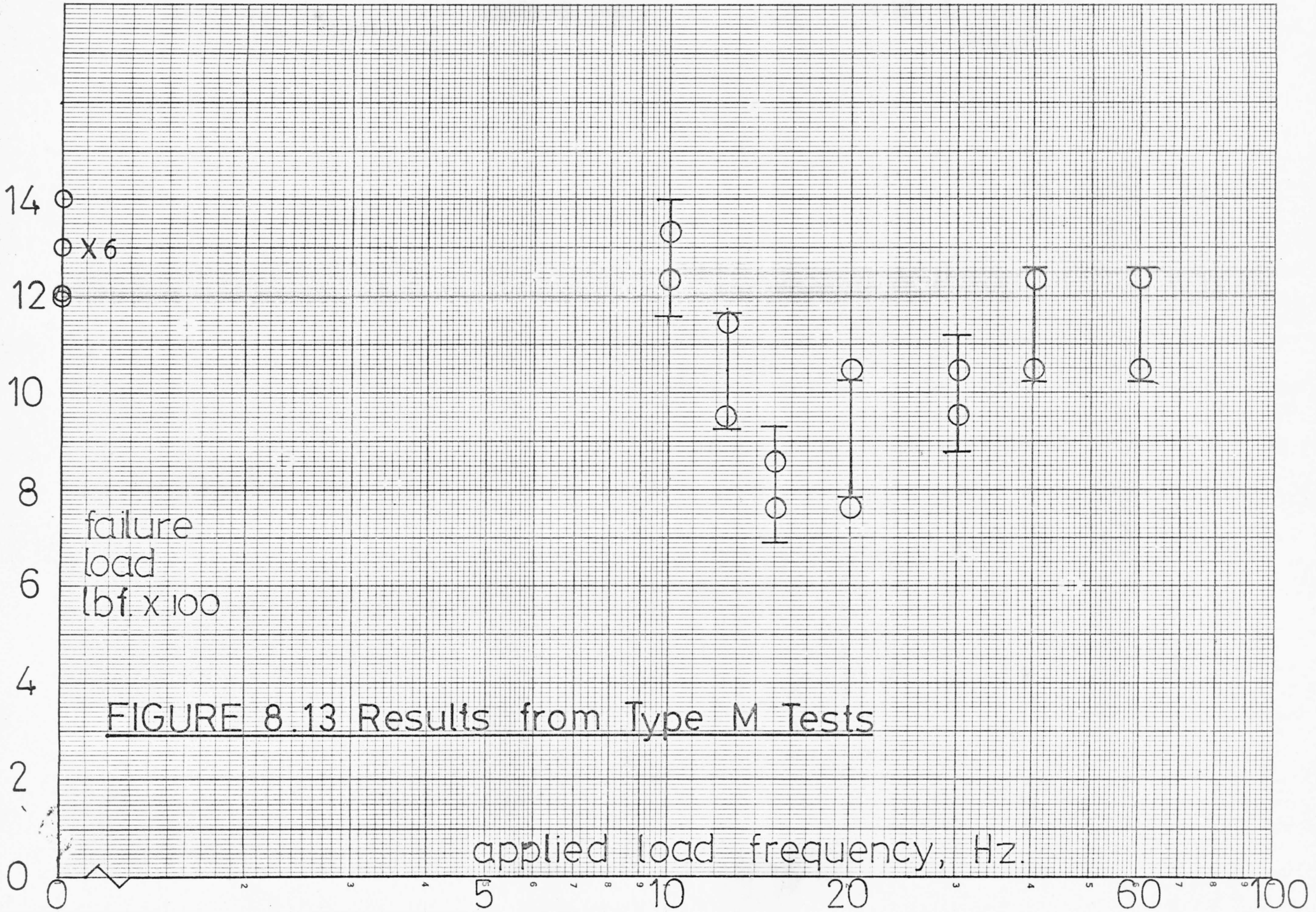


FIGURE 8.13 Results from Type M Tests

8.14 SUMMARY

The preceding data shows the results of varying, in turn, each of the following:-

(a) The frequency of the applied load vibrations in consideration of both scuffing and pitting.

(b) The mean disc speed.

(c) The slide/roll ratio.

(d) The disc surface roughness.

(e) The amplitude of the applied load fluctuations.

In the next sections results are given from subsidiary work, which was of an investigative nature.

8.15 ELECTRICAL INVESTIGATION OF ASPERITY CONTACT

Figures 8.15a to 8.15f show results from this work. In the photographs the upper trace displays the voltage across the contact. A line near the top of the picture represents full film, downward spikes from this line indicating asperity contact. The lower trace displays the pressure waveform.

8.16 RESISTANCE MEASUREMENT OF FILM THICKNESS

The results from this work are tabulated below.

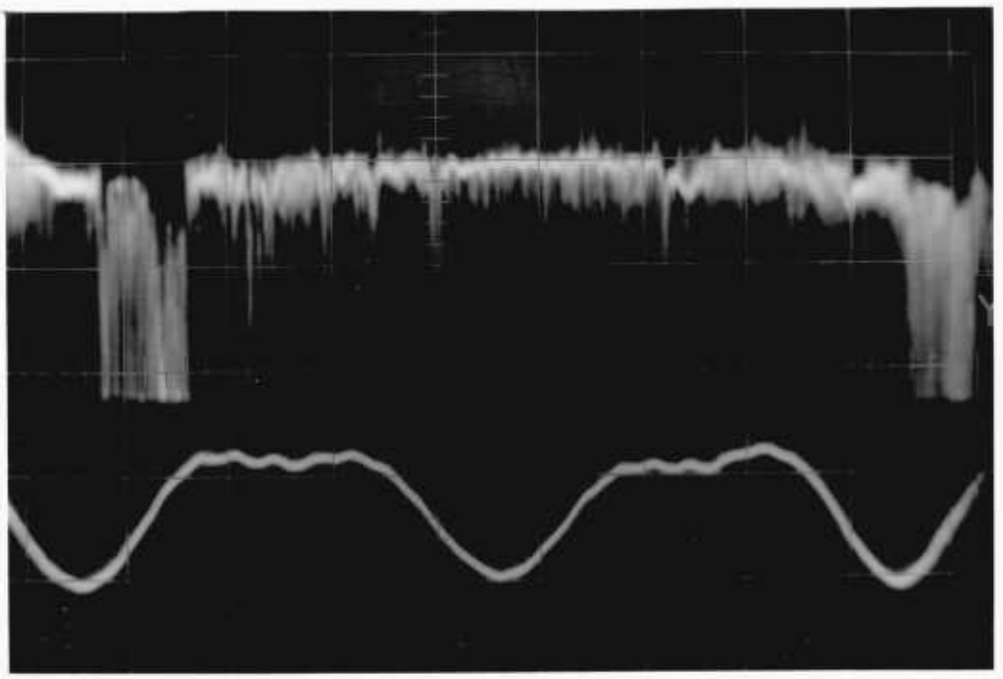


Figure 8.15a Electrical Investigation of Asperity Contact

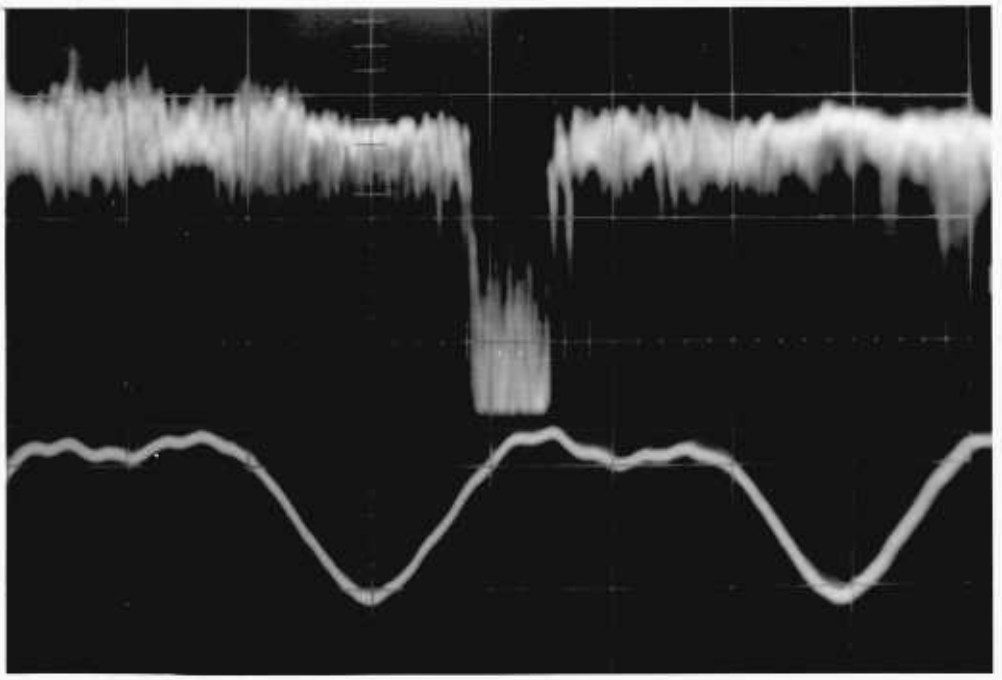


Figure 8.15b Electrical Investigation of Asperity Contact

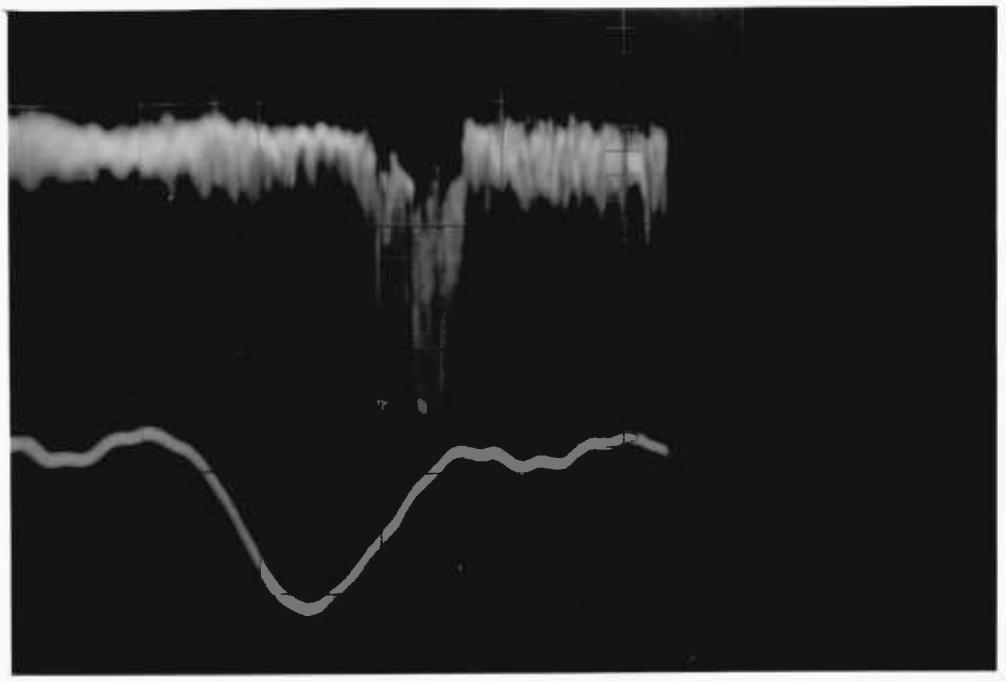


Figure 8.15c Electrical Investigation of Asperity Contact

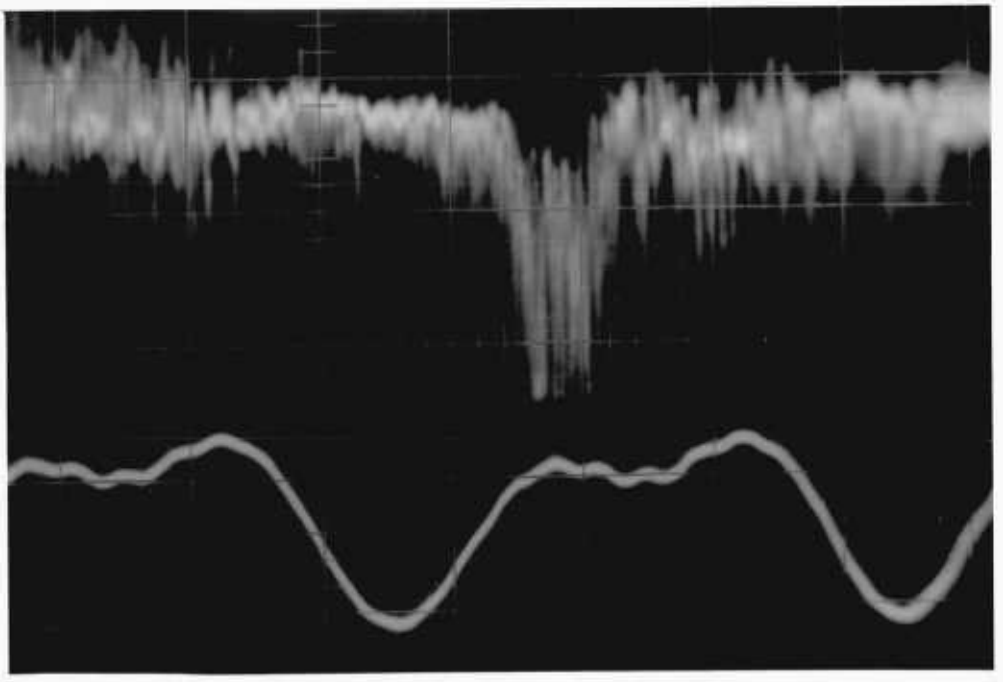


Figure 8.15d Electrical Investigation of Asperity Contact

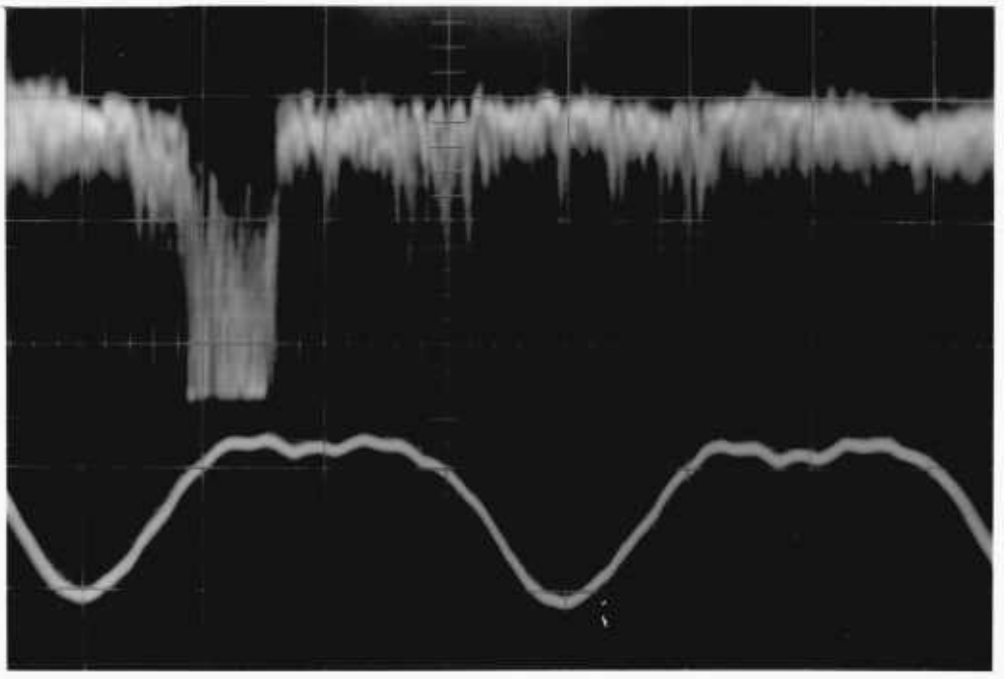


Figure 8.15e Electrical Investigation of Asperity Contact

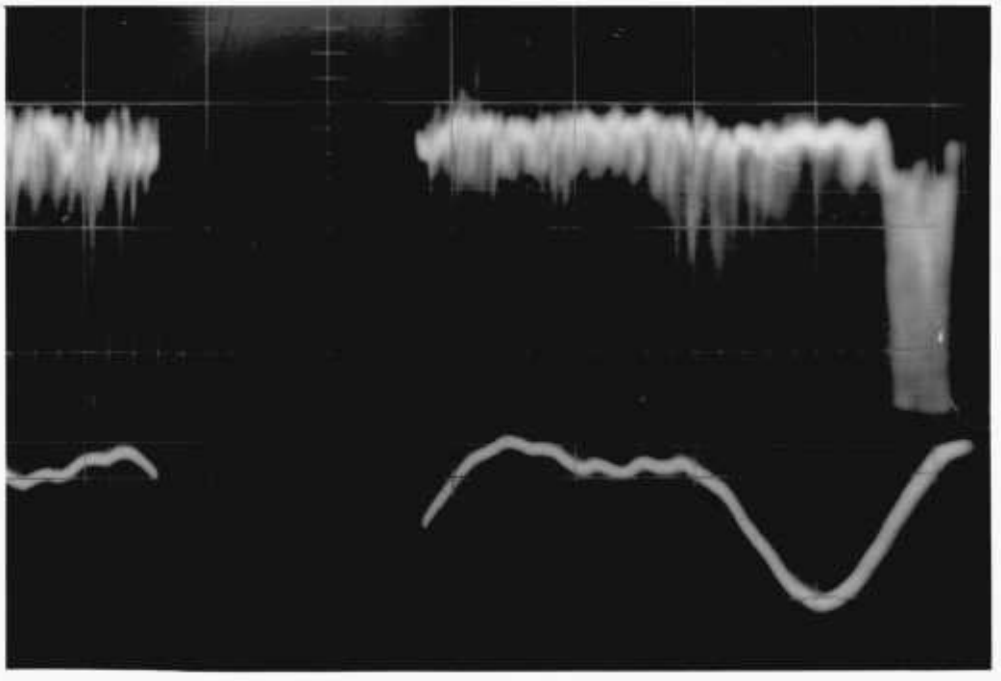


Figure 8.15f Electrical Investigation of Asperity Contact

Table 8.16 Average Resistance of the Oil Film (Ohms) at Various Test Conditions

Load lbf.	Disc Speed r.p.m.	Frequency of the Applied Load, Hz. 0	15	60
		Resistance		
250	400	180	180	330
250	1100	1000	560	1000
500	400	33	33	56
500	1100	180	180	100
1000	400	33	33	18
1000	1100	33	56	33
1500	400	10	5.6	10
1500	1100	18	18	18

8.17 RESULTS OF FILM THICKNESS MEASUREMENTS BY VOLTAGE DISCHARGE

Table 8.17 Film Thickness in Volts

Load lbf.	Disc Speed r.p.m.	Applied Load Frequency 0	15	60
		Volts		
250	400	0.8	0.9	0.9
250	1100	1.5	1.4	1.4
500	400	0.6	0.6	0.6
500	1100	1.2	1.2	1.3
1000	400	0.5	0.5	0.6
1000	1100	1.1	1.2	1.2
1500	400	0.5	0.5	0.5
1500	1100	0.8	0.7	0.8

8.18 RESULTS FROM TEST 224, COEFFICIENT OF FRICTION AND DISC SURFACE TEMPERATURE FOR DIFFERENT APPLIED LOAD FREQUENCIES

The data is shown in Figure 8.18.

8.19 PRELIMINARY ANALYSIS OF THE RESULTS

The following sections examine the effect of having a vibrating load. Table 8.19 collects together some of the basic findings from Type B to M tests.

Before the test data could be employed with confidence it was necessary to conduct two analyses. These were:-

(i) A statistical analysis of scuffing load data and its confidence limits.

(ii) A Fourier analysis of the pressure waveforms generated in the oil, to see whether different frequencies had comparable waveforms.

For convenience these are presented in Appendices Eleven and Twelve. The conclusions were that the noted variations in the scuffing load with vibrations were statistically significant, and dependent, at least to some extent on frequency of vibration, rather than waveform.

8.20 EFFECT OF VIBRATIONS ON THE SCUFFING LOAD

Appendix Eleven shows that in all the tests, except Type J, the application of a vibrating load at a particular frequency produced a significant reduction in the scuffing load.

It was not possible to determine a satisfactory relationship between the frequency at which the scuffing load was lowest and any other single or combination of factors occurring in the tests.

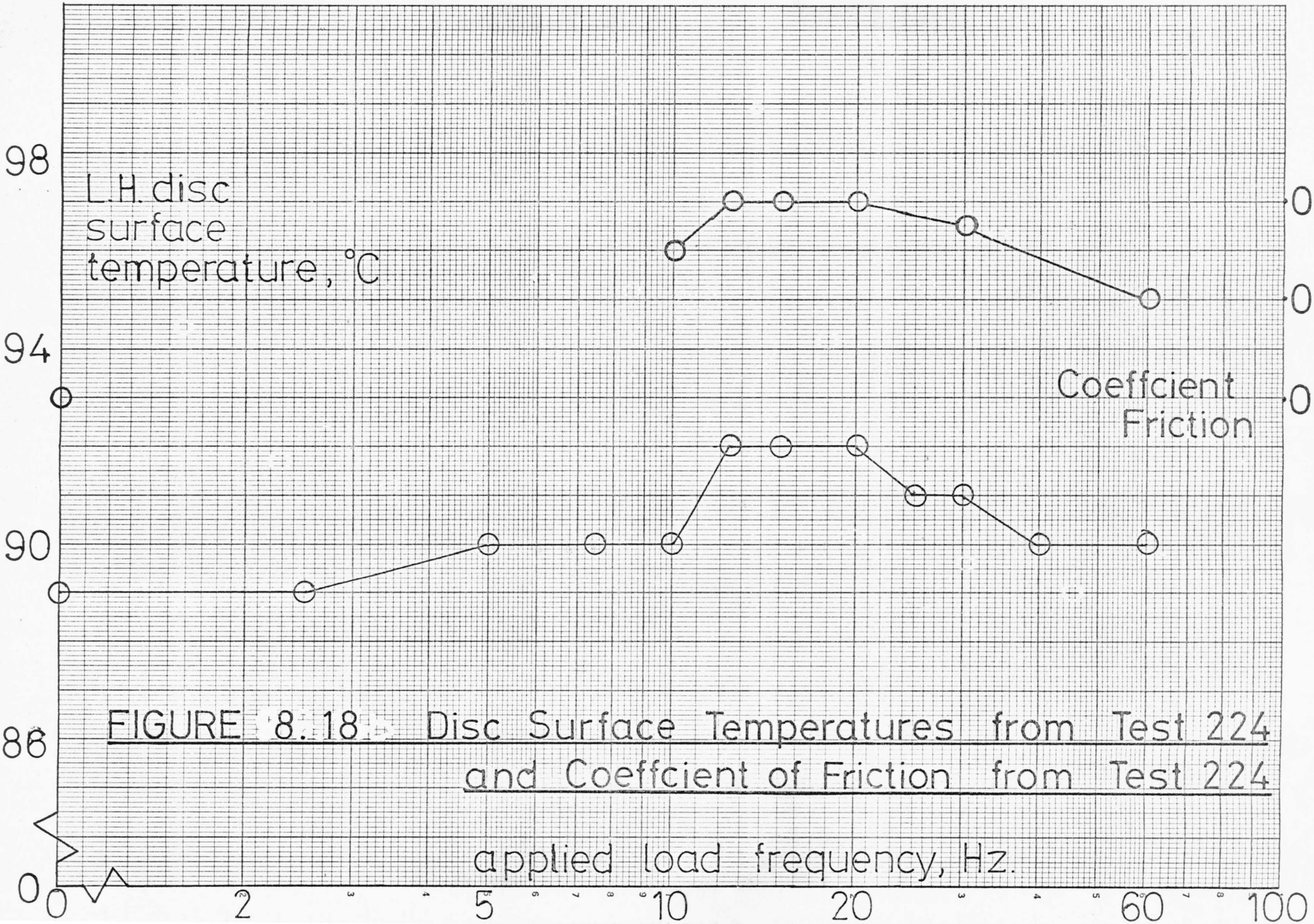


FIGURE 8.18 - Disc Surface Temperatures from Test 224 and Coeffcient of Friction from Test 224

8.19 TABULATION OF INFORMATION FROM TESTS

Type of Test	Failure Load at 0 Hz.	Mean Disc Speed	Min. Scuff. Load, % of 0 Hz Fail	Slide /Roll Ratio	μ Steady Loads, Mean	μ Dynamic Loads, Mean	% Recovery at 60 Hz	h Oil Film Thickness	λ Ratio	Left Hand Temp, Mean	Right Hand Temp, Mean	Total Temp., Mean	Stress at 0 Hz Failure	Frequency of Min. Scuffing Load
	Lbf.	r.p.m.	%				%	in.x 10^{-6}		^{o}C	^{o}C		Lbf/in^2 x 10^3	Hz.
B	1289	800	66	0.375	.049	.057	88	47	2.7	97	86	181	174	15
D	1133	1000	67	0.375	.051	.060	109	56	3.2	105	89	195	163	10
E	1300	600	58	0.375	.069	.069	95	38	2.2	103	90	204	174	15
F	1850	675	78	0.259	.063	.072	98	40	2.3	104	95	198	208	20
H	1933	1080	88	0.259	.060	.061	113	55	1.7	117	103	221	213	20
I	2350	800	75	0.259	.048	.059	97	44	2.5	104	93	197	235	10
J	2100	1000	≈100	0.259	.047	.050	97	51	2.9	110	100	212	222	-
K	2150	600	73	0.318	.053	.057	93	36	2.0	86	80	181	224	20
M	1289	800	63	0.375	.049		88	47	2.7				174	15

The extent of the reduction in the scuffing load varied between 11 and 41%, and is plotted against the oil film thickness at failure in Figure 8.20a. The trend indicated that as the oil film increased, the effect of the vibrations on the scuffing load was reduced.

Alternate factors for the tests were used as the ordinate on this graph but did not yield any useful relationships.

Finally the effect of the vibrations at 60 Hz were considered, and the scuffing loads, expressed as a percentage of those obtained with a steady load for the following types of test were:-

(a) Type B, 88%

(b) Type D, 109%

(c) Type H, 113%

(d) For the remainder of the tests it was approximately 100%.

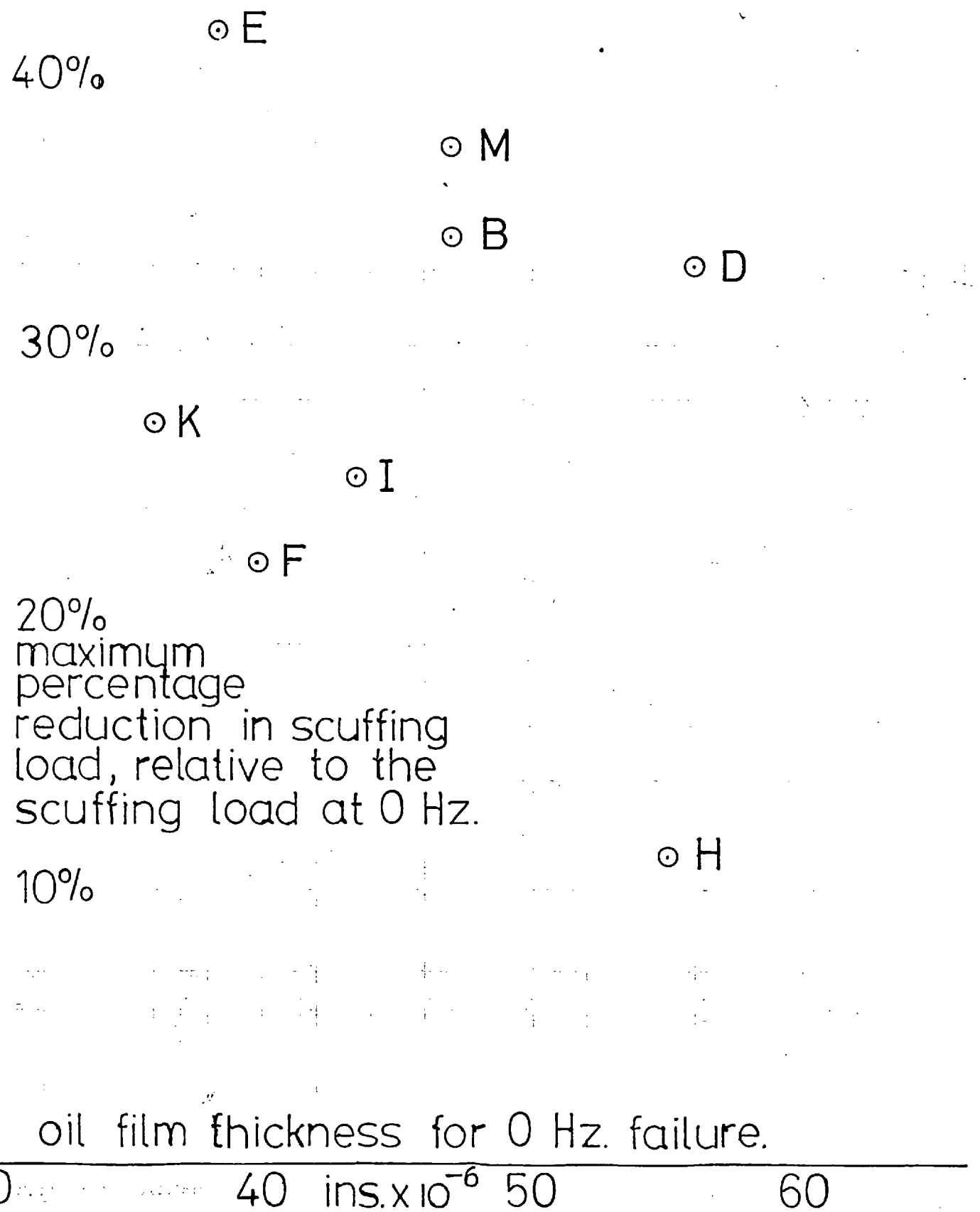
8.21 EFFECT OF VIBRATIONS ON THE COEFFICIENT OF FRICTION

Figure 8.21a shows the coefficient of friction plotted against the frequency of the applied load for each of the different test types. The average for the sets of results is also plotted.

This showed a significant increase in the coefficient of friction when a fluctuating load was used, the average increase being 11%.

Figure 8.18 showed that in Test 224 an increase in the coefficient of friction of up to 8% was obtained with a dynamic load. However, the data used for Figure 8.21a had been obtained when the discs were at the point of imminent

FIGURE 8.20a Extent of the Reduction in the Scuffing Load at different Oil Film Thicknesses.



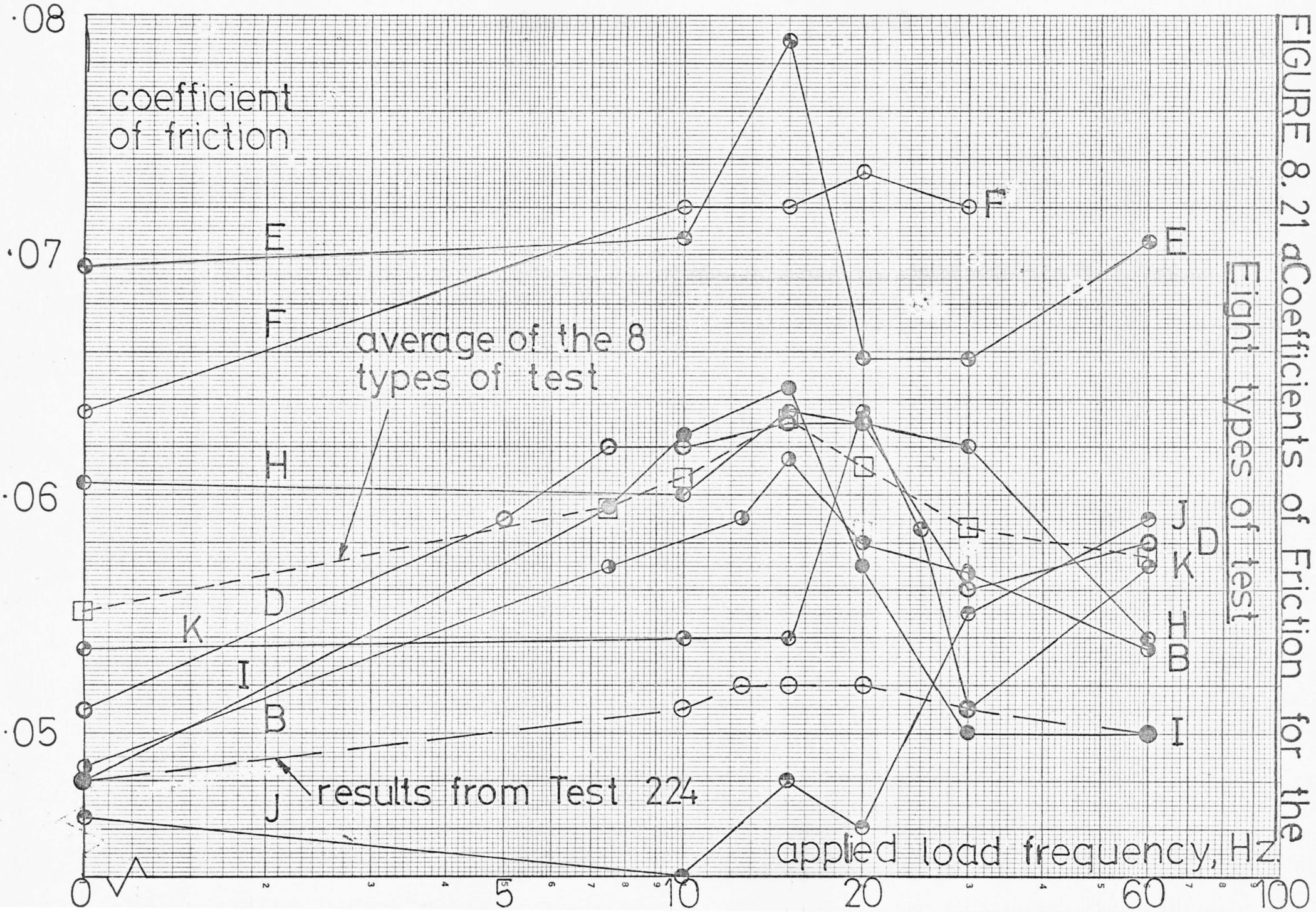


FIGURE 8.21 aCoefficients of Friction for the Eight types of test

failure.

Finally Figure 8.21b shows the coefficient of friction, just prior to scuffing plotted against the failure load. In general it appeared that tests which failed at a low load had a higher coefficient of friction than that measured when scuffing occurred at a high load. That this was not a consequence of variations in the surface roughness of the discs can be seen by examining the results from Type H tests. On the graph these are indistinguishable from those produced by the other tests.

8.22 EFFECT OF VIBRATIONS ON THE DISC SURFACE TEMPERATURE

From Figure 8.22 it can be seen that as the failure load increased higher disc surface temperatures were recorded with either a steady or fluctuating load.

Figure 8.18 showed that in Test 224 an increase in the disc surface temperature of up to $3^{o}C$ was obtained when a fluctuating load was used instead of a steady one. In particular, as with the coefficient of friction, the largest increase was over the range of frequencies for which the lowest scuffing loads had been obtained.

8.22.1 Effect of Oil Viscosity on the Coefficient of Friction

In this section it was shown that the reduction in the oil viscosity brought about by the above rise in the disc surface temperature was insufficient to yield the measured increases in friction.

Figure 8.22.1 shows the friction and surface temperature results from Test 224. From these figures the values

FIGURE 8.21 b Coefficient of Friction plotted against the load at Scuffing

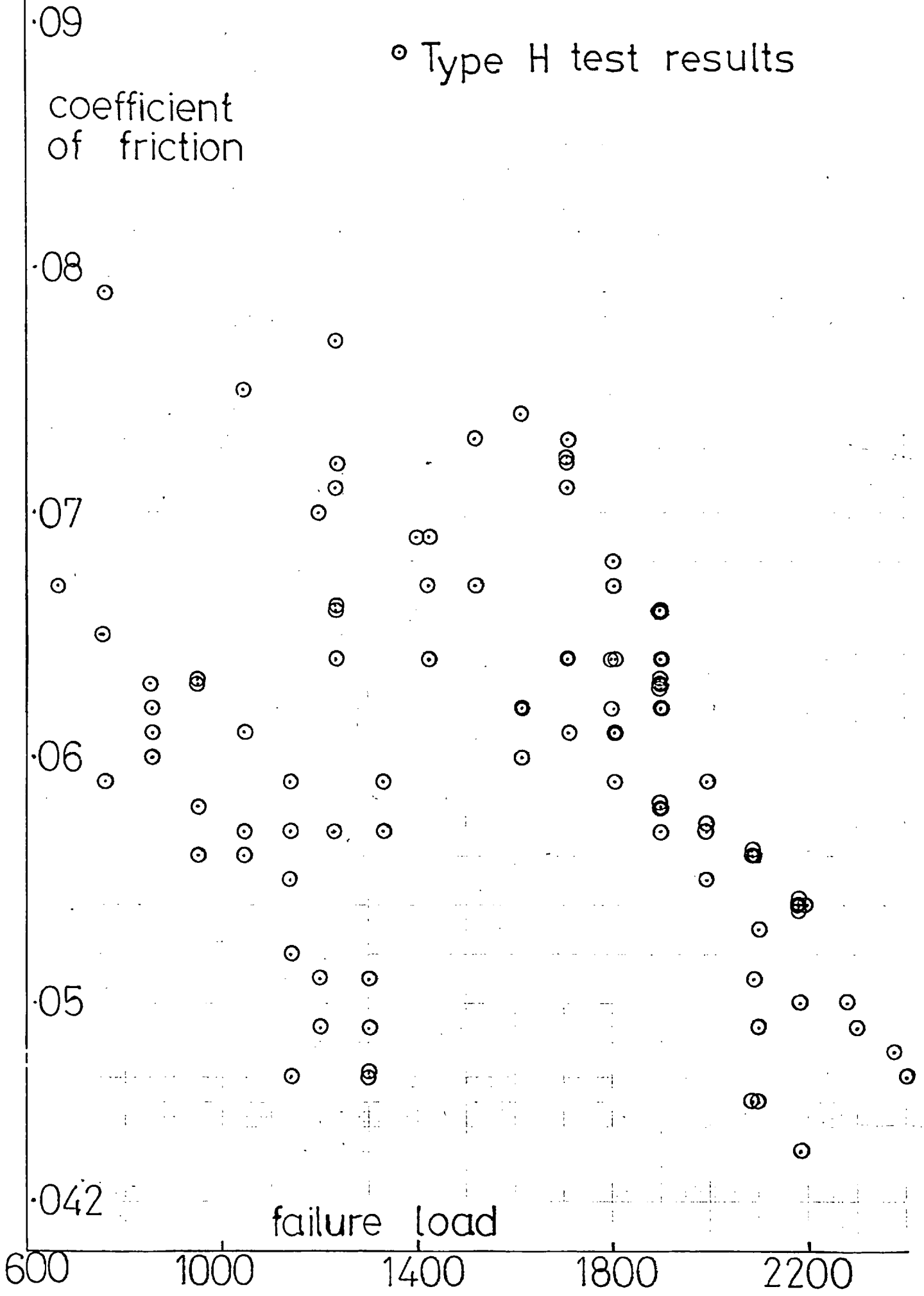
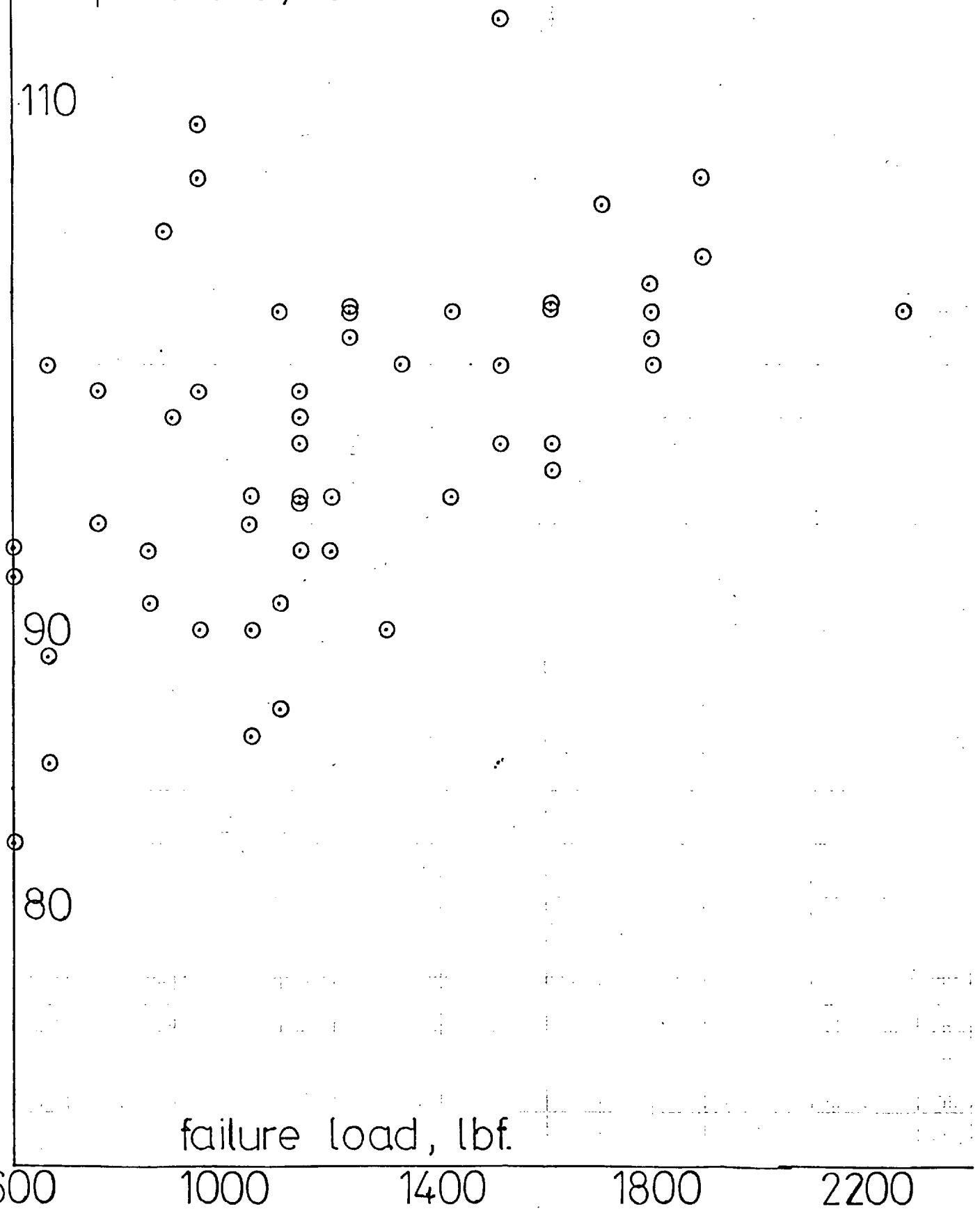


FIGURE 8.22 Mean Disc Surface Temp. for the two discs plotted against the Scuffing Load



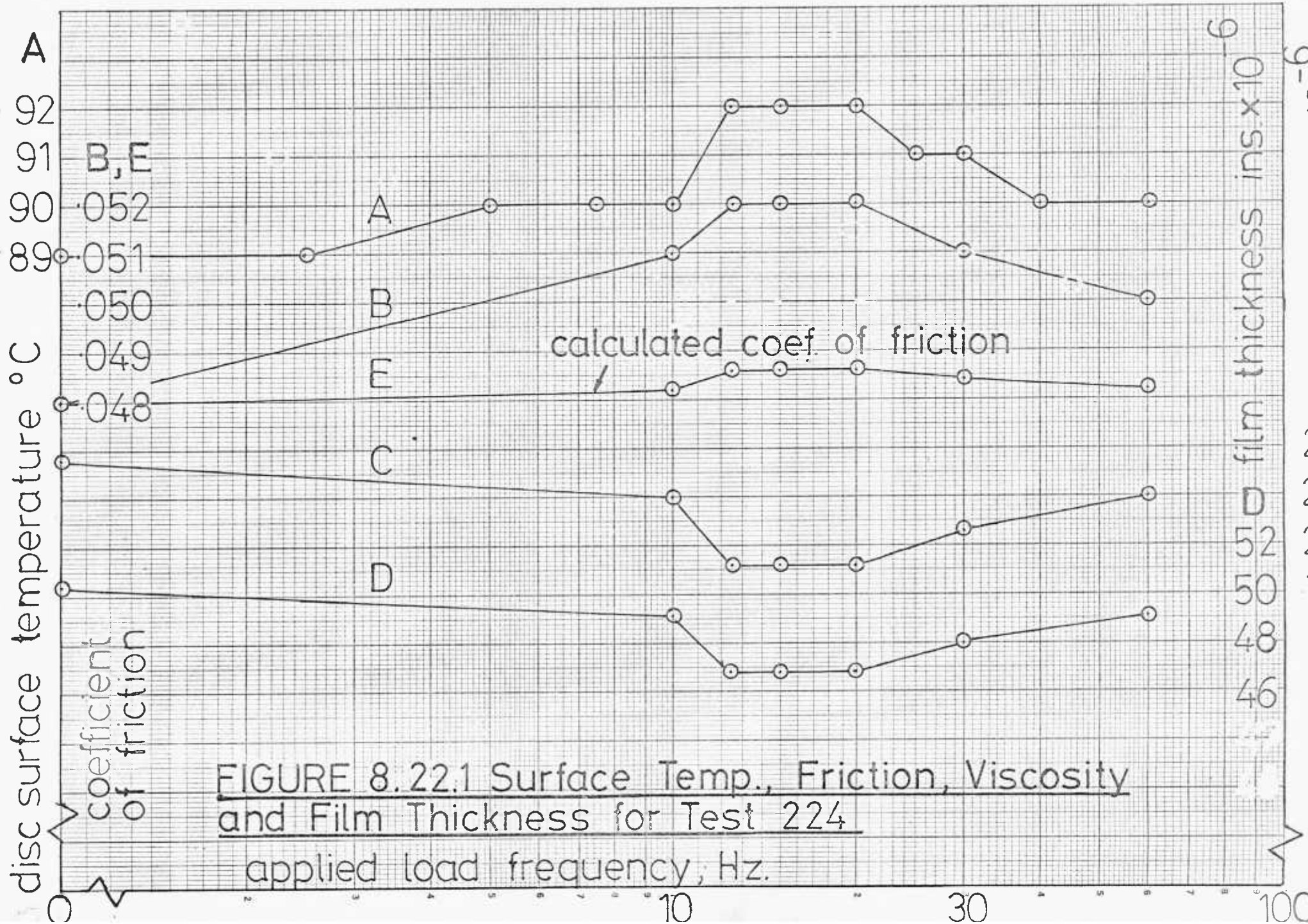


FIGURE 8.22.1 Surface Temp., Friction, Viscosity and Film Thickness for Test 224

of $\eta_{atm.}$ and h_o were calculated. They are also shown in the figure.

In section 10.17 work by O'Donoghue and Cameron (73) is discussed. They produced the following equation for the coefficient of friction in a disc machine.

$$\mu = 0.6\ (S+22)/(35\eta^{1/8}(V_1-V_2)^{1/3}(V_1+V_2)^{1/6}\ R^{1/2}) \qquad (60)$$

Using equation (60) and the values of $\eta_{atm.}$ in Figure 8.22.1 the coefficients were calculated. These are superimposed on Figure 8.22.1.

It was concluded that the reduction in the oil viscosity was insufficient to yield the measured increases in the coefficient of friction.

8.23 EFFECT OF VIBRATIONS ON FILM THICKNESS

Both resistance and voltage discharge techniques were used to measure this, and the results tabulated in Tables 8.16 and 8.17.

As discussed in 7.18 the analysis of the results from the former was limited to comparisons of the oil film resistances. These were estimated to the nearest value of resistance A. The experimental error was therefore one resistance stage, and it can be seen that any one load and speed the results lay within this, so no significant results were obtained.

It had been thought that with the voltage discharge technique a direct calculation of the film thickness would be possible. O'Donoghue and Cameron (71) deduced a calibration constant for voltage discharge of 4.2 volts/ thousandth of an inch. The present oil did not appear to

have the same calibration constant, thus only relative thicknesses could be found. Since the main interest was in changes in the film thickness, this was satisfactory. When recording a result from the oscilloscope the fluctuations in the trace meant that an estimate had to be made for the average voltage corresponding to a full film. As with the resistance measurements of film thickness, the recorded variations in film thickness at a particular load and speed were less than the experimental error.

It was concluded that the application of a fluctuating load at frequencies of 15 or 60 Hz. was not causing a large change, of the order of 30%, in the film thickness. However, neither method was sufficiently accurate in the disc machine to conclusively measure a change of the order of 10%.

8.23.1 Film Thickness and λ Ratio

The calculated oil film thicknesses at failure are in all cases several times greater than the disc surface roughness, given as a C.L.A. figure. However this is an average figure, and for ground surfaces the "peak-to-valley" figure would be up to about 48 to 72 μ ins., which is naturally greater than the oil film thickness. Scuffing necessitates that the asperities penetrate the oil film and weld together, before tearing apart.

The ratio of the oil film thickness to the combined surface roughnesses for the two surfaces is defined as the λ ratio.

$$\lambda \text{ ratio} = h/\text{combined r.m.s. surface roughness.}$$

h = Theoretical film thickness.

$Q_{r.m.s.}$ = r.m.s. surface roughness.

Q = surface roughness measured by a "Talysurf" machine, and expressed as a C.L.A. figure.

Assuming that the surfaces have a Gaussian distribution of heights,

$$Q_{r.m.s.} = (\pi/2)^{1/2} Q$$

The combined surface roughness is equal to

$$(Q_1^2 + Q_2^2)^{1/2}$$

Hence if both surfaces have the same surface roughness

$$\lambda = h/\pi^{1/2} Q.$$

8.24 EFFECT OF VIBRATIONS ON THE PITTING LIFE

This was examined in Tests 80 to 83 and Test 216. Previous tests with EN31 discs running under the same conditions, albeit at a steady load of 800 lbf., had produced pitting after 13 hours.

Tests 80 to 82 revealed that even after 70 minutes at a mean load of 760 lbf. the discs had pitted lightly with an applied load frequency of 15 Hz. It had been impossible to determine the onset of pitting from an examination of the torque trace so Test 83, which was run with a mean load of 665 lbf., was terminated after 30 minutes. Again the discs were found to have pitted.

A calculation of the coefficients of friction showed that the values were higher than those for a steady load test. The average figure now being 0.060 as opposed to 0.055.

To determine the effect of vibrations at 60 Hz. Test

216 was run at a mean load of 760 lbf. The discs ran for 11 hours before pitting. The average coefficient of friction after running in was 0.051.

8.24.1 Calculation of Stress required to cause Pitting

In this section the stress required to cause pitting after 30 minutes is calculated. This could be achieved knowing the stress to cause pitting after 13 hours and the shape of the S/N curve. From the work by Macpherson (3) it was known that the following relationship existed for the S/N curve for the surface pitting of gear steels. (The S/N curve relates fatigue life to the surface stress).

$$(p_{max1}/p_{max2})^9 = N_2/N_1$$

p_{max2} was calculated as follows:

1100 r.p.m. for 13 hours $N_1 = 858 \times 10^{-3}$

At 800 lbf. $p_{max1} = 137 \times 10^3$ lbf./in^2.

To calculate N_2:-

1100 r.p.m. for 30 minutes $= 33 \times 10^3$

15 Hz for 30 minutes $= 27 \times 10^3$

However the vibrations are distributed around the disc circumference, so the number of additional stress cycles at any point (see 14.2) = 70

$\therefore N_2 = 33 \times 10^3 + 70 = 33,070$

$p_{max2}^9 = p_{max1}^9 \times N_1/N_2$

$\therefore p_{max2} = \underline{197,000 \text{ lbf./in}^2}$.

The nominal stress at 700 lbf., which is the peak applied load, in Test 83 = 128,000 lbf./in^2. The above calculation showed that the stress required to cause pitting after 30 minutes was 197,000 lbf./in^2.

8.25 EFFECT OF USING DISCS WITH A ROUGHER SURFACE

Figure 8.7 shows the results from Type H tests, in which the discs had a surface roughness of between 16 and 20 μ ins. C.L.A. By comparison Figure 8.9 shows the results from Type J tests, run under similar conditions but using standard discs with a surface roughness of between 8 and 12 μ ins. C.L.A. Not surprisingly it was found that in Type H tests scuffing occurred earlier than in Type J tests for both steady and dynamic loads.

It was conceivable that the reduction in the scuffing load was related to the λ ratio (see section 8.23) for the contact. In which case Type H tests would have exhibited a similar reduction to that obtained in Type K tests (see Figure 8.10). This did not occur.

It was concluded that the effect of the vibrations was increased with greater surface roughness, but that it was not directly related to the λ ratio.

8.26 EFFECT OF USING A VIBRATION LEVEL OF $\pm$ 12½%

The results from Type L tests showed that this higher level of vibration could raise the failure load at 15 and 30 Hz. closer to that obtained with a steady load.

8.27 EFFECT OF CHANGES IN THE MEAN DISC SPEED

With a constant slide/roll ratio an alteration in the mean disc speed led to two main changes.

(a) A change in the sliding speed and

(b) an alteration in the oil film thickness which is proportional to $(U_1 + U_2)^{0.7}$.

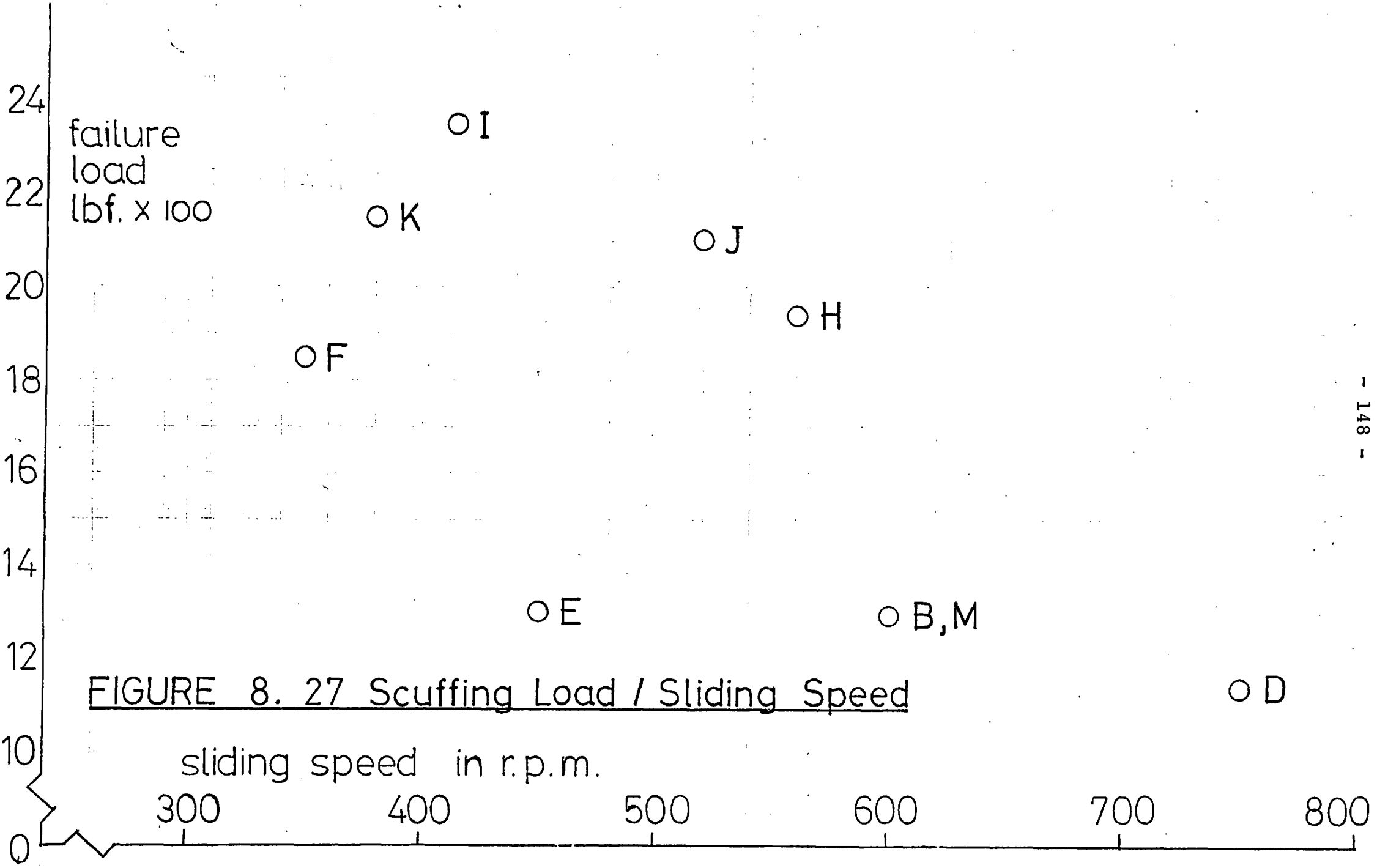


FIGURE 8. 27 Scuffing Load / Sliding Speed

An increase in the former tended to reduce the load at scuffing, as shown in Figure 8.27.

The calculated oil film thickness at failure for Type B to M tests ranged from 36 to 60 x 10^{-6} ins. However, within each test series the variation in film thickness was never more than 9% because the film thickness is proportional to $1/W^{0.13}$. Figure 8.20a showed that a thicker oil film tended to reduce the effect of the vibrations.

8.28 EFFECT OF CHANGES IN THE SLIDE/ROLL RATIO

When the slide/roll ratio was altered for a given mean disc speed the effect was to change the amount of sliding without changing the oil film thickness. Figure 8.28 shows that as expected the scuffing load, for tests with a steady load, decreased as the slide/roll ratio $(U_1 - U_2)/(U_1 + U_2)$ increased when the mean disc speed $(U_1 + U_2)/2$ was held constant.

8.29 SUMMARY OF RESULTS

(a) Compared with a steady load, vibrations could reduce the scuffing load by up to 41%, and failures could occur at stresses as low as 125,000 lbf./in^2.

(b) The effect of vibrations at 60 Hz. produced a significant increase in the scuffing load for Type D and H tests.

(c) A fluctuating load increased the average coefficient of friction for the eight types of test by up to 14%.

(d) Tests which scuffed at a low load had a higher coefficient of friction than the remainder.

(e) The effect of the vibrations on the disc surface temperature was to raise it by up to 3°C relative to that ob-

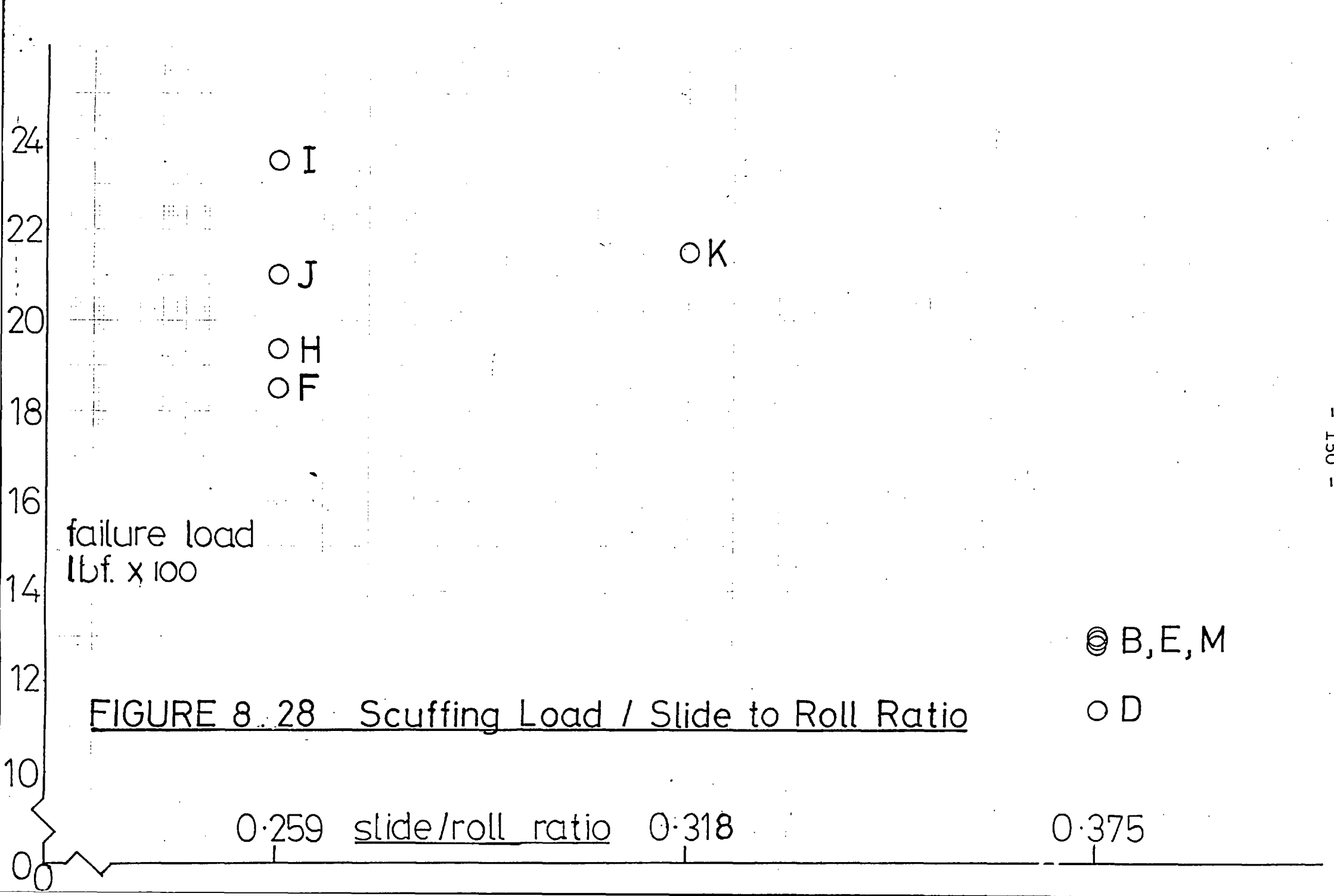


FIGURE 8.28 Scuffing Load / Slide to Roll Ratio

tained with a steady load.

(f) The application of a fluctuating load at frequencies of 15 or 60 Hz. was not causing a large change, of the order of 30%, in the average oil film thickness.

(g) The effect of vibrations at 15 Hz. was to reduce the pitting life from 13 hours to 30 minutes. At 60 Hz. the life to pitting was 11 hours.

(h) The effect of the vibrations was increased when rougher discs were used.

(i) An increase in the vibration level caused scuffing to occur at a load which was nearer to that obtained with a steady load.

(j) Alterations in the mean disc speed showed that scuffing could occur at a wide range of oil film thicknesses.

(k) Changes in the slide/roll ratio showed that an increase in the sliding speed led to a reduction in the scuffing load, for the same oil film thickness.

CHAPTER NINE

GENERAL DISCUSSION

9.1 INTRODUCTION

The most interesting result in Chapter Eight is that vibrations could markedly reduce the scuffing load for the disc machine. The rest of this thesis is concerned with investigating this effect and attempting to explain its origins.

9.2 MECHANISM OF SCUFFING

Scuffing occurs in the disc machine when the elasto-hydrodynamic oil film is no longer able to support the load. As the asperities interact localised heating occurs. This in turn reduces the oil film and welding takes place. With the movement of the discs the surfaces are torn apart. The discs rotate and this damaged portion of the surface re-enters the contact and suffers further damage.

The scuffed area is characterised by gross damage to the surface, with evidence of metal transfer, welding and tearing.

9.3 MAIN HYPOTHESIS TO EXPLAIN THE EFFECT OF A VIBRATING LOAD ON THE SCUFFING LOAD

In order that the above process should occur at a lower load a deterioration of the conditions in the contact is required.

A list of possible hypotheses to explain the reduction in scuffing load at certain frequencies was drawn up as follows.

(a) Resonance effects.

(b) Cavitation effects.

(c) Changes in film thickness.

(d) Excessive pressure in the contact.

(e) Total temperature effect.

Chapters Eleven to Fifteen look at each of these in turn, and discuss their merits.

It is found that until Chapter Fifteen the hypotheses advanced to not provide a satisfactory explanation for the findings in Chapter Eight.

These chapters are preceeded by Chapter Ten in which a literature survey of previous work relevant to the hypotheses is presented.

CHAPTER TEN

SURVEY OF PREVIOUS WORK ON THE EQUATIONS FOR SQUEEZE FILMS

10.1 INTRODUCTION

With the results of the analysis in Chapter Eight in mind a literature survey of the work on oil films subjected to an unsteady load was conducted, in order to examine the influence of this behaviour upon the oil film.

The equations for the oil film thickness, oil flow and pressure in a squeeze film have developed and become more sophisticated since the original work by Stefan in 1874 and Reynolds in 1886 (44). In obtaining his solution Reynolds had assumed the following.

10.2 REYNOLDS' ASSUMPTIONS

(a) Gravitational and inertia terms negligible.

(b) Isoviscous, incompressible Newtonian liquid.

(c) Thickness of squeeze film small compared with plate dimensions.

(d) No slip between the liquid and plate's surfaces.

Over the years workers have attempted to remove all these assumptions from the original equation.

10.3 EVOLUTION OF THE ANALYSIS

In 1947 Eirch and Tabor (45) investigated the dynamic behaviour of a squeeze film, subjected to impact loading. The pressure distribution, flow velocity, shear rate

and temperature rise within the film were calculated.

In 1961 Butter (45) introduced a pressure-dependent viscosity, and demonstrated that this raised the load capacity and maximum pressure produced by the squeeze film. However, we now know that the rise in viscosity of an oil subjected to a sudden large increase in pressure occurs over a finite time interval, and that in many forms of elastohydrodynamic lubrication, such as roller bearings there is insufficient time for the viscosity to reach the value measured in a conventional couette viscometer. Paul (47) using an impact viscometer showed that provided the pressure exceeded about 300 MN/m^2, then the viscosity became very time dependent. After 0.033 seconds the viscosity was only 10^{-3} of that measured after 320 seconds for a Paraffinic Cylinder Stock. Similarly, for Perfluorakyl Ether after 0.033 seconds the viscosity was 10^{-4} of that measured after 8700 seconds.

Butter's work was followed by Pinkus and Sternlicht (48) who considered viscoelastic fluids and incorporated fluid inertia into the equation for the pressure generated in a squeeze film under a round plate. Jackson (49) extended this using an iterative procedure and the continuity and radial momentum equations.

Shukla (50) in 1964 considered a Power Law fluid lubricant and went on to develop a hydromagnetic theory for squeeze films. Kuzma, Maki and Donnelly (51) investigated magnetohydrodynamic squeeze films theoretically and experimentally, using round glass plates with an interposed layer of mercury. Excellent correlation with experimental

data was obtained, when the theoretical analysis included fluid inertia and buoyancy forces.

10.4 SQUEEZE FILMS BETWEEN PLATES

Hays (52) extended the work of Reynolds and Stefan by investigating the case of rectangular plates. The squeeze film was assumed to have a double-Fourier pressure distribution, the coefficients of which were obtained by using variational methods and a digital computer. For the first time plate curvature was considered and found to result in a reduction in the time of approach, both for convex and concave plates. For the case of a flat rectangular plate Moore (53) in 1964 verified Hays' theory, and went on to produce an approximate theory for the case where there is a finite angle, which is proportional to the film thickness, between the plate and surface. This was verified by further experimental work which he undertook. As with a convex or concave plate it was found that having even a small decreasing angle between plate and surface led to appreciable decrease in film thickness.

Further sophistications were considered by Hays (52) and Archibald (54) who investigated plates which are non-planar. Archibald examined spherical and conical bearings, and the case of a circular plate with a concentric round hole. He was able to demonstrate an analogy between the squeeze film equation, the equation for viscous flow through a prismatic tube, and that for the uniform torsion of a bar. Using the results produced from

the theory of elasticity for the latter he was able to deduce expressions of the load capacity and time of approach of a rectangular plate.

As a result of the improvements in the theory since Reynolds' equation in 1886, Dowson (55) in "A generalised Reynolds equation for fluid film lubrication" removed the conditions of isoviscosity, incompressibility and permitted property variations across the film thickness.

10.5 EVOLUTION OF SQUEEZE FILM EQUATIONS

The following is a summary of the work covered on squeeze films by the above authors.

10.6 REYNOLDS SQUEEZE FILM EQUATION

In rectangular coordinates this is

$$\frac{\partial}{\partial x}\left[\frac{h^3}{\eta} \cdot \frac{\partial p}{\partial x}\right] + \frac{\partial}{\partial x}\left[\frac{h^3}{\eta} \cdot \frac{\partial p}{\partial z}\right] = 12 \frac{\partial h}{\partial t} \qquad (26)$$

This assumes that the fluid is incompressible.
p is the pressure in the film arising from squeeze action.
x and z are mutually perpendicular directions in the plane of the plate.

Assuming constant viscosity, parallel plate and surface, and h a function of time, equation (26) becomes

$$\bar{\nabla}^2_p = \frac{12\eta}{h^3} \cdot \frac{dh}{dt} \qquad (27)$$

If the plate is circular, elliptical, or rectangular (but infinite in the z direction, $\frac{\partial}{\partial z} = 0$), equation (27) integrates directly for p. Therefore

$$W = \int p \cdot d A \qquad (28)$$

This leads to the basic equation for a squeeze film

$$Wt = K\eta\, L_T^4\, (1/h^2 - 1/h_o^2) \qquad (29)$$

Where,

h_o is the initial film thickness.

L_T a typical length dimension for the plate.

K a constant for the shape of the plate.

If equation (29) is differentiated w.r.t. time equation 30 is obtained.

$$\frac{dh}{dt} = - \frac{W\, h^3}{2K\, \mu\, L_T^4} \qquad (30)$$

Figure 10.6a shows the relationship between h and t for a flat plate approaching a flat parallel surface.

It is obvious from equation (30) that for constant applied load W and constant viscosity the sinkage rate is proportional to the cube of the film thickness.

For smooth surfaces the effect of increasing W or η is shown in figure 10.6b.

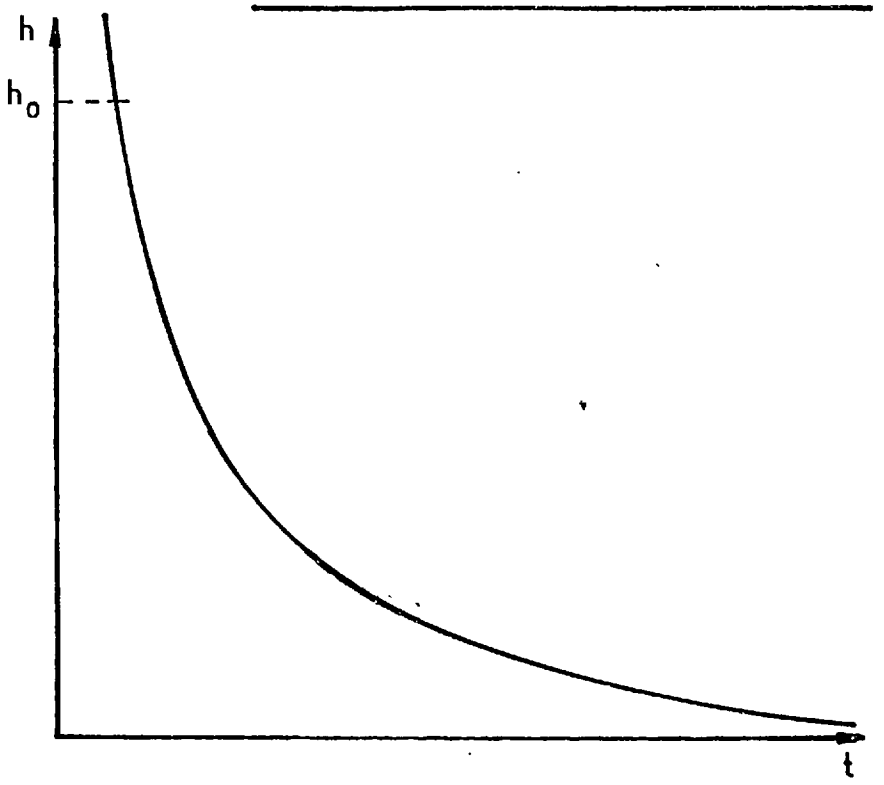
When a plate shape other than circular or elliptical was considered, the pressure distribution in the squeeze film was more complex, owing to the lack of rotational symmetry and corner effects.

10.7 RECTANGULAR PLATES

Hays, working with rectangular plates, of length L and width B assumed a pressure distribution of the form

$$p = \sum_M^\infty \sum_N^\infty A_{MN} \sin M\theta \sin N\phi \qquad (31)$$

FIGURE 10.6a Flat Plate Approaching a Flat Parallel Surface



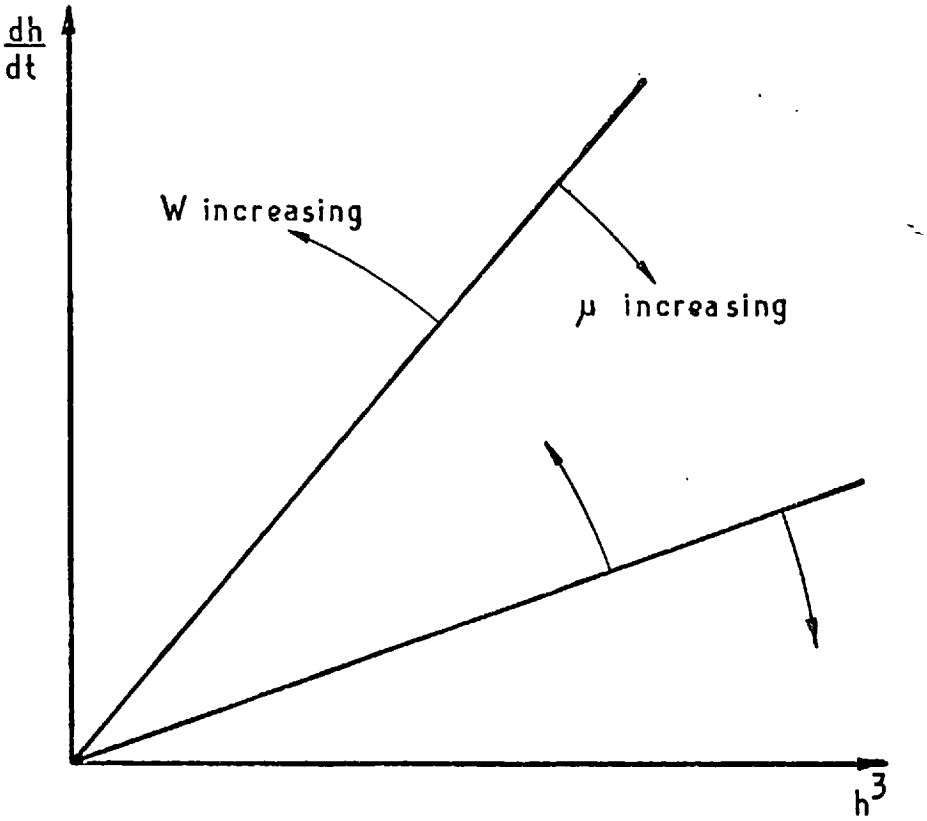


FIGURE 10.6b Effect of W or μ on the Sinkage Rate

Where M and N are odd integers from 1 to ∞, and

$\theta = \pi x/L$, and

$\phi = \frac{\pi z}{B}$, thus satisfying the boundary conditions that the pressure is zero at the edge of the plate. The series coefficient of A_{MN} was determined by variational techniques. The equation could then be arranged into the form of equation (29). The value of K is however a function of the ratio of B/L, and L_T is naturally influenced by the width of the plate.

For the plate shapes considered so far, the values of L_T and K are summarised below.

Shape of the plate	L_T	K
Circular, diameter D	D	$3\pi/64$
Elliptical, length 2a, breadth 2b	$\left(\frac{a^3 b^3}{a^2+b^2}\right)^{\frac{1}{4}}$	$3\pi/2$
Rectangular with no side flow, equivalent to B $\simeq \infty$	L	$\frac{1}{2}$
Rectangular, width B, length L	$(L^3 B)^{\frac{1}{4}}$	$\frac{1}{2}f$ (B/L)

Hays showed that the value of the function for a rectangular plate could be determined from the graph 10.7 which is plotted from his results.

Returning to equation (27), substituting equation (30) into it,

$$\overline{V}^2_p = - \frac{12\eta\ W\ h^3}{h^3\ 2K\eta\ L_T^4}$$

which reduces to

$$\overline{V}_p = - 6W/KL_T^4 \qquad (32)$$

and it can be seen that the right-hand side is constant.

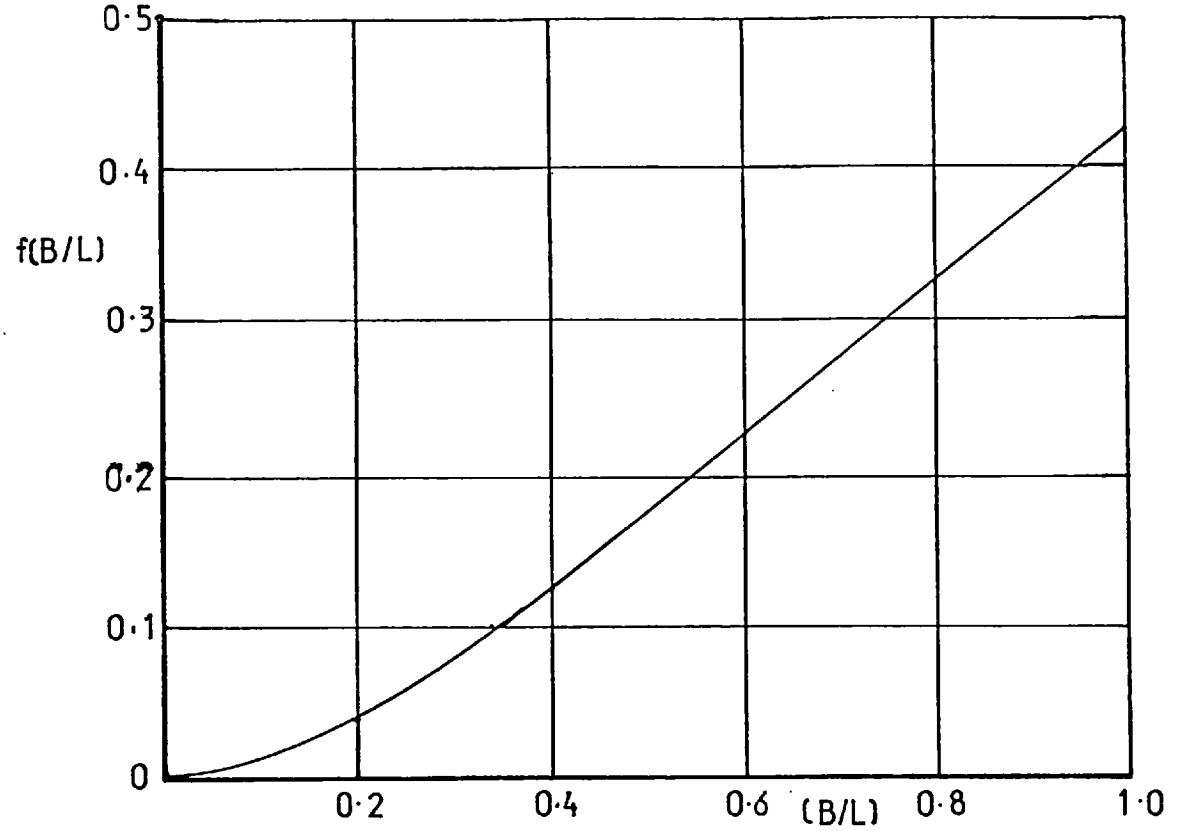


FIGURE 10.7 f(B/L) for Rectangular Plates

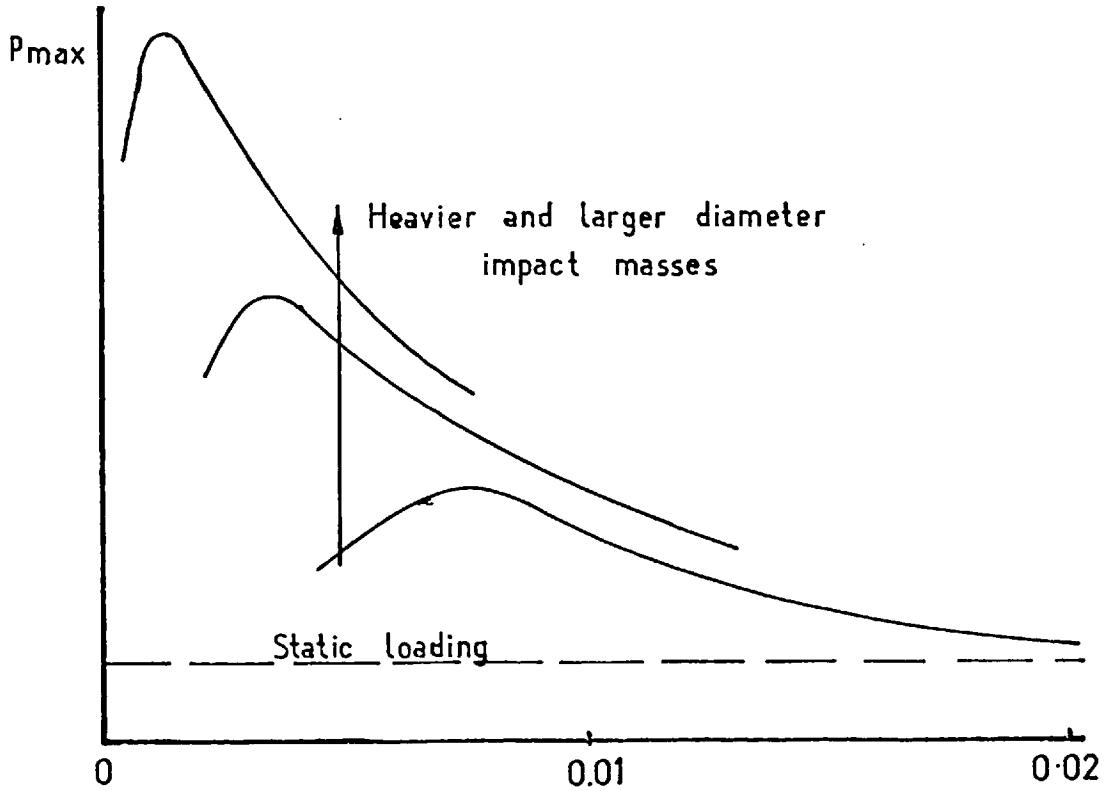


FIGURE 10.8a Squeeze Film Pressures for Impact Loading

(Arising from the assumption of negligible inertia effects. The pressure generated in the squeeze film is independent of time or h, and is a function of position only). For a circular plate, p = p(r) only because of rotational symmetry, and $\bar{V}^2_p$ is also a constant in this case. However for a rectangular plate, where two coordinates are required to describe position, the equation (27) must be modified as follows.

$$(1/LB)\int_o^L\int_o^B \bar{V}_p \,.\, dx.\, dz. = (12\eta/h^3)(dh/dt) \qquad (33)$$

Moore obtained an approximate solution for the case of a rectangular plate by assuming a parabolic pressure distribution in the x and z directions. He showed that for a square plate, length L

$$p = (36W/L^6)\; x\; z\; (L - x)(L - z) \qquad (34)$$

Putting $W = \int p\, dA$, and that p = 0 along x = 0 and L and along z = 0 and L it can be shown, using equation (30) that

$$dh/dt = -\,2\, Wh^3/\eta L^4 \qquad (35)$$

The above assumption by Moore is invalid because the leakage at the corners results in the pressure being less than that determined using a parabolic profile in two dimensions. This had been previously verified by Hays who, using more exact methods had obtained a coefficient of 2.37 instead of 2 for equation (35).

From the work of Eirich and Tabor the velocity distribution under a circular plate can be obtained from

$$V = (8Wrh^2)/(\pi\eta D^4)(1 - ((4y^2)/(h^2))) \qquad (36)$$

Where h is the film thickness (in the y direction).

The next advances in the theory considered the effect of having a variable viscosity or non-Newtonian fluid. Starting with the most commonly used pressure-viscosity relationship of $\eta = \eta_o e^{\alpha p}$ where α is a constant, usually 1.325×10^{-4} in^2/lbf. Butler was able to show that the maximum pressure in the centre of the plate was now greater than with constant viscosity. Assuming the above pressure-viscosity relationship to be true for all pressures, he then showed that there is an upper limit of η_o, above which no radial flow will occur. The peak pressure having reached an infinite value. This resulted in a limiting minimum film thickness. For several years now it has been known that even in conventional viscometers this law over estimates the viscosity of the fluid by a large extent at high pressures, rendering the above conclusions invalid.

The temperature rise in the contact, under impact conditions may be as high as several hundred degrees centigrade, as the energy is dissipated in shearing the fluid film. This temperature rise reduces the viscosity and the following relationship was used.

$$\eta \propto 1/TB \text{ where } 1.5 \leq B \leq 3 \qquad (37)$$

This consequently lead to a reduction in the time of sinkage and load capacity.

10.8 NON-NEWTONIAN FLUIDS

The effect of having a non-Newtonian fluid was considered by Shukla. A simple classification of New-

tonian and non-Newtonian fluids is given below.

Newtonian fluid	$\partial V/\partial y = T/\eta$
Non-Newtonian fluids	
Bingham	$\partial V/\partial y = (T + T_o)/\eta$
Viscoelastic	$\partial V/\partial y = T/\eta + (1/G)(dT/dt)$
Power Law	$\partial V/\partial y = (T/\eta)^{1/N}$

Where, V is a coordinate perpendicular to the plate,

G is the shear modulus,

and T_o is a constant.

Shukla dealt with a power law fluid and showed that for a round flat plate

$$W^{1/N}t = \frac{2N+1}{N+1}\left(\frac{2\pi}{N+3}\right)^{1/N}\eta^{1/N} L_T^{(1+3/N)}\left[\frac{1}{h^{1+1/N}} - \frac{1}{h_o^{1+1/N}}\right] \quad (38)$$

Where N is the power law index. When N = 1, equation (38) can be seen to simplify to equation (29) above. With a constant load W on the plate, the time of sinkage is greater when N > 1, and less with N < 1, than in the case of a Newtonian fluid. A similar expression has been obtained for a rectangular plate. In both cases the load capacity varies as the Nth power of the squeeze velocity.

Returning to the work of Eirich and Tabor (45), they reported Reynolds numbers of about 800 (laminar flow), using h as the length dimension, for the situation of flow in the film between an anvil and an impacting round hammer. They ignored inertia effects compared with viscous forces and thus assumed a balance between pressure and viscous forces. Unfortunately, for dynamically loaded films the assumption that the integral of p dA is equal to the load is not valid. The velocity of the hammer is reduced

as it descends through the film, so the authors substituted for this a statement equating the loss of kinetic energy of the hammer to the work done against the viscous forces. This is expressed as an equation below.

$$M\,(U^2 - (U - dV)^2)/2 = -\,dh \int_0^{B/2} p.\ 2\pi r.\ dr \qquad (39)$$

Where M is the mass of the hammer

U is its velocity.

Combining this with the equation for the balance of viscous and pressure forces gives the velocity of the hammer V at any height h in the squeeze film.

$$V = V_o - 3\pi\eta\ D^4\ (1/h^2 - 1/h_o^2)/64M \qquad (40)$$

This can be seen to be similar to equation (29). When h is considerably smaller than h_o there is an appreciable reduction in speed and thus the term $1/h_o^2$ can be neglected for most cases. Consequently the hammer is effectively brought to rest when h is given by

$$h = (3\pi\eta\ D^4/64M\ V_o)^{\frac{1}{2}}$$

From this height the hammer sinks under its own weight, and equation (29) is naturally valid. As would be expected Eirich and Tabor were able to show that the initial velocity of movement of the liquid surface of the film can be assumed to be V_o. Their results also indicate that the pressure, rate of shear and velocity of flow increase with decreasing D, the maximum values occurring as h tends to the dimensions of surface roughness.

The authors produced Figure 10.8a.

An expression for the temperature rise in the film,

assumed to be owing to viscous heating was given and the effect of adiabatic compression of trapped air bubbles included.

Hays (52) used variational techniques to obtain the coefficients of A_{MN} of an assumed pressure distribution, equation (31), for sine wave loading of non-rotating journal bearings. The Sommerfield Number for a specific journal bearing configuration with constant viscosity liquid is

$$S_o = K_2 \ (\omega/F_o) \tag{42}$$

Where K_2 is a constant, and

F_o the amplitude of the applied load.

He derived expressions for the load capacity, total flow and energy loss caused by viscous shear within the fluid. The results were non-dimensionalised and presented in graphical form. Pinkus and Sternlicht (48) showed that the Sommerfield Number is a function of the eccentricity ratio.

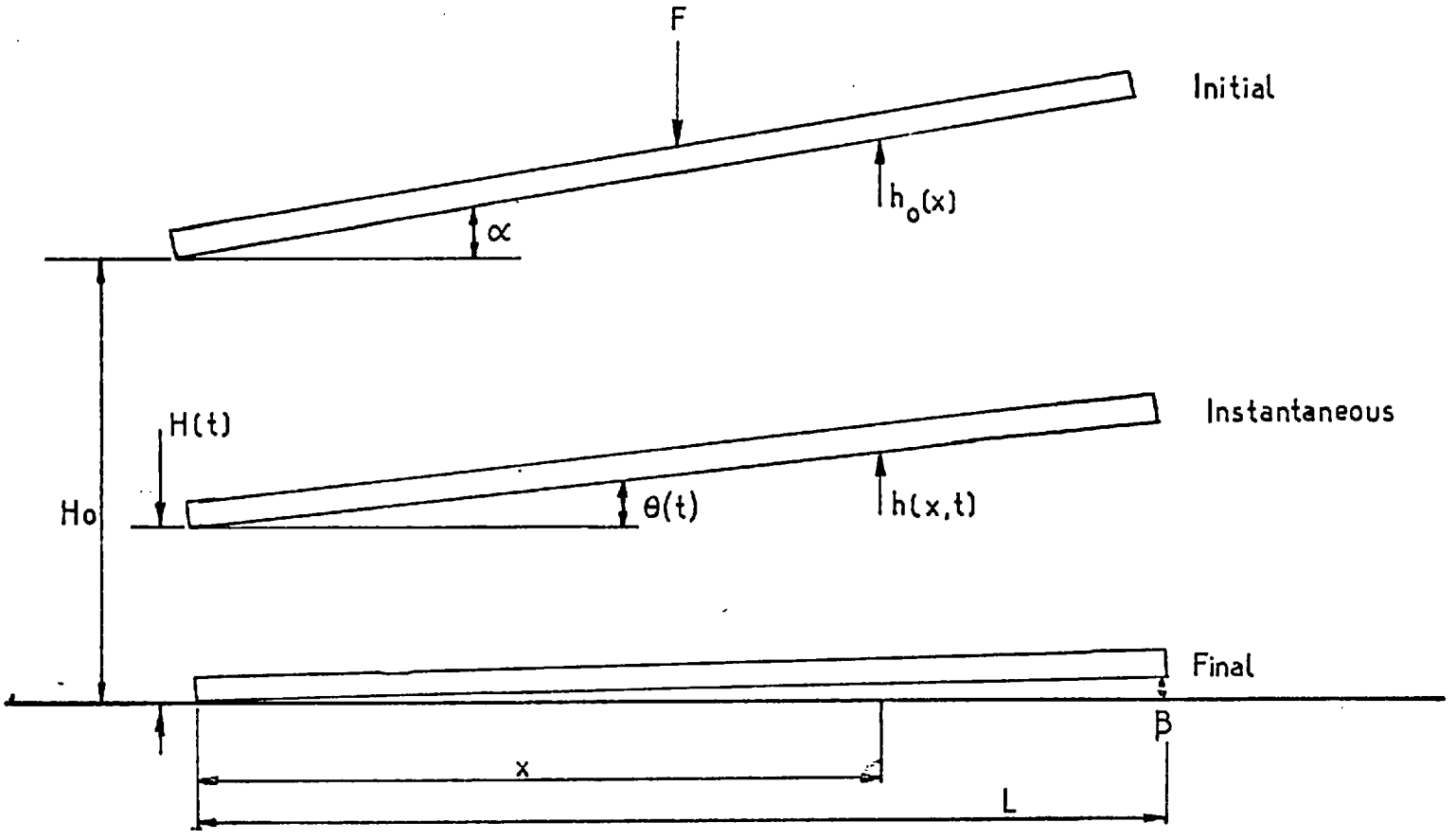
The effect of inclining the plate or having a rough, instead of smooth surfaces was first examined by Moore (53). Either of these will reduce the time of sinkage as expected. Inclining the plate gives an "angle of attack" and a rough surface gives drainage "channels".

He took the case where $\theta(t)$ decreases linearly with squeeze film thickness. The coordinates for the system are shown in Figure 10.8b.

For a square plate

$$h(t)/H_o = (\theta(t) - B)/(\alpha - B) \tag{43}$$

FIGURE 10.8b Co-ordinates for Inclined Sinkage



And, obviously $h(x_1\ t) = H(t) + \theta(t)\ x$ (44)

With small values of θ the pressure distribution may be assumed to be symmetrical, and thus equation (34) can be used. Combined with equation (44) and a modified form of equation (26), the rate of sinkage can be found from

$$\frac{dh}{dt} = -2.37\ \frac{Wh^3}{\eta_L 4}\left[1 + 1.5\ (\frac{\theta L}{H}) + 1.2\ (\frac{\theta L}{H})^2 + 0.1\ (\frac{\theta L}{H})^3\right] \quad (45)$$

The constant of 2.37 is obtained from Hays' work to account for corner effects. Comparison with equation (30) shows equation (45) to be of the same form.

When $\beta = 0$, $\theta L/H$ can be replaced by $\alpha L/H_o$ which is constant, the polynomial on the right hand side of equation (45) is constant. Figure 10.6c shows the effect on the sinkage rate of different values of β, and the large increase with an inclined plate. Moore confirmed these results with experimental work.

10.9 THE INFLUENCE OF ROUGH SURFACES AND ASPERITIES

With the plate parallel to the surface Moore looked at rough surfaces (56) and postulated the following equation, similar in format to equation (45).

$$\frac{dh}{dt} = -2.37\ \frac{Wh^3}{\eta L^4}\ \ 1 \pm C_1\ (\frac{\varepsilon}{h}) \pm C_2\ (\frac{\varepsilon}{h})^2 \pm C_3\ (\frac{\varepsilon}{h})^3 \pm .. \quad (46)$$

Where ε is either the root-mean-square, or peak-to-trough measurement of asperity size for the surface C_1, C_2, C_3 are constants for the surface.

ε/h was referred to as the dimensionless approach roughness.

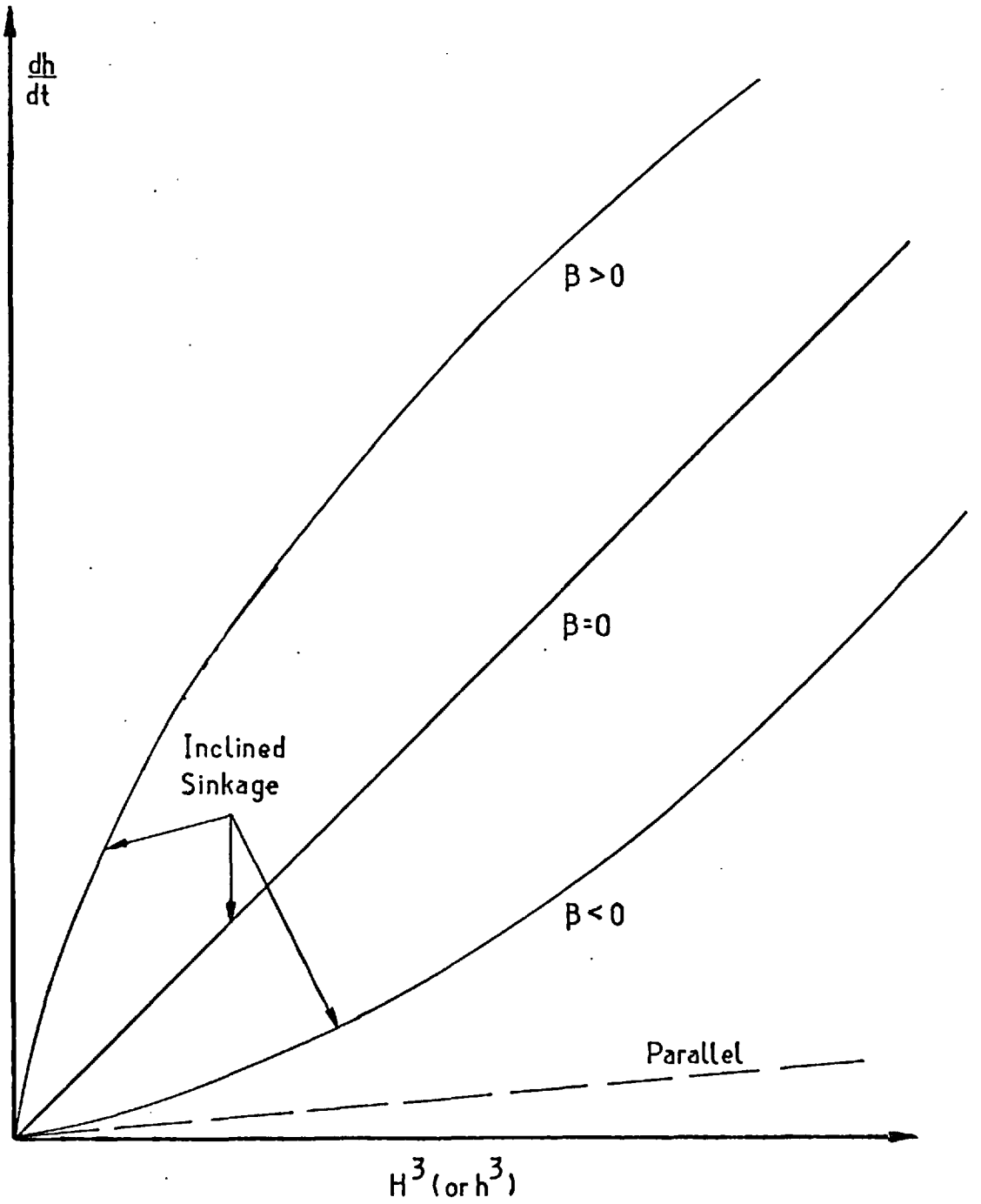


FIGURE 10.8c The Effect of β on the Sinkage Rate

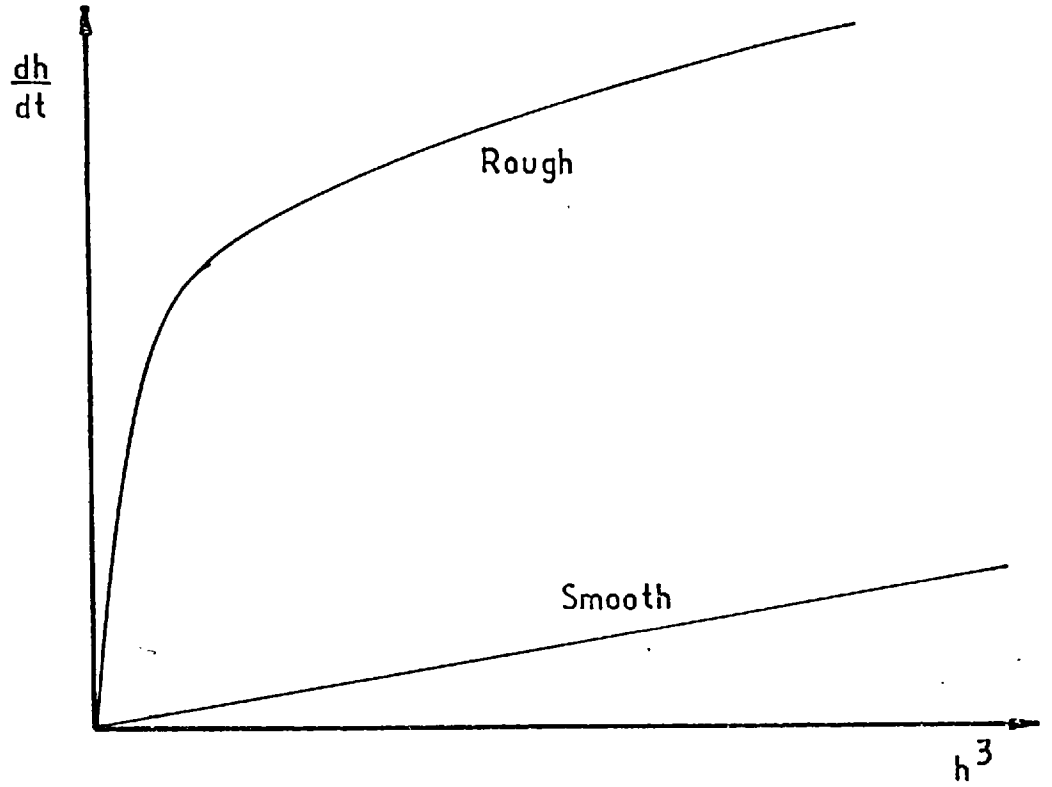
The effect of this surface roughness is shown in Figure 10.9a and 10.9b. Moore showed that there was excellent agreement with experimental data. He did however come across the perennial problem that there still is no really satisfactory method of defining the roughness of a surface, and consequently it is impossible to relate the coefficients to a surface.

This has lead to the use of two techniques to predict sinkage behaviour. The first being a superposition approach (this is a combination of viscous flow between asperities, based on Saint-Venant's equation (57) combined with the flow that occurs between the plate and the tips of the asperities). The second is a dimensionless number technique. Both methods have yielded equivalent results, and the latter is now described briefly.

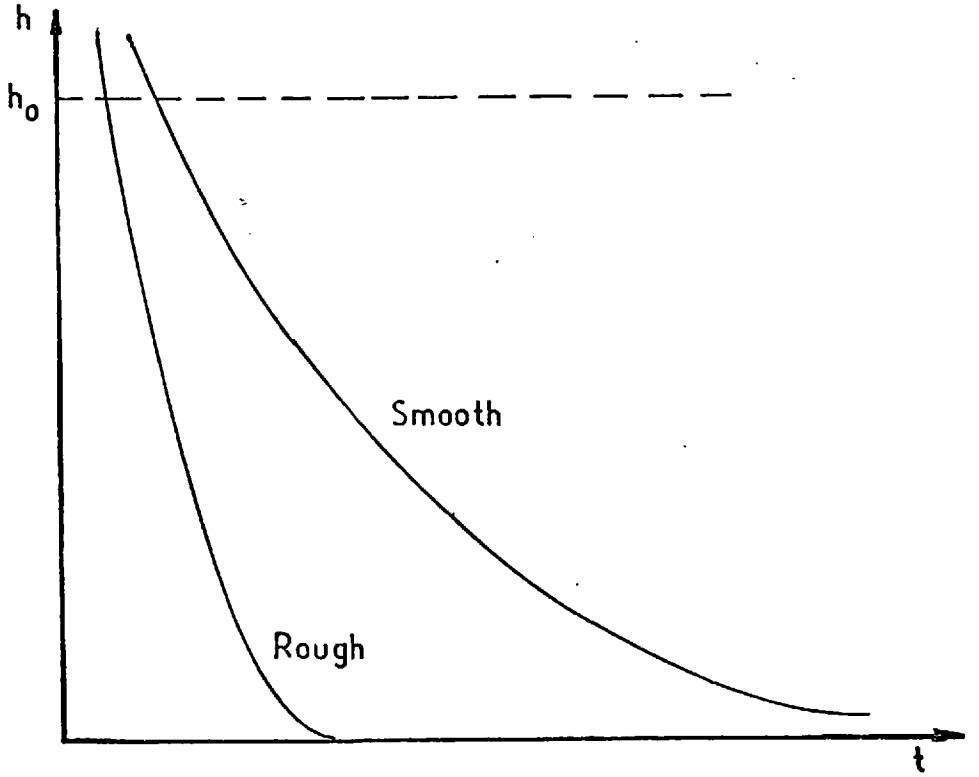
It is assumed that the geometry of a rough surface can be characterised by the shape, size and spacing of its asperities. For specified initial and final values of h then let t be the approach time in the case of a rough surface and similarly t_s for a smooth surface. Then,

$$t/t_s = f \text{ (shape, size, spacing)} \qquad (47)$$

Moore has suggested expressions for the terms in the brackets. He found that the mean hydraulic radius (equal to an equivalent outflow area between the asperities, divided by the wetted perimeter of flow), is a reliable measure of asperity shape, even with random roughness. This enables the ratio of t/t_s to be determined. For absolute values of t, t_s can be calculated from equation



FIGURES 10.9a & 10.9b Effect of Surface Roughness on Sinkage Rate



(29), or else the following may be used.

$$\frac{tW}{\eta A} = f \text{ (shape, size, spacing)} \qquad (48)$$

Where W/A is the specific load, as usual.

With respect to hydrodynamic and magnetohydrodynamic effects, Shukla (50) showed that with an incompressible, conducting lubricant the load capacity could be increased by applying a magnetic field between the plate and surface. As magnetic fields were not used in the present work, their influence will not be considered further.

10.10 ITERATIVE SOLUTIONS FOR THE INERTIA FORCES

Reynolds' equation assumes that steady flow conditions exist. Intuitively, inertia forces must be present to accelerate the fluid from the centre of the squeeze film towards the periphery. A further simplification is contained in the assumption that the integration of the squeeze film pressure over the plate area is equal to the load, which can only be true when the speed of descent is constant. A third approximation is the neglect of V_y, the velocity perpendicular to the surface, and again,intuitively it is obvious that at h, V_y is equal to dh/dt.

The effect of inertia though it is small compared with the viscous forces was examined by Jackson (49) in 1962. He used approximate iterative solutions of the continuity and momentum equations, based on the velocity distribution within the fluid. For a round plate and an

incompressible liquid he showed that the relative importance of the inertia and viscous effects is governed by the parameters

$$(\rho h/\eta)/(dh/dt) \; ; \; (hd^2 h/dt^2)/(dh/dt)^2$$

The first group is similar to a Reynolds' number, and if greater than unity then inertia effects will be significant. The second parameter can be termed an acceleration group, and gives a measure of the relative magnitudes of the local and inertia effects. The following equation gives the load carrying capacity of the film, including inertia effects.

$$W = -\frac{3\pi\eta\, D^4}{32\, h^3}\frac{dh}{dt} + \frac{\pi D^4 p}{64}\left[\frac{24}{35h^2}\left(\frac{dh}{dt}\right)^2 - \frac{3}{5h}\frac{d^2h}{dt^2}\right] \qquad (49)$$

The terms in the square brackets are due to inertia effects. It can be shown, substituting equation (30) in equation (49) that the inertia terms are zero only when the dimensionless squeeze film thickness h/D tends to zero.

10.11 ONE SURFACE SUBJECTED TO NORMAL SINUSOIDAL EXCITATION

In 1966 Hunt (58), at the University of Southampton, carried out a theoretical examination of the pressure distribution in a plane fluid film subjected to normal sinusoidal excitation. For the situation of a plane circular bearing comprising two parallel discs of diameter D, with the gap thickness h completely filled with fluid at atmospheric temperature and pressure, he was able to show that

$$\frac{p_{max}}{\mu\omega} = -3 \left(\frac{a}{h}\right) \left(\frac{D}{2h}\right)^2 \cos \omega t \left[1-3a \left(\sin \omega t\right)/h\right] \qquad (50)$$

Where μ is the absolute viscosity in Reyns,

a is the amplitude.

By plotting $\frac{p_{max}}{\mu\omega}$ against ωt for D/h = 2000 the equation could be seen to simplify to

$$\frac{p_{max}}{\mu\omega} = \pm 2.6 \left(\frac{a}{h}\right) \left(\frac{D}{2h}\right)^2 \left[1 + 1.5\ a/h\right] \qquad (51)$$

Returning to equation (50) he plotted the non-dimensional left-hand side against a/h for different values of D/h and obtained Figure 10.11.

To give an idea of what this graph means in a practical situation Hunt considered a pair of meshing gear teeth separated by an oil film of 10^{-4} ins. If the natural frequency of one of the gear teeth is 3 kc/sec., typically the dimension D for an equivalent circular area of contact is 0.50 ins., the lubricating viscosity is 5×10^{-6} Reyn and the ratio of vibration amplitude to oil film thickness a/h is 1/10, then from figure 10.11 p_{max} is 24,000 lbf/in^2. He considered that this pressure was unlikely to cause damage, but that any slight variation in any of the above parameters could bring the stress level up to that which could cause a short fatigue life. But before beginning to consider the effects of this he pointed out that at much lower ratios of a/h than 1/10 a more dangerous condition will occur. As p_{max} is experienced as both a positive and negative pressure, the condition of cavitation will occur in the fluid when $p_{max}/\mu\omega = 10^3$, which happens when a/h is merely 10^{-3}.

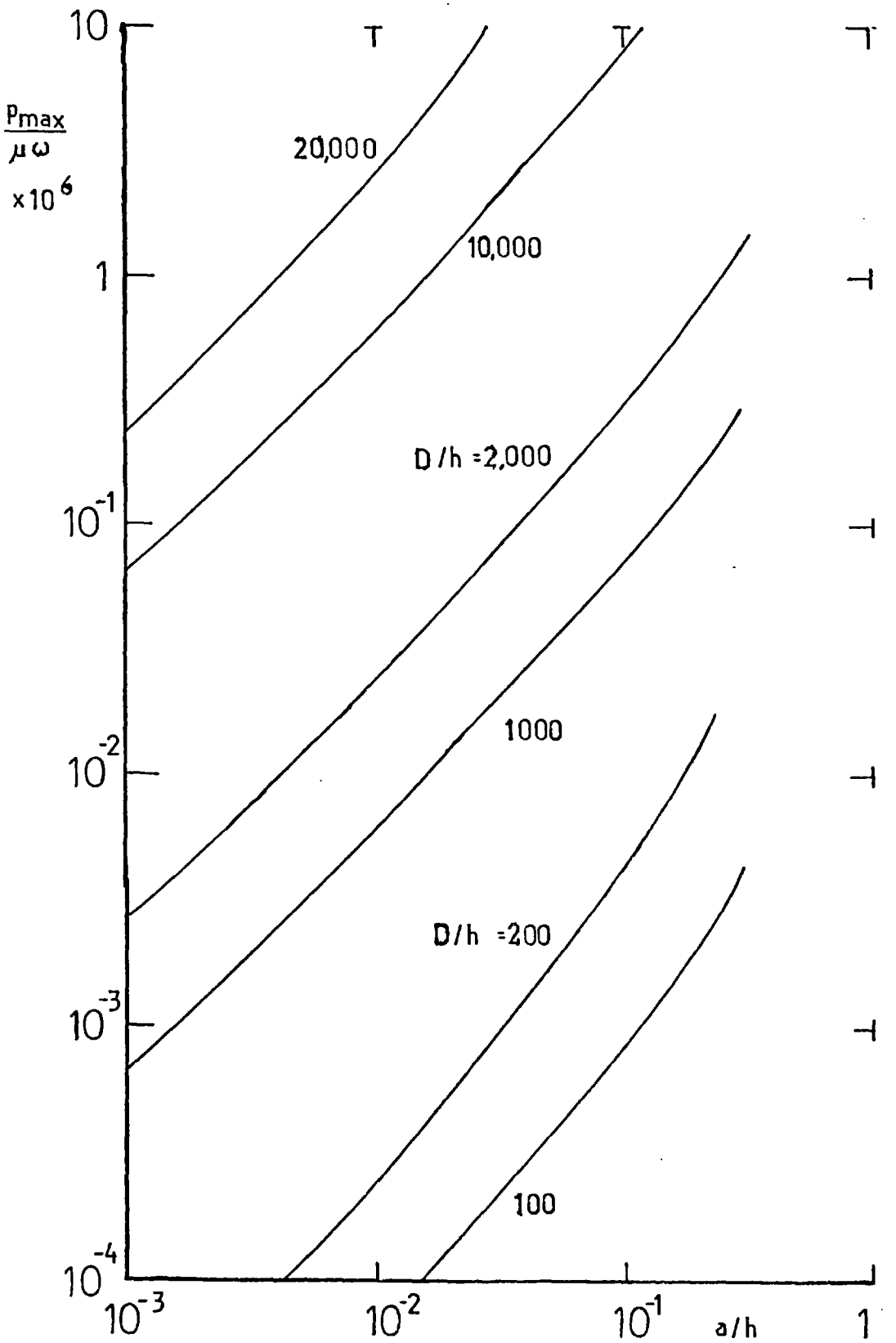


FIGURE 10.11 Variation of $\frac{p_{max}}{\mu\omega}$ with a/h

He concluded that in the above example cavitation would be unavoidable under running conditions, with subsequent fatigue damage of the surface.

To check the validity of equation (50) a rig was built to observe the onset of cavitation, characterised by the formation of bubbles in the fluid between two small circular steel discs, radius 3/16 in., using fluids with viscosities from 10^{-5} to 10^{-4} Reyn at $20^{o}C$. The experimental values of a/h agreed well with figure 10.11, and when cavitation was allowed to continue for 10^{6} cycles extensive pitting damage was found on both plates.

Hunt's work probably provides the greatest insight into the results obtained in the work of this thesis, and it will be discussed again in the next Chapter and used to illustrate the effects experienced in the disc-machine.

10.12 CHRISTENSEN'S WORK

Christensen (59), in a paper entitled "Elasto-hydrodynamics of Normal Approach", analysed a system comprising a rigid sphere approaching a semi-infinite elastic plate. He calculated pressure distributions, film shapes and load capacity, showing that the first became much narrower and more peaked as the film thickness decreased. Thus he was able to conclude that for small values of the film thickness the elastic distortion of the materials becomes of increasing importance, but his other conclusions had already been covered by previous workers, such as Butler (13).

Christensen (60) also investigated the pressures encountered between two cylinders under impact conditions. Considering first the theoretical aspect, the motion of the cylinders is given by

$$\frac{\partial}{\partial x}\left(\frac{h^3}{12\eta}\frac{\partial p}{dx}\right) = \frac{-\partial h}{\partial t} \tag{52}$$

Assuming that the fluid is incompressible and there is no side leakage. For the situation of elastic cylinders and a pressure dependent viscosity of the form $\eta = \eta_o e^{\alpha p}$, he was able to show that

$$\bar{h} = \bar{h} + \bar{x}^2 - \int_{-\infty}^{\infty} \bar{p}\ \ell n/\bar{x} - \bar{x}'/dx \tag{53}$$

$$\bar{p} = \alpha\bar{p} = -\ell n\left(1 - \zeta\frac{I(\bar{x})}{I(0)}\right) \tag{54}$$

and

$$W_c = \alpha W\pi\ \frac{(\alpha E)}{4R} = \int_{-\infty}^{\infty} \bar{p}\ dx \tag{55}$$

where $\zeta = 1 - e^{-\alpha p_o}$

His calculations revealed that pressure between elastic bodies are, as expected, less than the corresponding ones between rigid cylinders. The most unexpected aspect of his results was the discovery that the peak pressures occur with a specific, as opposed to zero film thickness, and that the assumption of a pressure dependent viscosity produced peak pressures in the centre, under lubricated conditions that were in excess of those experienced under dry Hertzian contact. As the film thickness tends to zero the pressures in the contact become equal to the Hertzian figures.

The effect of these high pressures was to trap

oil in the contact under impact conditions. The pressure-dependent viscosity increased to prevent flow and maintain a thicker oil film for a given load than would be experienced by gradually, but rapidly applying the load. However, as discussed before, Paul's (47) work showed that the response of the viscosity to step changes in the pressure was very time dependent. This makes it impossible to calculate any figures for the greater oil film thickness under impact conditions.

To verify the above findings Christensen conducted an extensive series of 360 tests in which a brass, aluminium or steel ball was dropped onto a similar specimen under dry or lubricated conditions. The tests covered five different loads on the ball, these being sufficient to produce permanent plastic deformation in the specimens. In every case the deformation was found to be greater when there was a lubricant between the surfaces.

He concluded that in the case of normal approach of two elastic cylinders separated by a lubricating film, high central pressures, greater than the Hertzian pressures were developed at a finite separation of the cylinders. Furthermore these pressures are related to the product αE.

In 1970 Herrebrugh (61) extended Christensen's work. He stated that the latter's method of direct integration was unsuitable in the region of relatively large deformations, and proceeded to use an integral equation approach. He made the following assumptions about the squeezing process.

FIGURE 10.12a Configuration used by Herrebrugh

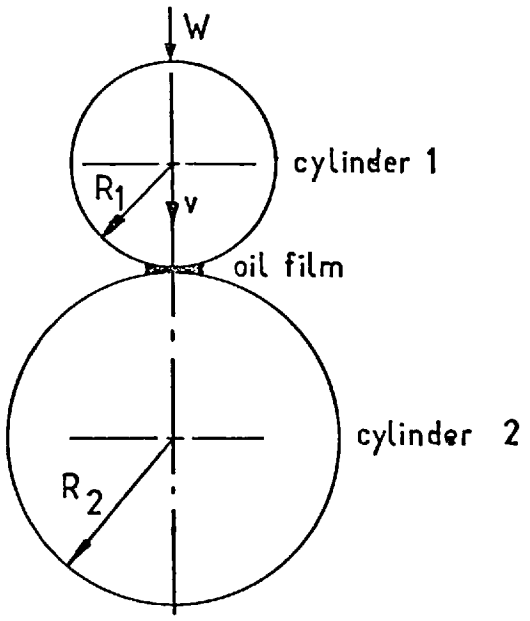
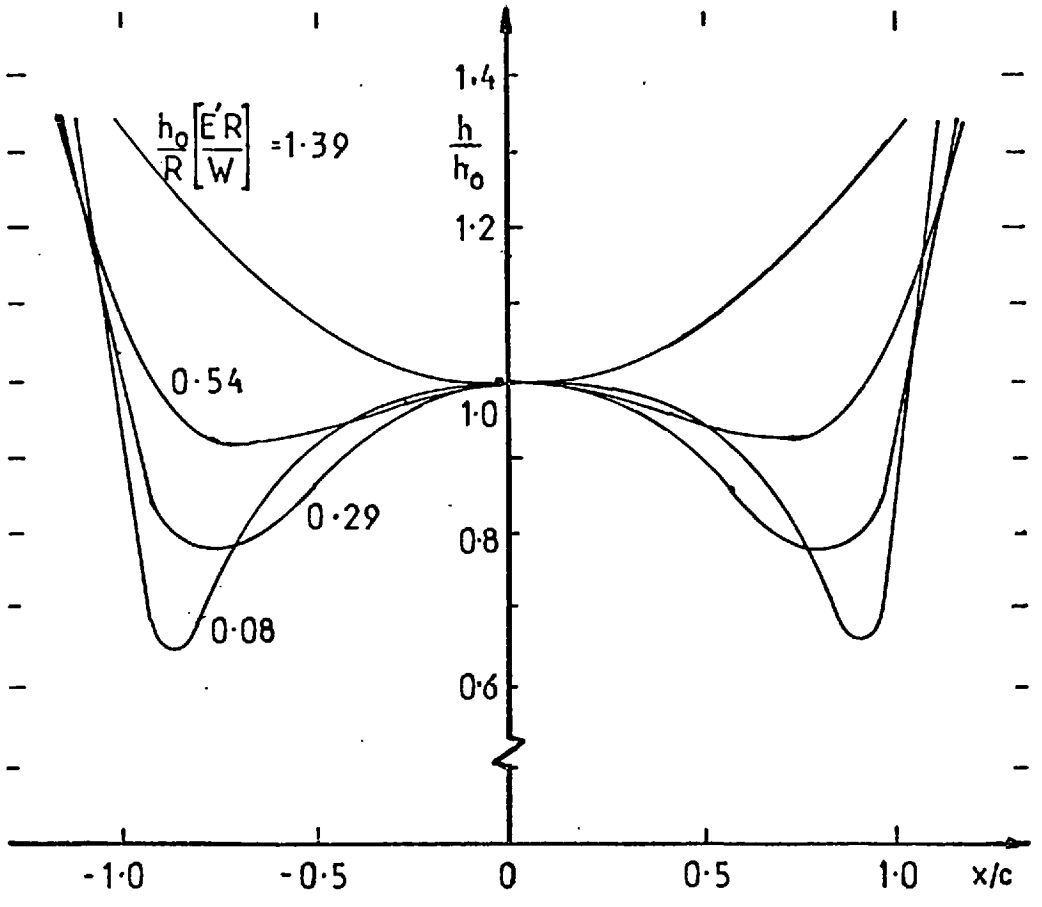


FIGURE 10.12b Dimensionless Film Profiles



(a) The cylinders were infinitely long.

(b) All inertia effects are negligible.

(c) The length of the oil film is much less than R.

(d) The film thickness is zero relative to R.

(e) The flow in the oil film is isothermal and the oil incompressible.

(f) Initial work assumed a constant viscosity but he did proceed later to the more general case of pressure-dependent viscosity.

Using the configuration shown in figure 10.12a he was able to show theoretically that there is an entrapment of fluid between the two cylinders as they come together, and graphically presented the film thickness profile across the contact and the pressure distribution.

His results showed that the application of an impact load could reduce the oil film thickness at the edge of the contact by up to 40% dependent upon the value of h_o E'/W.

10.13 EXPERIMENTAL MEASUREMENTS DURING TRANSIENT LOADING

Sanborn and Winer (62) turned to the experimental aspect of transient loading upon an oil film. They were able to measure film thickness and traction using interferometric techniques during and after a step load transient at sliding speeds from 13.7 to 92.1 inches per second. They selected lubricants which covered a wide range of η, and differing values of α (the pressure-viscosity coefficient). This resulted in the use of three Napthenic, six Paraffinic and four Synthetic fluids. The

use of a cine camera at 64 frames/second, and a strain gauge bridge for measuring the load combined with pneumatic bellows for the loading system enabled the load to be applied in less than 0.05 sec. The resulting interference fringes were continuously recorded. The inlet temperature was monitored, but was usually the same as that of the reservoir.

Traditional horseshoe oil-film thickness patterns were obtained, and as the pressure was increased from virtually zero to 150,000 lbf/in^2. in the contact, the oil film thickness was observed to fall to 2/3 of its initial value, but took between 0.10 and 0.20 sec. to reach this figure, independent of the sliding speed. That the time taken for the decrease is so relatively large (the maximum time for a point to pass through the contact is 10^{-3} sec.) is reasonable when the effect of the pressure-dependent viscosity is remembered. As the oil is virtually incompressible it has to flow out of the contact, and as the inlet is always fully flooded, the conditions there are basically unaffected by sliding speed.

They were able to draw the following conclusions.

(a) The minimum oil film thickness is in the side lobes of the horseshoe.

(b) The effect of the rapid increase in load, to 150,000 lbf/in^2. in the contact, upon the oil film thickness was not really significant, as a sudden, large reduction in film thickness was not experienced.

Their other conclusions were all related to the

chemical nature of the oils and the influence of long chain polymers on film thickness. This was not very significant for this study.

10.14 HYDRAULIC SQUEEZE FILM BEARING

An interesting application of the resistance to flow of a fluid in a contact whilst under pressure is that of the hydraulic squeeze film bearing. The bearing consists of a pair of parallel surfaces immersed in a liquid whilst one of the surfaces is oscillated at high frequency, perpendicular to the plane of the surfaces, but without causing cavitation. It was found that there is a net outward force produced, trying to separate the plates.

Kauzlarich (63) in 1971 showed that if one surface of the bearing is rigidly fixed, the load capacity can be found from

$$W = \frac{\pi R^4}{4g}\left[\frac{6\eta e\omega \cos \omega t}{h_o^2(1-e \sin \omega t)^3} - \frac{3\rho e\omega^2 \sin \omega t}{5(1-e \sin \omega t)} + \frac{15\rho\, e^2\omega^2 \cos^2 \omega t}{14(1-e \sin \omega t)^2} - \frac{3\ \rho\omega^2}{10}\right] \qquad (56)$$

Where the bearing configuration is as shown in Figure 10.13.

It can be seen that if the bearing is rotating the load capacity is reduced. Taking into account the fact that cavitation must be avoided in the bearing, otherwise the surfaces rapidly become pitted, the load capacity just before cavitation is given by

$$W = 0.393\ \pi\rho_o\ R^2\ (1/e - 1)\ (1/(1 - e^2)^{\frac{1}{2}} - 1) \qquad (57)$$

This was the first time the load capacity had been calculated for a hydraulic squeeze film bearing, though it had been done previously for gas squeeze bearings by Cameron (64). Kauzlarich conducted experiments, but owing to the large oil film gap he used, only managed to measure a load carrying capacity of 5 lbs.

10.15 CAVITATION

As it was considered at one time that the present results might partially be due to the effects of cavitation. Riddel, Pacor and Appledorn (65), in 1974 intended to simulate fatigue testing of rolling bearings by using cavitation. Total damage was probably caused by two different mechanisms.

A stressing of the metal caused by the implosion of the bubbles, and chemical attack of the surfaces, probably by atomic hydrogen coming from the lubricant and diffusing through the metal. The mechanical and chemical characteristics would thus determine the failure pattern of the specimens. Hard metals had a greater fatigue life and reactive metals would undergo more surface corrosion.

They were able to conclude that fatigue pitting was primarily chemical in nature. That is, the mechanical deformation caused by the load must be accompanied by chemical attack that weakens the structure internally, and this chemical reaction appeared to be mainly caused by hydrogen attack.

10.16 Elastic Impact of Cylinders

In 1974 a paper (69) with this title was presented by Weber, Stippes and Costello. They derived an equation for the maximum impact stress, and, by numerical integration, the time of contact. The former for dry conditions was given by:-

$$p = (q_m(k_1 + k_2)/(\pi(c_1 + c_2)))^{1/2} \qquad (58)$$

Where,

$q_m = Q_m/a$

$k_1 = 1/R_1$

$k_2 = 1/R_2$

$c_1 = (K_1 + 1)/8\mu_1$

$c_2 = (K_2 + 1)/8\mu_2$

μ = the shearing modulus

$K_1 = K_2 = 3 - 4\sigma$

$\alpha = ((k_1 c_1)^{1/2 (1+\alpha)} (k_2 c_2)^{1/2 (1-\alpha)})/4\pi$

$$Q_m^2 (3/2 + \log Q_m) = - (b V/c)^2 \qquad (59)$$

V = velocity of approach of the two cylinders at the beginning of the impact.

$\alpha = (c_1 - c_2)/(c_1 + c_2)$

$b = \pi a/(c_1 + c_2)$

$c = ((b m_1 + b m_2)/ a m_1 m_2)^{1/2}$

m_1, m_2 = mass/unit length of cylinders.

10.17 TOTAL TEMPERATURE AT SCUFFING

Forrester and O'Donoghue investigated methods of measuring surface temperatures. Their report (70) covered the methods of manufacture, uses and limitations of surface temperature sensing elements, with particular concentration on the following types.

(a) Trailing thermocouple suspended on a moving surface.

(b) Subsurface thermocouple or thermistor.

(c) Surface thermocouple, thermistor or resistance thermometer, whose junction forms part of the surface.

They showed that trailing thermocouples, if calibrated and used on a lubricated surface, as in the disc machine, could provide results within 5°C of the true value. The theoretical response and thermometric lag of surface and subsurface thermocouples were derived in their appendices.

In 1965 it was known from earlier work on gears that even when there was a sizeable oil film, scuffing could occur. O'Donoghue and Cameron (71) undertook research to determine the mechanism of scuffing which was causing this sudden instability in the running conditions. They used a 5 in. centres back-to-back tester with 30 : 30 gears of 6 D.P. A sophisticated thermocouple was built into the surface near the tip of one of the teeth, enabling the temperature of a layer extending to only 0.0005 ins. below the surface to be found. The response time was 1/10 millisecond. Voltage discharge techniques were used to determine the oil film thickness at the pitchline and tip of the teeth. Calibration yielded a constant of 4.2 volts/thousandth of an inch.

It was seen that at constant speed the steady de-

crease in film thickness with increasing load was a result of the increase of surface temperature leading to a lowering of the viscosity.

They reviewed previous work on the critical temperature at scuffing. In many instances it had been shown that the total temperature at scuffing was constant and independent of the sliding speed. In the earlier work by Ibrahim and Cameron (76) the sudden onset of scuffing when the surfaces were separated by an adequate oil film suggested that this was a consequence of the total temperature in the contact having reached the critical value for that oil/material combination.

Tests with a ball rotated at 1 r.p.m. on a hardened silver steel washer showed that a transition temperature existed for the oil at about 150°C. Up to this temperature the coefficient of friction was fairly constant at about 0.11, and thereafter it rose rapidly.

The total temperature in the work by Ibrahim and Cameron was calculated as 190 to 200°C, that is, above the transition temperature. It was concluded that the mechanism of scuffing was as follows: Any chance contact which occurred, owing to asperities touching, on metallic debris would cause welding and subsequent tearing of the surfaces. On the next revolution this would continue and the situation would escalate as the temperature rose further beyond the critical value.

Reference 73 by O'Donoghue and Cameron covered an extensive investigation into the relationship between the coefficient of friction between two discs in a disc machine and the other factors for the test.

They were able to derive the following relationship for μ the coefficient of friction.

$$\mu = 0.6(s + 22)/(35\eta^{1/8} (V_1 - V_2)^{1/3} (V_1 + V_2)^{1/6} R^{1/2}) \quad (60)$$

Where,

s = total initial surface roughness, micro-inches C.L.A.

V_1, V_2 = surface speeds of discs 1, 2 inches/second.

η = viscosity of the oil, centistokes.

R = reduced radius of contact, ins.

In the present disc machine tests the coefficient of friction was usually obtained directly by measurement, so the above equation has not been required.

The authors also studied the disc surface temperatures, but the majority of their results were similar to those given in reference 71.

10.18 PRESSURE AND DEFORMATION BETWEEN NORMALLY APPROACHING LUBRICATED CYLINDERS

Lee and Cheng (72) extended the earlier work by Christensen and Herrebrugh on the impact of lubricated cylinders. They were able to produce pressure and deformation profiles, using the Newton-Raphson method to solve the coupled, time-dependent elastohydrodynamic equations. The extent of this advance can be seen in that they were able to include the effects of lubricant compressibility, local surface velocities and a composite pressure-viscosity coefficient.

Results were presented covering a range of centre pressures from 2.5×10^4 to 1.5×10^5 p.s.i. It was seen that

a centre entrapment was produced, the film thickness was plotted for different conditions, and the results compared with those given in Christensen's work (60). The local approach velocity was found to play an important role during the final stages of normal approach. With a composite-exponential lubricant the load was strongly dependent upon the centre pressure.

The quantitative results are not presented here as they will be used in detail in Chapter Fifteen.

10.19 SCUFFING OF CIRCUMFERENTIALLY GROUND DISCS

Dyson's paper (74) proposed that discs scuff when the asperities contact because it is no longer possible to generate high pressures by the main elastohydrodynamic system, through the operation of the modified Reynolds' equation.

$$dp/dx = 6\eta\ (U_1 + U_2)(E(H) - (E(H))_m)/E(H^3) \qquad (61)$$

Where E is the expectation operator (positive values only) given by

$$E\ (H^n) = \int_0^\infty H^n\ F\ (H)\ dH$$

F(H) is the probability density distribution of H, which is the load gap between the surfaces.

$H = h - h_1 - h_2$

h = mean separation of the surfaces.

h_1, h_2 = height of the two surfaces, measured outwards from the surface.

$(E(H))_m$ is the value of E(H) at the position of zero gradient of the mean pressure.

The conditions for failure may be predicted if the surface height distribution and force-compliance relation are known.

He proposed that as the disc bulk temperature gradually increases during the course of a test, the surfaces tend to approach one another more closely to maintain the effectiveness of the pressure generating system. This approach was limited by the discs configuration in dry contact. Failure occurs when the necessary high pressures are not developed to prevent direct asperity contacts. Dyson then used the results from this theory to compare theoretical scuffing points with those obtained from experiment. The correlation was satisfactory.

Dyson's paper was the first to attempt to predict scuffing conditions from first principles, and in which the effect of surface roughness both on the contact mechanics and on the hydrodynamics was considered.

10.20 CONCLUSIONS

The study of squeeze films and the effect of oscillating loads, which started with the work of Stefan and Reynolds has evolved to encompass surface chemistry, pressure-viscosity effects and non-Newtonian fluids. The generalised Reynolds' equation has been modified to eliminate many of the original assumptions, and Dowson (55) was able to produce a modern version, albeit far more complex, in which the only assumptions were the following:

(a) The radius of curvature of bearing components is large compared with film thickness.

(b) The lubricant is a Newtonian fluid.

(c) Inertia and body terms are small compared with the viscous and pressure terms in the equations of motion.

(d) From the geometry of the fluid film, the derivations of u and v with respect to z are large compared with all other velocity gradients.

(e) There is no slip at the boundaries.

The work of the above authors indicated that considerable changes would occur in the contact whilst subjected to an oscillating load. For example, the load at any instant would not be equivalent to the integral $\int p \, dA$. In the next Chapters the findings of the above authors will be related to the present results to explain the observed phenomena.

CHAPTER ELEVEN

HYPOTHESIS THAT LOW SCUFFING LOADS WERE ATTRIBUTABLE TO RESONANCE

11.1 INTRODUCTION

Type B to M tests had shown that scuffing occurred at a lower load for certain applied load frequencies. It was possible that this was induced by either a resonance condition, or that the applied load frequency was an integral multiple of the disc rotational frequency. This chapter investigates the validity of this hypothesis, beginning with the possibility that, in one mode or another, the disc machine was resonating at the applied load frequency.

11.2 INVESTIGATION OF THE DISC MACHINE USING A MOBILITY METER

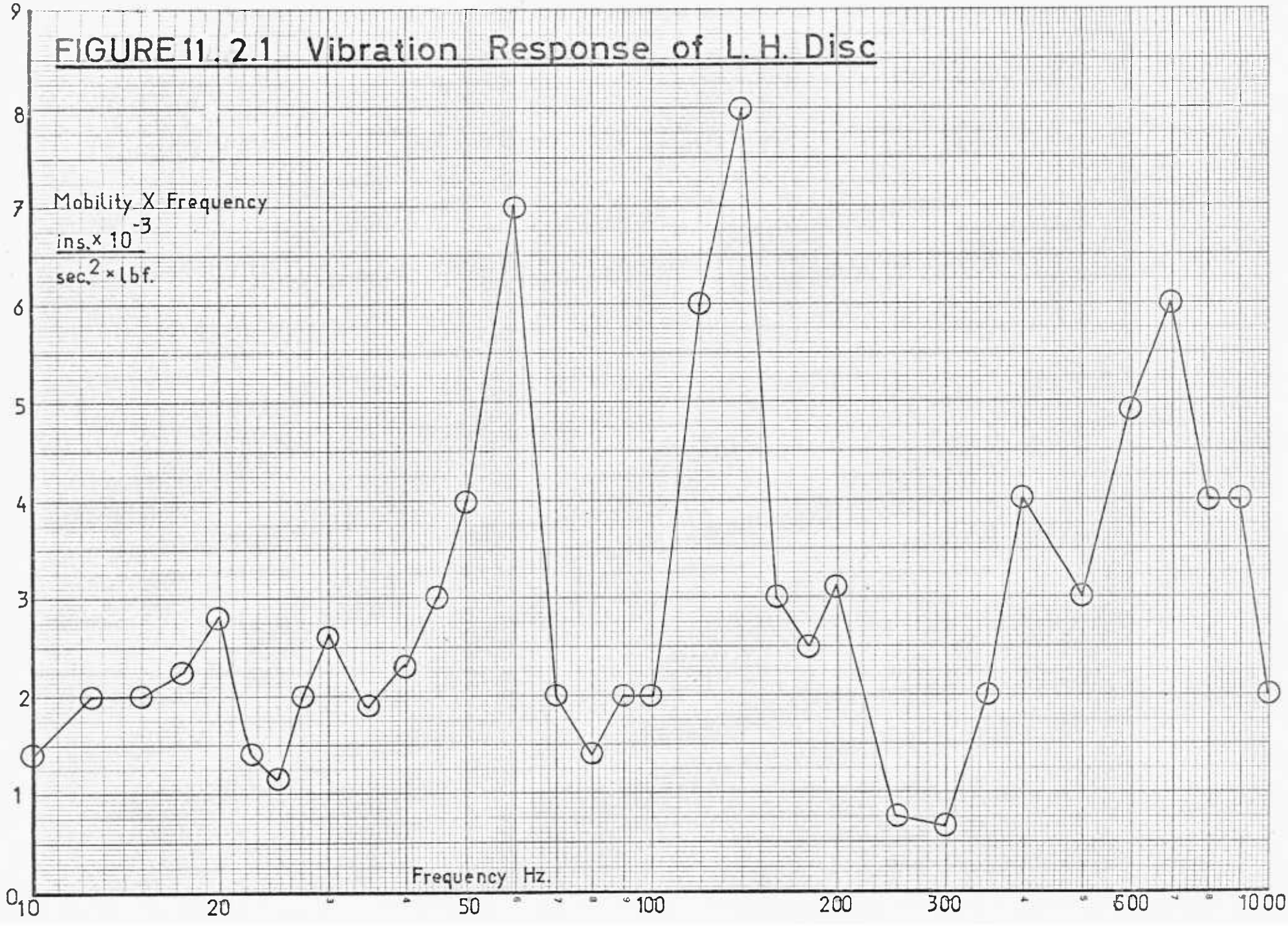
With the discs mounted on their spigots a mobility meter, frequency generator and accelerometer were used to determine any disc resonances, as follows.

11.2.1 Test 1

The left hand disc was excited on its spigot, whilst an accelerometer was attached at the point which would normally be in contact with the right hand disc. With the gap between the disc and spigot filled with oil the signal generator was swept through the frequency range from 10 to 1000 Hz. The results are plotted on graph 11.2.1.

11.2.2 Test 2

For this test the excitation was applied to the disc casing, which forms the disc support housing and the


FIGURE 11.2.1 Vibration Response of L.H. Disc
Mobility X Frequency
ins. x 10^-3
sec.^2 x lbf.
Frequency Hz.
0
1
2
3
4
5
6
7
8
9
10
20
50
100
200
300
600
1000

response of the right-hand disc on its support measured through the same frequency range. The accelerometer was attached at the point where contact would normally occur with the left-hand disc. The results are shown in graph 11.2.2.

11.2.3 Test 3

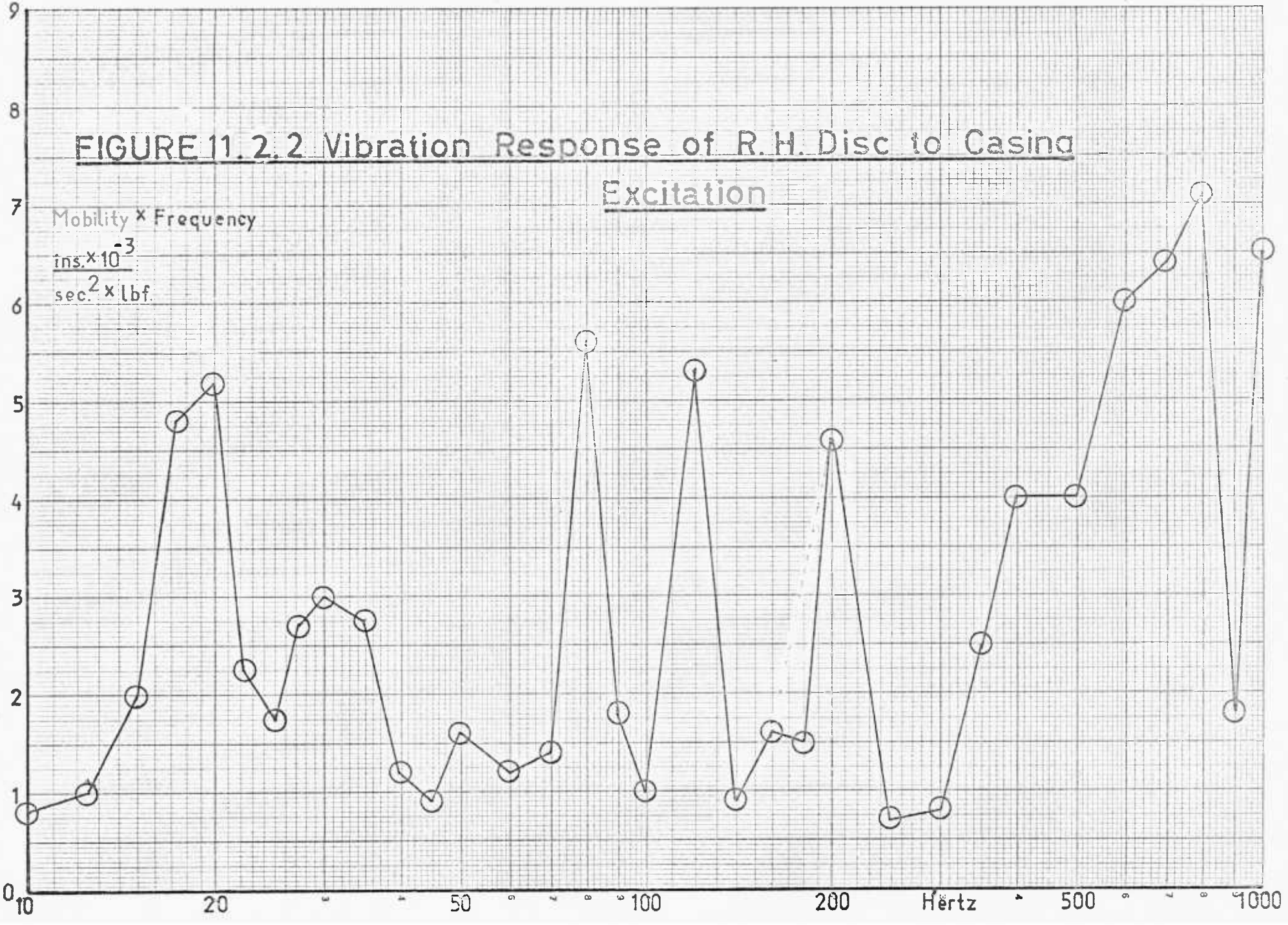
The resultant response of the two discs in combination was measured by exciting the left-hand disc. The frequency range from 10 Hz. to 1 kHz. was covered. Care was taken to ensure that the gap between the discs and spigots was filled with oil. The data is plotted in graph 11.2.3.

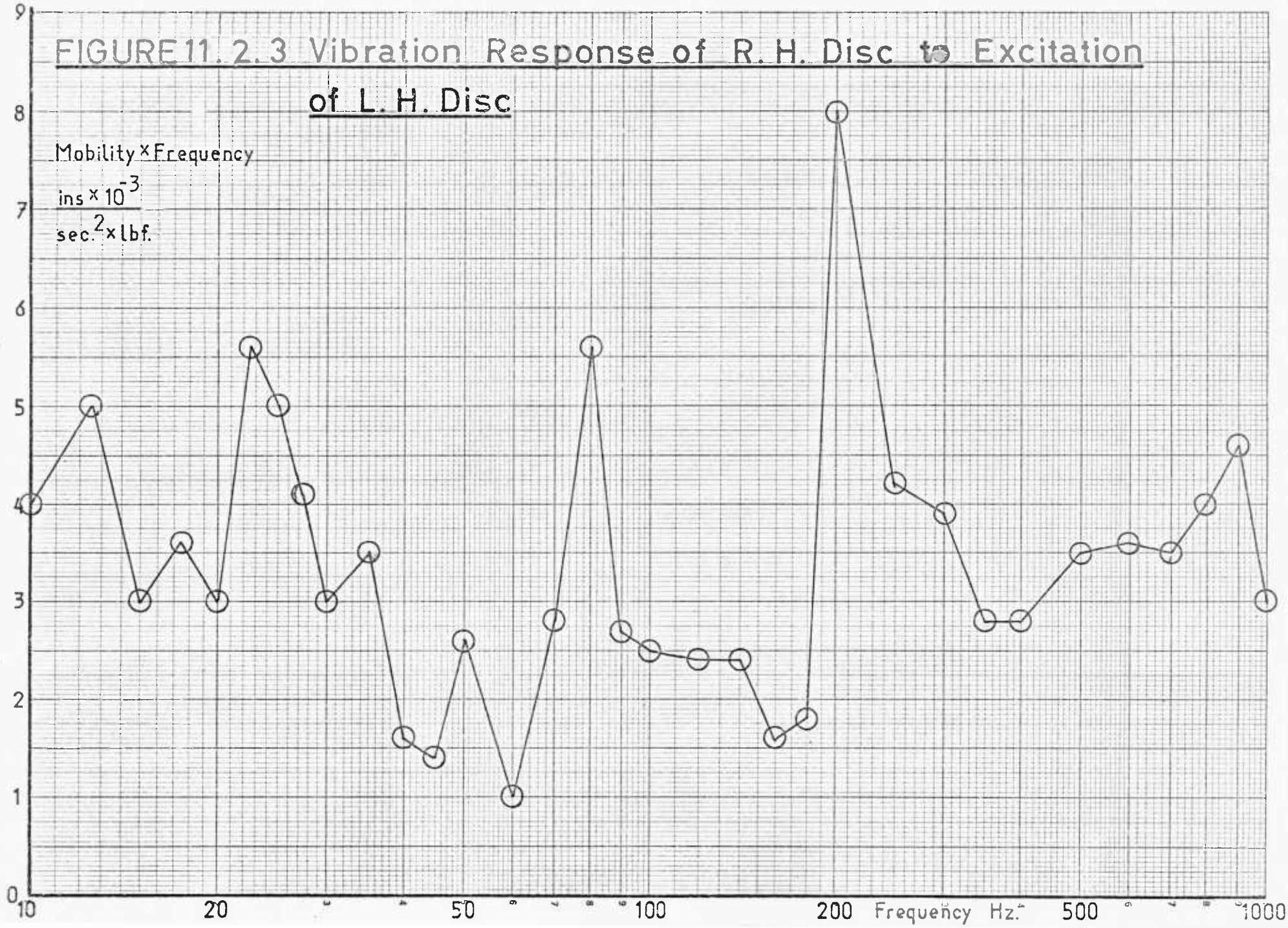
11.3 DISCUSSION OF MOBILITY METER RESULTS

An initial examination of the three graphs indicated that distinct peaks are occurring. However the vertical axis of the graphs reveals first, that all the responses are within an order of magnitude and secondly that the actual magnitude of the response throughout the frequency spectrum was small.

When an investigation is conducted for resonance a far greater variation in the amplitude level is normally expected. The low level of response to the applied excitation was due to the oil providing effective damping to any movement.

It was concluded that no resonance of the discs on their spigots was occurring, either independently or in combination, between 10 and 1000 Hz.


FIGURE 11.2.2 Vibration Response of R.H. Disc to Casing Excitation
Mobility x Frequency
ins. x 10^-3 / sec.^2 x lbf.
0
1
2
3
4
5
6
7
8
9
10
20
50
100
200
Hertz
500
1000


FIGURE 11.2.3 Vibration Response of R.H. Disc to Excitation of L.H. Disc
Mobility x Frequency
ins x 10^-3
sec.^2 x lbf.
0
1
2
3
4
5
6
7
8
9
10
20
50
100
200
500
1000
Frequency Hz.

11.4 EXAMINATION OF THE TORQUE FOR DISC RESONANCES

The strain gauges measuring the torque on the discs are mounted on driving blades, which engage with the disc driving rings. The inertia of the system is thus very low, and any fluctuations in the torque are immediately detected. Under normal running conditions a 2,000 μF capacitor is connected across the inputs to the pen recorder to remove high frequency "noise" from the torque trace.

If the discs were experiencing resonant or unstable conditions then these should cause fluctuations in the torque. The output from the strain gauges was connected to the second channel of the cathode-ray oscilloscope, on which the pressure waveform was displayed.

The discs were run at 1100 and 500 r.p.m., under a load of 665 lbf. Oscillating this load at a level of $\pm$ 5% throughout the frequency range from 2½ to 60 Hz. enabled measurements to be taken from the oscilloscope, of the torque.

11.5 RESULTS FROM DISPLAYING THE TORQUE ON THE OSCILLOSCOPE

Surprisingly, at all frequencies the variations in the torque, expressed as a strain gauge voltage were between 0.6 and 0.8 mV, and were of a random, high frequency nature. Synchronisation of the pressure and torque traces could not be observed. 0.8 mV represents a level of $\pm$ 12½% on the mean value and arises from asperity contacts.

It was concluded that the discs were not in a state of resonance, either mechanical or hydrostatic.

11.6 CHECKING THE FLEXIBLE PIPES FOR HYDRAULIC RESONANCES

It was possible that a standing wave was occurring in one or more of the flexible high pressure oil pipes supplying the three oil pressure pockets. To examine whether this was the case, a steel adaptor was machined which enabled the oil pressure transducer to be installed in any of the high pressure pipes at the point where it entered the disc housing (Figure 11.6). The resonant frequency of the pressure transducer was in excess of 10 kHz., which would ensure that it registered any dynamic pressure variations present.

The first test was conducted as in 11.4. This was followed by recording the dynamic pressures when there was no applied fluctuation, but the disc speeds were varied between (a) 875/375 and (b) 1375/625 r.p.m. with a load of 700 Lbf.

11.7 RESULTS FROM INSTALLING THE PRESSURE TRANSDUCER ADJACENT TO THE DISC HOUSING

Considering the latter tests first it was found that variations in the disc speed did not affect the pressure in the pipes. Any ovality of the discs or variation in the oil film thickness passed undetected. However, there was a consistent variation in the pressures of 15 lbf./in^2. occurring in all the pipes at 72 Hz., caused by the three pistons in the oil pump which rotates at 1440 r.p.m. It was considered that this variation was sufficiently small to be ignored.

Returning to the first test, the pressures at the disc end of the flexible pipes to the left-hand disc were identical to those at the outlet from the servovalve. No form of standing wave or resonance could be detected, and

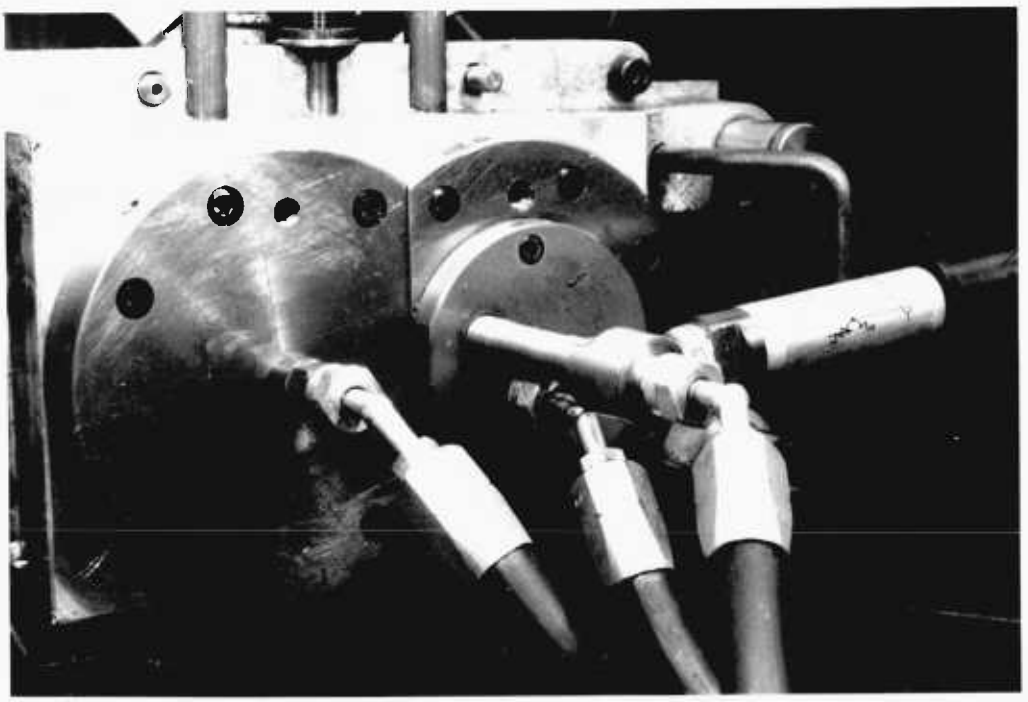


Figure 11.6 Pressure Transducer Installed next to the Disc Housing.

control of the waveform amplitude and frequency was unimproved.

Installation at the end of either of the flexible pipes to the right-hand disc showed that the fluctuating pressure in these lines was similar to that for the left-hand disc, in frequency, phase and shape. However the amplitude was always less, as in each pipeline to the right-hand disc there was a capillary, installed in the disc spigot.

Again it was concluded that no resonances or standing waves could be generated throughout the frequency range.

11.8. DISCUSSION

Although the above sections showed that the existence of a resonant situation was very unlikely, another form of mechanically induced failure could occur, as follows.

11.9 COMPARISON OF THE DISC AND APPLIED LOAD FREQUENCIES

If the situation existed that the change in load was at the same point on the disc each time, it was reasonable to expect that rapid damage to the surface would result. To examine this possibility Table 11.9a and 11.9b were drawn up, and it is seen that such a condition did not occur.

Table 11.9a Rotational Frequencies in Hz. occurring in the Disc Machine

Type of Test	L.H. Disc	R.H. Disc	Difference in Speeds	Frequency at which same points come together	Frequency at which the lowest scuffing load was obtained
B	18.3	8.3	10.0	1.67	15
D	22.9	10.4	12.5	2.08	10
E	13.7	6.2	7.5	1.25	15
F	14.2	8.3	5.8	0.83	20
H	22.7	13.3	9.4	1.33	20
I	17.8	9.9	7.9	0.99	10
J	21.0	12.3	8.7	1.24	-
K	13.2	6.8	6.4	0.49	10
M	18.3	8.3	10.0	1.67	15

The table 11.9b extends to the fourth Fourier component as this could be a significant portion of the waveform.

Table 11.9b Frequencies of the first Four Fourier Components, in Hz.

Basic Frequency	Harmonics 2nd	3rd	4th
10	20	30	40
12½	25	37½	50
15	30	45	60
20	40	60	80
30	60	90	120
60	120	180	240

11.10 CONCLUSIONS

From the above it was concluded that the low loads at which scuffing occurred in some of the tests were not attributable to either:

(a) Hydraulic or mechanical resonance in the disc machine altering the load between the discs from the specified one, or

(b) A state of synchronisation occurring between the disc rotational frequency and any significant harmonic of the applied load frequency, such that each load cycle or harmonic was repeatedly commencing at the same point on the disc surface.

CHAPTER TWELVE

HYPOTHESIS THAT CAVITATION WAS CAUSING THE REDUCED SCUFFING LOADS

12.1 INTRODUCTION

The occurrence of cavitation during vibration in the disc machine might well precipitate scuffing. The following section examines the merits of this hypothesis.

12.2 CAVITATION

As stated in 10.15, Riddel, Pacor and Appeldorn (65) investigated cavitation induced pitting and showed that it was the result of combined mechanical and chemical effects.

The discs in the disc machine were forced together with a load which was never less than 95% of the mean value. Furthermore, the inlet was kept fully flooded. Cavitation under these conditions is very unlikely, as verified by the work of Hunt (58).

He showed that small oscillations in the relative position of two surfaces could produce large changes in the pressure between them. He expressed the relationship as follows (using British units).

$$p_{max} = \pm 2.6\ \mu\omega\ (a/h)\ (R^2/h^2)\ (1+1.5\ (a/h)) \qquad (62)$$

Where the position of one surface, relative to the other can be expressed by the equation

$$\varepsilon = h + a \sin \omega t$$

Where,

R is the radius of the contact in the plane of the contact.

a is half the total amplitude of vibration of the surfaces.

h is the mean separation of the surfaces.

ω is the frequency of the surface oscillations in rad/sec.

The $\pm$ occurs because the pressure peaks apply in both senses, adding or subtracting from the mean level. Cavitation occurs when the pressure in the contact is negative. With a load of 760 lbf., and assuming a value of a/h as high as 0.2, the minimum frequency to cause cavitation can be calculated as follows.

$$133{,}000 = \pm\ 2.6 \times 5.8 \times 10^{-6} \times \omega \times (0.2)\ (4.08 \times 10^{-2} / 5.04 \times 10^{-5})^2 \times (1 + 1.5\ (0.2))$$

Therefore $\omega = 8{,}238$ Hz.

This was well outside the range of frequencies employed and any such oscillation would be damped by the oil film (see 11.2). The resonant frequency of the discs, in radial oscillations, without damping had been measured as just under 300 Hz. From the dynamics of the system, any oscillations, whether free or forced at frequencies above this would be rapidly attenuated.

12.3 CONCLUSION

From these investigations cavitation can thus be ruled out as a viable failure hypothesis.

CHAPTER THIRTEEN

HYPOTHESIS THAT SCUFFING OCCURRED AT CONSTANT TOTAL TEMPERATURE

13.1 CRITICAL TEMPERATURE HYPOTHESIS

The influence of the load on scuffing is mainly through its effect on temperature as discussed by Macpherson (3), O'Donoghue and Cameron (71) and Dyson (74). O'Donoghue and Cameron (71) showed that in many instances the total or peak temperature at scuffing was constant and independent of sliding speed. With plain oils the total temperature equalled 150 to 200°C at scuffing. They showed that this critical temperature was related to the transition temperature for the oils, (see 10.17) in that the discs or gears would scuff once it had been exceeded.

If this hypothesis were valid for the disc machine then it would be extremely useful in predicting failures.

13.2 TOTAL TEMPERATURES IN THE DISC MACHINE

The total peak temperature in the contact is the sum of the measured disc surface temperature plus the flash temperature rise calculated from

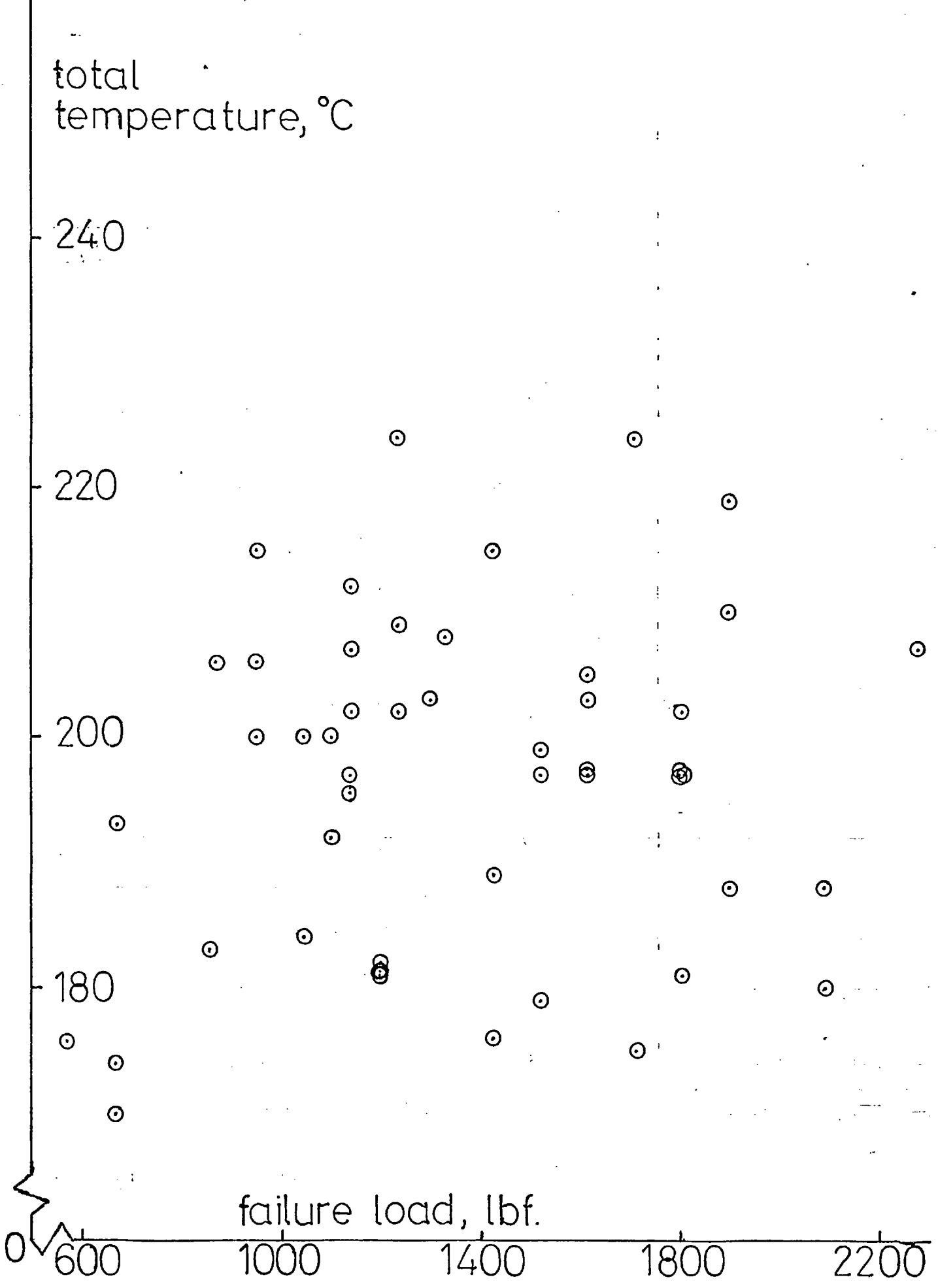
$$TF = (2bk/\pi)^{1/2} \, (\mu W/JLbK) \, ((U_1-U_2)/(U_1^{1/2}+U_2^{1/2})) \qquad (65)$$

For the disc machine (65) reduces to

$$TF = 0.0171 \, \mu \, W \, (N_1^{1/2} - N_2^{1/2})/b^{1/2} \qquad (66)$$

The total temperatures at failure in the disc machine tests varied between 170 and 224°C, and are plotted in Figure 13.2. The distribution of the results is less than would have

FIGURE 13.2 Total Temperature / Load at Scuffing



expected from the range of sliding speeds, which vary between 5.0 and 10.7 ft./sec. and the consequent failure loads which range from 665 to 2375 lbf.

Hence it was conceivable that the discs were scuffing in accordance with the critical temperature hypothesis. Before this could be confirmed it was necessary to determine the accuracy of the calculated total temperature figures and also measure the transition temperature for the oil/material combination.

In Appendix Nine the total possible error in the value for the total temperature was calculated as $\pm$ 14°C. This does not encompass the actual variations in the total temperature, which amounted to $\pm$ 27°C.

Appendix Eight describes the work done to measure the transition temperature for the oil/material combination. With a conventional mineral-based lubricant a rapid increase in the coefficient of friction would be expected above a certain temperature, as the oil ceased to lubricate satisfactorily. This temperature is known as the transition temperature for the oil.

The present oil did not exhibit such a transition, and this probably arises because the oil is synthetic, and has a considerable anti-wear additive content. Accordingly, it is to be expected that a fairly wide range of total temperatures at failure would be obtained.

13.3 CONCLUSIONS

At first sight it appeared that the disc machine failures were in accordance with a critical temperature at failure hypothesis. However two factors led to the rejection

of this hypothesis. These were:

(a) The spread of 54°C in the calculated value for the total temperatures. This could not be accounted for by experimental error, and

(b) Over the range of temperatures encountered in the disc machine a transition temperature did not exist for the oil/material combination.

CHAPTER FOURTEEN

HYPOTHESIS THAT SURFACE FATIGUE WAS INDUCING SCUFFING

14.1 INTRODUCTION

Although no signs of pitting could be detected on the scuffed specimens, it was possible that the repeated stressing could have caused the discs to fail. A decrease in the scuffing load as the frequency was raised (see Figures 8.3 to 8.13) implied that a fatigue mechanism was acting.

The stress report by Westland Aircraft (13) demonstrated a practical method of applying Miner's Law (the cumulative damage hypothesis) to the results obtained from an unsteadily loaded gearbox. As the magnitude, frequency and Fourier components of the applied waveforms, were known in the present tests, the application of Miner's Law was practical using the same method.

14.2 APPLICATION OF MINER'S LAW

The following had to be calculated:-

(a) The number of load cycles that had been experienced by a point on the disc at the time of failure, and

(b) the surface stress occurring during each load cycle.

The former is considered first and was the sum of two contributions.

1. The stress cycles due to passing through the contact.

2. The stress cycles caused by the load fluctuations. However these were distributed around the periphery of the disc, so the percentage occurring at any point was calculated as follows:-

At 1300 lbf. the Hertzian band width for the contact is 35×10^{-3} ins. found from

$$b = ((8 \times W \times R) / (\pi \times L \times E))^{1/2}$$

Where b is half the Hertzian contact width in cms.

It can be seen that h is proportional to $W^{1/2}$. For the purposes of this investigation it was assumed to be the same at all loads, as the actual value is not critical.

Dividing the circumference of the disc by the contact width showed that at any moment 0.34% of the periphery was in the contact. With the assumption that the load fluctuations were evenly distributed around the disc, the number of stress cycles at a point could be calculated. Table 14.2 was drawn up for an applied load frequency of 20 Hz.

The application of Miner's Law also required that the surface stress was known. As the calculated surface stress is proportional to $W^{1/2}$ (see 8.1) a load fluctuation of $\pm$ 5% would produce a stress change of $\pm$ 2½%. These stresses are shown in Table 14.2.

Table 14.2 Surface Stress and Number of Cycles at Failure

Cycles due to passing through the contact		Cycles at a point due to the fluctuating load	Calculated mean stress at failure	Calculated peak stress during load cycle
L.H.	R.H.	No.	lbf./in^2.	lbf./in^2.
For a failure at 760 lbf. load stage				
27,500	12,500	102	133,000	137,000
For a failure at 1615 lbf. load stage				
71,500	32,500	267	195,000	200,000

Miner's Law states that failure will occur when,

$$\sum_{n=n_1}^{n=n_x} n/N = 1$$

Where n_1, n_2, ... n_x are the number of cycles of stress to which the surface was subjected at stress levels for which failure would occur after N_1, N_2, ... N_x cycles.

Table 14.2 shows that the increase in the number of stress cycles when a fluctuating load was used was less than 1%. The increase in the stress level during these cycles was 2½%.

The graph of applied stress versus number of cycles to failure for surface fatigue of gear steels has a relatively shallow slope $((p_{max2}/p_{max1})^9 = (N_1/N_2)$. Thus Miner's Law could only account for a reduction, in the total number of cycles to failure, of 1.25%. The average reduction in scuffing load, at the worst point for each of the types of test, was 29%, which corresponds with a considerably greater reduction in the number of stress cycles.

14.3 CONCLUSIONS

Not at any stage during the testing had peaks been observed in the output from the pressure transducer. These would have indicated that an amplification of the applied load changes was occurring in the contact. With the discs subjected to surface stressing as calculated, Miner's Law could not account for the measured scuffing loads.

CHAPTER FIFTEEN

HYPOTHESIS THAT SCUFFING WAS INITIATED BY THE FORMATION OF A TEMPORARY ENTRAPMENT

15.1 INTRODUCTION

From the work of Christensen (59, 60) Herrebrugh (61) and Lee and Cheng (72) a possible mechanism to advance the onset of scuffing with a vibrating load was as follows.

When the discs are forced towards one another with each increase in the applied load, a pocket is formed in the disc surface, which supports the load, albeit at a far higher oil pressure. However, around the edges of the pocket the film thickness is less than normal. This produces higher flash temperatures and increased asperity contact which, after several passes through the contact, is sufficient to initiate scuffing. This occurs at a load which is less than that which could be supported with a constant film thickness.

This model was used for the following discussions.

15.2 THE PRESSURE AND DEFORMATION PROFILE BETWEEN TWO CYLINDERS IN NORMAL APPROACH

Christensen (60) in 1961 was the first to undertake a detailed theoretical study of the lubricated impact between a sphere or cylinder and a flat surface.

The starting point for any such investigation is Reynolds' equation, which for a cylinder and plane is

$$\frac{\partial}{\partial x}\left(\frac{h^3}{\eta}\frac{\partial p}{\partial x}\right) = -12\frac{\partial h}{\partial t}$$

and has boundary conditions

$$p = 0 \text{ for } x = \pm\infty$$

The contacting surfaces deform because of the high pressures induced, and these deformations effect the manner in which the oil film thickness varies. Hence the rate of change of oil film thickness $\partial h/\partial t$ at any particular time will vary throughout the contact in a manner which is initially unknown, as discussed by Conway (79). The pressure generated will increase the viscosity and density of the oil, which will in turn react with the pressure. Shear in the oil will produce heat, and the consequent temperature rise will reduce the viscosity. Finally, at high approach speeds the inertia of the oil may need to be considered.

Solutions to the problem thus necessitate relatively large assumptions, or the use of a numerical iterative process utilising a computer. Conway and Lee (77) did the former, whilst Christensen (59, 60), Herrebrugh (61) and Lee, K.M. and Cheng (72) have attempted iterative solutions.

15.3 OIL FILM IN A CLOSING GAP

Christensen (60) in a paper with this title presented a solution for the normal approach of two elastic cylinders separated by a lubricating film whose viscosity depended on pressure. He showed that very high pressures may be developed in the centre of the contact at a finite separation of the cylinders. This confirmed earlier findings by Rabinowicz (78) namely that in the impact between a sphere and a flat surface, the presence of oil caused dents which were deeper and more conical in shape than the more spherical ones of dry impact. In certain cases, the lubricated dents were smaller, but deeper than the dry impact areas.

Christensen's findings were applied to the conditions existing in this disc machine. A representative running condition, for which reduced failure loads had been obtained with a dynamic load, was chosen.

Christensen's work was used to determine the effect of each sudden pressure change upon the film and pressure profile. The data is tabulated in Table 15.3.

Table 15.3

Data for Type B or M tests at a Mean Load of 950 lbf.

L.H. Disc Speed	1100 r.p.m.
R.H. Disc Speed	500 r.p.m.
Initial load	900 lbf.
Final load, after servovalve switches	1000 lbf.
R, Equivalent radius of the contact	0.815 ins.
E, Equivalent Young's Modulus	32.6×10^{6} lbf./in^2.
α, pressure-viscosity coefficient	10.4×10^{-5} ins^2/lbf.
L, width of the contact	0.25 ins.
σ, Poisson's ratio	0.285
p_o, Maximum pressure for a steady-state load of 1000 lbf.	153×10^{3} lbf./in^2.
h_o, steady-state film thickness with a load of 900 lbf. (see 8.1)	49.3×10^{-6} ins.
h_o, steady-state film thickness with a load of 1000 lbf.	48.6×10^{-6} ins.
$\eta_{atm.}$, Viscosity at ambient pressure and 50°C	5.8×10^{-6} Reynes.
b, half Hertzian bandwidth for a steady load of 1000 lbf.	0.0153 ins.
$\rho_{atm.}$, oil density at ambient pressure	0.89 grms./ml.

G, αxE	3390
$\bar{\alpha}$, αx p_o	15.6
W, w/ER @ w = 1000 lbf.	15×10^{-5}

Where,

$$R = 1/(1/R_1 + 1/R_2)$$

$$E = 2/((1/E_1 + 1/E_2)(1 - \sigma^2))$$

Subscript $_o$ indicates that the quantity refers to the centre of the contact.

The following assumptions have been made.

(1) The cylinders are infinitely long.

(2) All inertia effects are negligible.

(3) The length of the oil film is much smaller than R.

(4) The film thickness is vanishingly small compared with R.

(5) The flow in the oil is isothermal and incompressible.

Christensen also used the following normalised, non-dimensional variables.

$$\bar{W} = \pi W \alpha^2 E/8LR$$

$$\bar{h}_o = \pi^2 \alpha^2 E^2 h_o/32R$$

He plotted the non-dimensional load against central film thickness for pressure-dependent viscosity and elastic material, as shown in Figure 15.3a.

If one assumes that the 900 lbf. load was being supported by the rolling action of the discs, then with the sudden increase in load at 1000 lbf. the cylinders would momentarily behave as discussed in Christensen's work. Assuming that the extra 100 lbf. is momentarily supported as an impact

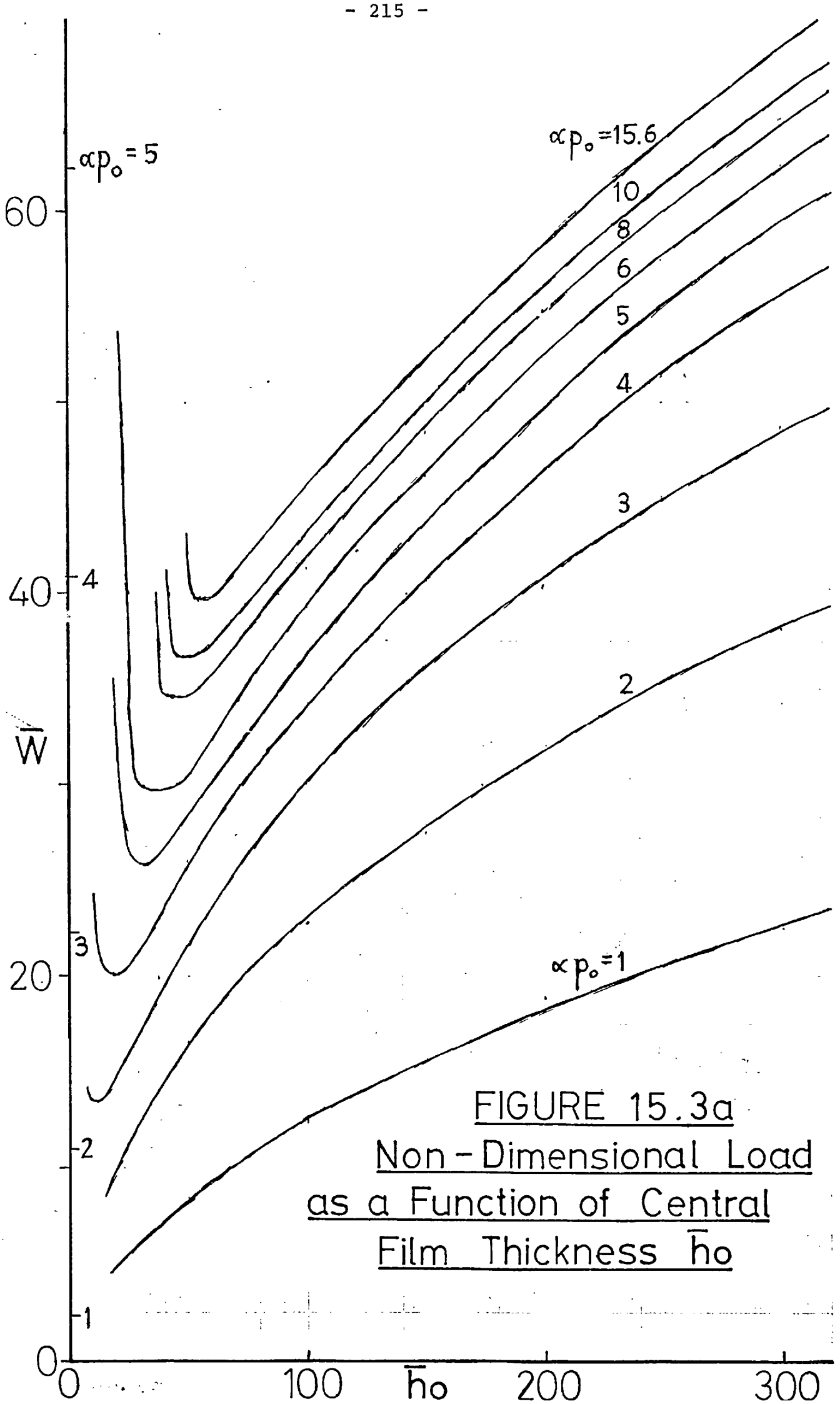


FIGURE 15.3a
Non-Dimensional Load as a Function of Central Film Thickness $\bar{h}o$

load his results were applied as follows.

For the conditions under consideration in Table 15.3, $\overline{W} = 680$, $h_o = 211$ and $\alpha p_o = 15.6$. It can be seen that in Figure 15.3a the point corresponding with $\overline{W} = 680$ and $h_o = 211$ is well above the curve for $\alpha p_o = 15.6$. From the figure a central pressure of $\alpha p_o = 15.6$ could only support a normalised load $\overline{W}$ of 62. Consequently far higher central pressures would have to be produced in the contact to support a normalised load of 680. In a case analysed by Christensen (where $\alpha p_o = 10$, R = 1.97 ins., $\alpha E = 1400$ and W/L = 856 lbf./in.) he showed that only 15% of the Hertzian load could be applied if the maximum pressure was not to exceed the Hertzian value. However this point occurred at the lowest point of the curve for $\alpha p_o = 10$ in Figure 15.3a, whereas in the disc machine the calculated normalised film thickness was several times greater than that at the lowest point of the curve $\alpha p_o = 15.6$, and thus the conditions in the disc machine were less severe.

Christensen (60) showed that with a pressure-dependent viscosity at a sufficiently high αp_o (which is satisfied by $\alpha p_o = 15.6$) a small increase in the load would bring about a large increase in maximum pressure.

He recalculated the pressures for his case when αE was increased by 100% to 2800, p_{max}, Hertzian was 37,500 and h_o was 15. This showed that for an increase in load of only 6.6%, the maximum pressure had increased by 25%. This pressure would act over an area smaller than the Hertzian contact zone for a short time. Such a pressure distribution would produce large shear stresses close to the surfaces and considerably reduce the fatigue lives of the specimens.

FIGURE 15.3b Film and Pressure Profiles for $h_o = 99$

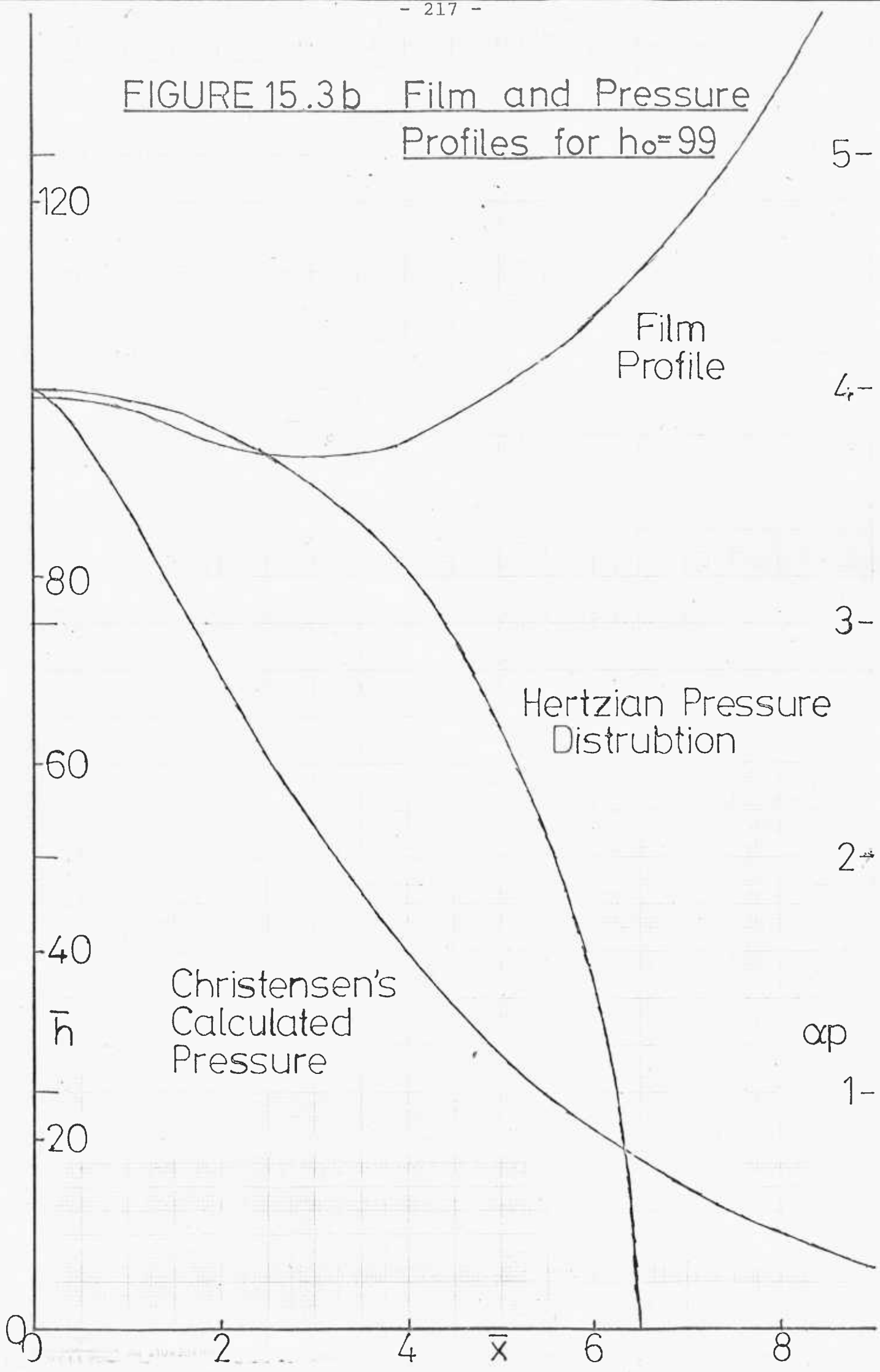


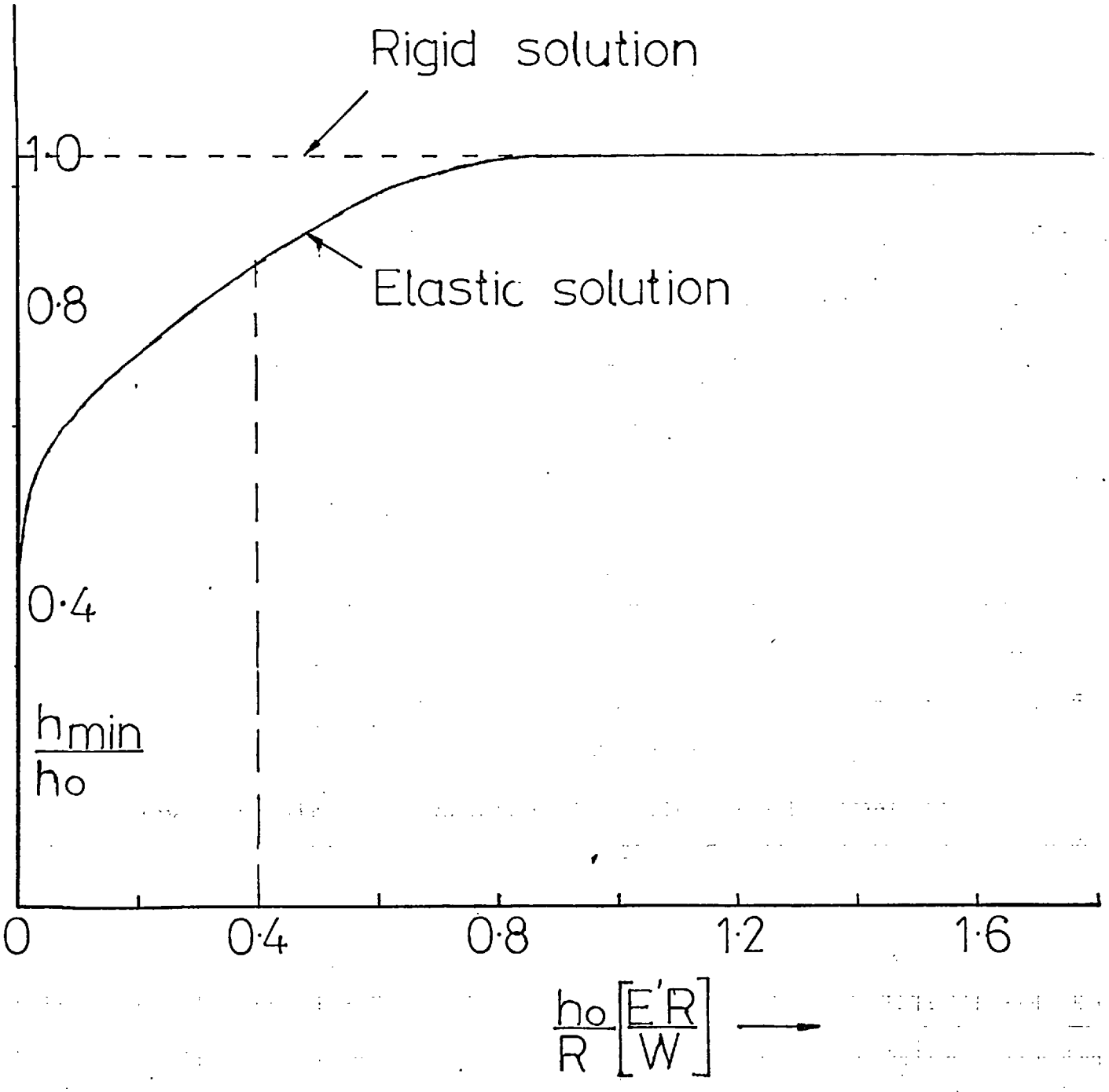
Figure 15.3b shows Christensen's calculated pressure distribution and film profile for $h_o = 99$. In the figure the Hertzian pressure distribution is superimposed. It can be seen that for the same load a far higher central pressure is required in the impact case, in comparison with the Hertzian condition. The fact that the cylinder's surface had formed an entrapment was verified by experimental work.

15.4 ELASTOHYDRODYNAMIC SQUEEZE FILM BETWEEN TWO CYLINDERS IN NORMAL APPROACH

Herrebrugh (61) extended the examination to cover the range of conditions where large deformations occurred, and thus more closely simulated the conditions occurring in the disc machine. Unfortunately his investigation was based on the assumption of uniform velocity distribution and a constant fluid viscosity, which limited the accuracy of the results obtained to those of a first approximation.

Using the film thickness parameter h_o ER/WR he separated the central film thickness from the squeeze velocity, and related many of his results to this dimensionless parameter. In Figure 10.12b the central film thickness was plotted for varying values of h_o ER/WR, and it may be seen that during impact loading an entrapment is again formed. That this should occur with an isoviscous fluid is very significant, as it shows that this film profile will not solely arise with fluids having a pressure dependent viscosity. Figure 15.4 shows the minimum film thickness at the edges of the contact plotted for a range of values of the film thickness parameter.

FIGURE 15.4 Minimum Film Thickness as a Function of Film Thickness Parameter



With the assumptions, as before, that the load behaves as an impact load at the moment of the pressure increase, the data in Table 15.3 produced a value for h_o ER/WR of 0.396. From the graph it can be seen that even with an isoviscous fluid the film thickness at the edges was 15% less than at the centre.

Herrebrugh (61) also produced pressure profiles for the contact, which displayed a sharper peak than the Hertzian profile, when the loads were high.

15.5 ELASTOHYDRODYNAMICS OF NORMAL APPROACH

Christensen (59) produced a graph similar to 15.3a the normal approach for a rigid sphere and semi-infinite plane through a fluid with a pressure dependent viscosity. The graph showed that for any given central pressure the load capacity decreased as the central film thickness reduced, until a point was reached, close to the surface, where a sharp reversal occurred, the load capacity increased rapidly, and at zero film thickness the load had recovered to the Hertzian value.

His main conclusions were:-

(a) For values of the central film thickness larger than the transition value, which is the situation in the disc machine, load and relative velocity are far more influenced by the increase in viscosity with pressure than by the effects of elastic distortion.

(a) For metalic contacts lubricated with mineral oil, the transition film thickness can be quite small, even compared to the surface roughness of finely machined surfaces. This was demonstrated in 15.3, where the transition film

thickness in Figure 15.3a for αp_o = 15.6 was about 60, as opposed to the actual value at a load of 1000 lbf.of 211.

(c) Very high pressure, considerably in excess of the Hertzian maximum value, can be generated by normal approach. Furthermore, once the pressure has reached a high value, a small further increase in load will cause a disproportionately larger increase in maximum pressure.

This last conclusion is of particular relevance to the disc machine. The Hertzian pressure at commencement of the step pressure rise was 145,000 lbf./in^2., and thus αp_o was 15.1. This compares with the highest value examined by Christensen (60) which was 10.0.

15.6 THE PRESSURE AND DEFORMATION PROFILES BETWEEN TWO NORMALLY APPROACHING LUBRICATED CYLINDERS

Lee and Cheng (72) considerably extended Christensen's work, introducing the effects of surface velocities due to local deformation, and lubricant compressibility, and the effect of a lubricant with composite pressure-viscosity coefficients.

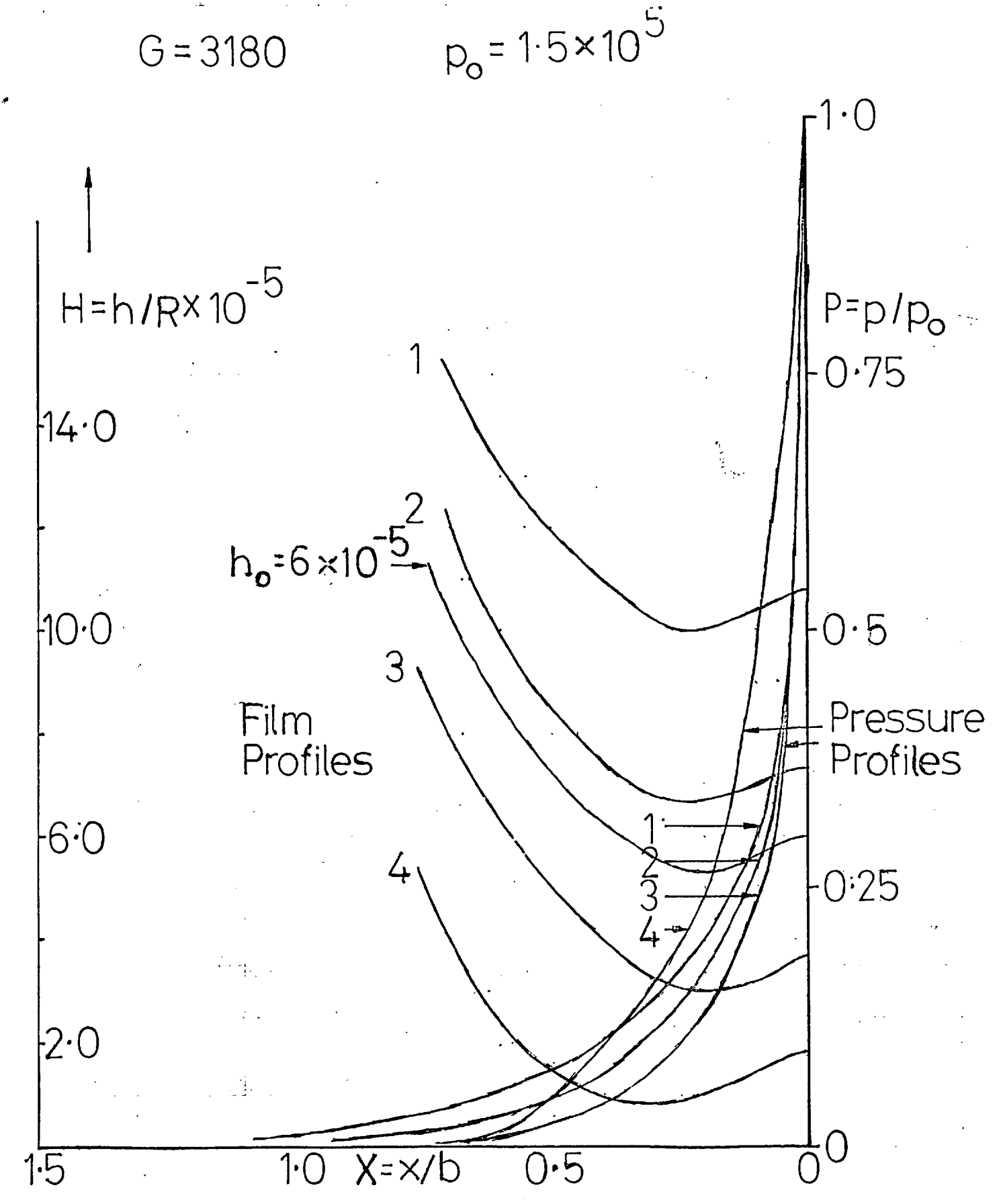
The results were plotted as a series of graphs of pressure, film thickness, load and approach velocity at a prescribed central pressure and at successive reductions of central film thickness. Their solutions were obtained by iterative numerical procedures which require all the other parameters to be fixed. Figure 15.6a shows the pressure and deformation profiles when

p_o = 150,000 lbf./in^2.

G = 3180

and $\eta = \eta_{atm.}\ e^{\alpha p}$

FIGURE 15.6a Pressure and Deformation Profiles for a Straight Exponential Lubricant



ricant. A higher centre pressure produces a deeper pocket, which is also slightly narrower.

c) With a "straight exponential lubricant" ($\eta = \eta_{atm.}\ e^{\alpha p}$) they produced curves similar to Christensen's in 15.3. of load against film thickness for varying values of $\bar{\alpha}$. These confirmed his findings, that for a given central pressure, the load is strongly dependent upon the pressure-viscosity coefficient. Higher values of $\bar{\alpha}$ produced a much smaller load. The two sets of results did differ however, in that Lee and Cheng obtained a higher load for a given $\bar{\alpha}$ and film thickness. This was attributable to the greater sophistication of their analysis.

In the second part of their work they considerably improved the realism of their model by the use of a "composite-exponential" lubricant, as follows.

It was known that a "straight-exponential" lubricant produced fluid viscosities which were excessive at pressures over 100,000 lbf./in^2. To overcome this Lee and Cheng used a model in which the viscosity increases exponentially with pressure, according to a large exponent in the low pressure region, and much smaller exponent in the high pressure region. This was expressed as follows.

$$\eta = \eta_{atm.}\ e^{\alpha p} \quad \text{for } p < p_1$$

$$\eta = \eta_{atm.}\ e^{(\alpha p_1 + \beta(p - p_1))} \quad \text{for } p > p_2$$

Where, $p_1 = 40{,}000$ lbf./in^2.

$p_2 = 70{,}000$ lbf./in^2.

$\alpha = 9.4 \times 10^{-5}$ in^2/lbf.

and $\beta = 6.5 \times 10^{-6}$ in^2/lbf.

The above values were chosen from their results as being close to those in the disc machine, where

p_o = 150,000 lbf./in^2.

G = 3390

and $H_o, (h_o/R) = 6.0 \times 10^{-5}$

The curve corresponding to these values was added to Figure 15.6a. The following were immediately apparent.

(a) The pressure profile was extremely steep, with a high centre pressure, and

(b) The cylinder's surface had formed an entrapment with a lower film thickness at the edges.

From their results Lee and Cheng concluded the following:-

a) At large film thicknesses the pressure level decreases steadily throughout the contact region with decreasing film thickness until it reaches a stage when the integrated load becomes a minimum. After this stage the pressure in the middle region reverses its tread and begins to rise, but the pressure in the inlet region still continuously decreases as the centre film further reduces. In all cases, the pressure rise is confined within a small fraction of the Hertzian bandwidth, and it does not appear to reach the Hertzian semi-elliptical shape.

b) With respect to the film thickness, a pocket is formed elastically at the contact centre, during the early stage of normal approach, and its shape does not change much for the subsequent reductions of the centre film thickness. The pocket depth, defined as the difference between the centre film thickness H_o (h_o/R) and the minimum film thickness, is dependent upon the centre pressure for a given lub-

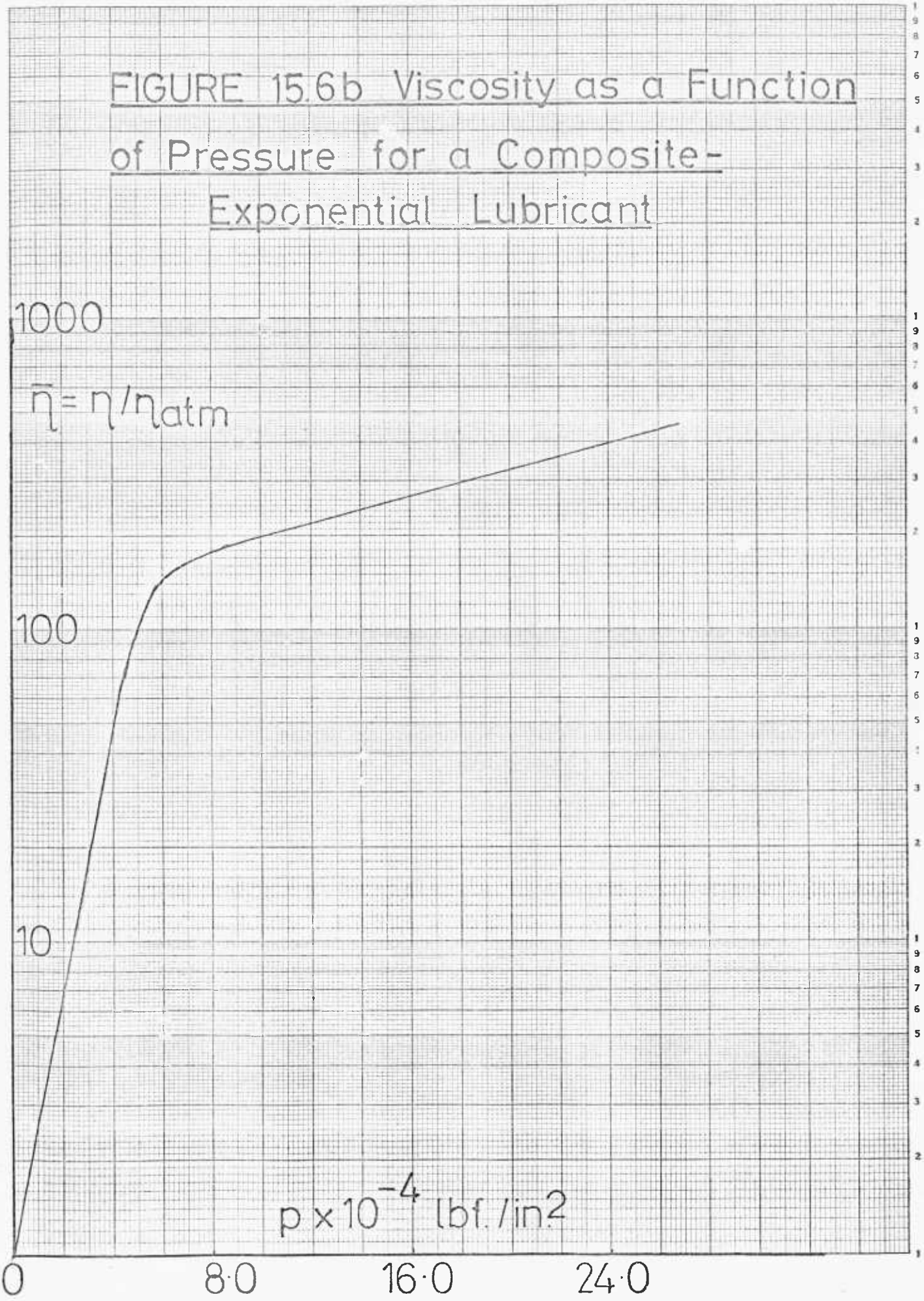


FIGURE 15.6b Viscosity as a Function of Pressure for a Composite-Exponential Lubricant

This is shown in Figure 15.6b.

The above value of α was fairly similar to that measured for the disc machine oil. The value of β for the disc machine oil was unknown. However, Macpherson (3) in a private communication stated that Figure 15.6b corresponded reasonably with the oil used, and that results produced using data from the graph would be significantly closer to the real values than those produced using a straight-exponential lubricant.

15.7 RESULTS PRODUCED USING A COMPOSITE- EXPONENTIAL LUBRICANT

Figures 15.7a and 15.7b show the effect of this modification to the theory. The difference in the results is immediately apparent, and led Lee and Cheng to draw the following conclusions.

(a) The pressure gradient is much more moderate near the contact centre, showing the absence of a pressure spike.

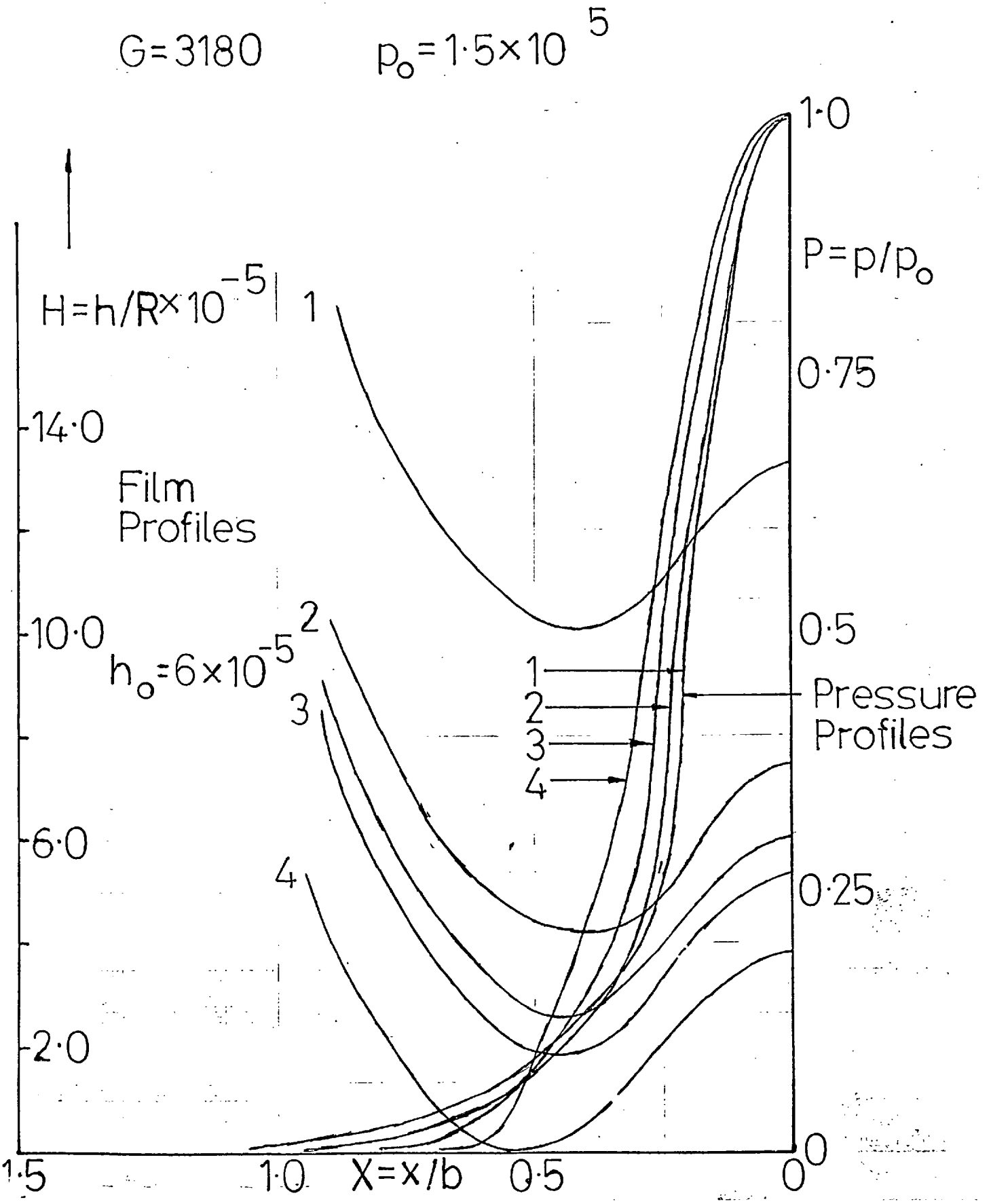
(b) The pocket formation is considerably more pronounced and has a greater depth than in the case of the straight-exponential lubricant.

(c) Outside the pocket the pressure is practically zero. The width of the pocket is approximately half the Hertzian contact width, based on the same centre pressure.

(d) The loads for the composite exponential lubricant are much larger, and were seen to be strongly dependent upon centre pressure. However, owing to the smaller contact width, the load never reached the Hertzian value, even when the minimum film thickness reached zero.

(e) The local approach velocity does not deviate signi-

FIGURE 15.7a Pressure and Deformation Profiles for a Composite Exponential Lubricant



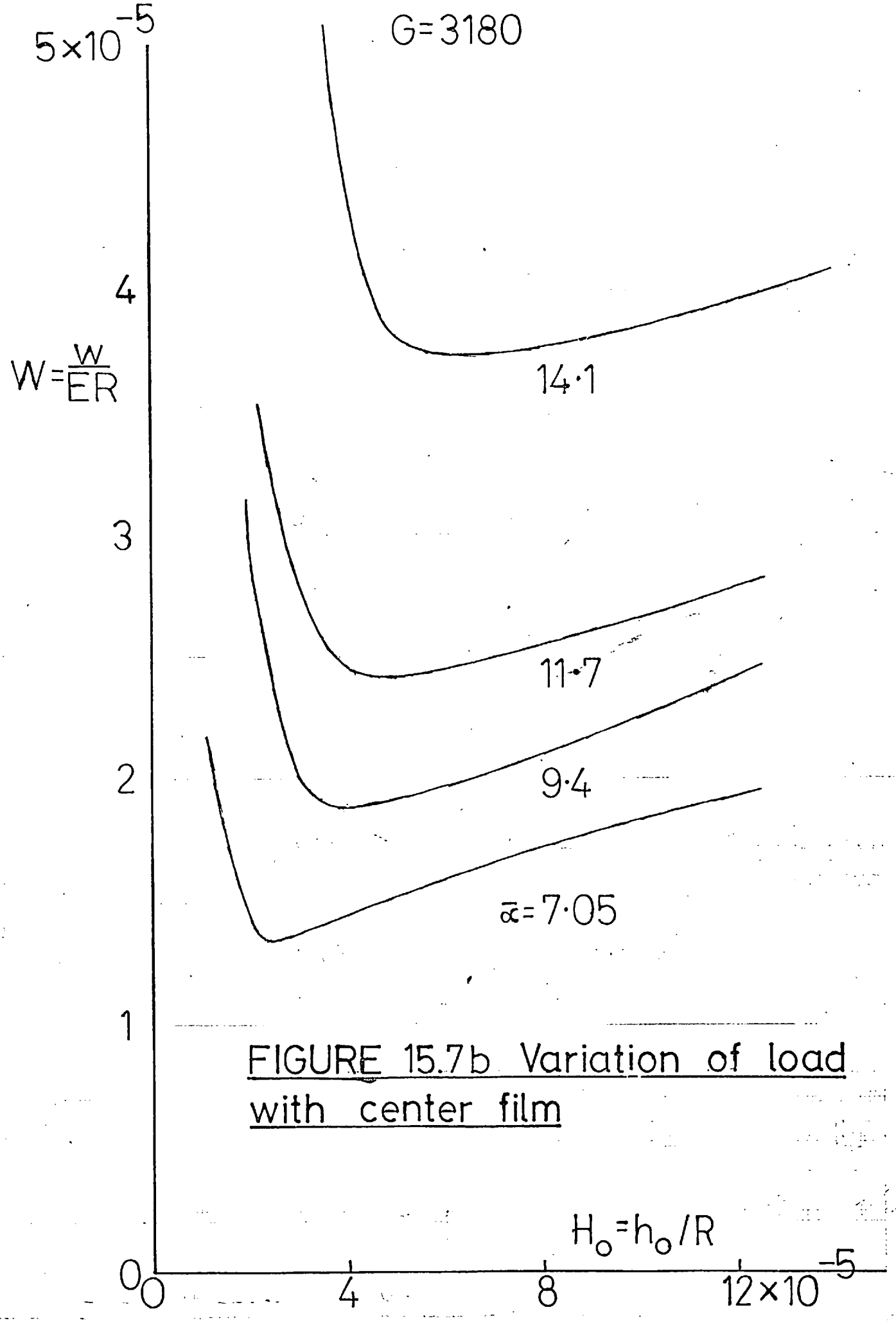


FIGURE 15.7b Variation of load with center film

ficantly from the centre value at early stages of the normal approach. However, for the final stages the local velocity is many times the centre value, indicating that the centre film thickness is almost at a standstill whilst the film thickness all round it continuously decreased.

15.8 DISCUSSION

As discussed in 15.3 the momentary increase in load with the switching of the servovalve will cause the cylinders to behave as described by Lee and Cheng, until the conditions stabilise under the new load. The two main differences between the disc-machine and the situation analysed by Lee and Cheng are:-

a) In the disc machine the starting point for the normal approach is the conditions existing with a 900 lbf. steady load. Lee and Cheng start with a large gap and zero load.

b) The surfaces of the discs are not only subject to normal approach, but also to considerable motion parallel to the contact, due to the rotation of the discs.

The first of these two is irrelevant, merely defining a film thickness at which to apply Lee and Cheng's findings.

The significance of the second is not known, but if a comparable situation does exist, even momentarily in the disc machine, then the consequences could be considerable, as will be seen in the following three sections.

Lee and Cheng's work represented an appreciable advance in the solution of the normal approach problem for two lubricated cylinders, and removed nearly all the major

assumptions. Their results are now used, with the Figures in Table 15.3 to predict the film profile and pressure distribution between the discs.

15.9 PRESSURE PROFILE FOR THE CONTACT

For a load of 1000 lbf. the calculated Hertzian pressure was 153,000 lbf.in^2. and the Hertzian bandwidth was 0.0306 ins. In Figure 15.7a, with a central pressure of 150,000 lbf./in^2., the bandwidth has been reduced by 50%, for pressures over 7% of the maximum.

In the disc machine the load and not the central pressure is the controlled variable. Hence, knowing the load (1,000 lbf.) and the pressure profile, the corresponding central pressure could be calculated. (It is assumed that at pressures above 150,000 lbf./in^2. pressure profile will remain similar to that in Figure 15.7a for $H_o = 6 \times 10^{-5}$. This is justified,as Lee and Cheng showed that it altered only slightly when the central pressure was doubled. See Figure 15.7a and 15.9).

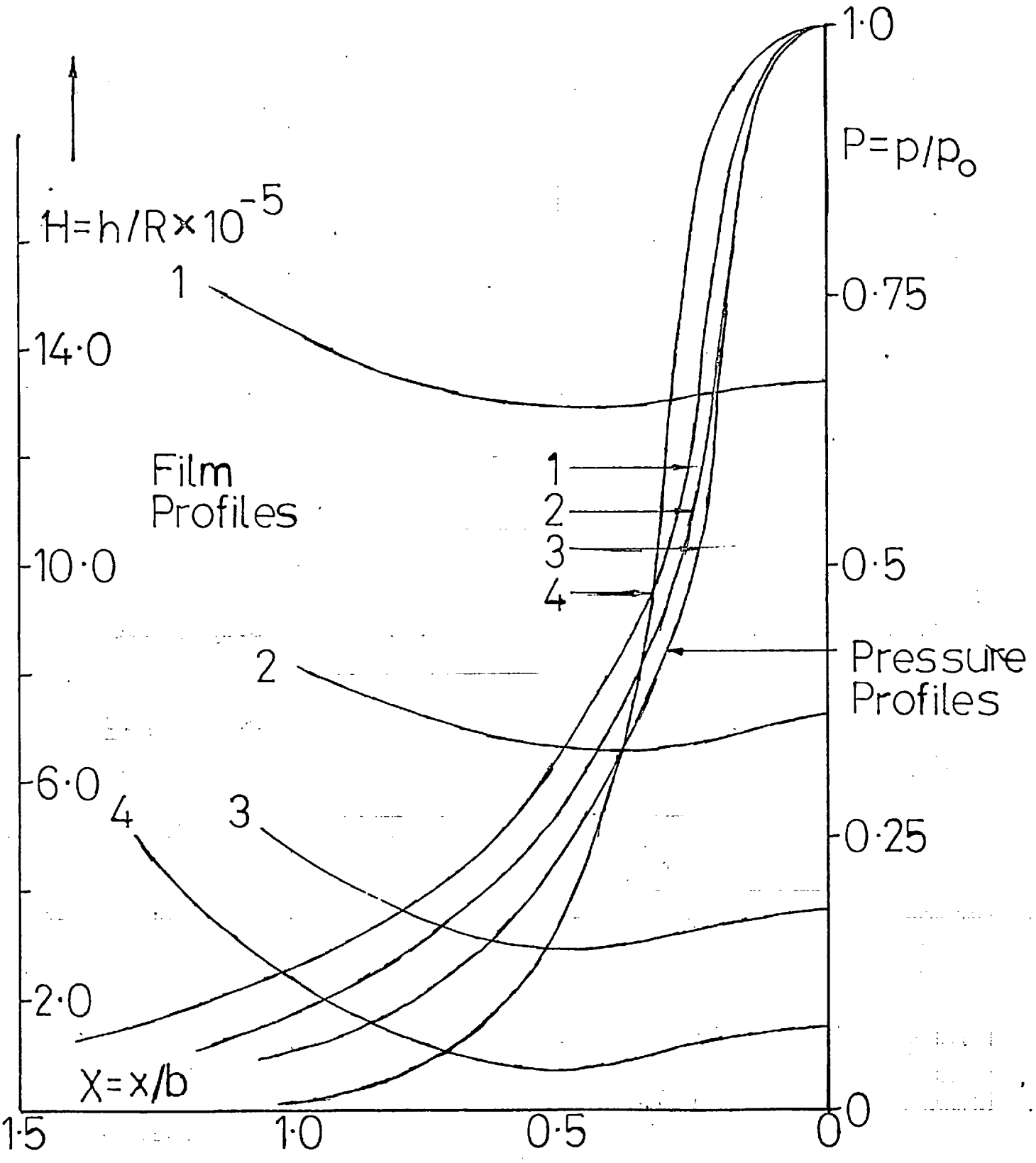
In Appendix Ten it is shown that the corresponding central pressure for a load of 1,000 lbf. is 258,000 lbf./in^2.

15.10 FILM PROFILE FOR THE CONTACT

Figure 15.7a shows that for a central film thickness of 6.0×10^{-5}, the film thickness at the edges of the contact is 2.5×10^{-5}, which is only 40% of that in the centre. This corresponds with an oil film thickness of 20×10^{-6} ins.

Lee and Cheng showed that a doubling of the central pressure produced a deeper pocket, (see Figure 15.9 and 15.7a) hence this situation would only be aggravated with a higher

FIGURE 15.9 Pressure and Deformation Profiles for a Composite Exponential Lubricant, p_o = 75,000 lbf./in.^{2}, G = 3180



central pressure.

15.11 FLASH TEMPERATURE RISE

The equation for calculating the flash temperature rise (75) in the disc machine reduces to

$$TF = 0.0171\ \mu W\ (N_1^{\frac{1}{2}} - n_2^{\frac{1}{2}})/b^{\frac{1}{2}} \qquad (66)$$

If, as shown in Figure 15.7a, the contact width during the sudden increase in load was reduced to half the normal value, then from equation (66) this would produce about a 40% greater flash temperature rise, during impact loading.

Furthermore, section 8.21 showed that when the discs failed at a low load the average coefficient of friction was greater than for the failures at a higher load. This is not surprising, as Lee and Cheng have indicated that in these conditions the film thickness in the lobes would be less than 40% of that in the centre of the contact. Asperity contact within the lobes will be greater and so cause higher friction. Reference to equation (66) shows that this would also increase the flash temperature rise.

When the above effects are combined the flash temperatures produced will be at least 40% above those for comparable steady running. This conclusion indicated that the hypothesis of a critical temperature should be re-examined. This was undertaken and new sets of total temperatures were calculated. However, even with weighted multiplying factors for TF, the values for the total temperatures still spread over a temperature range of at least 45°C.

15.12 CONCLUSIONS FROM LEE AND CHENG'S WORK

From Lee and Cheng's work it was concluded that the effects of using a fluctuating load in the disc machine were:-

(a) An entrapment was forming, which had a width of half the normal Hertzian value, and a film thickness at the edges of less than 40% of that in the centre. For a load of 1,000 lbf. the film thickness at the edges was 20.0×10^{-6} ins. In tests run with a steady load the minimum calculated film thickness at failure was 36.1×10^{-6} ins.

(b) The pressure profile for pressures over 7% of the peak value extended over merely half the normal Hertzian contact width. This produced a smaller load capacity for a given central pressure. For a load of 1,000 lbf. the central pressure was calculated as 258,000 lbf./in^2.

(c) An examination of the equation for TF, the flash temperature rise, indicated that for the conditions in (a) above, the flash temperature rise would be at least 40% greater than that for steady running. Thus the total temperatures would be greater than those given in Section 13.2. The distribution of these total temperatures was too great to satisfy a critical temperature at failure hypothesis.

This view was reinforced when an attempt to measure the transition temperature in Appendix Eight showed that such a value did not exist for this oil/material combination.

The following sections present evidence which substantiates the above conclusions.

15.13 COEFFICIENT OF FRICTION AND ASPERITY CONTACT

In Section 8.21 it was shown that there was a sig-

nificant increase in the coefficient of friction when a fluctuating load was used.

In Section 8.15 the results from an electrical investigation of asperity contact showed that the positive pressure changes caused an increase in the occurrence of asperity contact. As an aside it was also apparent that asperity contact was related to the rotation of the discs, certain areas on them causing more asperity contact than others.

The load, speed and applied frequency were varied. This generally gave displays similar to Figures 8.15a to 8.15f, but at high frequencies the incidence of asperity contact tended to become random. Attempts to quantify the extent of asperity interactions proved to be futile.

In Section 15.10 it was shown that Lee and Cheng found that the minimum film thickness under impact could be reduced to less than 40% of the central film thickness. This concurs with the measured increase in friction, and is strongly substantiated by the evidence that the positive pressure changes were causing increased asperity contact, which was more than would be produced by a comparable increase in steady load.

15.14 DISC SURFACE TEMPERATURE

In Figure 8.18 the results of Test 224, with an infra-red microscope, showed that the disc surface temperatures were up to $3^{o}C$ hotter with dynamic as opposed to steady loading.

The analysis of the flash temperature rise in Section 15.11 indicated that values over 40% higher than

normal would be obtained during dynamic loading. This increase would only occur during the positive pressure change. Furthermore, for the majority of the time the disc surface is outside the contact. Hence a 40% increase in disc surface temperature would not be expected. The maximum measured increase of 7% indicated that significant changes were occurring between steady and dynamic running, and that increases of over 40% in the flash temperature rise might have occurred.

15.15 DISC SURFACE STRESS

In Section 8.24 it was shown that for Test 83, with a fluctuating load of 15 Hz., a surface stress of 197,000 lbf./in^2. was required to produce pitting in 30 minutes. The Hertzian maximum stress for the test was 128,000 lbf./in^2.

In Section 15.9 the use of Lee and Cheng's results led to a deduced central pressure of 258,000 lbf./in^2. when the load was raised from 900 to 1,000 lbf. In the same situation the Hertzian peak pressure was calculated as 153,000 lbf./in^2. Thus a dynamic load would produce a large increase in surface stress above the Hertzian value. The results from Tests 80 to 83 indicated that this was happening. For Test 83 the calculated actual increase was 54%.

15.16 MECHANISM OF SCUFFING

The consequences for scuffing arising from the results of Lee and Cheng's work are now discussed.

Scuffing requires the asperities to penetrate the oil film and so interact, to produce localised heating and welding of the surfaces, as outlined in section 9.5.

During each sudden increase in load scuffing could be initiated as follows.

The formation of an entrapment in the disc surface, with a consequent reduction of the film thickness at the edges would greatly increase the extent of asperity contact (as confirmed in 15.13). For the case examined in 15.10, with a central film thickness of 49.3×10^{-6} the film thickness at the edges was reduced to 20×10^{-6} ins. This is less than that for scuffing in any of the steady load tests, the figures for which varied between 36 and 55×10^{-6} ins.

Simultaneously the change in contact width and profile could raise the flash temperature by over 40%.

The combined asperity interaction and increased flash temperature caused scuffing to occur at a load which would have been supported satisfactorily had it not been subject to fluctuations.

15.17 CONCLUSIONS

The results in the sections 15.13 to 15.15 substantially support the findings by Lee and Cheng, as applied to the disc machine in Section 15.9 to 15.11. Though the conditions analysed by them differ from those in the disc machine, the same mechanism appears to exist. The conclusions from their work were listed in 15.12, but are given again here. Briefly these were:-

(a) An entrapment was forming during each sudden pressure rise. It had a width of half the normal Hertzian value, and a minimum film thickness at the edges of less than 40% of the central film thickness.

(b) Outside the entrapment the pressure was very low.

Hence for a given load a far higher central pressure was required.

(c) Due to the change in the contact width and increased contact friction the flash temperature rise while the entrapment existed, would be at least 40% greater than for steady running.

The consequences from the above were:-

(1) Scuffing occurred at much lower loads, due to the greatly reduced film thickness at the edges of the entrapment causing increased asperity contact and increased flash temperature rise.

(2) The coefficient of friction was higher when a dynamic load was used.

(3) The disc surface temperature was also higher.

(4) The pitting life of the discs could be considerably reduced, due to peak pressures in the contact which were of the order of 50% higher than in the comparable case for steady running.

CHAPTER SIXTEEN

HYPOTHESIS TO ACCOUNT FOR VARIATION OF THE SCUFFING LOAD WITH FREQUENCY

16.1 INTRODUCTION

The variations in scuffing load with frequency have yet to be explained. The first part of this chapter presents a tentative hypothesis to explain the increases in scuffing load observed when the applied load frequency was raised from 20 Hz. to 60 Hz. (see 8.3 to 8.13).

16.2 HYDRAULIC SQUEEZE BEARING

In Kauzlarich's paper (63) he analysed the hydraulic squeeze film bearing. Earlier workers had shown that when one of two parallel plates immersed in a fluid is forced up and down a load could be carried, provided the fluid was compressible. Kauzlarich was able to remove this restriction, and showed that the inertia terms in the Navier-Stokes equations predicted a nett load capacity, equal to

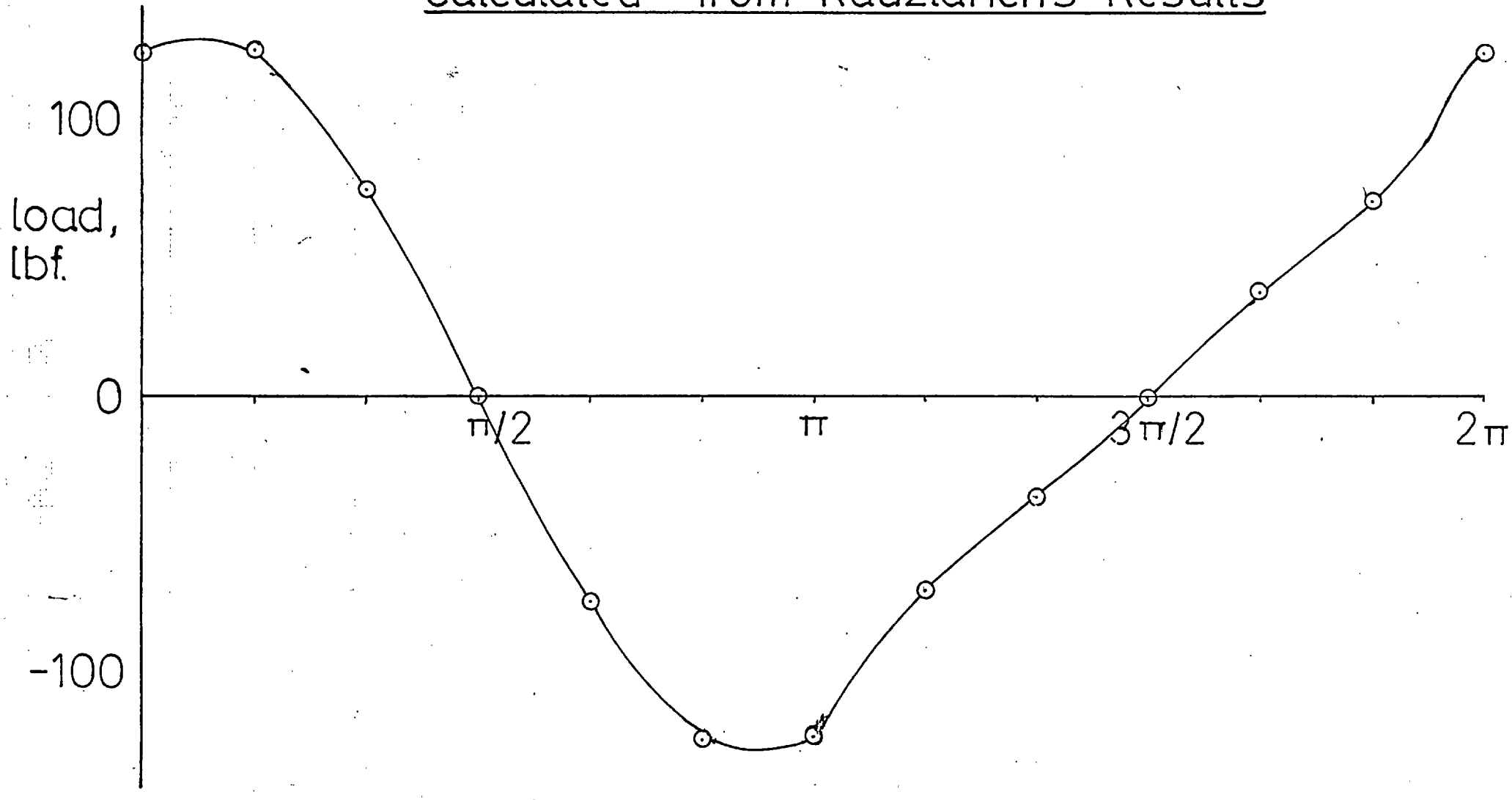
$$F = 33\ \pi\rho\omega^2\ R^4\ (1/((1 - e^2)^{1/2}) - 1)/280g$$

Using the figures in Table 15.3 this produces a value for F of 0.0059 lbf. at 60 Hz. when e = 0.2, which is negligible.

Kauzlarich showed that the squeeze film force at any moment could be found from equation (56) in section 10.14. This was used with e = 0.1 and ω = 60 x 2π rad./sec. to produce Figure 16.2.

This shows that though the nett force was very low,

FIGURE 16.2 Squeeze Film Forces during a Pressure Cycle
Calculated from Kauzlarich's Results



fairly significant forces were in existance during the cycle. As the major portion of this force arises from the first term in equation (56) it can be seen that the magnitude was proportional to the frequency of the applied load.

16.3 PRESSURE DISTRIBUTION IN A PLANE FLUID FILM SUBJECTED TO NORMAL SINUSOIDAL EXCITATION

Hunt (58) also investigated incompressible fluids in his paper with the above title. He showed that the pressure at any moment could be found from

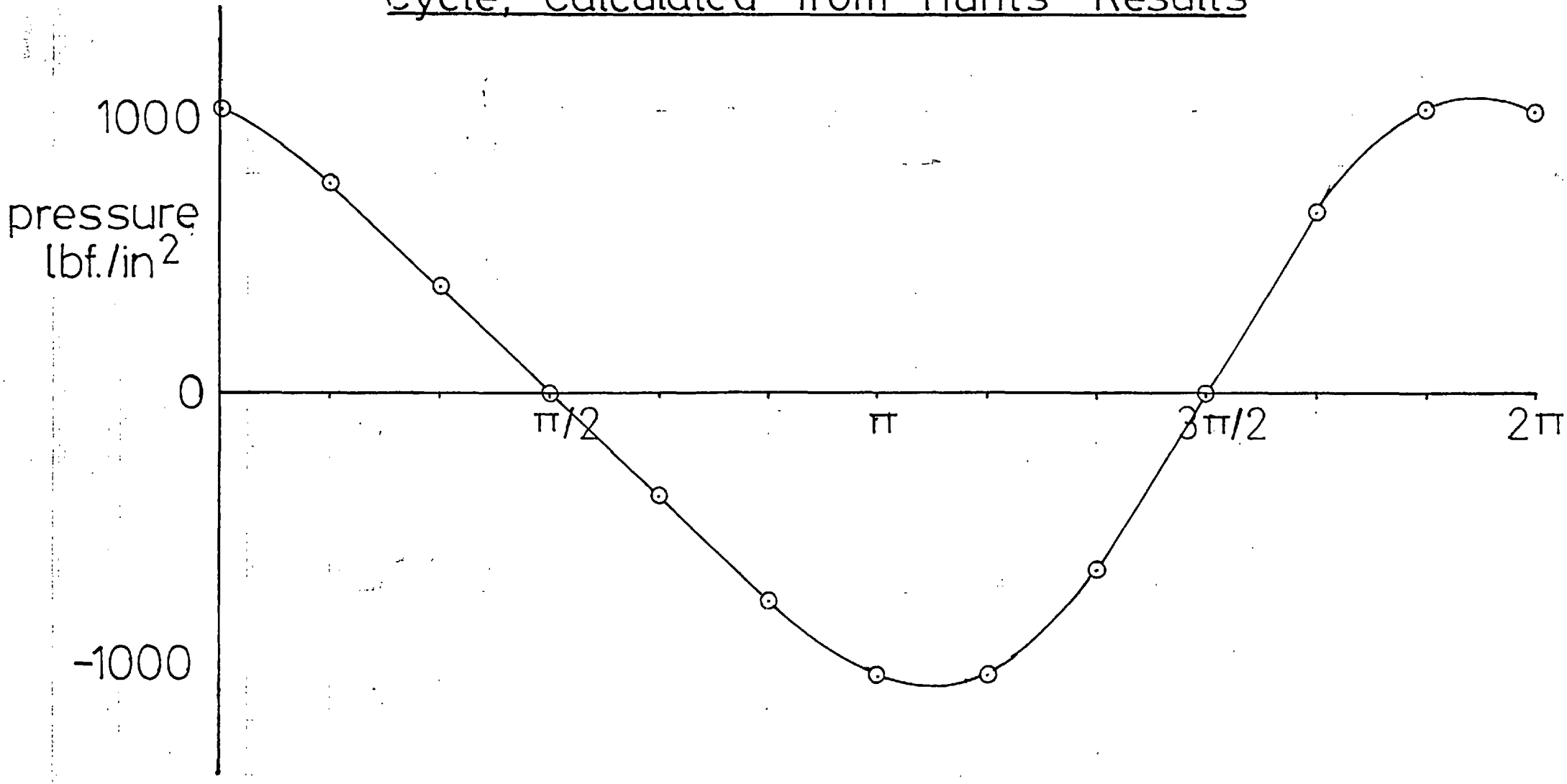
$$p_{max} = -\eta\omega 3(a/h)(R/h)^2 \cos \omega t \left[1-3(a/h) \sin \omega t \right] \qquad (68)$$

Again, substituting the values from Table 15.3, Figure 16.3 was produced. This is similar to that produced by Kauzlarich. However the equations (68) and (56) assume that the viscosity is the same as that at ambient pressure. If instead, the viscosity appropriate for a fluid with a pressure dependent viscosity at a pressure of 150,000 lbf./in^2. was used, then the pressures produced by the oscillations would have been considerably greater. Again it can be seen that the magnitude of the pressures is porportional to the frequency of the applied load.

16.4 DISCUSSION

Kauzlarich's and Hunt's work indicated that when a dynamic load was used in the disc machine the discs could behave as a squeeze film bearing. As the frequency rose the effect of the squeeze film bearing increased, and this would provide additional support for the load. If it is assumed that this led to a slight increase in the average oil film

FIGURE 16. 3 Squeeze Film Pressures during a Load Cycle, Calculated from Hunt's Results



thickness, then the effect of each sudden increase in pressure, as discussed by Lee and Cheng, would be reduced. It has already been shown in section 8.20 that as the oil film increased the effect of the vibrations decreased. This was to be expected as Lee and Cheng showed that the shape of the entrapment was fairly constant with changes in the separation of the surfaces (see Figure 15.7a). Thus, when the applied frequency rose from 20 to 60 Hz. it is possible that a slightly thicker oil film protected the surfaces from increased asperity contact arising from the sudden pressure increases.

16.5 LUBRICATION OF ROUGH SURFACES

In considering the influence of frequency, the effect of a varying load is similar, due to the movement of the surfaces, to the situation of transverse, long wavelength surface roughness.

To seek a more realistic representation of engineering surfaces, sinusoidal (83), saw-tooth (84) and random (86) surface roughnesses have been analysed, and their influence on lubrication examined. Christensen (85) used stochastic models for the surfaces and arrived at conclusions similar to those produced by the above authors.

Though the approaches and assumptions varied, in general the authors were in agreement on the following conclusions.

(i) The coefficinet of friction was higher for a rough surface (even for hydrodynamic lubrication of fully separated surfaces). Tzeng and Saibel, and Davies calculated increases

ranging from 10 to 55%. Davies also measured, with slight success, a similar increase when rough surfaces were substituted for smooth ones.

(ii) The load carrying capacity was significantly increased when rough surfaces were used. However Burton stated that if the temperature-viscosity effect predominates, the surfaces can be drawn together as a result of the surface roughness, and thus a type of instability may contribute to film breakdown in some marginal lubricant situations.

(iii) The roughness effects were more pronounced when the asperities were close together. For the present discussion this is similar to having a high frequency of applied load.

The magnitude of the changes in load capacity were less than experienced in the disc machine. The work by the authors highlighted the effect of asperity interaction, and the somewhat unstable nature of the oil film separating them.

It was concluded that the effect in (iii) above provided further indication that a form of squeeze film effect was protecting the asperities at higher frequencies of applied load.

16.6 SCUFFING LOAD AT LOW FREQUENCIES

When the frequency was reduced below 10 Hz. the pressure waveform was so elongated that each pressure change became a discrete occurrence. In the disc machine, surface reaction between the material and additives in the oil raises the scuffing point in comparison with using a plain oil. This was demonstrated in Chapter Four, when discs with a surface coating scuffed at lower loads than plain discs. It was possible that the reaction time for the surface additives was

of the order of the time between load changes (80).

It was concluded that probably the situation described by Lee and Cheng was occurring, but possibly the pressure changes were sufficiently infrequent that the disc surface films could chemically recover between vibrations. Discussions with other workers failed to produce a satisfactory explanation for the variations in scuffing load at low frequencies.

16.7 EXPERIMENTAL INVESTIGATIONS

An attempt has been made to determine the magnitude of any change that was occurring in the average film thickness as the applied load frequency was changed from 0 to 15 to 60 Hz. For this voltage discharge and resistance measurement techniques were used and the results discussed in 8.23. It was concluded that unfortunately neither method, when used in the disc machine, was sufficiently accurate that a change of 10% could be measured conclusively. However it was apparent that changes in the average film thickness of the order of 30% were not occurring.

To provide an alternate approach Test 216 was run as a pitting test with an applied load frequency of 60 Hz. The results were given in 8.11 and discussed in 8.24.

In Tests 80 to 83 it had been found that under similar conditions, but with an applied load frequency of 15 Hz., the effect of the vibrations was such that the pitting life of the discs had been reduced, in one test, to 30 minutes. Test 216 showed that at 60 Hz. the discs ran for 11 hours before pitting. This compares with 13 hours when a steady load was used (see section 3.7.1).

Finally, in Type D and H tests with a frequency of applied load of 60 Hz., an increase in the scuffing load was obtained. This amounted to 9 and 13% respectively.

16.8 CONCLUSIONS

It was concluded that at low frequencies, below 10 Hz., each pressure change was possibly sufficiently separated in time from the next one that a deterioration in the overall condition of the disc surfaces did not occur.

The results from the pitting tests appeared to support the conclusions in 16.4, that probably as the applied frequency rose from 15 Hz. to 60 Hz., an increased oil film, arising from the discs behaving as a squeeze film bearing, was protecting the surfaces. This was despite the four-fold increase in the number of cycles at 60 Hz.

Lack of time has prevented a fuller investigation into the above hypotheses, and both are advanced tentatively.

CHAPTER SEVENTEEN

SUMMARY, CONCLUSIONS AND RECOMMENDATIONS FOR FUTURE WORK

17.1 SUMMARY

The main object of the work in this thesis was to investigate the effect of vibrational loading on gear scuffing. This has been achieved, over the frequency range from 5 to 60 Hz., using a kinematically equivalent hydrostatic bearing disc machine.

As an introduction into the conditions existing in a gear pair under dynamic loads, the effect of retained austenite in the surface of a gear steel, and surface coatings were examined.

A laboratory-type, naturally aspirated diesel engine was modified to enable the occurrence of scuffing between the piston ring and liner to be observed and recorded continuously. The factors effecting scuffing were then examined.

In Chapter Six a literature survey was presented covering previous work on dynamic loads in gears.

The disc machine was modified to enable dynamic loads of known frequency, shape and amplitude to be applied between the discs. A series of tests were run with a dynamic load. This was followed by investigations into the conditions in the contact, for example, an electrical investigation of asperity contact, and surface temperature measurement with an infra-red microscope.

The results from these tests were analysed and the effect of vibrations on the various parameters examined.

Before the analyses were undertaken a statistical investigation of the test results and Fourier analyses of the pressure waveforms were conducted. These are given in Appendices Eleven and Twelve.

The main tests had shown that at certain frequencies of applied load a reduction in the scuffing load was obtained. A list of possible hypotheses to explain this was drawn up, and a literature survey of the previous work relevant to those hypotheses presented.

In Chapters Eleven to Fifteen each of the following hypotheses was investigated.

1. That resonance was occurring in the disc machine, or that the load changes were repeatedly occurring at the same point on the disc.
2. That cavitation was taking place.
3. That scuffing was occurring when the critical temperature was reached.
4. That the vibrations were causing scuffing through surface fatigue.
5. That scuffing was initiated by the formation of a temporary entrapment in the disc surface.

It was shown that the last hypothesis provided the best explanation of the disc machine results.

In Chapter Sixteen a hypothesis was advanced to explain the variations of scuffing load with frequency.

17.2 CONCLUSIONS

These were as follows:-

(a) A repeatable scuffing test with an oscillating load has been established.

(b) At any point during a test it was possible to simultaneously monitor the coefficient of friction, disc surface temperature, applied load, bulk oil temperature, disc speeds, and magnitude, shape and frequency of the applied load waveform.

(c) By suitable positioning of the servovalve on the disc machine, a load cycle could be obtained with Fourier components which were nominally independent of applied frequency.

(d) The application of a fluctuating load could reduce the load at scuffing by up to 40%.

(e) A fluctuating load could also reduce the pitting life by a factor of about 30.

(f) Lee and Cheng's findings provide a probable explanation for the changes occurring when a fluctuating load is used. Though the situation analysed by them was not identical with that in the disc machine the same mechanism appears to exist. Their findings, as applied to the disc machine, indicate that the application of a sudden pressure rise momentarily produces an entrapment in the disc surfaces. This causes three main effects.

(i) The film thickness around the edges of the contact reduces to less than 40% of that in the centre.

(ii) The width of the entrapment is only half the normal contact width, and the peak pressure in the contact is 60% greater than normal. This causes a reduction in the pitting life.

(iii) The combination of slightly higher friction with a fluctuating load and narrower contact width

increases the flash temperature rise by about 40%.

These severe conditions initiate earlier scuffing than with steady loading.

(g) A satisfactory hypothesis for the variation in scuffing load at low frequencies could not be deduced. It may be related to the reaction times of the surface additives.

(h) At high frequencies Hunt's and Kauzlarich's work indicated that the discs might behave as a squeeze film bearing. If this was occurring it could improve the scuffing load at high frequencies by taking some of the load and causing a subsequent increase in the oil film thickness.

17.3 RECOMMENDATION FOR FUTURE WORK

This is the first instance of the application of a controlled fluctuating load to a pair of simulated gear teeth. Consequently, considerable further research is required. In particular investigation of the following could yield extremely useful information:-

1. Higher frequencies of vibration. This should include the frequencies of blade vibrations in gas turbines.

2. Lee and Cheng's work considered the situation of normal approach, without any lateral motion of the surfaces. The film profile for conventional elastohydrodynamic lubrication of two rolling surfaces can now be obtained by a relatively simple computer program. It would be extremely interesting to see if Lee and Cheng's results could be modified to include the effect of the disc's rotation, and new film and pressure profiles computed.

3. Knowing the probable mechanism causing failure it should be practical to deduce methods of nullifying it, and the following might justify further investigation.

(a) From the theory, reducing the value of E would reduce the peak stress ($p_{max} \propto E^{1/2}$) and the flash temperature rise ($TF \propto E^{1/4}$).

(b) It is conceivable that metallurgical changes, or surface-active chemicals could reduce μ and thus TF ($TF \propto \mu$).

(c) Improvements in the surface finish would reduce the film thickness required to maintain separation of the edges of the contact. It was shown in 8.25 that improvements in the λ ratio substantially reduced the effect of the vibrations.

(d) Finally, an additive which could fill the valley bottoms with a solid film would be expected to be very effective in avoiding or postponing scuffing.

4. In Type D and H tests an improvement in the load at scuffing had been obtained with the highest applied load frequency. It is possible that surfaces could carry additional load, when subjected to externally applied, controlled vibrations.

APPENDIX 1

DESCRIPTION OF THE TEST ENGINE FOR THE INVESTIGATION OF PISTON RING SCUFFING

1.1 THE PETTER AV1 LABORATORY ENGINE

The Petter AV1 Lab. engine is a four-stroke, compression ignition engine. It is physically robust and extensively used for lubricant testing. The design is such as to allow for easy fitting and removal of the piston and cylinder liner.

The engine was mounted on a sprung test bed and connected to a D.C. electrical dynamometer which absorbed the power produced. This electrical energy was dissipated in banks of water cooled resistors. The dynamometer could also be used for motoring the engine for starting and as an aid to running-in.

1.2 CYLINDER LINER MODIFICATIONS

As the Petter engine is used for various British Institute of Petroleum Standard Tests, specially matched sets of liners and pistons are available. These are manufactured to much closer tolerances than the commercial items, and matched assemblies were used throughout the present work.

A flat, approximately 1½ inches wide, was machined on the outer diameter of the liner, extending 3½ inches along its axis (from the top) to accept the heater face (see figure 5.3). This reduced the minimum thickness of the liner on the centre line of the heater to 0.125 inches. Half way down the flat a groove was cut for a Ni Cr - Ni Al thermo-

couple which was cemented into position. The thermo-couple lead was connected to a direct reading electronic thermometer. Below the heater and on its vertical centre line, a hole 3/16 inch diameter was drilled through the liner.

All the machining on the liner was done after it had been pressed into the block. In this way difficulties in lining up were avoided. Any misalignment would have led to sealing problems.

1.3 PISTON MODIFICATIONS

With the standard single oil control ring the large supply of oil to the top compression ring was such as to partially obscure the view and further, difficulty was found in making the rings scuff. Accordingly three, three-element oil control rings were fitted to the piston. The groove above these held a standard tapered compression ring, while the top groove was fitted with a chromed compression ring.

To fit the extra scraper rings it was necessary to increase the existing ring grooves from 1/8 inch to 3/16 inch, and drill oil drain holes through the rear of the grooves. Figure 1.3 shows a modified piston with its new ring pack.

1.4 LINER HEATER

The heating element consisted of 1/8 inch diameter stainless steel wire, and would pass up to 200 amperes. This was supplied from a variable, low voltage transformer. The face of the element was assembled against the flat mach-

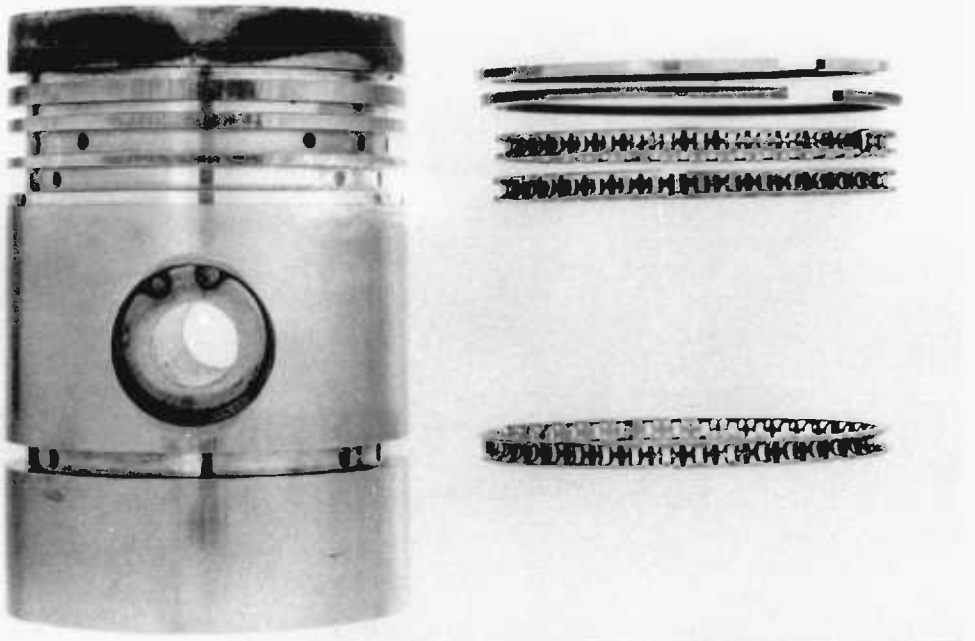


Figure 1.3. Modified Piston and its New Ring Pack.

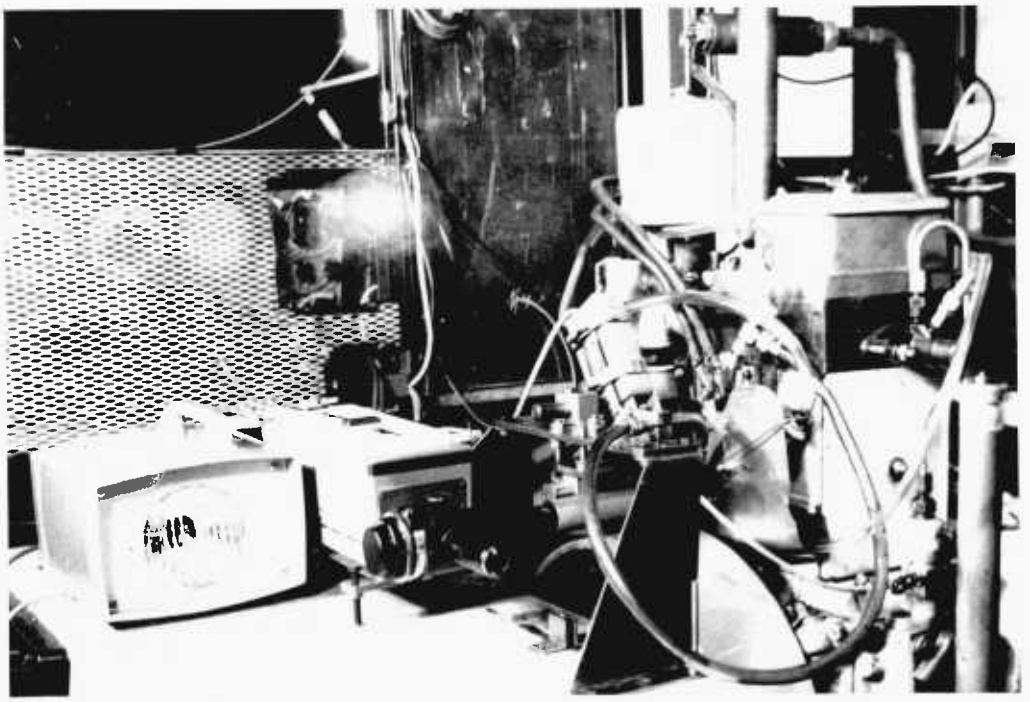


Figure 1.5. General View of the Diesel Engine Rig.

ined on the liner.

1.5 OPTICAL AND RECORDING SYSTEM

The top piston-ring was viewed through the hole in the cylinder liner using a low-power microscope and a television camera system. Illumination was provided by a Xenon-arc stroboscope focussed through a lens system and mirror (see figure 5.3). The microscope and camera system were mounted separate from the test bed, to avoid vibration. The stroboscope was triggered at the bottom of the induction stroke by a photo-electric pick-up and a disc on the end of the camshaft. The video-recorder was a CCIR standard, high resolution model using ½ inch tape. The audio facility on it allowed observations and readings to be recorded. The T.V. picture was not synchronised with the stroboscope flash, as an adequate picture was obtained without this refinement. Figure 1.5 shows a general view of the engine, microscope, T.V. camera and stroboscope units.

1.6 OIL AND WATER SYSTEMS

The oil temperature was held at $95 \pm 2^{o}C$, during tests by heaters and coolers.

The water temperature at outlet from the water jacket was thermostatically controlled at $95^{o}C$ by a 3 KW heater and a cooler.

1.7 ENGINE INSTRUMENTS

Instrumentation of the following data was grouped on a control panel.

(a)	Water jacket inlet temperature	(^{o}C)
(b)	Water jacket outlet temperature	(^{o}C)
(c)	Sump oil temperature	(^{o}C)
(d)	Engine oil pressure	(p.s.i.)
(e)	Engine speed	(r.p.m.)
(f)	Temperature of the heated portion of the liner	(^{o}C)
(g)	Liner heater current	(amps)
(h)	Oil heater voltage	(volts)
(j)	Dynamometer volts	(volts)
(k)	Dynamometer current	(amps)
(l)	Engine torque	(lbf./ft.)

Figure 1.7 shows the engine control panel, television and video-recorder.

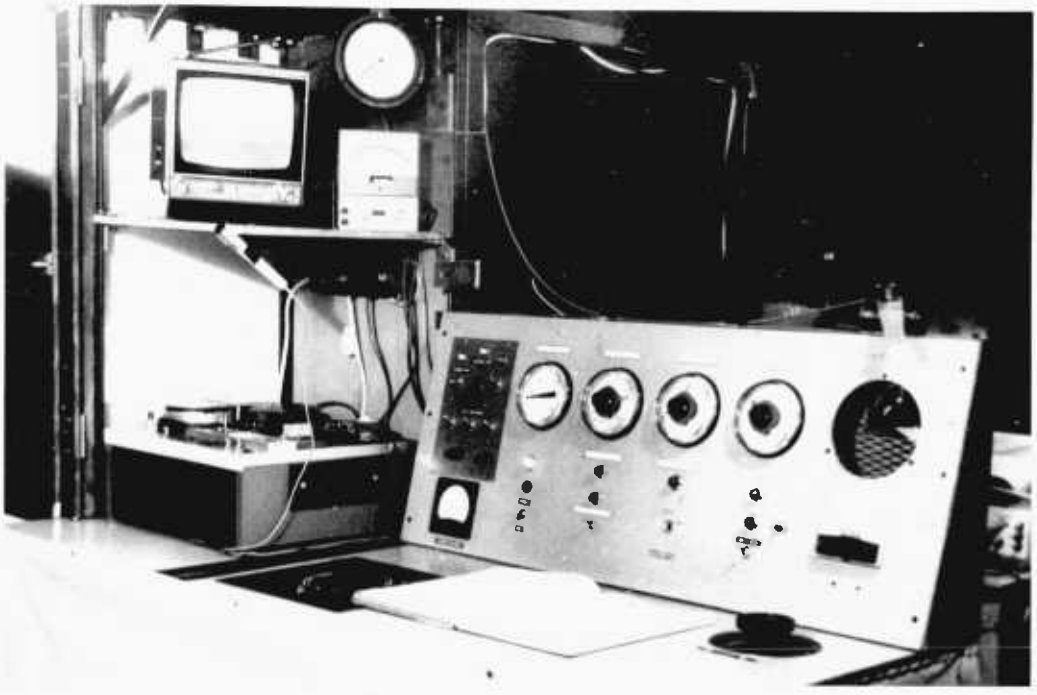


Figure 1.7. Control Panel, T.V. and Video Recorder.

APPENDIX 2

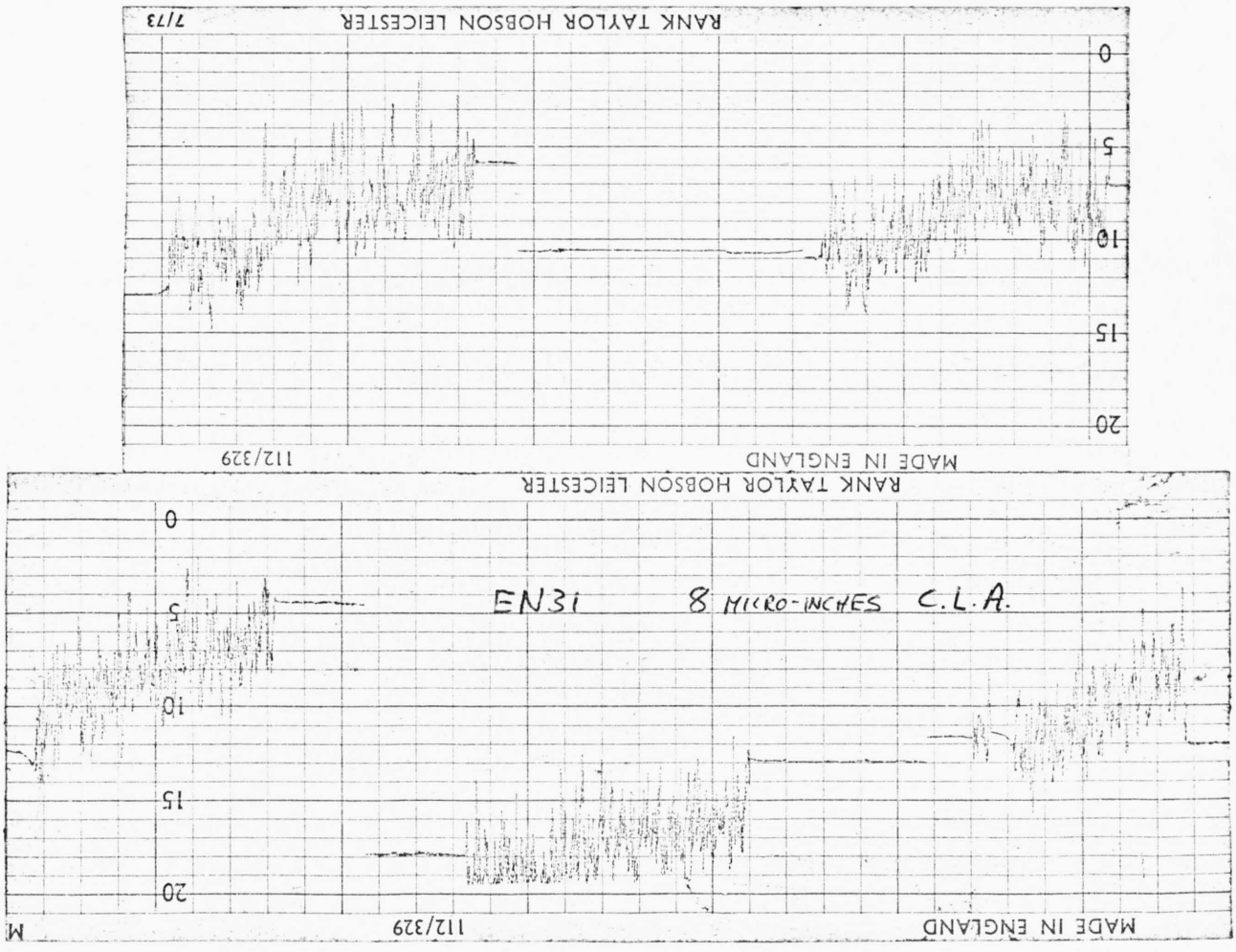
SURFACE ROUGHNESS AND HARDNESS

DETAILS OF EN 31 DISCS

Hardness:- 821 $\pm$ 20 Vickers Hardness Number

Surface Roughness:- 8 $\pm$ 2 micro-inches C.L.A.

Surface Traces attached from "Talysurf" Machine.



APPENDIX 3

SURFACE ROUGHNESS AND HARDNESS

DETAILS OF EN 39B DISCS

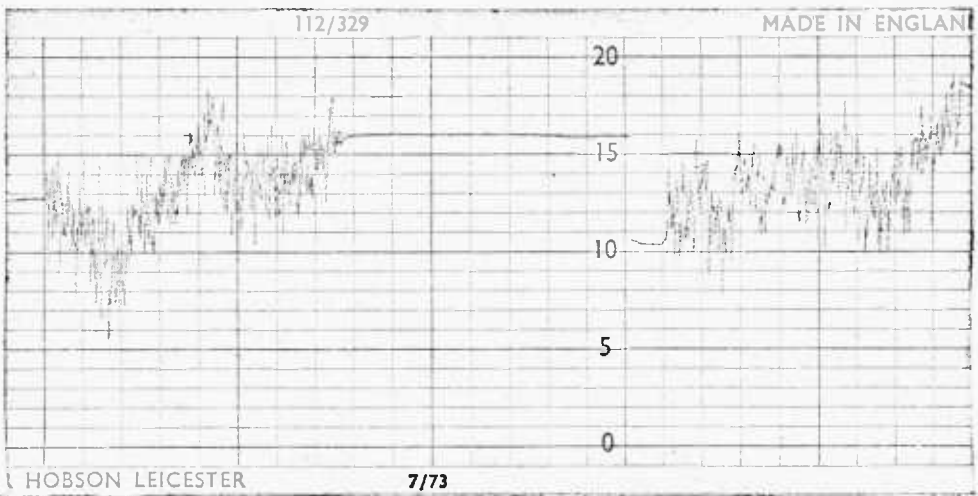
Surface Roughness:- 7 $\pm$ 2 micro-inches C.L.A.

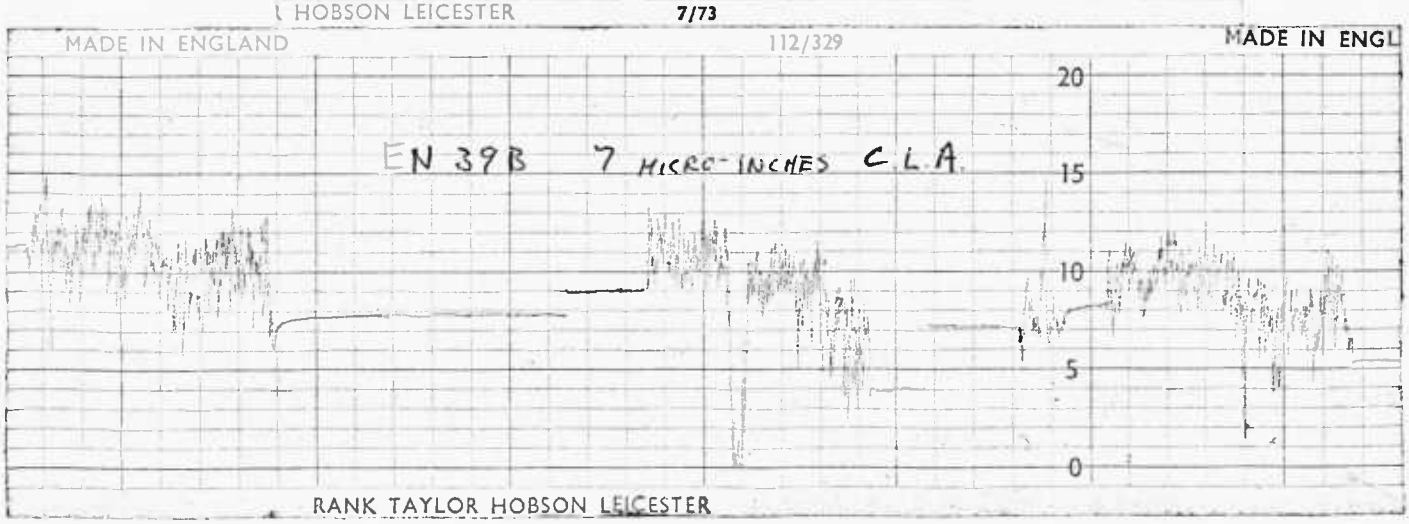
Surface Roughness Traces from "Talysurf" machine attached.

Surface Hardness:- Untreated EN 39B 802 $\pm$ 20.

Deep frozen treated EN 39B 852 $\pm$ 20.

(Vickers Hardness Number).





APPENDIX 4

COMPOSITION AND QUALITIES OF EN 31

Specific gravity	7.8
Co-efficient of linear expansion	11×10^{-6}
Young's Modulus	200×10^{9} N/m^2.
C	0.90 - 1.20 %
Cr	1.00 - 1.60 %
Si	0.10 - 0.35%
Mn	0.30 - 0.75%
S	0.050 % max.
P	0.050 % max.

Applications:- (37)

When supplied in the softened condition it shall have a Vickers hardness not exceeding 229.

Used mainly in the hardened and lightly tempered condition for parts requiring a high surface hardness with a deeper hardened zone than can be obtained with case-hardened steels. It can be oil quenched in sections up to 1 in. diameter and water hardened in larger sections to produce a very hard, wear resistant surface.

Typical uses:- ball and roller bearings, bearing rings, connecting rod big end bushes, lathe centres, gears, cams and pawls, punches, fuel nozzles, instrument pivots and spindles, tools, shear blades, blanking and forming tools.

APPENDIX 5

COMPOSITION AND QUALITIES OF EN 39B

Specific gravity	7.86
Coefficient of linear expansion	11×10^{-6}
Young's Modulus	206×10^{9} N/m^2.
C	0.12 - 0.18 %
Cr	1.00 - 1.40 %
Si	0.10 - 0.35 %
Mn	0.50 % max.
S	0.050 % max.
P	0.050 % max.
Ni	3.80 - 4.50 %
Mo	0.15 - 0.35 %

Applications:- (37)

In the softened condition the material shall have a Vickers Hardness number not exceeding 227.

These steels may be carburized and hardened to produce a hard wear resistant case, and developing a core strength of the order of 85 tons/in^2. with good resistance to shock.

Typical uses:- high duty gears, heavy duty worms, crown wheels and pinions, heavy roller bearings, breech mechanisms and small arms components, camshafts, clutch plates, valve rockers, gudgeon pins, and tappets.

APPENDIX 6

DEEP FREEZING TREATMENT PROCEDURE FOR EN 39B DISCS

The procedure is as follows:-

1. Gas carburize with 0.7% nominal carbon content at 925°C.
   Furnace cool to 850°C.
   Vestibule cool in non-oxiding atmosphere.
2. Anneal at 650°C.
   Furnace cool.
3. Harden at 790°C into oil.
4. Sub-zero treat.
5. Temper at 140°C for 4 hours.

Explanations of the above processes are as follows.

Gas carburizing is the only method permitted for gears. Case depths quoted for carburizing are those obtained after grinding. Surfaces to be treated must naturally be clean, free from dirt, oil, grease rust or foreign material.

Sub-zero treatment is carried out immediately after hardening and before tempering. Cool to - 60°C or below at a rate not greater than 20°C per hour and hold at this temperature for 1 hour. On regaining room temperature temper.

The case depth is established assuming that it ends when the hardness falls below 520 HV.

Microscopic examination of the case structure of a test piece to be carried out after etching in a 3 - 5%

NITOL solution at magnifications of x 200 and x 500 for the following features.

(1) The case to be of fine martensite. No bainite or pearlite is acceptable.

(2) No decarburization is to be observed except where it would be removed by grinding.

(3) Retained austenite is unacceptable if present in amounts greater than 20%.

(4) Small isolated globular carbides are permissible, carbides in continuous networks are causes for rejection. (To assist detection of carbides it was suggested to repolish and etch the section in boiling alkaline sodium piorate).

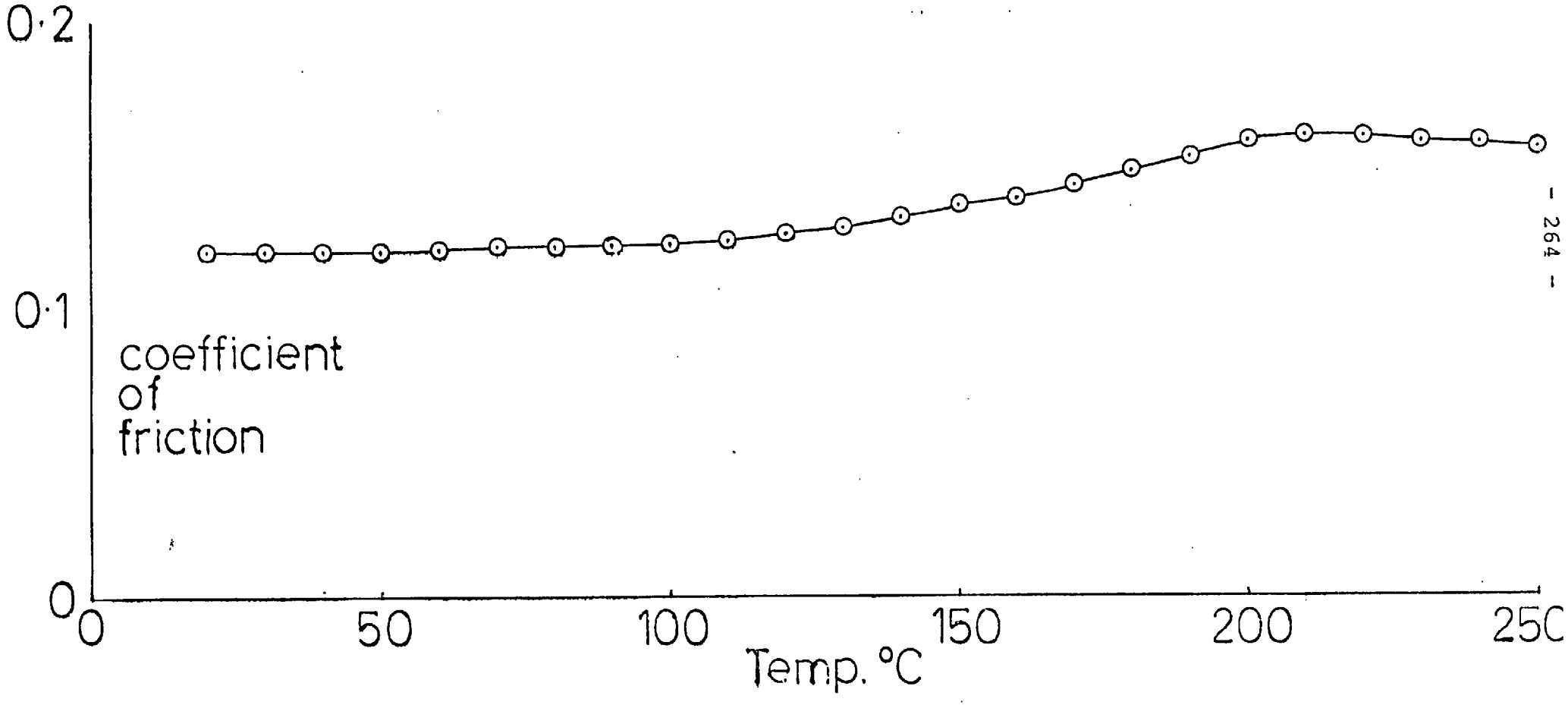
APPENDIX EIGHT

TRANSITION TEMPERATURE MEASUREMENT

FOR Eng. R.D.2487

This was measured with a cone on triplane machine (81, 82). The EN31 cone had an effective radius of 3/8 inch. and was pressed against three EN31 rollers of 3/16 inch. diameter with a load of 40 lbf. The cone was rotated at 1 r.p.m. and lubricated with oil to specification Eng. R.D.2487. Whilst the apparatus was heated to 250^{o}C and then cooled to room temperature, readings were taken of the coefficient of friction. These are shown in Figure 8.

FIGURE 8 Slow Speed Friction Measurement for Disc Machine Oil



APPENDIX NINE

CALCULATION OF THE ACCURACY OF THE TOTAL TEMPERATURES

The total temperature is the sum of the disc surface temperature plus the calculated flash temperature rise. The experimental error for both had to be determined and then added together, as follows.

The disc surface temperature could be measured to within $\pm$ 5°C, as shown by Macpherson (3) and discussed in section 10.17.

The flash temperature rise (TF) was dependent upon the following four factors.

(1) The load, which could be measured with an accuracy of $\pm$ 1%.

(2) The coefficient of friction, which was generally accurate to within 3%.

(3) The low speed disc speed, which was maintained within 2% of its true value.

(4) The high speed disc speed, which was accurate to within 1%.

$$TF \propto W^{3/4} \times \mu \times (U_1^{1/2} - U_2^{1/2})$$

The percentage maximum error in TF was determined for the worst case when the slide/roll ratio was 0.259.

Error in TF (%)

$$= 100\ (1.01^{3/4} \times 1.03\ ((1.7 \times 1.01)^{1/2} - 0.98^{1/2})/(1.7^{1/2} - 1.0)$$

$$= 9\%.$$

As the average flash temperature rise was 100°C, the maximum error in this value was approximately 9°C. Thus the total possible error in the value of the total temperature was $\pm$ 14°C.

APPENDIX TEN

CALCULATION OF CENTRAL PRESSURE, USING LEE AND CHENG'S RESULTS (72), FOR A LOAD OF 1000 lbf.

By experimentation it was determined that the following equation was a close fit with the pressure profile, in Figure 15.7a, for $H_o = 6.0 \times 10^{-5}$

$$p = p_o - 2.828\ p_o\ X^{3/2}$$

For positive values of X where, X = x/b.

Ignoring inertia effects the load is equal to $\int pdA$

load/inch = $\int p\ dx$

$$1000/0.25 = 2b\int_o^{\frac{1}{2}} (p_o - 2.828\ p_o\ X^{3/2})\ dX$$

$$= 2b\ (p_o\ X - 1.1313\ p_o\ X^{5/2})_o^{1/2}$$

$$= 0.600\ b\ p_o$$

But from the equation for b

$$b = 4R\ p_o/E$$

Substituting, $\therefore\ 4000 = 2.4\ R\ p_o^2/E$

$$\therefore \quad p_o = 258{,}000\ \text{lbf./in}^2.$$

APPENDIX ELEVEN

STATISTICAL ANALYSIS OF SCUFFING LOADS

The aim of this analysis was to determine whether the failure loads obtained with a dynamic load differed significantly from the equivalent steady load test results. The statistics text book by R.A. Fisher (67) was consulted to compare the two sets of data and establish the probability that they could actually have arisen from one data set.

The analysis was applied to the results from Type B tests, since previous testing had required nine Type B tests with a steady load. There were also five Type B tests for an applied load frequency of 15 Hz. The significance of the difference between the two sets of results could be determined by calculating the following:-

Let the two samples be

$x_1, x_2, \ldots\ldots x_{n_1+1}$ and

$x_1^1, x_2^1, \ldots\ldots x^1_{n_2+1}$

$$\bar{x} = (1/(n_1 + 1)) \sum (x)$$

$$\bar{x}^1 = (1/(n_2 + 1)) \sum (x^1)$$

$$s^2 = \left[\sum (x - \bar{x})^2 + \sum (x^1 - \bar{x}^1)^2\right] / (n_1 + n_2)$$

$$t = (\bar{x} - \bar{x}^1) \left[(n_1 + 1)(n_2 + 1)/(n_1 + n_2 + 2)\right]^{1/2}/s$$

Where, $\bar{x}$ and $\bar{x}^1$ are the mean of the two populations.

s is the standard deviation for the two populations combined, and

t is a theoretically derived figure, related to the variance of the two means.

For Type B tests

$\bar{x} = 1289$ $\bar{x}^1 = 855$

$s = 63$ and $t = 12.35$

From (67) and knowing t the probability that the two sets of scuffing loads were in fact one single set was thus less than 0.002.

This examination was repeated for two other examples, chosen as follows:-

(a) The results at 15 Hz. for Type D tests, as they were fairly typical and

(b) The results at 20 Hz. as they exhibited a large spread.

The two probabilities were 0.03 and 0.04 respectively.

Thus it was concluded that the changes observed in the scuffing failure load with alterations to the test conditions were statistically significant.

To assist in the analysis the standard deviation s, under dynamic loading was calculated for each type of test, at the frequency with the greatest number of data points.

$$s^2 = (1/(n - 1))\sum_1^n (x - \bar{x})^2$$

This produced the following results.

Table 11 Standard Deviation for Each Type of Test

Type of Test	Applied Load Frequency, Hz.	Standard Deviation s, lbf.
B	15	67
D	15	164
E	10	91
F	20	162
H	20	134
I	60	134
J	15	110
K	25	67
M	40	134

The mean of all the above is 118 lbf. Accordingly error bands have been shown on the graphs in 8.3 to 8.13 at $\pm$ 120 lbf. about the mean for each test frequency. These bands are seen to encompass 88% of the data points.

APPENDIX TWELVE

FOURIER ANALYSIS OF THE PRESSURE WAVEFORMS

Before comparing the effects of different frequencies of vibration on scuffing load, it was necessary to establish that the actual pressure waveforms produced in the oil were comparable. Otherwise the possibility remained that the scuffing load differences arose simply from different waveforms at different frequencies, rather than the actual applied frequencies themselves.

To investigate the magnitude of the variations with frequency the input waveform was processed by a computer, using a Fourier analysis program, specially written. This is shown at the end of this Appendix. The six waveforms used in Type B to L tests and their corresponding Fourier components are shown in Figures 12a to 12l. Table 12.1 gives the first three harmonics at each frequency.

Table 12.1 Fourier Components of Pressure Waveforms

Frequency Hz.	Fourier Components % Harmonics		
	1st	2nd	3rd
10	21	16	11
12½	26	22	12
15	21	19	17
20	34	20	3
30	35	18	4
60	48	5	2

In analysing the waveforms, harmonic components of less than 5% of the waveform were considered to have negligible effect. Relevant points from the analysis are now listed.

1. In all cases the first harmonic predominated.
2. Variations existed between the amplitude of the higher harmonics.
3. The 12½ and 15 Hz. waveforms contained very similar Fourier components.
4. The 20 and 30 Hz. waveforms were also very similar.

Had these analyses shown that all the waveforms contained the same harmonic components, then the pressure cycle between the discs would have been the same at all frequencies. The variations were interpreted as follows.

In rising from 10 Hz. to 60 Hz. the waveform was altering from being a very approximate square wave, to a shape which was closer to a sine wave.

The similarity in the components of the 12½ and 15 Hz. waveforms meant that it was practical to compare directly the scuffing failure loads at these two frequencies. The waveform for both frequencies was designated as waveform A.

The same applies to the pressure waveforms at 20 and 30 Hz., and were designated as waveform B.

In Figure 12.1 the mean failure loads for each type of test was plotted at these four frequencies. It can be seen that in virtually every case the failure load with waveform B at 30 Hz. was greater than that at 20 Hz. For Type B tests the failure load with waveform A at 15 Hz. was less than that at 12½ Hz.

It was concluded that the changes in the scuffing performance were not simply due to variations in the pressure waveform.

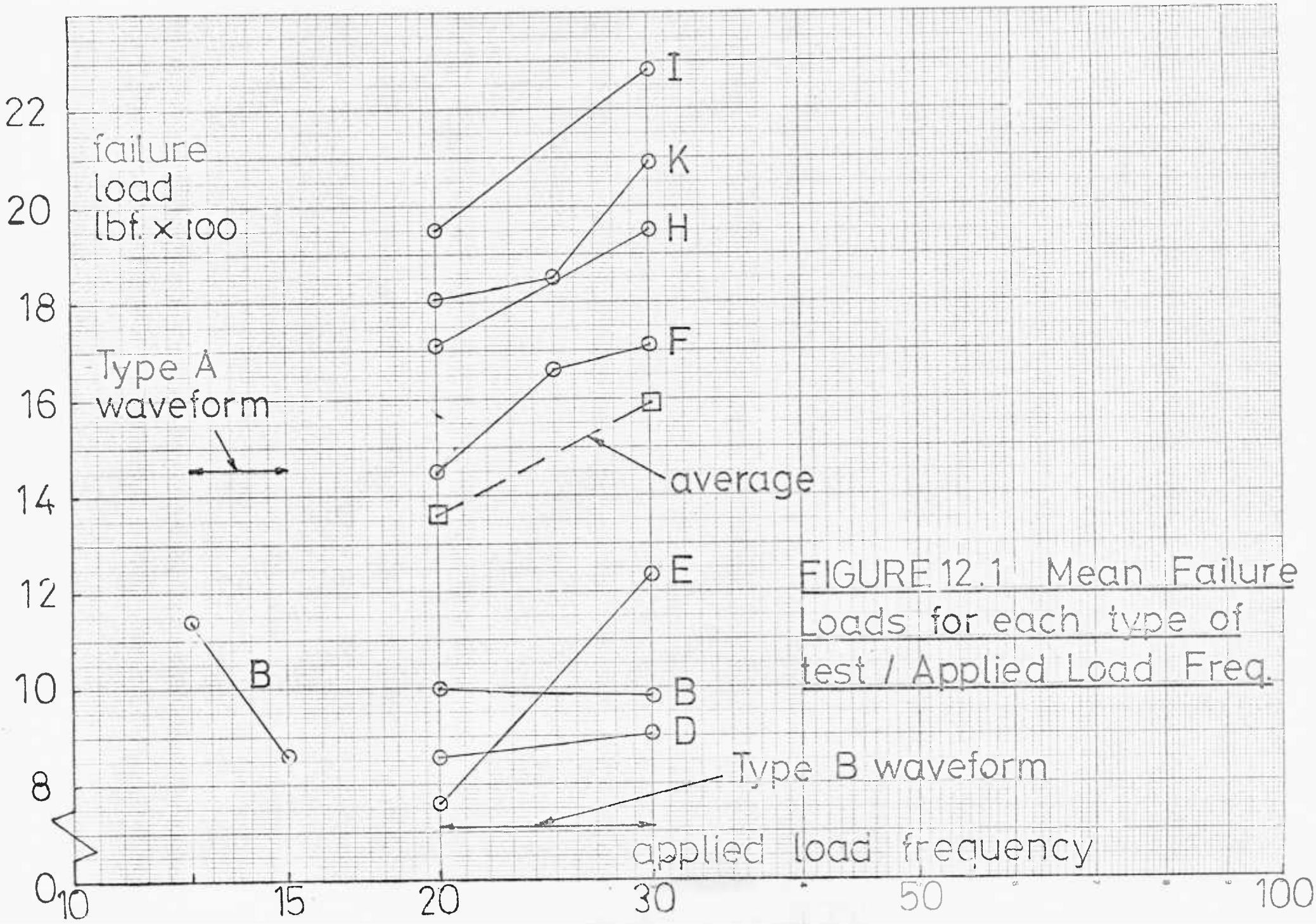


FIGURE 12.1 Mean Failure Loads for each type of test / Applied Load Freq.

12.2 FOURIER ANALYSIS OF PRESSURE WAVEFORMS FOR TYPE M TESTS

The servovalve was remounted on the disc machine (see Figure 7.13) so that a waveform was produced which was very nearly independent of frequency. Figures 12.2a to 12.21 show these pressure waveforms and their Fourier components. Table 12.2 gives the first three harmonics at each frequency.

Table 12.2 Fourier Components of Pressure Waveforms used in Type M Tests

Frequency Hz.	Fourier Component % Harmonics		
	1st	2nd	3rd
10	34	19	10
12½	35	18	10
15	36	19	10
20	29	18	10
30	32	19	10
60	31	20	11

It can be seen that the components are very similar, and thus the scuffing loads over the whole range of applied load frequencies could be compared directly, for Type M tests.

Figure 8.13 shows the results of these tests, and from them two things in particular can be deduced.

(1) With a constant waveform shape a reduction in the scuffing load was obtained between the frequencies of 12½ and 60 Hz.

(2) By comparison with the results from Type B tests it can be seen that the effects produced by the two waveforms are very similar.

Fig. 12a 10 Hz. Waveform

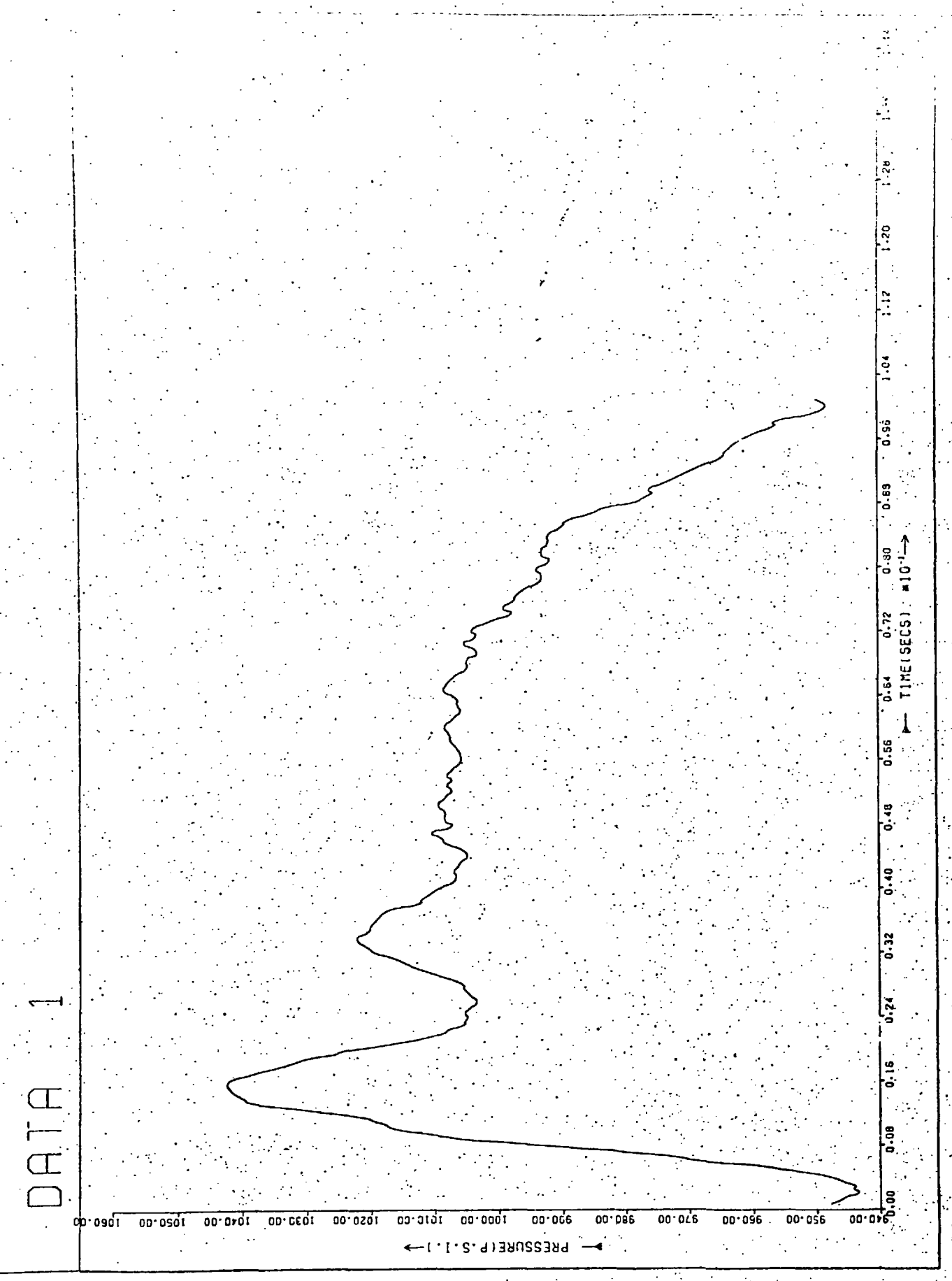


Fig. 12b Fourier Components of 10 Hz. Waveform

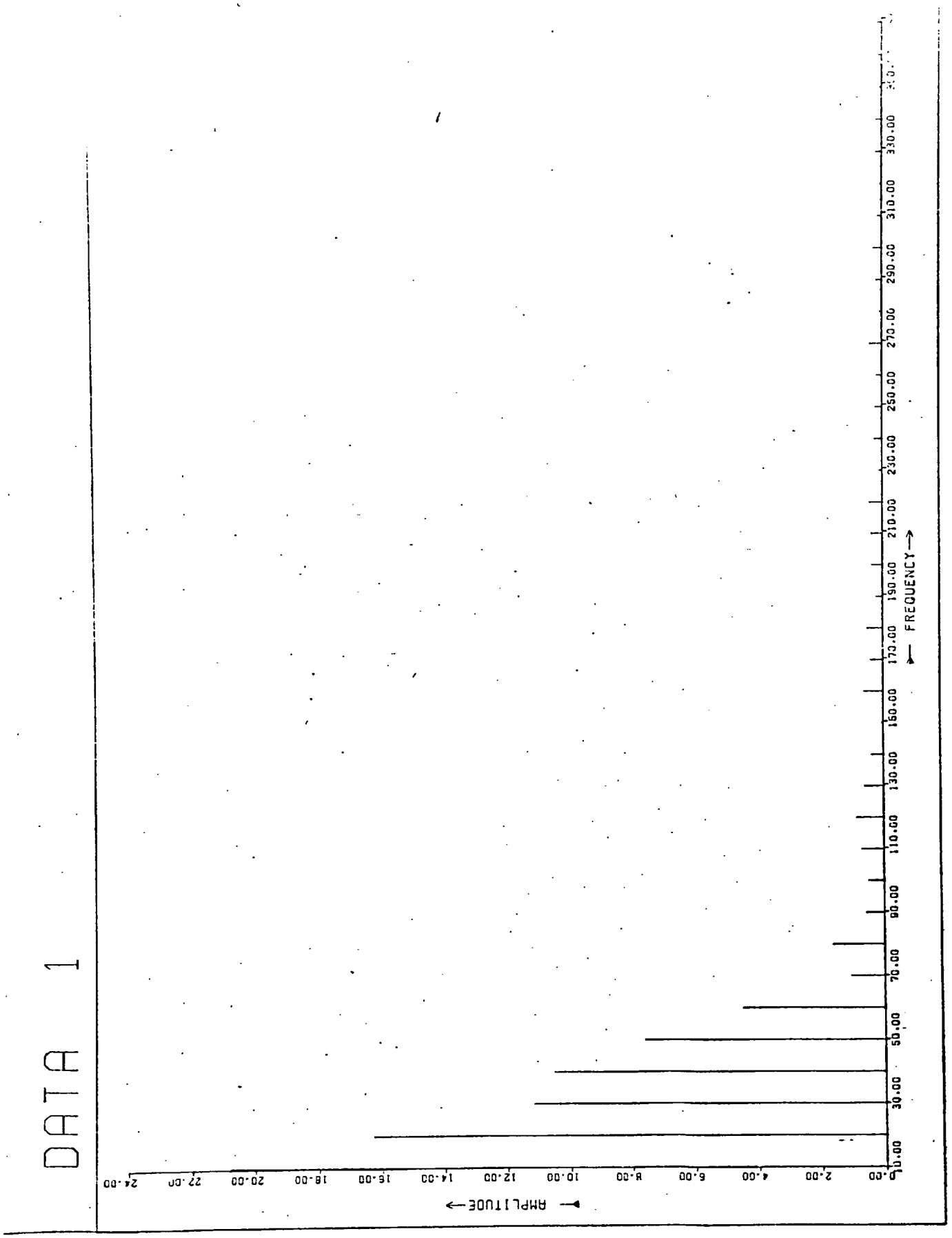


Fig. 12c 12½ Hz. Waveform

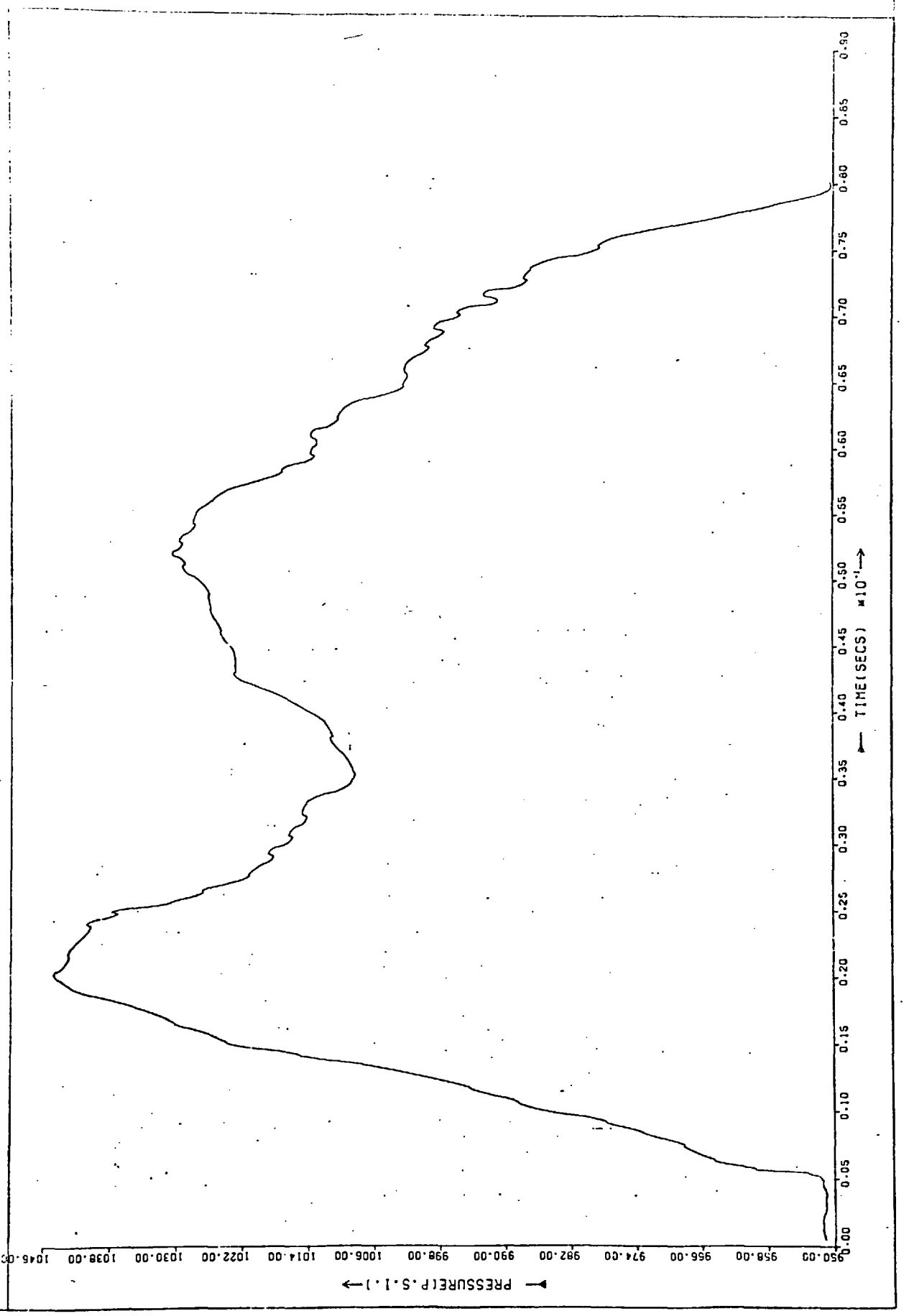


Fig. 12d Fourier Components of 12½ Hz. Waveform

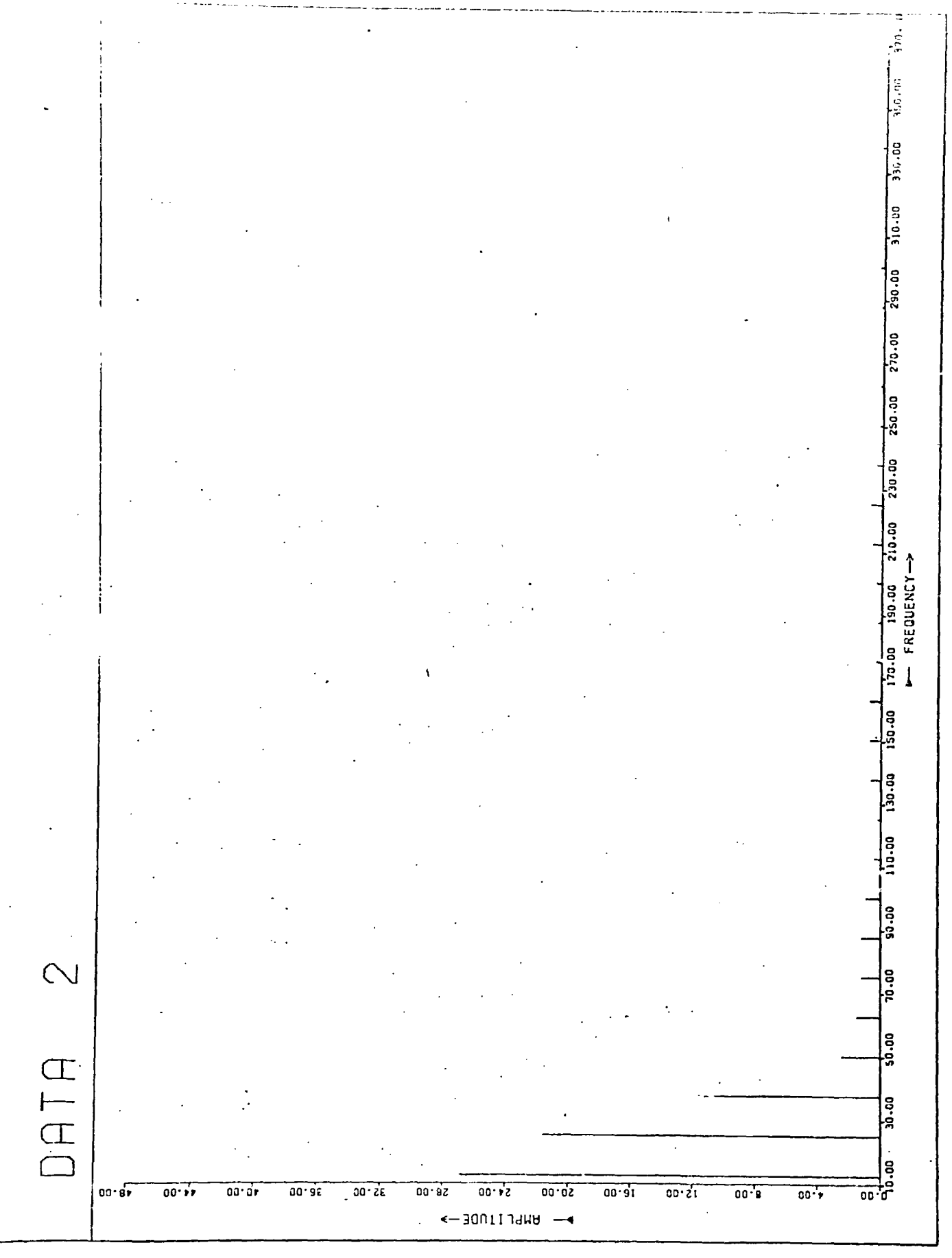


Fig. 12e 15 Hz. Waveform

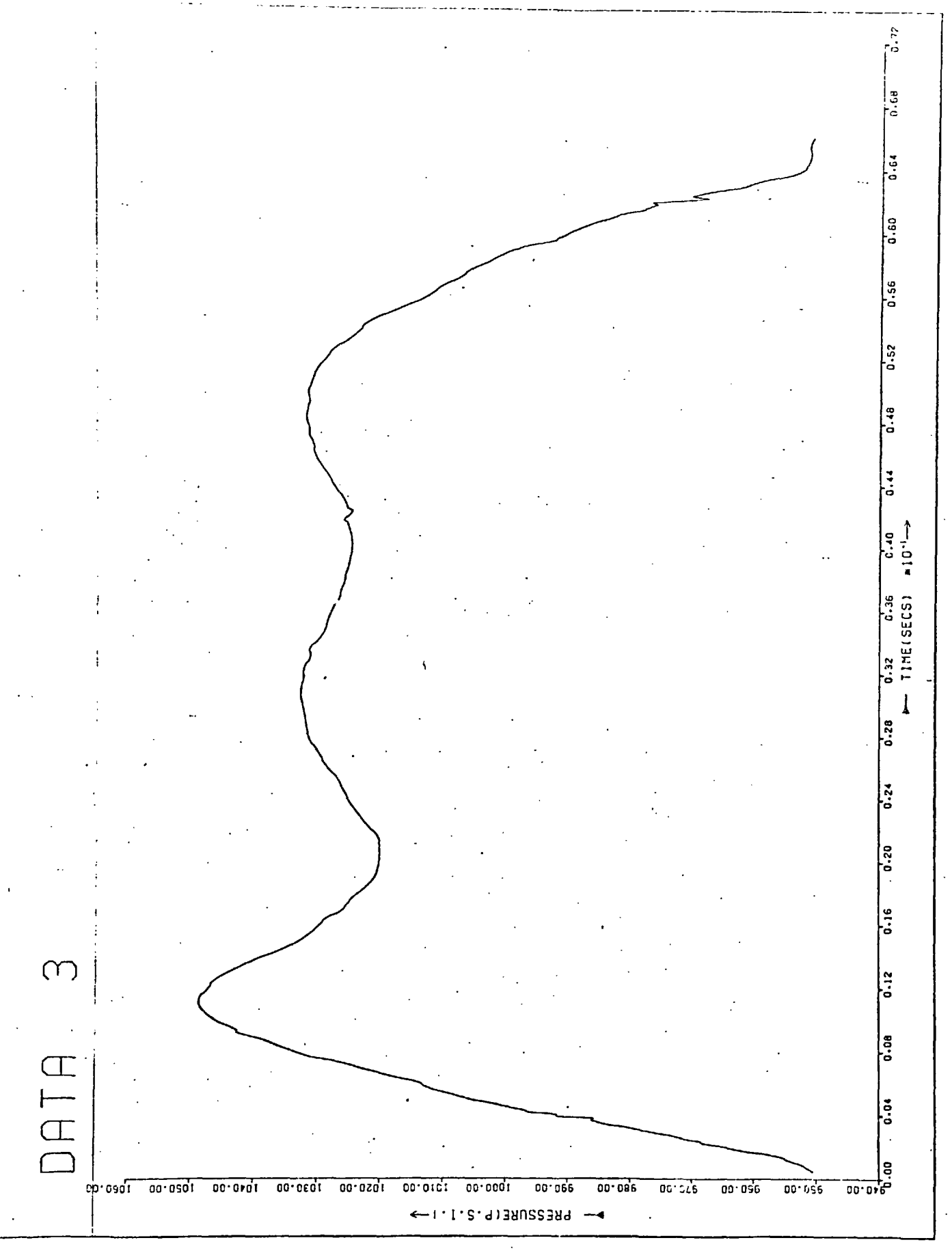


Fig. 12f Fourier Components of 15 Hz. Waveform

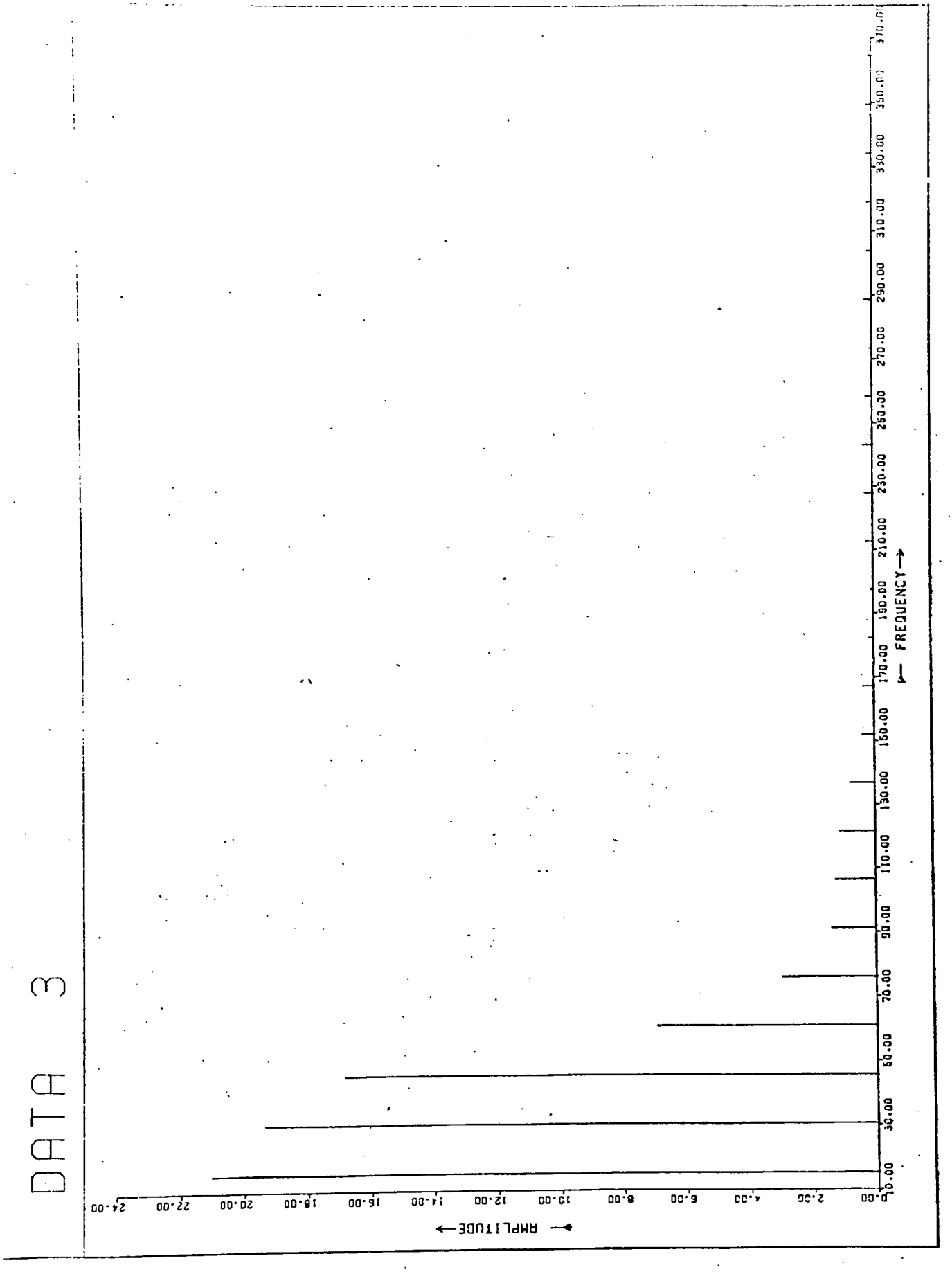


Fig. 12g 20 Hz. Waveform

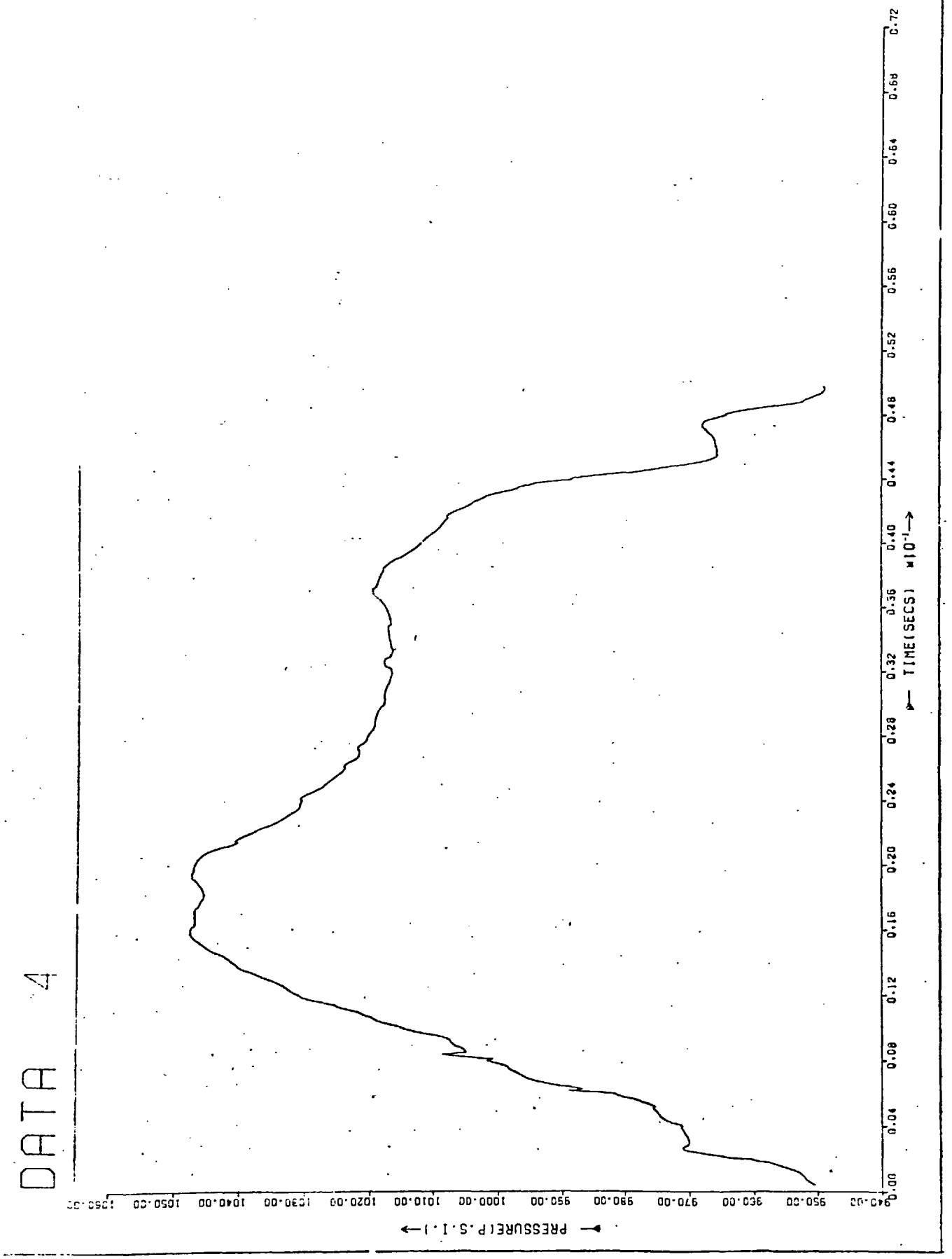
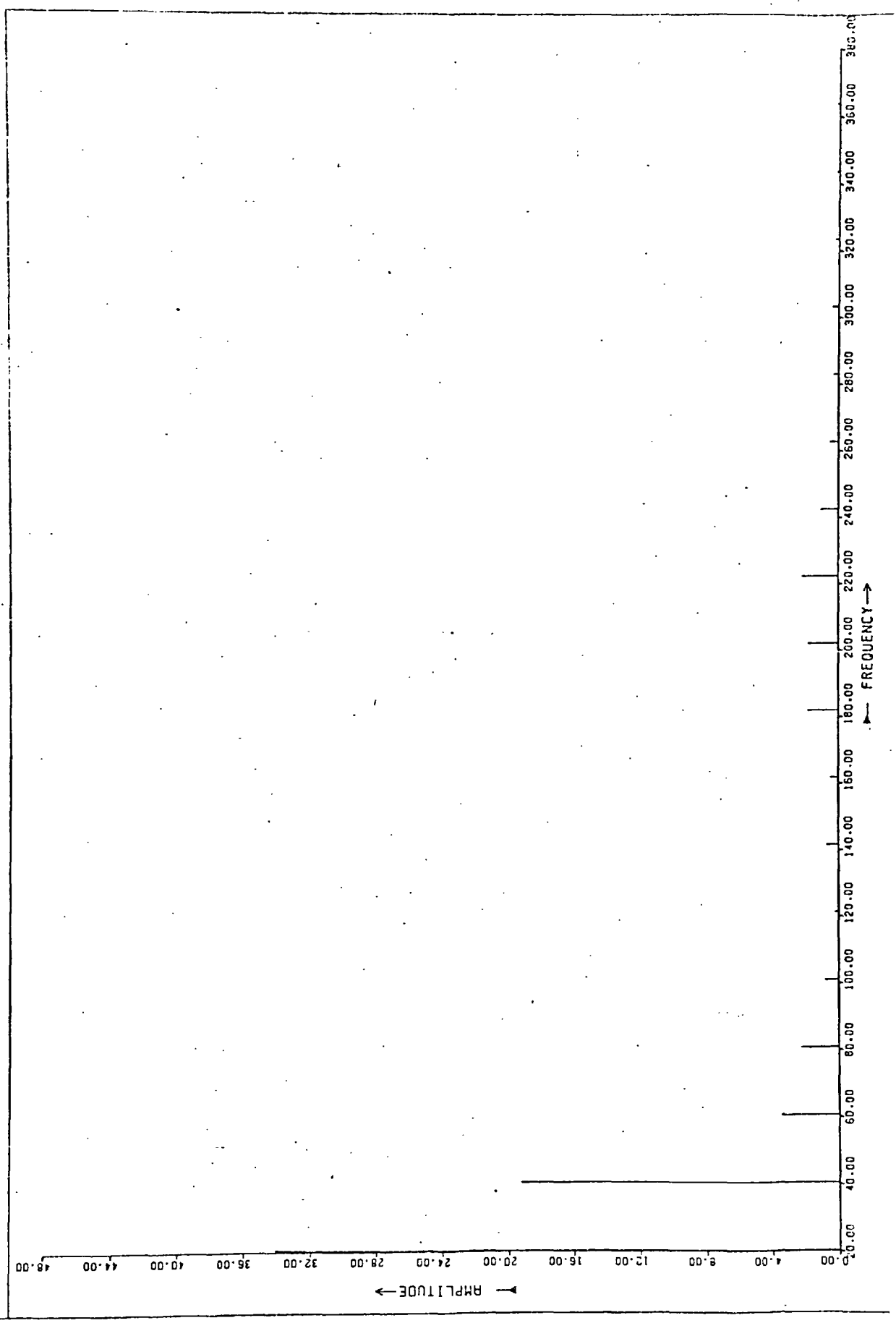


Fig. 12h Fourier Components of 20 Hz. Waveform



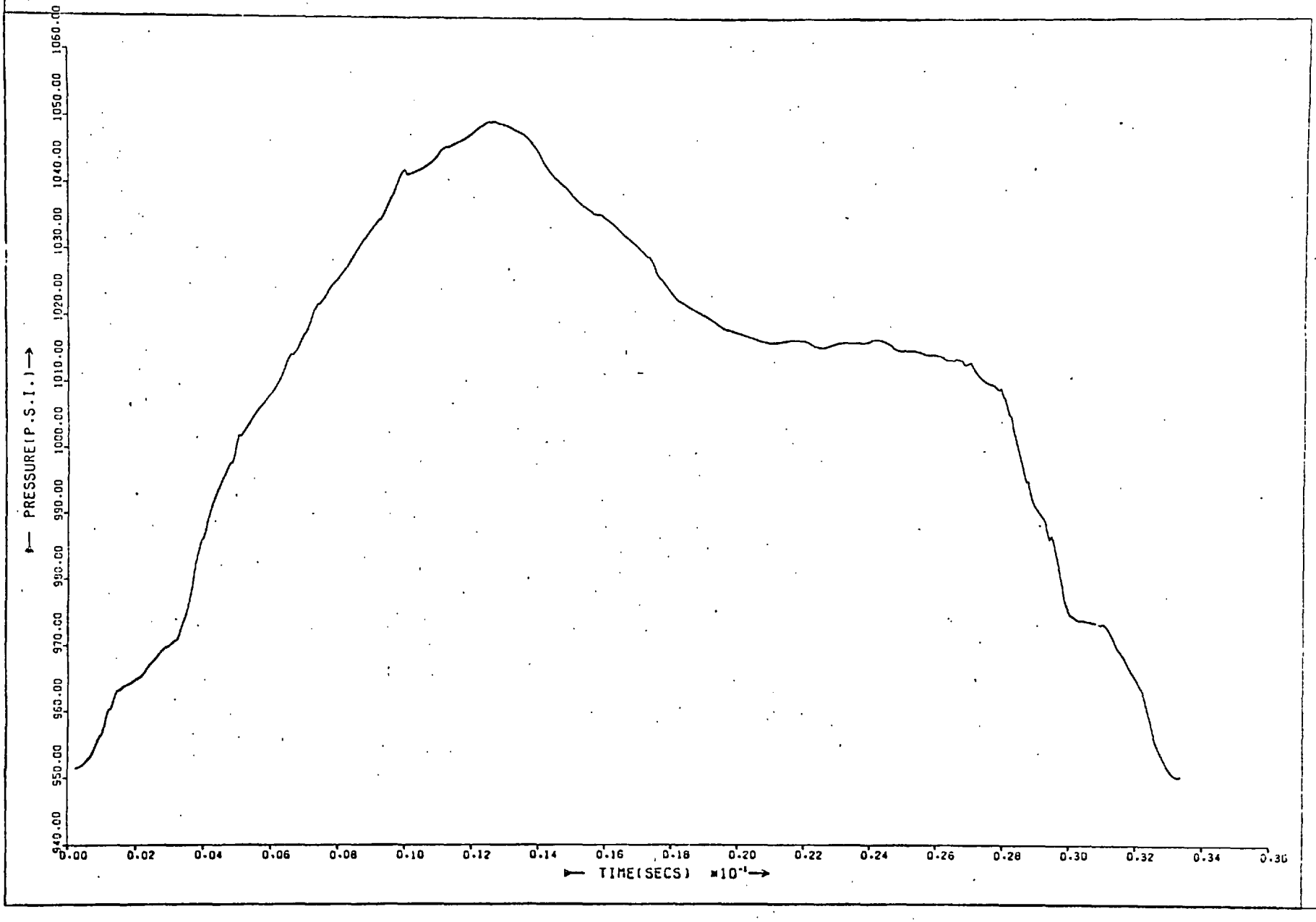


Fig. 12i 30 Hz. Waveform

Fig. 12j Fourier Components of 30 Hz. Waveform

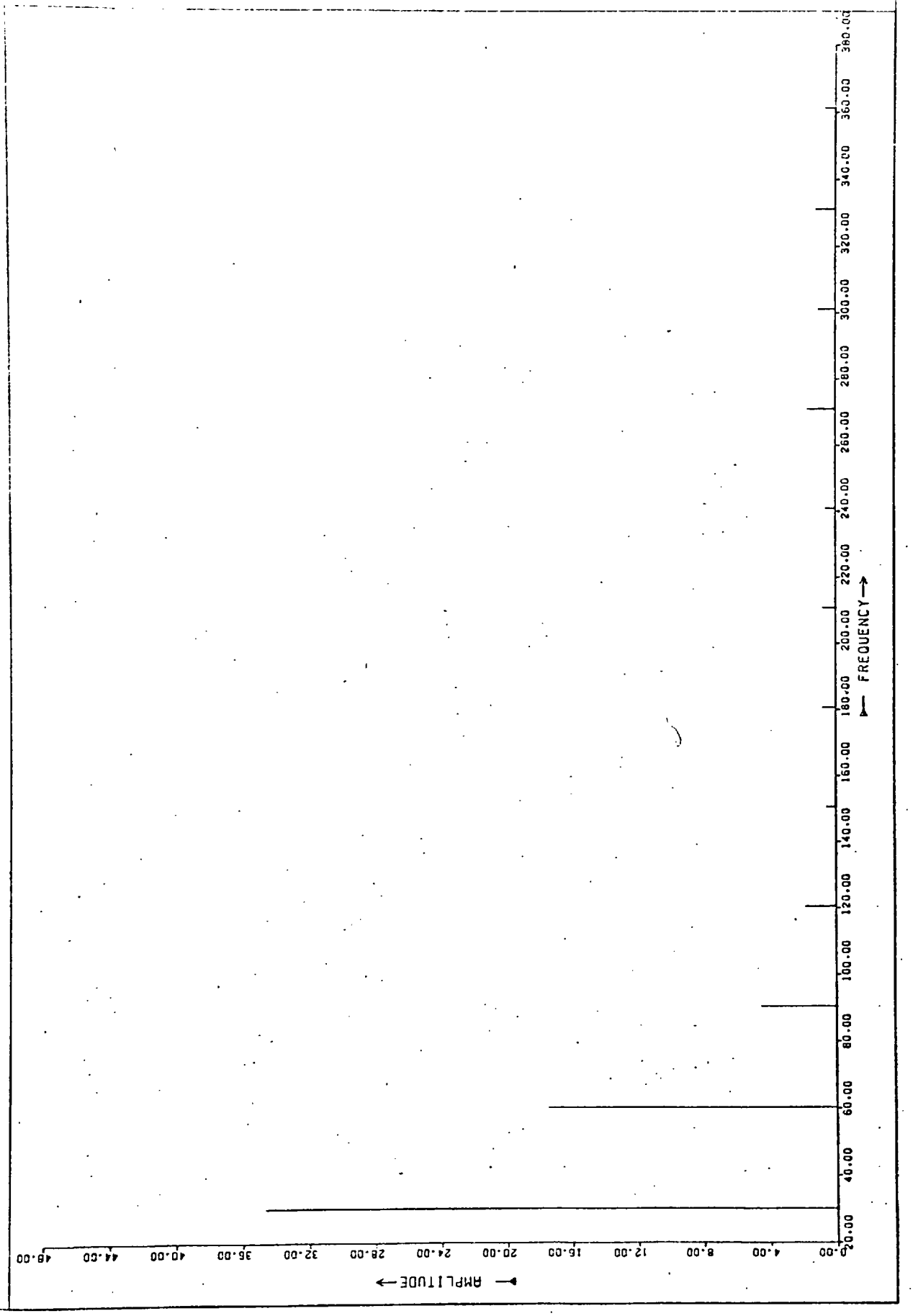


Fig. 12k 60 Hz. Waveform

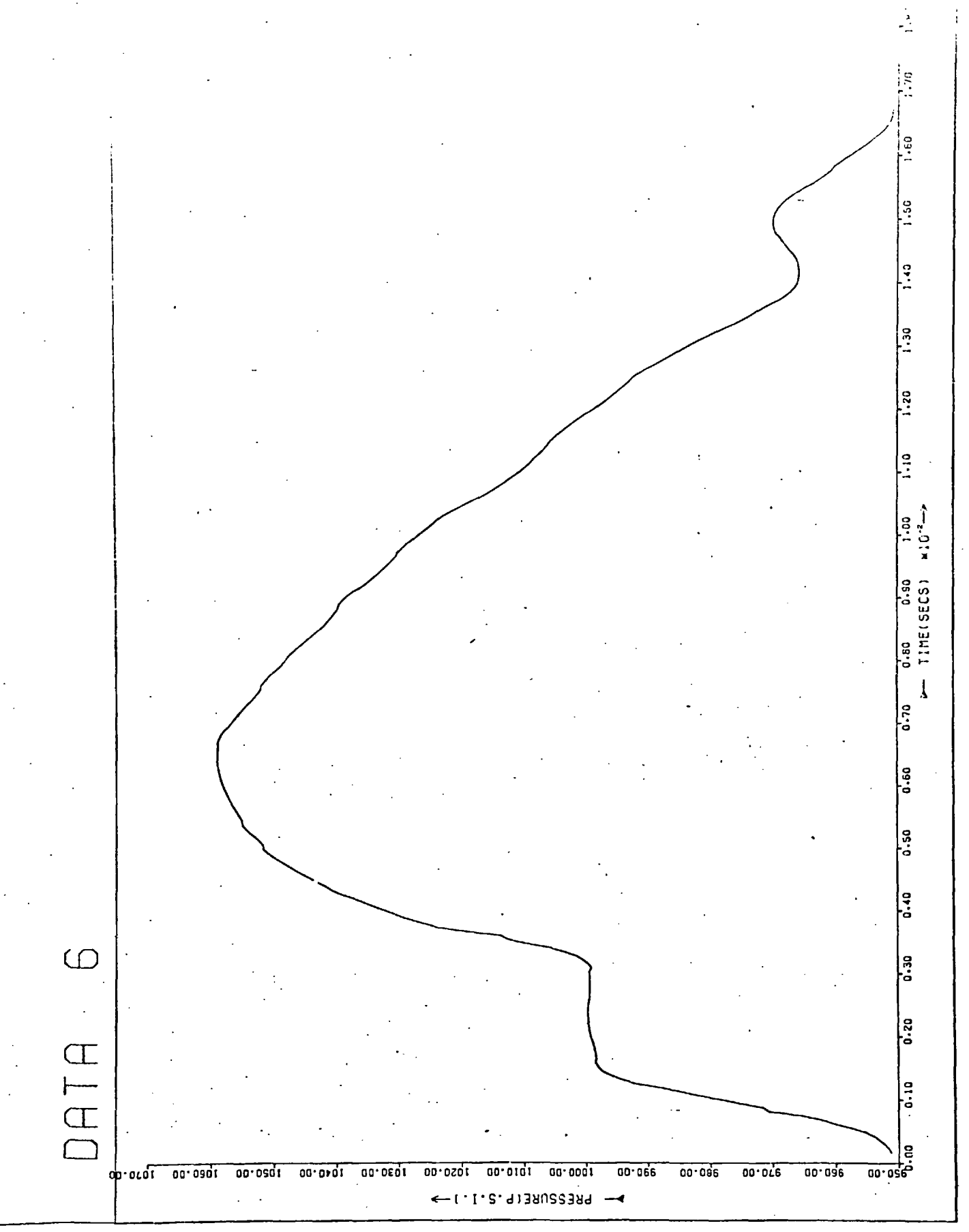


Fig. 121 Fourier Components of 60 Hz. Waveform

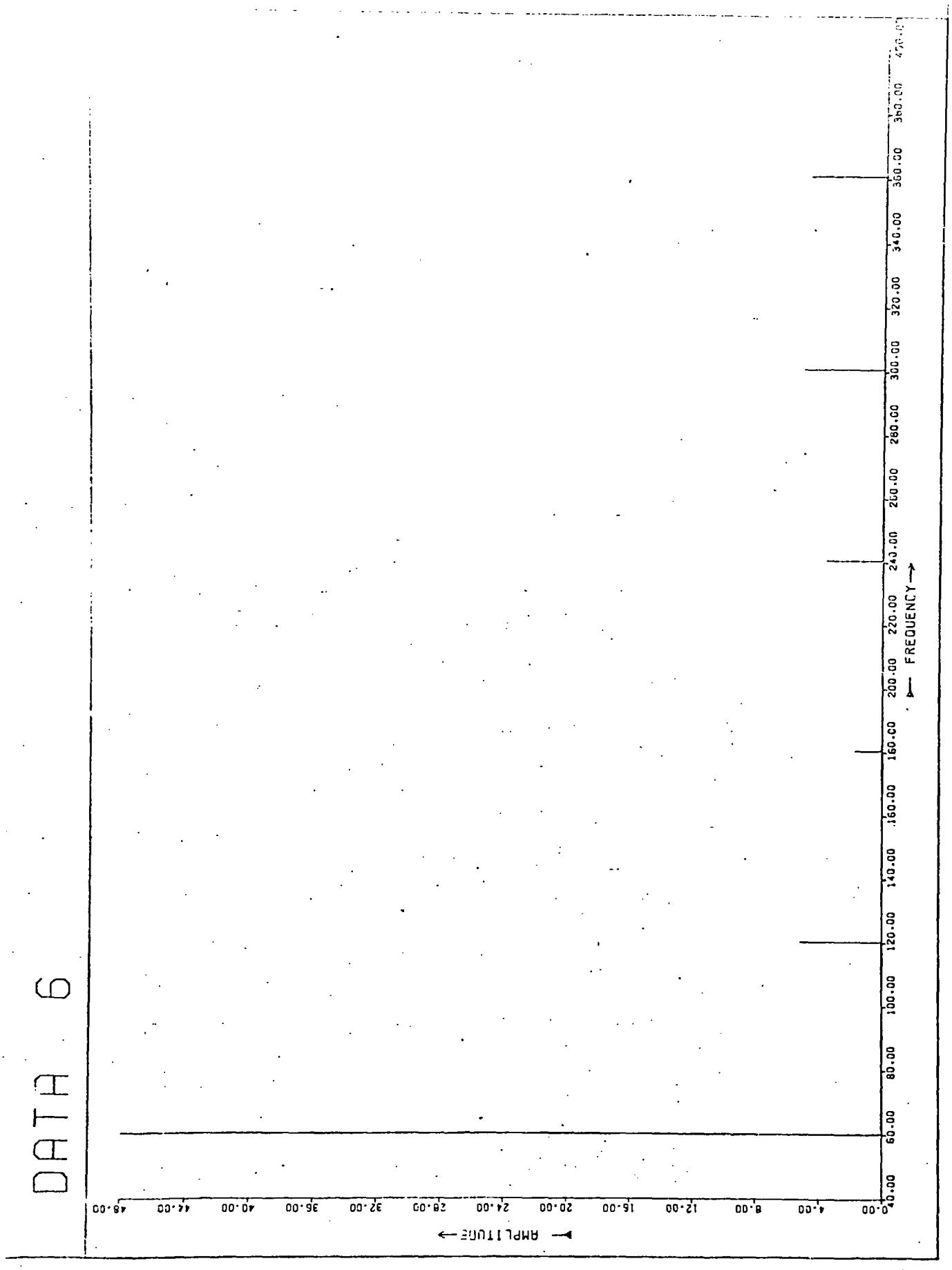


Fig. 12.2a 10 Hz. Waveform

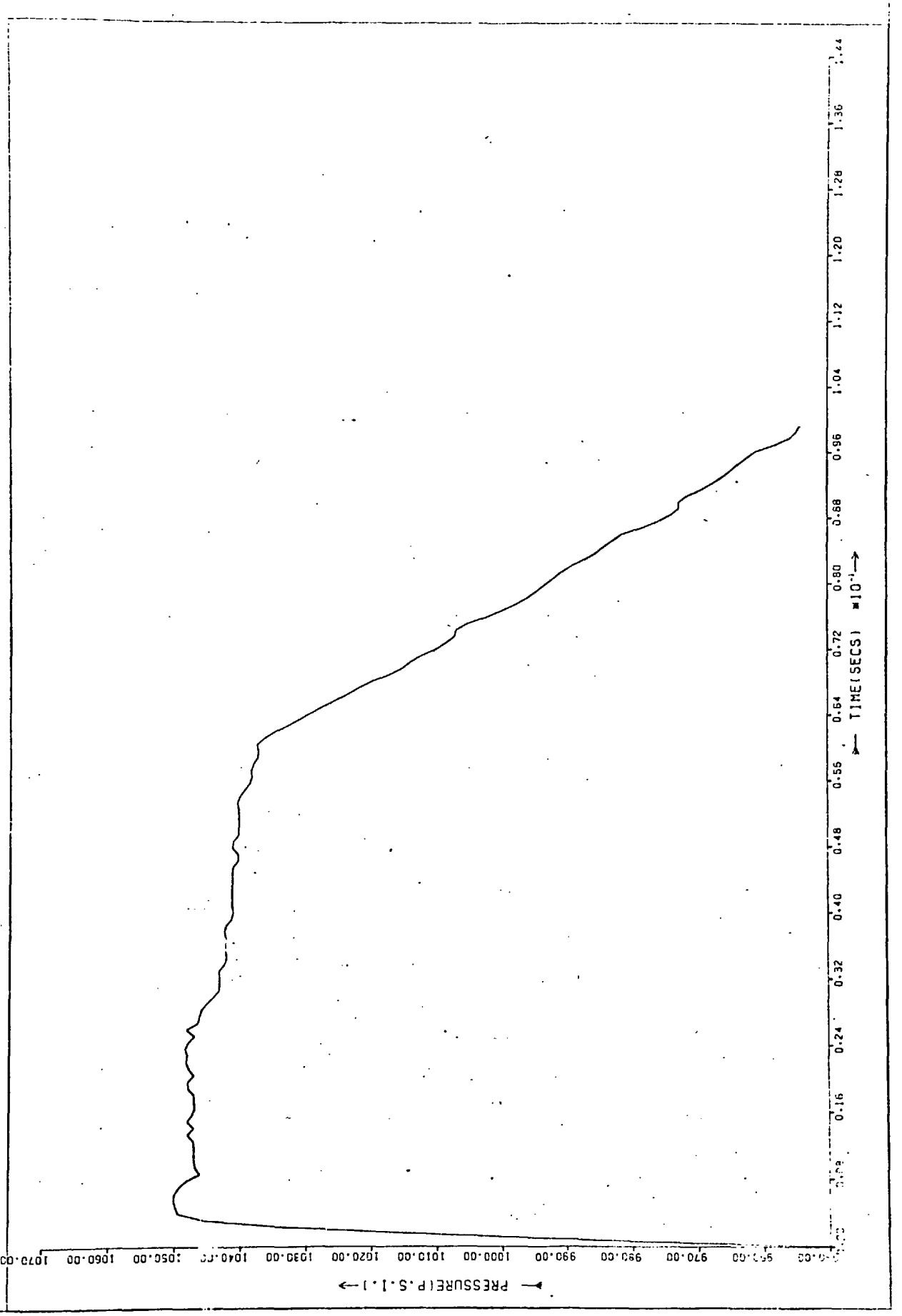


Fig. 12.2b Fourier Components of 10 Hz. Waveform

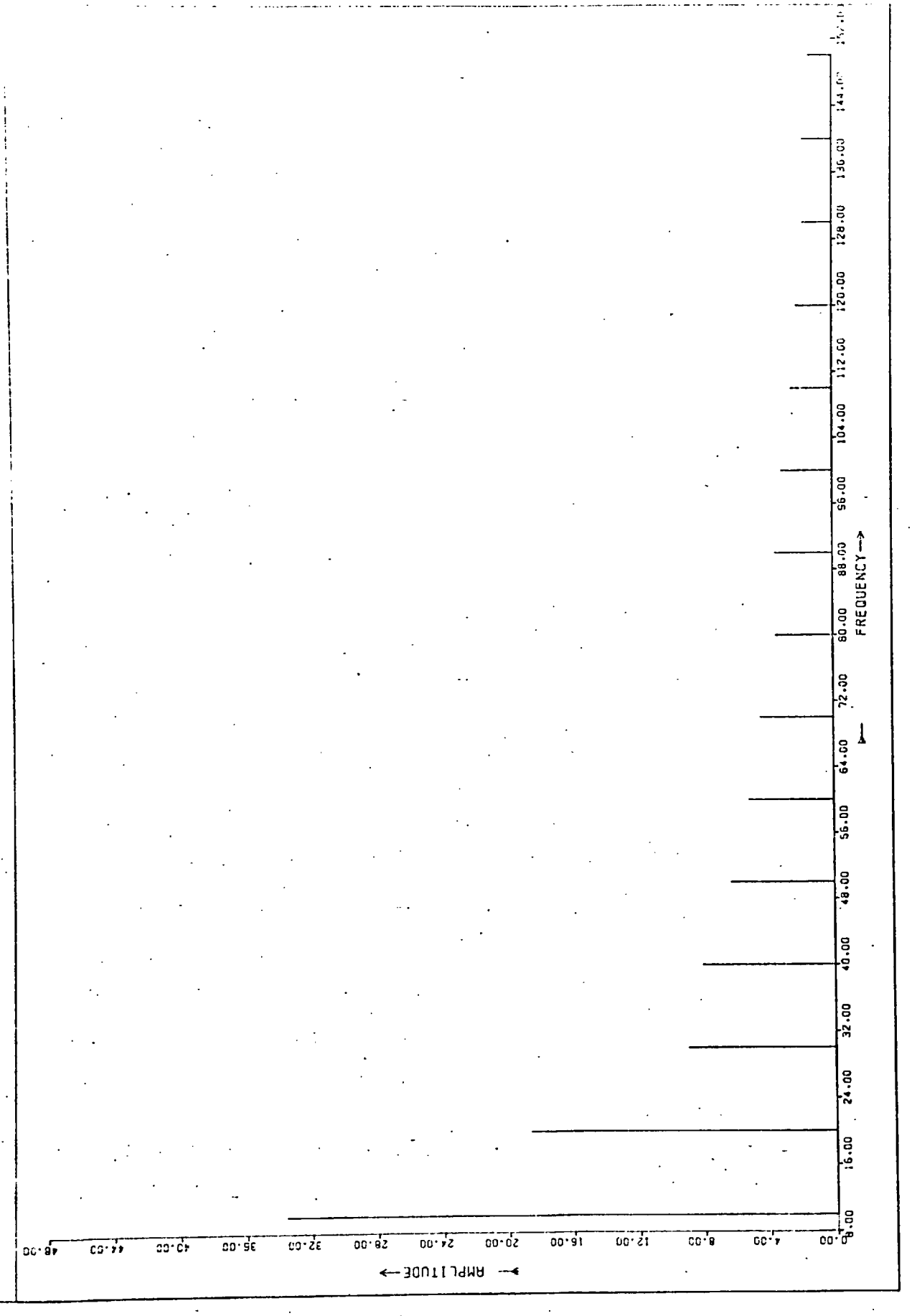


Fig. 12.2c 12½ Hz. Waveform

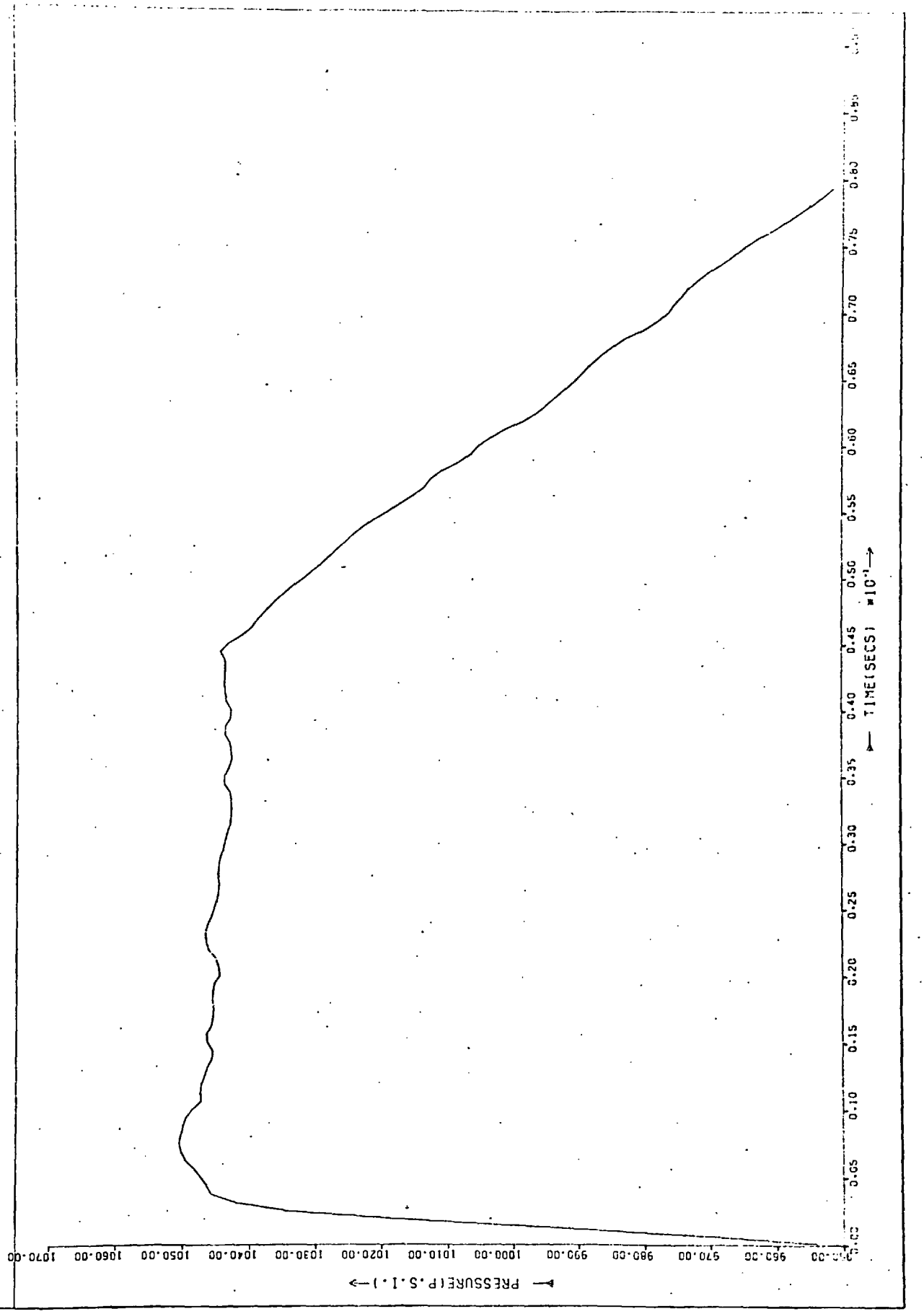


Fig. 12.2d Fourier Components of 12½ Hz. Waveform

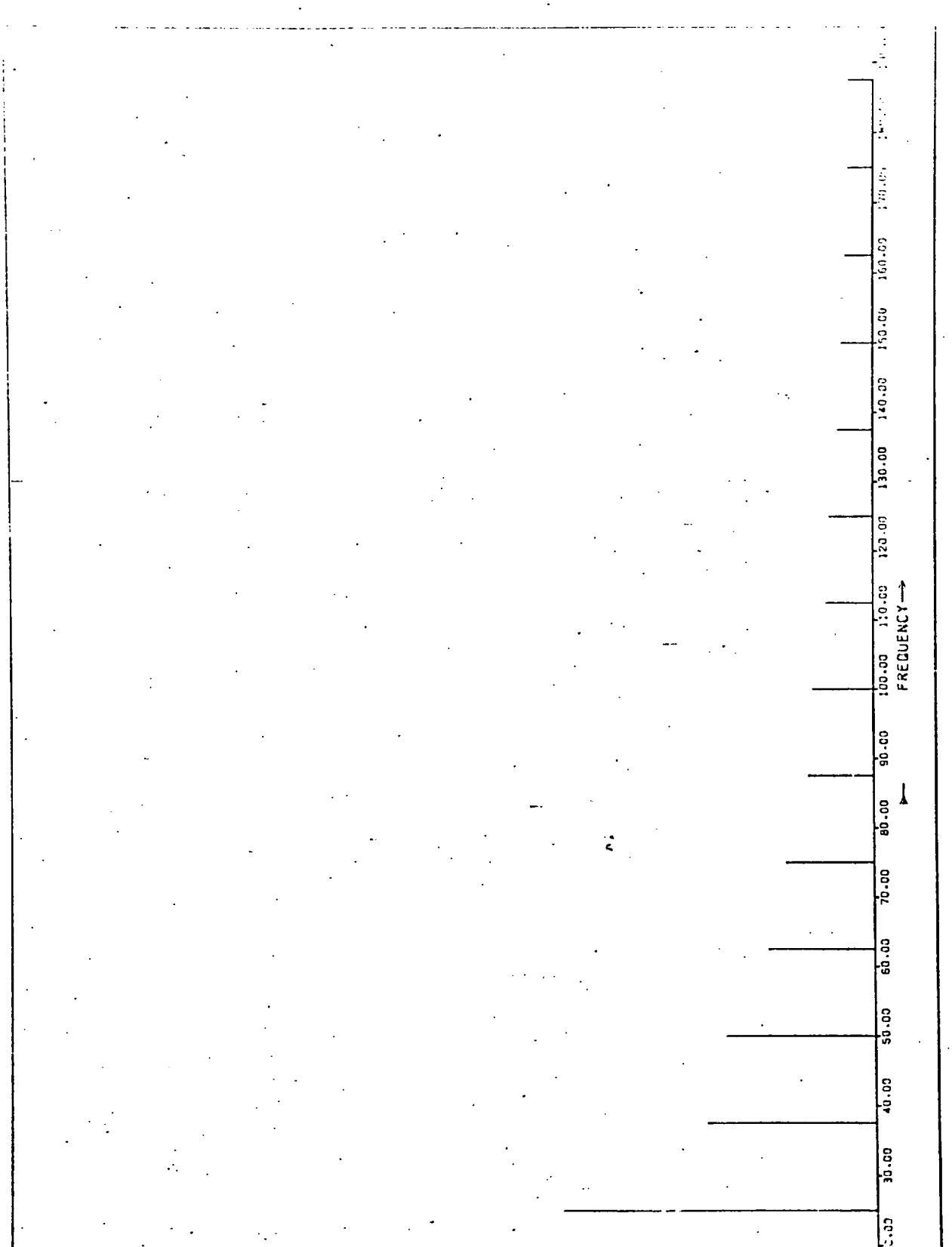


Fig. 12.2e 15 Hz. Waveform

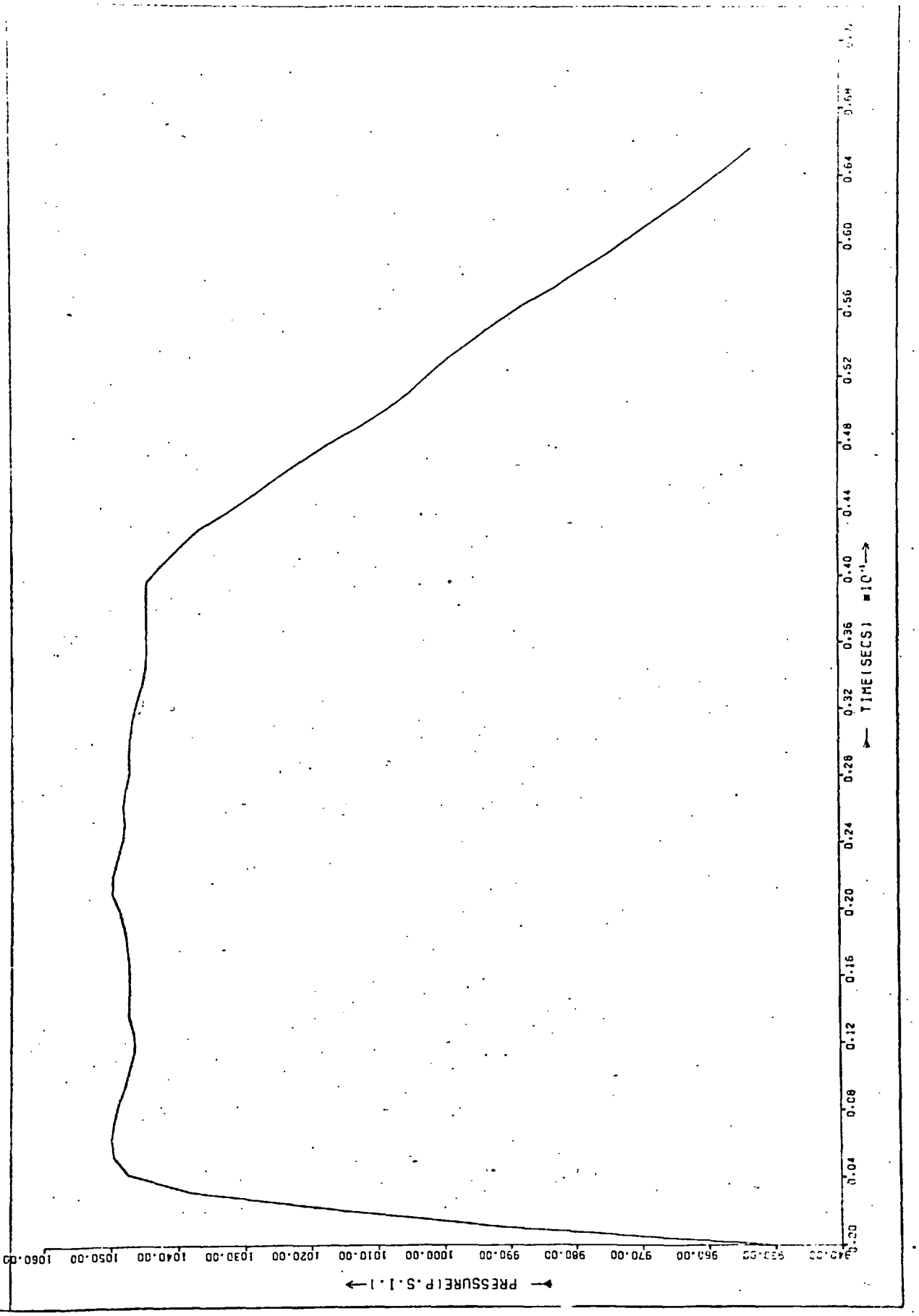


Fig. 12.2f Fourier Components of 15 Hz. Waveform

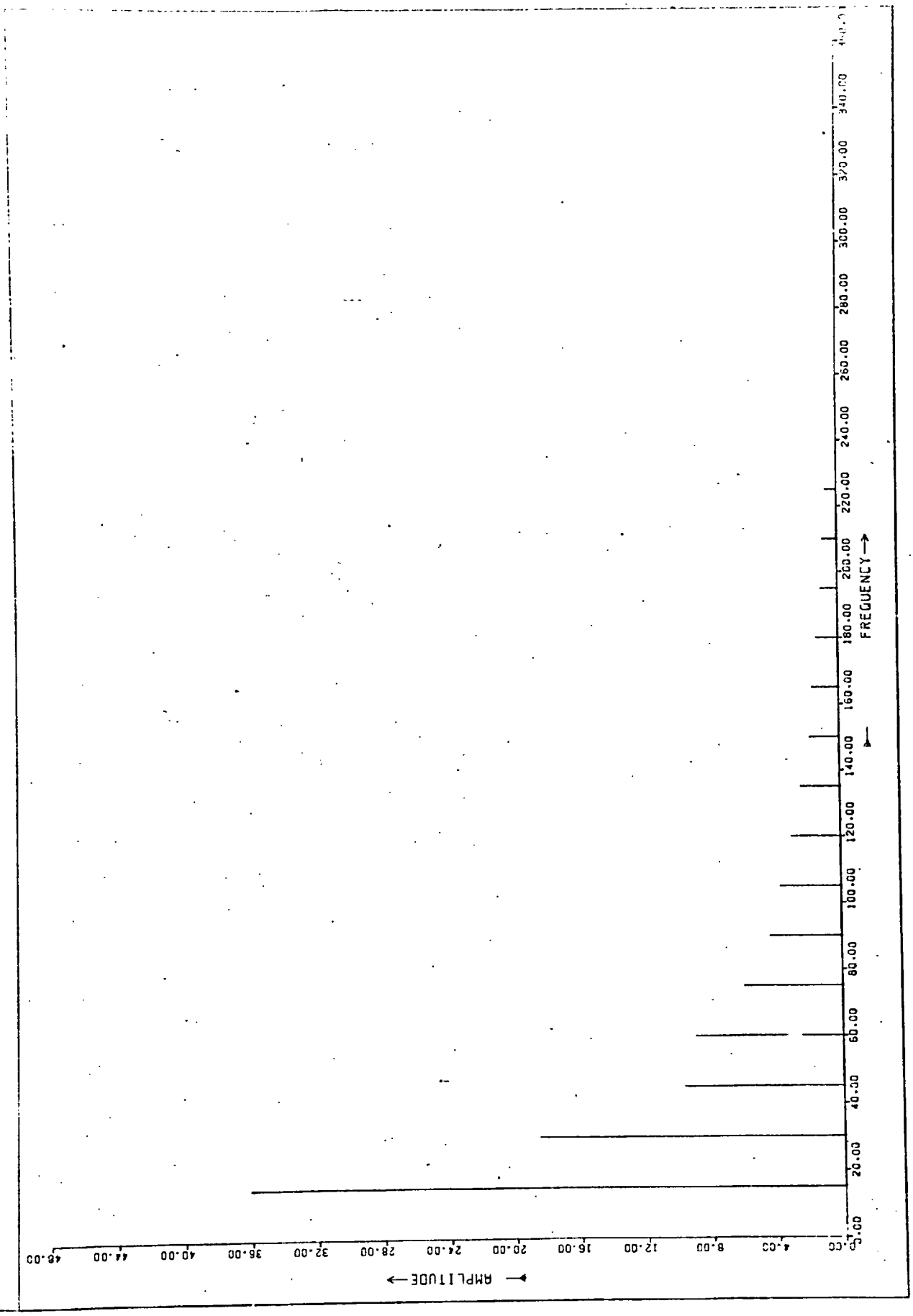


Fig. 12.2g 20 Hz. Waveform

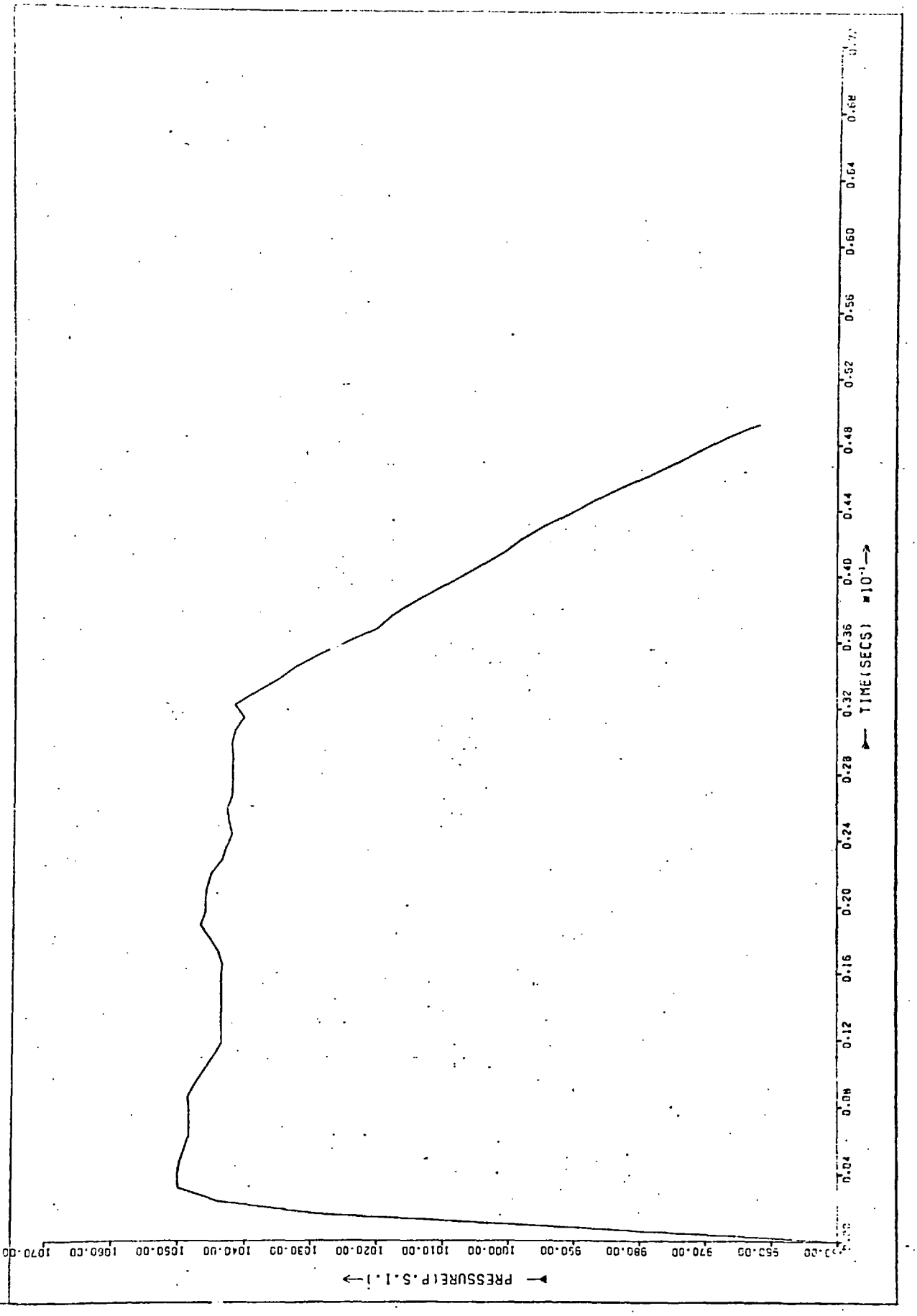


Fig. 12.2h Fourier Components of 20 Hz. Waveform

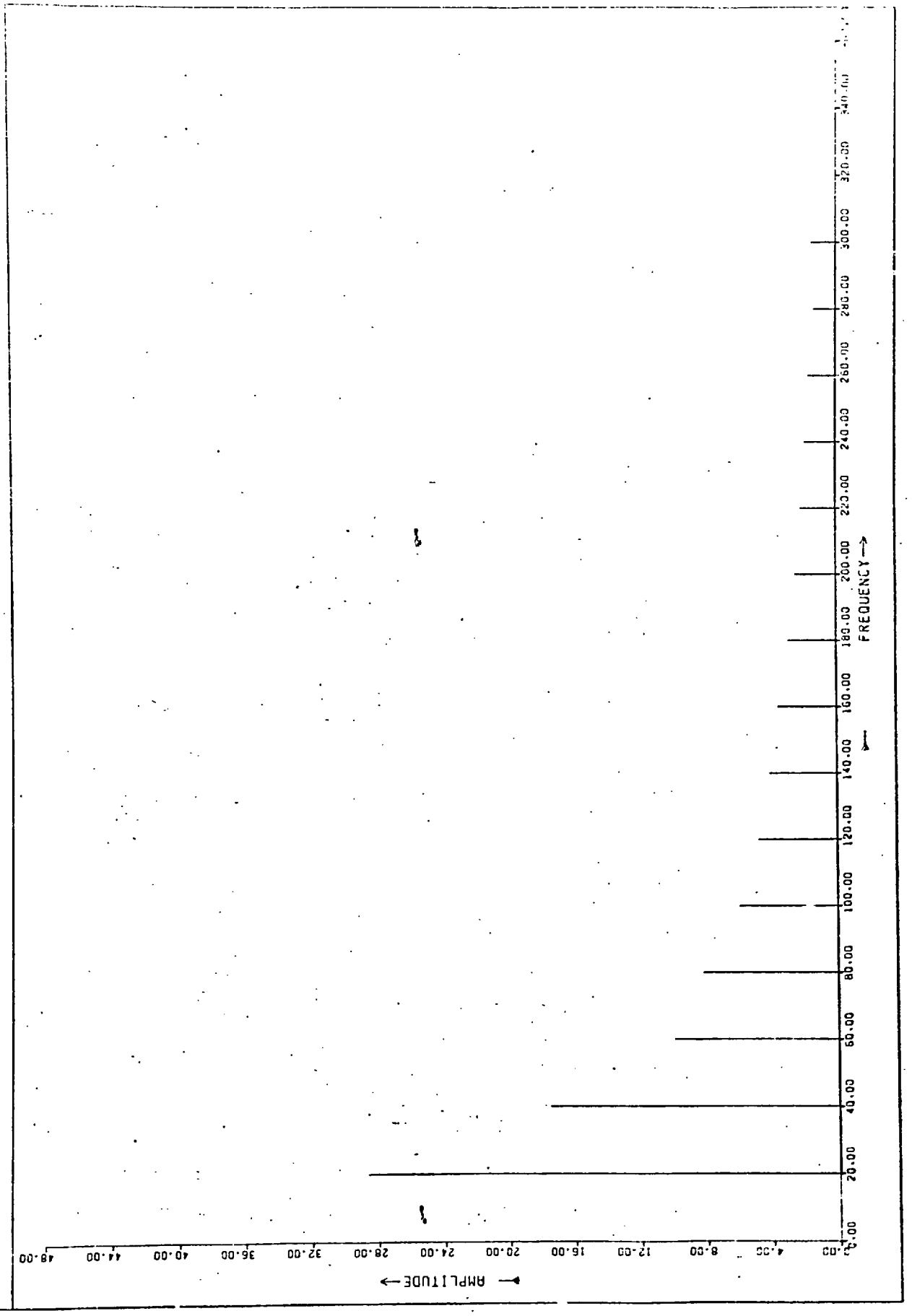


Fig. 12.2i 30 Hz. Waveform

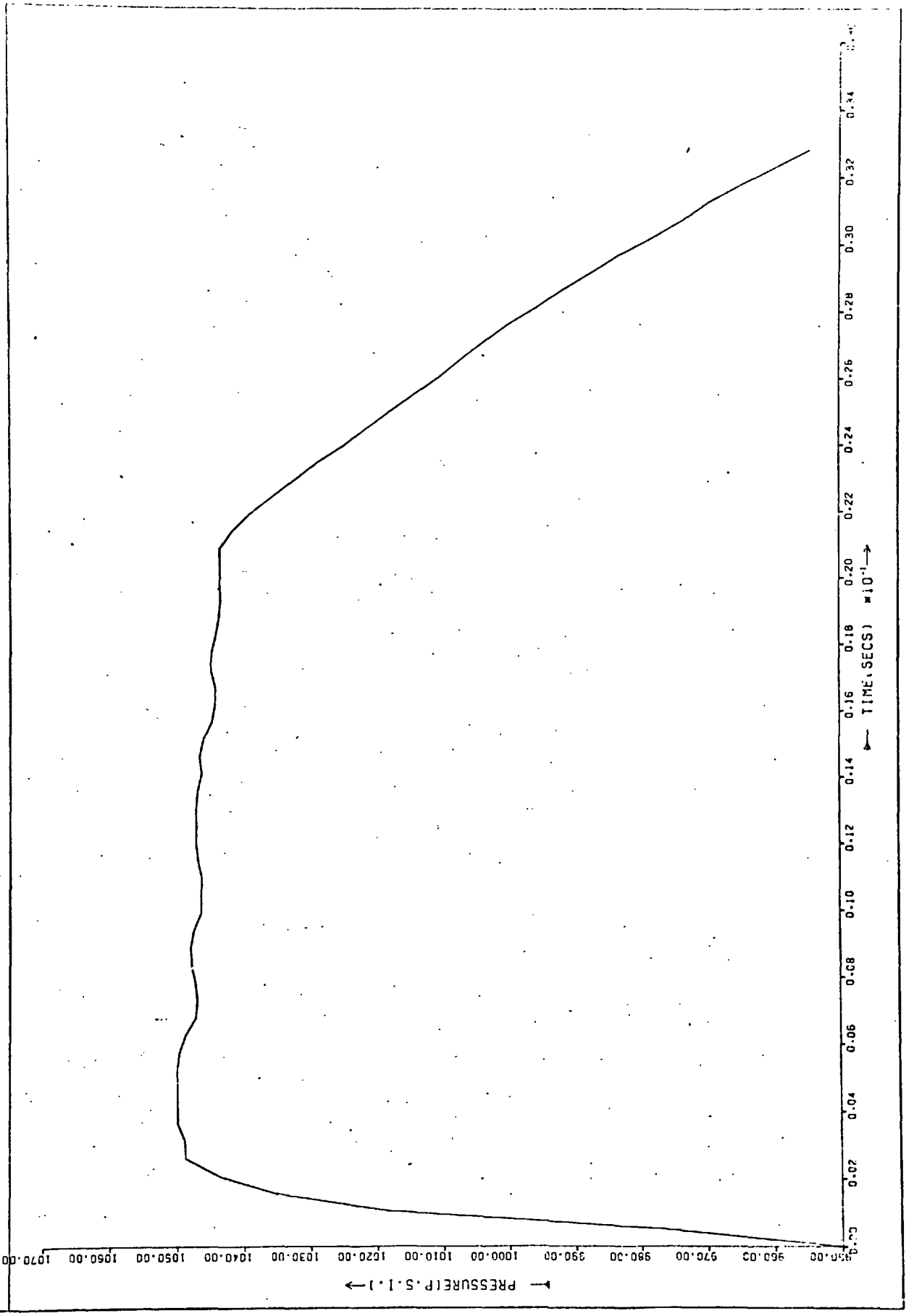


Fig. 12.2j Fourier Components of 30 Hz. Waveform

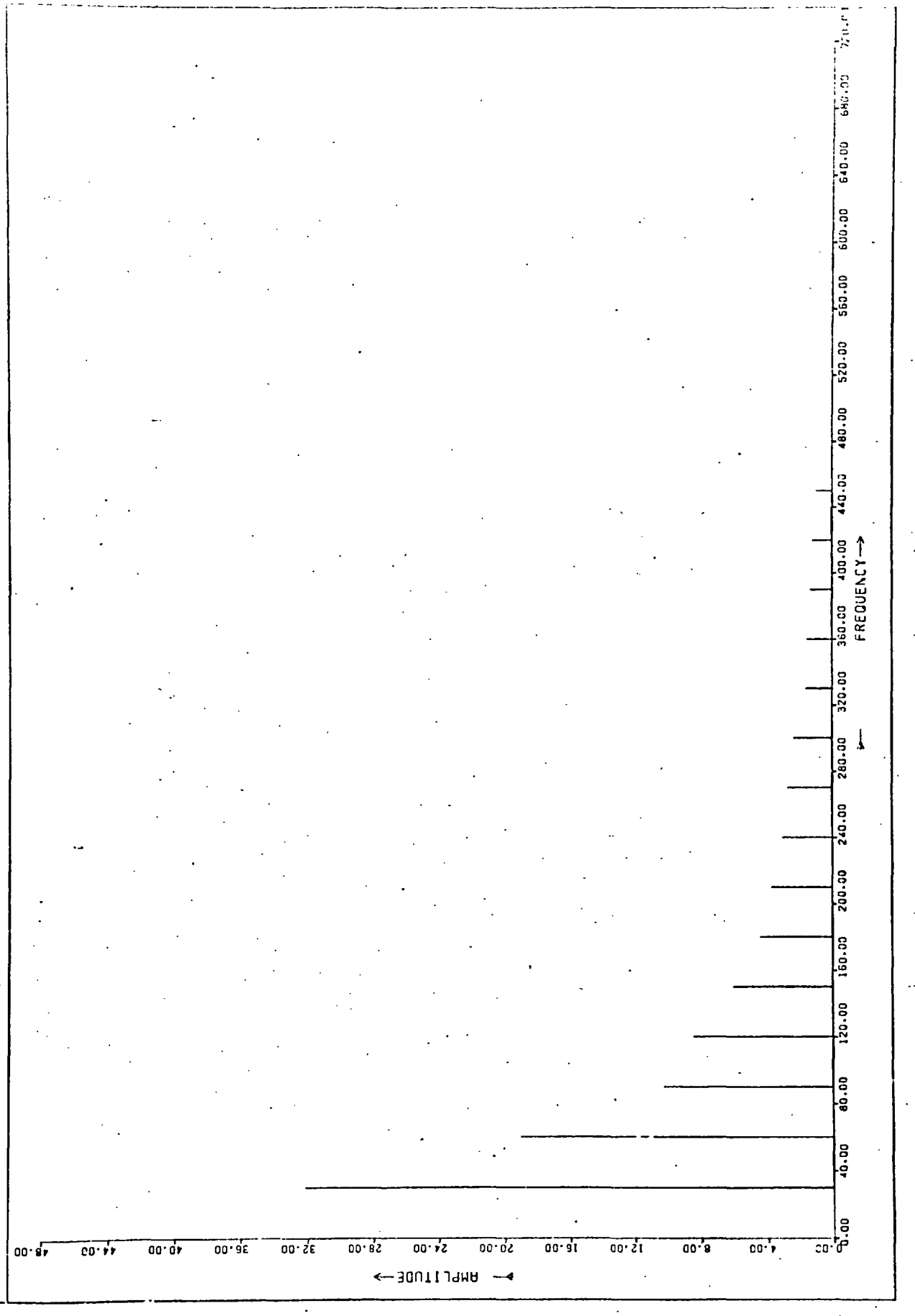


Fig. 12.2k 60 Hz. Waveform

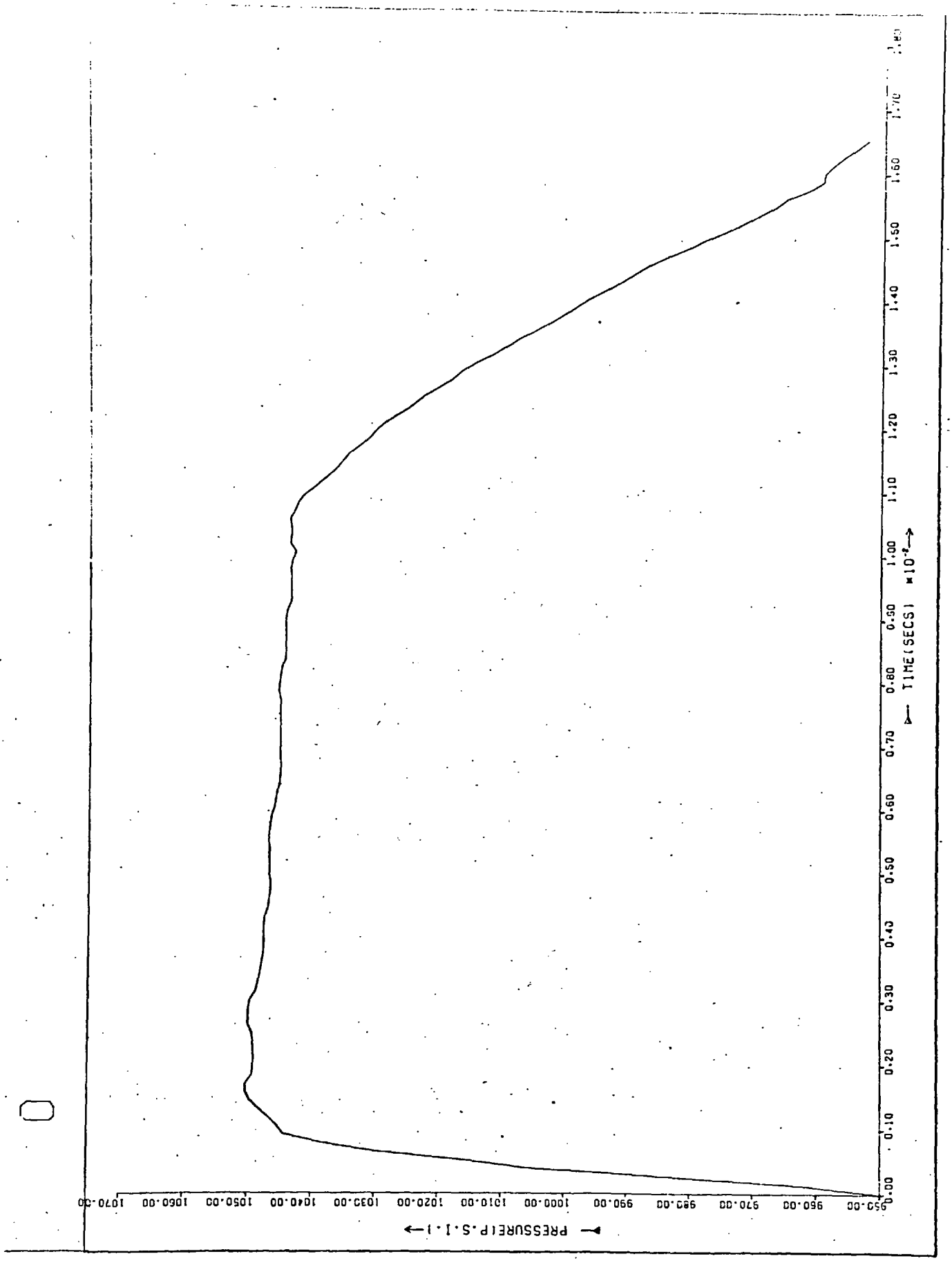
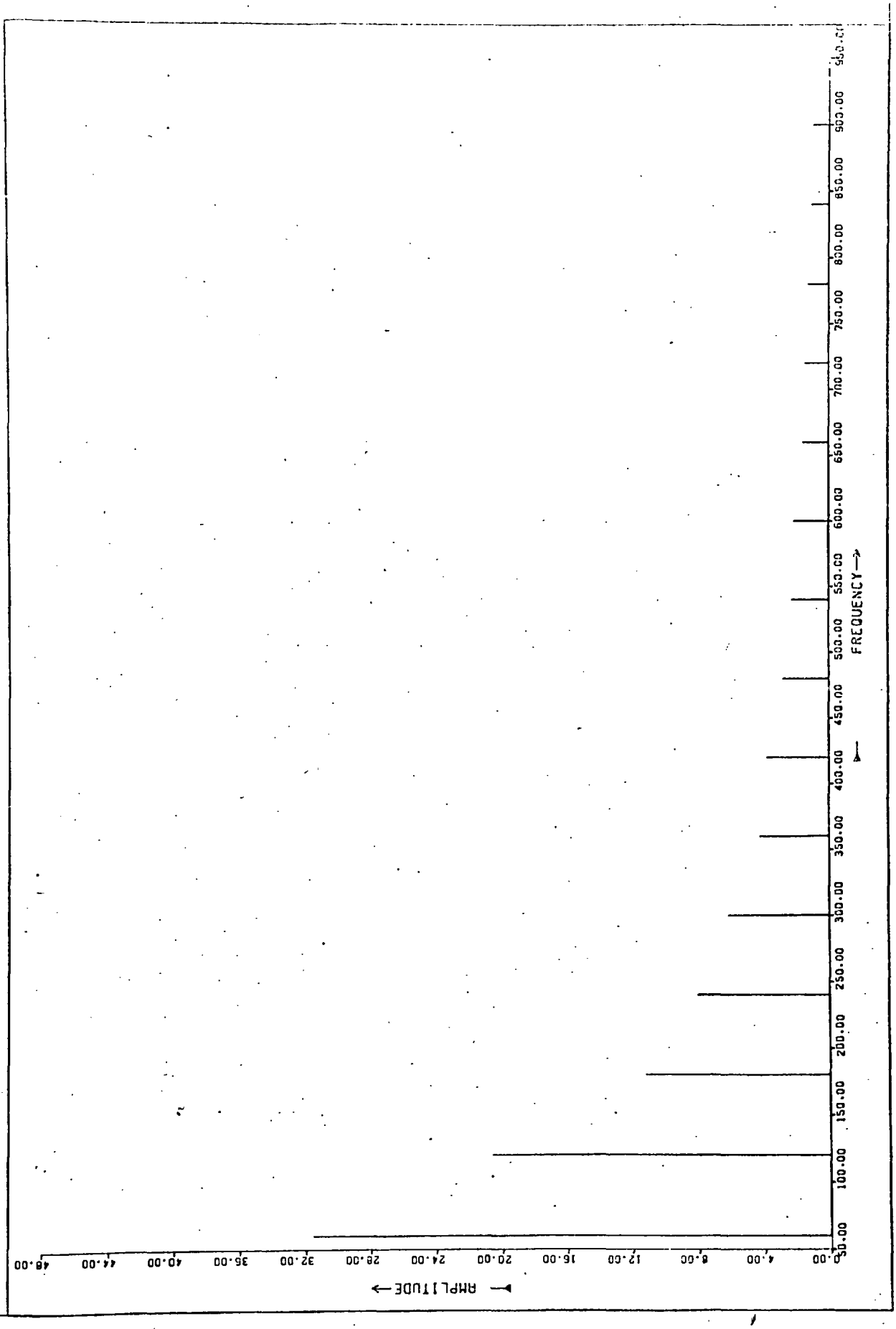


Fig. 12.21 Fourier Components of 60 Hz. Waveform



12.3 Computer Program for Fourier Analysis of Pressure Waveforms

```
CCDSOJ     CCDSOJ                          *** IMPERIAL COLLEGE COMPU

JOBNUMBER  CU     UU   MM     MM  EEEEEEEEE  MM     MM  MM     MM      11      555555
JOBNUMBER  CU     UU   MMM   MMM  EE         MMM   MMM  MMM   MMM     111      55
JOBNUMBER  CU     UU   MM MM MM  EE         MM MM MM  MM MM MM MM    1111      55
JOBNUMBER  CU     UU   MM  MM  MM  EE         MM  MM  MM  MM  MM  MM     11      55
JOBNUMBER  CU     UU   MM      MM  EE         MM      MM  MM      MM     11      55
JOBNUMBER  CU     UU   MM      MM  EEEEEEEE   MM      MM  MM      MM     11      555555
JOBNUMBER  CU     UU   MM      MM  EE         MM      MM  MM      MM     11        5555
JOBNUMBER  CU     UU   MM      MM  EE         MM      MM  MM      MM     11
JOBNUMBER  CU     UU   MM      MM  EE         MM      MM  MM      MM     11
JOBNUMBER  CU     UU   MM      MM  EE         MM      MM  MM      MM     11
JOBNUMBER  CUUUU JUU   MM      MM  EEEEEEEEE  MM      MM  MM      MM  11111111   555555
JOBNUMBER   CUUU JU    MM      MM  EEEEEEEEE  MM      MM  MM      MM  11111111     5555
```

```
      PROGRAM TOMY(INPUT,OUTPUT,TAPE5=INPUT,TAPE6=OUTPUT,TAPE1,TAPE2,
     +TAPE62)
      DIMENSION T(400),P(400),T1(400),P1(400),A(400),B(400),ILST(40),
     +F(400)
      CALL START(2)
      DO 99II=1,6
      CALL READIN(T1,P1,NN)
      PIE=3.141592654
      WL=T1(NN)-T1(1)
      N=2**((INT(ALOG(FLOAT(NN))/(ALOG(2.))))+1))
      TINC=WL/FLOAT(N)
      WRITE(6,)N
      DO1 I=1,N
      T(I)=FLOAT(I-1)*TINC+T1(1)

        FIND NEAREST T1....

      DIF=10000000000.
      DO2 J=1,NN
      IF(ABS(T(I)-T1(J)).GT.DIF)GO TO 2
      DIF=ABS(T(I)-T1(J))
      L=J
    2 CONTINUE
      CALL QUADINT(NN,AA,BB,CC,L,T1,P1,AREA)
    1 P(I)=AA*(T(I)**2)+BB*T(I)+CC
      N2=N/2
      N1=N2+1
      M1=(2*(INT((ALOG(FLOAT(NN))/ALOG(2.))))+2
        SPLIT IN HALF

      DO3 I=1,N2
      A(I)=P(I)
    3 B(I)=P(I+N2)

      CALL FOURIER TRANSFORM
```

```
      CALL CC6AAF(A,B,N1,.F.,M1,ILST)


        GENERATE FREQUENCY SPECTRUM


      DO 4 I=1,N2
      F(I)=FINC*FLOAT(I)
        P1 NO LONGER IN USE    FILL WITH AMPLITUDES.....

    4 P1(I)=SQRT(A(I+1)**2+B(I+1)**2)
      DO 5 I=1,N1
    5 WRITE(2,1000)T(I),P(I),F(I),A(I),B(I)
 1000 FORMAT(F8.5,9X,F8.6,13X,F8.6,9X,F8.5,9X,F8.6)
      DO 6 I=N1+1,N
    6 WRITE(2,2000)T(I),P(I)
 2000 FORMAT(F8.5,9X,F8.6)
      CALL GRAF(T,P,N,1,0,11H TIME(SECS),11,17H PRESSURE(P.S.I.),17,18.,
     +12.)
      CALL NUMBER(2.,3.5,0.5,II,0.,-1)
      NP=3*N2
      DO 999I=1,N2
      NN=(3*I)-1
      P(NN)=P1(I)
      P(NN-1)=0.
      P(NN+1)=0.
  999 T(NN)=T(NN-1)=T(NN+1)=F(I)
      CALL GRAF(T,P,45,1,0,18H          FREQUENCY,18,18H AMPLITUDE,13,18
     +.,12.)
      CALL NUMBER(2.,0.5,0.5,II,...,-1)
      WRITE(2,)'TIME(SECS)     PRESSURE(P.S.I)     ANGULAR FREQ.       SI
     +NE COEFFTS     COS COEFFTS'

   99 CONTINUE
      CALL ENPLOT
      STOP
      END
      SUBROUTINE READIN(T,P,N)
      DIMENSION T(400),P(400),IX(10),IY(10)
      LOGICAL PROG
      READ(1,)PSC,TSC,P0,T0
      N=0
      PROG=.F.
     PSC IN PSI/IN, TSC IN SEC/IN



      READ(1,1000)IX0,IY0,IX1,IY1,IX2,IY2
 1000 FORMAT(6I4)
```

```
      IX1,IY1


         I


      IX0,IY)-IX2,IY2
```

```
      PB=FLOAT(IX2-IX0)/199.
    1 READ(1,2000)(IX(I),IY(I),I=1,10)
 2000 FORMAT(20I4)
      DO 2 I=1,1:
      IF(IX(I).LT.0)GO TO 3
      N=N+1
      P(N)=(FLOAT(IY(I)-IY0)/PD)*PSC+P0
    2 T(N)=(FLOAT(IX(I)-IX0)/TD)*TSC+T0
      GO TO 1
    3 CONTINUE
     CHECK TRACE CONTINUITY....


      DO 4 I=2,N
      IF(T(I).GT.T(I-1))GO TO 4
      WRITE(6,)'TIME ',N,' LESS THAN OR EQUAL TO TIME ',N-1
      FROG=.T.
    4 CONTINUE
      IF(FROG)STOP
      RETURN
      END
      SUBROUTINE QUADINT(N,AA,BB,CC,NP,X,Y,AREA)
      DIMENSION X(200),Y(200)
      NN=NP
      NNN=0
      IF(N.NE.NN)GO TO 2
      NN=NN-1
      NNN=1
    2 CONTINUE
      IF(NN.NE.1)GO TO 77
      NN=2
      NNN=-1
   77 CONTINUE
      A1=(X(NN)**2-X(NN-1)**2)/(X(NN-1)-X(NN))
      A2=(X(NN+1)**2-X(NN-1)**2)/(X(NN-1)-X(NN+1))
      A3=(Y(NN-1)-Y(NN+1))/(X(NN-1)-X(NN+1))
      A4=(Y(NN-1)-Y(NN))/(X(NN-1)-X(NN))
      AA=(A3-A4)/(A1-A2)


      B1=AA*(X(NN)**2-X(NN-1)**2)
      B2=Y(NN-1)-Y(NN)
      B3=X(NN-1)-X(NN)
```

```
      BB=(B1+B2)/33
      CC=Y(NN-1)-AA*(X(NN-1)**2)-BB*(X(NN-1))



        CHECK RESULT IN DEBUG MODE



      A1=AA*(X(NN+1)**2)+BB*(X(NN+1))+CC-Y(NN+1)



      IF(ABS(A1).GT.1.E-11)WRITE(6,1)NN



      1  FORMAT(* ++++QUADRATIC SOLVING ERROR AT *,13,*TH CALL OF



      SUBROUTINE++++)



        COMPUTE AREA OF SEGEMENT NN-1 TO NN



      IF (NNN.EQ.-1)GO TO 88
      NN=NN+NNN
   88 A1=AA*(X(NN-1)**3)/3.+BB*(X(NN-1)**2)/2.+CC*(X(NN-1))
      A2=AA*(X(NN)**3)/3.+BB*(X(NN)**2)/2.+CC*(X(NN))

      AREA=A2-A1
      RETURN
      END
```

REFERENCES

1. Buckingham, E. "Analytical Mechanics of Gears", McGraw-Hill Book Co. Inc. 1949, p. 428.

2. Tuplin, W.A. "Dynamic Loads on Gear Teeth", Machine Design, Oct. 1953.

3. Macpherson, P.B. "Lubrication in Gear Scuffing and Pitting", Ph.D. Thesis, Univ. of London, Nov. 1971.

4. Johnson, D.C. and Bishop, R.E.D. "A note on the Excitation of Vibrating Systems by Gearing Errors", Journal of the Royal Aero. Soc. June 1955, Vol. 59, p. 434.

5. Reswick, J.B. "Dynamic Loads on Spur and Helical Gear Teeth", Trans. ASME, July 1955, p. 636.

6. Crook, A.W. "Simulated Gear-Tooth Contacts: some Experiments upon their Lubrication and Sub-surface Deformations", Proc. of Inst. Mech. Engrs., Vol. 171, No. 5, 1957, p. 187.

7. Johnson, D.C. "Excitation of Resonant Vibration by Gear Tooth Meshing Effects", Proc. Inst. Mech. Engrs., Int. Conf. on Gearing, Sept. 1958, p. 18.

8. Bishop, R.E.D. "Note on a Torsional Failure caused by Gear Inaccuracy", Journal of Mech. Eng. Sci., Vol. 4, No. 2, 1962, p. 188.;

9. Cleare, G.V. "Gear Tooth Failures in Highly Stressed Transmission Gears", Proc. Inst. Mech. Engrs., Int. Conf. on Gearing, 1958, p. 57.

10. Gregory, M.A., Harris, S.L. and Munro, R.G. "Dynamic Behaviour of Spur Gears", Proc. Inst. of Mech. Engrs., Vol. 178, Pt. 1, No. 8, 1963-64, p. 207.

11. Harris, S.L. "Dynamic Loads on the Teeth of Spur Gears", Proc. Inst. Mech. Engrs., Vol. 172, 1958, p. 87.

12. Weber, C. "The Deformation of Loaded Gears, and the Effect on their Load Carrying Capacity", D.S.I.R. Sponsored Research (Germany), Report No. 3, 1949.

13. Westland Aircraft Ltd. "A Method for Deriving the Power/N curve for a Gear from Test Results which include unwanted, but known Rig Vibration". Stress report S.D. 738, Gearbox Fatigue Testing, Westland Aircraft Ltd. 30/6/1960.

14. Manton, S.M., O'Donoghue, J.P., and Cameron, A. "Temperatures at Lubricated Rolling/Sliding Contacts", Proc. Inst. Mech. Engrs., Vol. 182, Pt. 1, No. 41, 1967-68, p. 813.

15. Merritt, H.E. "Gear Tooth Contact Phenomena", Proc. Inst. Mech. Engrs., Vol. 176, 1962, p. 141.

16. Kohler, H.K., Pratt, A. and Thompson, A.M. "Dynamics and Noise of Parallel-axis Gearing", Proc. Inst. Mech. Engrs., Vol. 184, Pt. 30, 1970, p. 111.

17. Welbourn., D.B. "Gear Errors and their Resultant Noise Spectra", Proc. Inst. Mech. Engrs., Vol. 184, Pt. 30, p. 131.

18. Dowson, D. and Wholmes, T.L. "The Effect of Surface Roughness upon the Lubrication of Rigid Cylindrical Rollers", Wear, Vol. 18, 1971, p. 129.

19. Dowson, D. and Wholmes, T.L. "Effect of Surface Quality upon the Traction Characteristics of Lubricated Cylindrical Contacts", Proc. Inst. Mech. Engrs., Vol. 182, Pt. 1, 1967-68, p. 292.

20. Mahalingham, S. and Bishop, R.E.D. "Dynamic Loading of Gear Teeth", Journal of Sound and Vibration, Vol. 36, Pt. 2, 1974, p. 179.

21. Nieman, G., Rettig, H., and Lechner, G. "Scuffing Tests on Gear Oils in the FZG Apparatus", ASLE Trans., Vol. 4, 1961, p. 71.

22. IP/IAE Gear Rig Tests Sub-Panel, "The IAE 3¼ ins. centres Gear Rig Estimation of Precision", Proc. Symp. on Gear Lub., Inst. Pet., 1966.

23. Benedict, G.H., and Kelley, B.W. "Instantaneous Coefficients of Gear Tooth Friction", Trans. ASLE, Vol. 4, 1961, p. 59.

24. Cameron, A., Lewis, J., and Macpherson, P.B. "Hydrostatic Disc Machine - Preliminary Details", Conf. on Externally Pressurised Bearings, Inst. Mech. Engrs., Nov. 1971, p. 317.

25. Popov, V.S., and Brykov, N.N., Matallov i Termicheskaya Albrabotka Metallov, No. 3, Mar. 1966, p. 25.

26. Balter, M.A., and Turovskii, M.L., Matallov i Termicheskaya Albrabotka Metallov, No. 3, Mar. 1966, p. 2.

27. Nieman, G. and Lechnev, G. Erdöl and Kohle 20 No. 2, Feb. 1967, p. 96.

28. Grew, W. "Role of Austenite and Mineral Oil in Lubricant Failure", Nature, Vol. 217, No. 5127, Feb. 1968, p. 481.

29. Matveevsky, R.M., Sinaisky, V.M., and Bayanovsky, I.A. "Contributions to the Influence of Retained Austenite content in Steels on the Temperature Stability of Boundary Lubricant Layers in Friction", Science of Machines Inst. Moscow, U.S.S.R., ASLE, Oct. 8 - 10, 1974.

30. Whyte, R.B. "Laboratory and Field Evaluation of an S.A.E. 70 Grade Gear Oil", Proc. Symp. on Gear Lub., Inst. of Petroleum, Vol. 3, 1966, p. 88.

31. Neal, M.J. "The Problems of Piston Ring and Cylinder Liner Scuffing in Internal Combustion Engines", Ministry of Tech. Report BR 21433.

32. Pike, W.C., Pywell, R.F., and Rulston, S.G. "Wear Phenomena of Chromium Plated Rings as revealed by Radioactive Tracers", S.A.E. Meeting at Houston, 4 - 7 Nov. 1969, Paper No. 690773.

33. Baüler, H. "Examining Scuffing Formation in a Motor Vehicle Diesel Engine", Motortechnische Zeitschrift, Vol. 24, No. 9, 1963, p. 299.

34. Bailey, M.W. "Critical Conditions in the Lubricated Sliding of Metals", Ph.D. Thesis, Univ. of London, Nov. 1971.

35. Bailey, M.W. "Critical Conditions in the Lubricated Sliding of Metals", Ph.D. Thesis, Univ of London, 1971, p. 150.

37. British Iron and Steel Research Association "The Mechanical and Physical Properties of British Standard EN Steels", Pergamon Press, 1966.

38. Dowson, D., and Higginson, G.R. "Elastohydrodynamic Lubrication", Pergamon Press, 1966, p. 96.

39. Cameron, A. "The Principles of Lubrication", Longmans, Green and Co. Ltd., 1966, p. 512, p. 24.

40. Dowson, D., and Higginson, G.R. "New Roller Bearing Lubrication Formula", Engineering, Vol. 192, 1961, p. 158.

41. Nieman, G., and Assman, H. "Experience with the FZG Apparatus for Testing Gear Oils", Journal of the Institute of Petroleum, Mar. 1966, p. 88.

42. IP Gear Lubricant Rig Tests Sub-Panel "An Investigation into the Correlation between the IAE and FZG Gear Type Lubricant Test Machines", Journal of the Inst. of Petroleum, Mar. 1966, p. 98.

43. Dudley, D.W. "Gear Handbook", McGraw-Hill Book Co. Inc., 1962, p. 9.

44. Reynolds, O. "On the Theory of Lubrication", Trans. Roy. Soc. (London) Vol. 177, 1886, p. 190.

45. Bowden, F.P., and Tabor, D. "The Friction and Lubrication of Solids", Oxford Univ. Press, 1954, Chaps. 13 and 15.

46. Butler, L.H. "The Hydrodynamic effect between Approaching Surfaces", Journal Inst. Pet. Vol. 46, No. 435, 1961, p. 63.

47. Paul, G. "Time Dependent Viscosity following a Pressure Rise measured on an Impact Viscometer",

American Soc. Lub. Engrs., ASLE/ASME Conference, Montreal, Canada, Oct. 8 - 10, 1974.

48. Pinkus, O., and Sternlicht, B. "Theory of Hydrodynamic Lubrication", McGraw-Hill Book Co. Inc., New York, 1961.

49. Jackson, J.D. "A Study of Squeezing Flow", Appl. Science Res., Section A, 11, 1962, p. 148.

50. Shukla, J.B. "Theory for the Squeeze Film for Power Law Lubricants", ASME Paper No. 64-Lub. S-4, 1964.

51. Donnelly, R.J. "The Magnetohydroydnamic Squeeze Film", Journal of Fluid Mechs., Vol. 19, Pt. 3, 1964, p. 395.

52. Hays, D.F. "Squeeze Films for Rectangular Plates", ASME Paper No. 62-Lub. S-9, 1962.

53. Moore, D.F. "On the Inclined Non-Inertial Sinkage of a Flat Plate", Journal of Fluid Mechs., Vol. 20, 1964, p. 321.

54. Archibald, F.R. "Load Capacity and Time Relations For Squeeze Films", Trans. ASME, Vol. 78, 1956, p. 29.

55. Dowson, D. "A generalised Reynolds Equation for Fluid Film Lubrication", Journal Mech. Sci., Vol. 4, 1962, p. 152.

56. Moore, D.F. "Drainage Criteria for Runway Surface Roughness", Journal of the Roy. Aero. Soc., 1965.

57. Den Hartog, J.P. "Advanced Strength of Materials", McGraw-Hill Book Co. Inc., New York, 1952, p. 19.

58. Hunt, J.B. "Pressure Distribution in a Plane Fluid Film subjected to Normal Sinusoidal Excitation",

Nature, Vol. 211, No. 5054, 9/9/1966, p. 1137.

59. Christensen, H. "Elastohydrodynamics of Normal Approach", Proc. Inst. Mech. Engrs., Vol. 182, Pt. 3, 1967-68, p. 248.

60. Christensen, H. "Oil Film in a Closing Gap", Proc. Roy. Soc., Vol. A266, 1961, p. 312.

61. Herrebrugh, K. "Elastohydrodynamic Squeeze Films between two Cylinders in Normal Approach", Trans. ASME, Journal of Lub. Tech., April 1970, p. 292.

62. Sanborn, D.M., and Winer, W.O. "Fluid Rheological Effects in Sliding Elastohydrodynamic Point Contact with Transient Loading", Journal of Lub. Tech., Trans. ASME, April 1971, p. 282.

63. Kauzlarich, J.J. "Hydraulic Squeeze Bearing", ASLE Trans., Vol. 15, 1, Lub. Conf. Oct 5-7, 1971, p. 37.

64. Cameron, A. "The Principles of Lubrication", John Wiley and Sons., New York, N.Y., 1966, p. 395.

65. Riddle, V., Pacor, P., and Appledorn, J.K. "Cavitation Erosion and Rolling Contact Fatigue", Wear, Vol. 27, 1974, p. 99.

66. Lewis, W. "Dynamic Loads on Gear Teeth", ASME Research Publication, 1931.

67. Fisher, R.A. "Statistical Methods for Research Workers", Oliver and Boyd, 1958, p. 114.

68. Dyson, A. "The Thickness of Very Thin Films in Elastohydrodynamic Lubrication", Faraday Society Special Discussion on Thin Films and Boundary Layers, Cambridge, Sept. 28-30, 1970.

69. Weber, J.R., Stippes, M.C. and Costello, G.A. "Elastic Impact of Cylinders", Trans. ASME, Journal of Applied Mechs., Dec. 1974, p. 1137.

70. Forrester, J.S. and O'Donoghue, J.P. "Measurement of Surface Temperature", Joseph Lucas Ltd., Group Research Report No. G.R. 90,425, 5th. Jan. 1966.

71. O'Donoghue, J.P., and Cameron, A. "Temperature at Scuffing", Proc. Inst. Mech. Engrs. 1965-66, Vol. 180, Pt. 3B, p. 85.

72. Lee, K.M. and Cheng, H.S. "The Pressure and Deformation Profiles between two Normally Approaching Lubricated Cylinders", Trans. ASME, Journal of Lub. Tech., July 1973, p. 308.

73. O'Donoghue, J.P. and Cameron, A. "Friction and Temperature in Rolling Sliding Contacts"., ASLE Trans., Vol. 9, 1966, p. 186.

74. Dyson, A. "The Failure of Elastohydrodynamic Lubrication of Circumferentially Groud Discs", Proc. Inst. Mech. Engrs., Vol. 52, 1976, p. 699.

75. Blok, H. "Measurement of Temperature Flashes on Gear Teeth", Inst. Mech. Engrs., General Discussion on Lubrication. Vol. 2, 1957, p. 14.

76. Ibrahim, M. and Cameron, A. "Oil Film thickness and the Mechanism of Scuffing in Gear Teeth", Paper No. 20, Conf. Lub. and Wear, Inst. Mech. Eng., Bournemouth, 1963.

77. Conway, H.D. and Lee, H.C. "Impact of a Lubricated Surface by a Sphere". Trans. ASME, Journal of Lub. Tech., Oct. 1975, p. 613.

78. Tabor, D. "Collisions through Fluid Layers", Engineering, Feb. 18, 1949, p. 145.

79. Conway, H.D. "The Rate of Change of Film Thickness in the Elastohydrodynamic Squeeze Film Process", Trans. ASME, Journal of Lub. Tech., Vol. 95, July 1973, p. 308.

80. Spikes, H.A. Private communication.

81. Khrushchov, M.M. and Matveesky, R.M. Amer. Soc. Mech. Engrs. Conf. on Lubrication, Washington (1964), Paper 64.

82. Lovell, A. D.I.C. Thesis, Imperial College, London 1965.

83. Burton, R.A. "Effect of Two-Dimensional, Sinusoidal Roughness on the Load Support Characteristics of a Lubricant Film", Trans. Am. Soc. Mech. Engrs., 1963, Vol. 85, Series D, p. 258.

84. Davies, M.G. "The Generation of Pressure between Rough, Fluid Lubricated, Moving, Deformable Surfaces", Lub. Engineering, 1963, Vol. 19, p. 246.

85. Christensen, H. "Stochastic Models for Hydrodynamic Lubrication of Rough Surfaces", Proc. Inst. Mech. Eng., 1969-70, Vol. 184, Pt. 1, p. 1013.

86. Tzeng, S.T. and Saibel, E. "Surface Roughness Effect on Slider Bearing Lubrication", ASLE Transactions, Vol. 10, 1967, p. 334.

87. Dowson, D., and Whomes, T.L. "Effect of Surface Quality upon the Traction Characteristics of Lubricated Cylindrical Contacts", Proc. Inst. Mech. Engrs., 1967-68, Vol. 182, Pt. 1, p. 292.